Design and Construction of Therapeutic Bacterial Sensors in *Escherichia coli* Nissle 1917

Tanel Ozdemir

A thesis submitted in partial fulfilment of the requirements for the degree of:

Doctor of Philosophy

of

University College London

Primary supervisor: *Dr. Chris P. Barnes*

Secondary supervisor: *Prof. Geraint Thomas*

September, 2017

Declaration

I, Tanel Ozdemir confirm that the work presented in this thesis is my own. Where information has been derived from other sources, I confirm that this has been indicated in the thesis.

Acknowledgements

I would like to start by expressing my sincere gratitude to Dr Christopher Barnes. Although sometimes a bit too pessimistic for my liking, he has been a tremendous supervisor. He was stern when I was dawdling and compassionate when I was struggling. I am proud of how far I have come under his guidance and grateful for the variety of opportunities he encouraged me to pursue. I am delighted to have been in his group. Alongside Chris, Alex Fedorec has been critical to my PhD and sometimes made me doubt whether it truly was independent research. As well as being a vital source of help throughout, he provided an underlying sense of camaraderie and friendship to the lab. Even so, I will never forgive him for his ridiculous desk fern. I would also like to thank Professor Geraint Thomas for his guidance as my secondary supervisor, and the BBSRC for funding my PhD through the fantastic LiDo Programme.

Up until they fled the nest and abandoned me in my final year at UCL, Miriam and Lewis added a valuable sparkle to my PhD life. I am grateful for the staggering number of coffees, G&Ts and laughs that we shared. Abbie, Sahana, Sandra and Xiang were alongside me when we collectively decided to dip our toes into the murky world of academia after our MSc. I am glad to have embarked on this journey with them, and eagerly look forward to witnessing the diverse paths we take from here. Outside of UCL, there has been a long established group who were an abundant source of rowdy encouragement and joy. Dan, Ed, Rob, Shabir and Tyler were there throughout to provide me with a welcome chuckle, drink or escape. There is no doubt in my mind that this will continue to be the case now that I am finished.

In more ways than one, I would not have been able to complete the PhD if it was not for Dad, Mum, Nilay and Tanser.

It has been a formative half-decade at UCL. All of these people have been instrumental in making it pleasant. For that, I am eternally grateful.

Abstract

The human microbiota refers to the ecosystem of microorganisms living on or within the human body, and is increasingly being implicated as a regulator of health and disease. Abnormal alterations in the development or composition of the intestinal microbiota are referred to as dysbiosis. However, the reciprocal interactions between the microbiota and the host's diet, immunology and genetics can in turn make it extremely difficult to distinguish the cause and effect of dysbiosis in pathologies. Synthetic biology has facilitated the design and creation of more complex and clinically relevant genetic circuits. The commensal nature of the intestinal microbiota and its constituents provide a number of well tolerated microorganisms such as *Escherichia coli* NISSLE 1917 (EcN) that could be used as powerful investigative tools.

The use of antibiotic selection within synthetic circuits would eventually hinder their investigative power during microbiota experiments. Toxin-Antitoxin (TA) post segregational killing systems are a naturally occurring bacterial mechanism to maintain plasmid stability. Here we show that the Axe/Txe TA system from *Enterococcus faecium* was able to significantly outperform the more widely used Hok/Sok system to maintain the stability of fluorescent and luminescent reporter plasmids in EcN without antibiotic selection during both liquid culture and *in vivo* animal experiments.

In addition, we created a sensor circuit that in EcN could detect both exogenous and bacterial-derived reactive nitrogen species, which are thought to play a crucial role in the human host inflammatory response. We also developed biosensors for pH and the short-chain fatty acid propionate. Finally, we demonstrated that an EcN sensor could detect and report on environmental signals *in vivo* from the intestines of the *Caenorhabditis elegans* worm. Synthetic biological tools such as these could help further elucidate the underlying role of the microbiota in conditions such as inflammatory bowel disease and cancers of the gasterointestinal tract.

UCL Impact Statement

The research presented here has the potential to have a wide impact inside and outside academia. We have shown that we can apply synthetic biology principles and methodologies to engineer a commonly used probiotic strain of *Escherichia coli* called *Escherichia coli* Nissle 1917. We initially demonstrated that a less well characterised plasmid stability mechanism functions better in this strain than the current standard mechanism. After publication of these findings, this will enable researchers to create more robust experiments and gain deeper insights into the intestinal microbiome.

Next, we created and characterised a variety of bacterial biosensors with this strain. This will have an initial academic impact on the research carried out within intestinal microbiome engineering. Furthermore, this academic research could help eventually create clinically relevant treatments that can help understand and combat pathologies such as inflammatory bowel disease and cancers of the gasterointestinal tract.

Lastly, we demonstrated that the *Caenorhabditis elegans* worm can be used as a simple, powerful and economical animal model for live intestinal experiments. Once published, these findings will encourage researchers to use this model as a useful biological tool for intestinal microbiome investigations. In line with the principles of 3Rs (replacement, reduction and refinement) within animal research, this can help significantly reduce the use of regulated vertebrate animals such as mice, and subsequently, it will also help reduce the amount of money and time needed to carry out these type of experiments.

Contents

List of Figures

Abbreviations

- AT = Axe/Txe
- DNA = Deoxyribonucleic Acid
- EcN = *Escherichia coli* Nissle 1917
- FCM = Flow-cytometry
- GFP = Green Fluorescent Protein
- HS = Hok/Sok
- IBD = Inflammatory Bowel Disease
- IPTG = Isopropyl β-D-1-thiogalactopyranoside
- LB = Lysogeny Broth
- MCC = Microcin
- MCS = Multiple Cloning Site
- M9 = Minimal M9 media
- NGM = Nematode Growth Medium
- NOS = Nitric Oxide Synthase
- PSK = Post-segregational Killing
- RBS = Ribosome Binding Site
- ROI = Region of Interest
- RNS = Reactive Nitrogen Species

- SNP = Sodium Nitroprusside (Nitric Oxide Donor)
- SCFA = Short Chain Fatty Acid
- TA = Toxin-Antitoxin

1. Background

1.1 Introduction to the Human Microbiome

As a result of co-evolution over millions of years, the skin, respiratory and intestinal tracts of humans are colonised by over a 1000 species of microbes soon after birth. The terms 'microbiota' and 'microbiome' are used to describe the collective microbial community which inhabit a certain environment and the collective genomic contents of this community, respectively. It is now known that these microbes have essential roles in maintaining normal physiology [1]. Ongoing consortium studies like the Human Microbiome Project and MetaHIT (Metagenomics of the Human Intestinal Tract) have established that the human microbiome contributes 360 times more unique protein-coding genes than human cells (8 million in comparison to 22,000) [2, 3]. Having identified this vast and unexplored genomic 'dark-matter', a significant emphasis has been placed on slowly unraveling the physiological importance of the microbiota in relation to human health and disease. For the purpose of clarity, this piece of work will only focus on the gut microbiota which encompasses the entire gastrointestinal tract (Figure 1.1).

Instead of several segregated components, the human gut microbiome can be considered a complex and multifaceted ecosystem that exhibits spatiotemporal synergy [5], metabolic competition and cooperation [6, 7] and intercellular interactions such as quorum sensing [8]. Quorum sensing is one of the most widely characterised microbial communication systems. Using a diffusible molecule (AHL), the system creates a signalling interaction which results in the correlation of gene expression in response to fluctuations in the population density of a community [9]. In a densely populated environment such as the intestines, multi-species communities also use mobile genetic

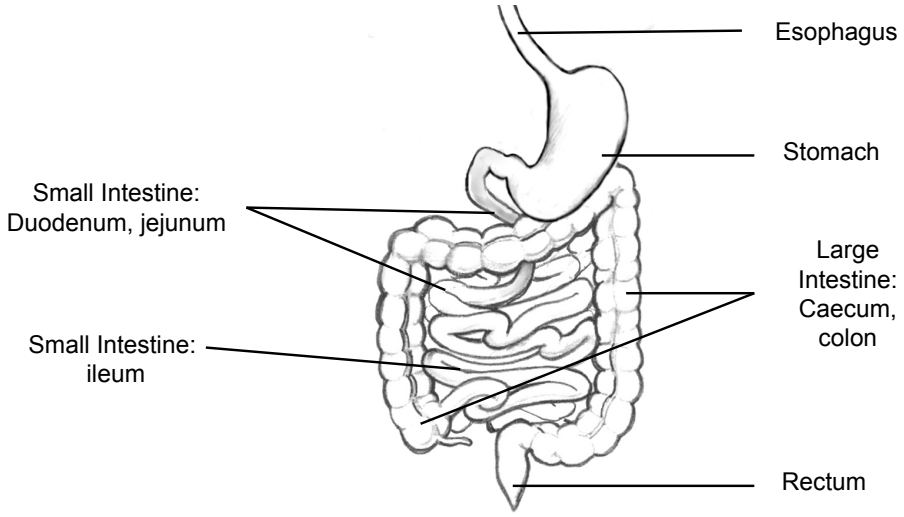

Figure 1.1: Drawing of the human gastrointestinal tract indicating the esophagus, stomach, small intestines, large intestines and rectum. Image adapted from [4].

elements such as plasmids and bacteriophages for horizontal gene transfers (HGT) to share beneficial genes with neighbours and preserve the stability of the niche [10, 11, 12].

1.1.1 The Gut Microbiome in Human Health

The host immune system has evolved to simultaneously allow colonisation by symbiotic microbiota whilst also containing the capacity to fight against pathogens. It is hypothesised that individual members of the microbiota maintain this gut homeostasis by balancing pro-inflammatory and regulatory host responses throughout the development of the immune system [13]. It is now known that the host age [14], diet [15] and immunological state [16] can significantly affect the gut microbiota (Figure 1.2). This coevolution is known to be beneficial to the host as the microbiota aids in the development of the infant immune system [17] and provides protection against pathogenic colonisation [18]. Recently, the discovery that the gut microbiota can also communicate with the central nervous system through neural and endocrine pathways led to the realisation of a microbiota-gut-brain axis that is linked to the host's brain and behaviour [19]. Another vital role for the microbiota is that additional genes provided by the microbiome facilitate the extraction of a wide range of otherwise inaccessible nutrients from the diet. A major example of this is microbial fermentation of ingested carbohydrates into short-chain fatty acids (SCFAs) such as butyrate, acetate and propionate [20, 21].

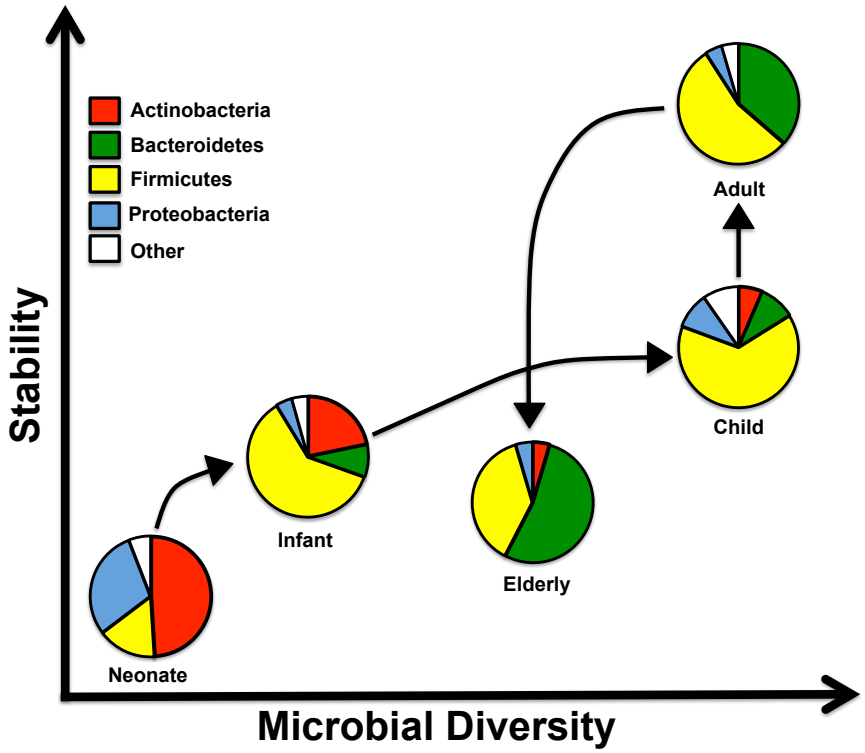

Figure 1.2: Human gut microbiome composition across the life cycle [22, 23]. The graphic shows that from a young age, the diversity and stability of the gut microbiome increases. However, this stability and diversity is reduced during old age.

1.1.2 Dysbiosis

Due to the integrated relationship with the host, both the microbiota and the microbiome can be significantly altered during human disease. This abnormal alteration is referred to as dysbiosis [24]. The reciprocal interactions between the microbiota and the host's diet, immunology and genetics can in turn make it extremely difficult to distinguish the cause and effect of dysbiosis in pathologies. It is also known that a diseased state can lead to changes in the microbiota through various mechanisms such as changes in bowel functions, eating habits and the use of antibiotics [25]. However, recent findings are indicating that certain host genetic variants predispose individuals towards dysbiotic states and these alterations in turn are a key feature in disorders of metabolism [26] and immunity [27].

1.1.3 Disease

As the epithelial cells of the gut lumen are constantly exposed to the microbiota and its metabolites, the host immune response can be a source of a number of maladies.

Inflammatory bowel diseases (IBD) such as ulcerative colitis and Crohn's disease are thought to be caused by a dysfunctional immune response that leads to dysbiosis and in turn chronic low levels of inflammation [13]. It is hypothesised that this erroneous immune response is due to a combination of environmental and genetic factors [28]. The gut microbiota has also subsequently been implicated in allergies [29] and autoimmune conditions such as rheumatoid arthritis [30], lupus [31] and type 1 diabetes [32].

1.1.4 Diet

The host diet has a vital role in shaping the microbiota composition and in turn the downstream secondary metabolites that are produced directly in the gut lumen. In fact, it is now known that up to 10% of the metabolites found in mammalian blood are of bacterial origin [33]. The role of diet-induced obesity on the gut microbiota was first established over a decade ago when it was shown to decrease the abundance of *Bacteroidetes* phyla whilst increasing the proportion of *Firmicutes* phyla [34]. It was then subsequently shown that this altered obese microbiota composition was enough to cause an increase in total body fat in germ-free mice by increasing the capacity to harvest energy from their diet [35]. Further research also demonstrated that the gut microbiota is implicated in other metabolic disorders such as cardiovascular disease [36] and type 2 diabetes [37]. One of the most widely investigated interactions of microbial metabolites is with colorectal cancer, the third most common cause of cancer mortality in the world [38]. Certain fermentation products such as SCFAs have been shown to prevent colorectal carcinogenesis by having anti-inflammatory [39] and anti-apoptotic [40] effects on the cells of the gut lumen. Conversely, other pro-inflammatory bacterial metabolites such as secondary bile acids and hydrogen sulphide are thought to contribute to colorectal carcinogenesis through reactive oxygen species (ROS) and reactive nitrogen species (RNS) [41, 42, 43]. Secondary bile acids are formed from colonic bacteria metabolising the primary bile acids that are synthesised by the liver. Alongside their pro-inflammatory effects, these compounds have also recently been associated with providing resistance to pathogenic *Clostridium difficile* infection [44].

1.2 Introduction to Synthetic Biology

Over the last 15 years, synthetic biology has emerged as an interdisciplinary field that integrates many facets of biology and engineering. Since the characterisation of deoxyribonucleic acid (DNA), the steady unravelling of this fundamental code of life has revealed the complexity of the genetic framework and the biological systems that it so delicately regulates. The genetic networks found in cells utilise a network of interacting genes and proteins for signalling, growth, division, and differentiation. Through the assimilation of techniques from disciplines such as chemical engineering, computer science, and electrical engineering, synthetic biology is concerned with further elucidating these complex biological systems and in turn manipulating them for a novel or alternative purpose. These purposes span several fields within themselves and includes the synthesis of valued chemicals, environmental remediation and disease therapy [45, 46].

1.2.1 Engineering Approaches in Synthetic Biology

Since the early emergence of the field, engineering concepts such as abstraction, decoupling, and standardisation were proposed to enable the efficient scaling up of the biological design process [47]. In order to be able to handle the complex genetic process, the concept of abstraction encourages a hierarchal dissection into different design levels such as DNA, parts, devices and whole systems. Together with decoupling, a strategy used to reduce a complicated problem into several simpler tasks that can be reassembled, the design of a specific part, device, or system can be compartmentalised and simplified. The standardisation of both the design process and the physical assembly was encouraged to enable a platform on which data, parts, and devices could be shared. Due to the complexity of engineering biological systems, these approaches still lead to a relatively slow and laborious 'design, test and build' cycle. While proof-of-concept circuits with a small number of standardised parts are achievable, the move towards large-scale systems with numerous circuits require a more complex design cycle (Figure 1.3). This modelling, redesign and verification of parts and systems *in silico*, rapidly reduce the cost and length of time needed.

An efficient and productive design cycle becomes a necessity when using complex

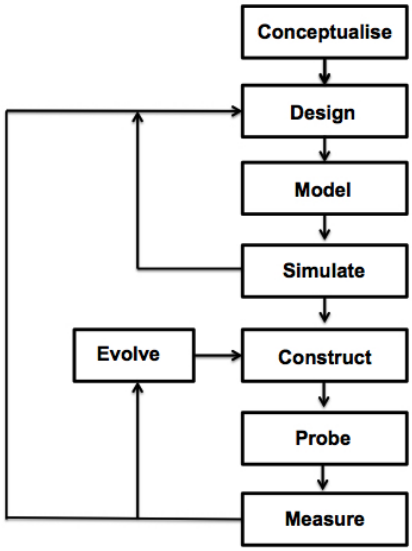

Figure 1.3: Design cycle for engineering genetic circuits. Diagram demonstrating the multiloop process in the design cycle of genetic circuits.

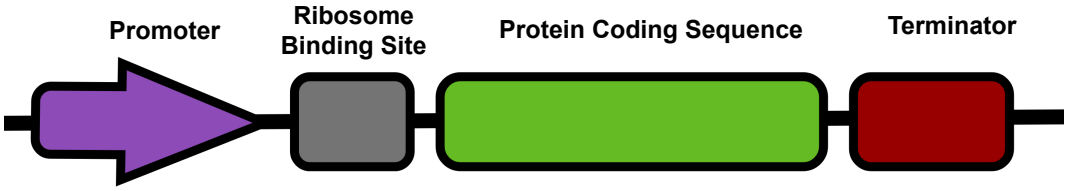

Figure 1.4: Biological parts in a synthetic protein coding device. A protein coding sequence could be for Green Fluorescent Protein (GFP).

parts and devices to enable programmable functionality from engineered genetic circuits [46]. Borrowing from fields such as electric engineering, synthetic biology has formed biological parts that act as a building block in a genetic circuit and perform a specific function such as regulating transcription, regulating translation or binding protein domains. The combination of a promoter, a ribosome binding site, a protein coding sequence, and a terminator is all that is needed for the expression of a single protein and to kickstart the circuit design process (Figure 1.4). With an ever increasing catalogue of different parts, several independent libraries have now been publicly released with the relevant information about their compatibility and function [48]. Building on this growing catalogue of parts, synthetic biologists have been able to construct several types of higher-order circuits. These components include switches [49], time delayed circuits [50], memory elements [51], logic gates [52] and genetic oscillators [53].

1.2.2 Therapeutic Applications of Synthetic Biology

Through the use of DNA as building blocks, this interdisciplinary field has gone on to vastly expand our knowledge base and push the boundaries of both prokaryote and eukaryote biology. These span from fundamental advancements such as the creation of non-natural xeno-nucleic acids (XNA) and polymerases [54] to the redesign and production of numerous fully functioning chromosomes from the eukaryote *Saccharomyces cerevisiae* yeast [55]. The ever expanding toolbox of synthetic biology has resulted in numerous therapeutic applications that not only rely on genome engineering but also on the design and integration of synthetic genetic circuits.

Using yeast, metabolic engineers were able to vastly reduce the cost of producing artemisinic acid, the precursor to the life-saving and expensive antimalaria drug artemisin [56]. More recently, the same concepts were applied to demonstrate that yeast could be engineered to biosynthesise opioids [57]. In order to tackle the increasing burden of antibacterial resistant microbes, it was shown that the effectiveness of three major classes of antibacterial drugs can be improved 5000-fold by using engineered bacteriophages to disrupt the microbial defence response to the drugs [58]. Other strategies include the design of genetics circuits that enabled laboratory *E. coli* to specifically recognise, migrate towards and kill pathogenic *Pseudomonas aeruginosa* [59]. Due to the fact that several genera of bacteria are known to naturally accumulate in the hypoxic environment of tumours, synthetic biology techniques have also been used in the field of cancer therapeutics [60]. It was shown that through a synthetic circuit, the activity of HIF-1α, a hypoxia-inducible factor, could be coupled to the production of cytosine deaminase, an enzyme that converts the 5-fluorocytosine prodrug to the much more toxic and chemotherapeutic 5-fluorouracil [61]. When *E. coli* was engineered to incorporate this circuit, it would localise at tumours and increase the prodrug sensitivity to human cancer cells expressing HIF-1α. The recent development of DNA-editing tools such as CRISPR/Cas9 has paved the way for precise and rapid genome engineering experiments across many species, including bacteria [62]. A recent example in the field of regenerative medicine showed that CRISPR/Cas9 could be used to inactivate 62 copies of the porcine endogenous retrovirus (PERV) in a pig cell line in hope of eventually improving the safety of porcine-to-human xenotransplantation [63].

1.3 Approaches to Investigating and Engineering the Microbiota

1.3.1 Introduction

The use of synthetic biology to engineer the intestinal microbiota has the potential to provide a wide variety of therapeutic applications. This community consists of a wide variety of well-tolerated microorganisms that occupy a very large and interactive buffer zone between the host and the external environment. With a broadening set of experimental tools and approaches being developed, these microogranisms are becoming increasingly engineerable. Researchers have tried to harness this commensal ability to deliver synthetic genetic circuits and novel therapeutics to the host via the intestines. These approaches have used a number of different bacterial species and looked at tackling a range of conditions such as pathogenic infection [64], metabolic disease [65] and cancer [66]. Recent work has even demonstrated that probiotics engineered with multifaceted genetic circuits could be used to monitor environmental signals within the mammalian gut [67, 68].

It can be argued that the incorporation of even more advanced components and techniques from synthetic biology is vital for the realisation of the full therapeutic and diagnostic potential of engineering the microbiota. Even with the use of chassis that are generally recognised as safe (GRAS) organisms, there now must also be serious considerations for the regulation, safety and biocontainent of such approaches. One particular safety concern is the spread of recombinant DNA from engineered strains to native strains as natural horizontal gene transfer is known to be prevalent in the intestines [69]. Another major concern is the escape of the engineered organism into the environment or another human being. Incorporating conditional kill-switches into circuits [70], or developing auxotrophic strains that cannot replicate outside of the gut [71] are methods that have successfully been used for biocontainment. Indeed, auxotrophy was the sole biocontainment strategy used during early clinical trials with engineered probiotic *Lactobacilli* strains [72].

1.3.2 Bacterial Vectors for Intestinal Microbiota Engineering

With the human microbiome consisting of over 1500 species, there is a great deal of variety in the vectors chosen by researchers. This decision is primarily based on two factors; the ease with which the strain can be manipulated in a laboratory setting and its suitability to the destined niche (Figure 1.5). A balance must be struck between convenience in the laboratory and the eventual relevancy to the target.

The intestines are found to be mostly anaerobic with some variation in oxygen concentration throughout. In line with this, microbes found in the intestines are either obligate anaerobes (that are harmed by the presence of oxygen), aerotolerant anaerobes (which can tolerate the presence of oxygen) or facultative anaerobes (which can grow with or without the presence of oxygen) [73]. With advancements in molecular biology methods and an expansion in the repertoire of genetic parts and methods, an ever increasing selection of bacteria have been used in the laboratory to augment our understanding of the gut microbiome (Figure 1.6). Recent innovations in our ability to culture new strains from the human gut will undoubtedly expand this toolbox [74].

In addition to some *Lactobacilli* strains, *E. coli* NISSLE 1917 (EcN) is one of the most widely studied clinical probiotic strains to date. This particular strain was isolated by Alfred Nissle in 1917 from the faeces of a soldier who did not fall ill with infectious diarrhea like his companions [75]. Since then, it has been classed as a non-pathogenic and non-invasive member of the *E. coli* family and does not produce any enterotoxins or cytotoxins. In addition to this, it has also been demonstrated that the strain possesses immunomodulating properties, reinforces the intestinal-epithelial barrier and acts antagonistically against other pathogenic entero-bacteria [76]. Due to these characteristics, several clinical studies have shown that EcN can be therapeutically effective

Laboratory Suitability	Destined Niche Suitability
- How convenient it is to culture (time, money, equipment)	- Prevalence in the destined niche
- How easy it is to perform DNA manipulation	- Stability in the destined niche
- Genome information	- Virulence in the destined niche
- Repertoire of available genetic parts	- Clinical data
- Safety and virulence	
- Published methods and tools	

Figure 1.5: Considerations behind choosing a chassis for microbiota investigations.

Obligate Anaerobes	Aerotolerant Anaerobes	Facultative Anaerobes
Bacteroides thetaiotaomicron	*Bifidobacterium longum*	*Escherichia coli* NISSLE 1917
Bacteroides fragilis		*Salmonella spp*
		Lactococcus spp

Figure 1.6: Examples of engineered commensal microbes [64, 80, 81, 82, 83, 84, 85].

in the treatment of ulcerative colitis, Crohn's disease and acute diarrhea [77, 78, 79].

After oral administration, the strain is capable of rapidly colonising the large intestine and cecum for up to several months in a stable manner [76, 86]. As a result of the clinical investigations of EcN, an effort was also recently made to sequence and publish the entire genome of the strain [87]. Due to these characteristics and the fact that EcN is a member of the *E. coli* family, a number of researchers have used the strain to investigate the potential of synthetic biology to engineer and monitor the intestinal microbiome. It can be argued that as a plethora of suitable genetic parts, culturing methods and other microbiology tools already exist for *E. coli*, EcN is therefore an ideal commensal vector for microbiota engineering.

1.3.3 Current Approaches

To date, there have been multiple approaches with different bacterial chassis in an attempt to use synthetic biology to design therapeutic tools to monitor and fight diseases. The most basic of these approaches include the engineering of a chassis to produce a beneficial compound directly in the gut. One of the first examples was the engineering of *Lactococcus lactis* to secrete recombinant human anti-inflammatory cytokine IL-10 directly in the intestines to reduce colitis as a form of treatment for IBD [88]. A more recent example is the transformation of EcN with a plasmid producing N-acylphosphatidylethanolamines (NAPEs), the precursors to a family of lipids which are synthesised in the intestines in response to feeding and known to reduce food intake [65]. Mice that received this modified EcN strain showed significantly lower food intake, adiposity and insulin resistance in comparison to control bacteria. In a similar approach, EcN was also successfully engineered with a plasmid to produce β-carotene in hope of eventually preventing vitamin A deficiency in the developing world [89].

Another example of this approach involved the use of engineered EcN to disrupt

the quorum sensing pathways of *V. cholerae*. This pathogen is known to control its population density and the amount of cholera toxin being produced via quorum sensing molecules cholera autoinducer 1 (CAI-1) and autoinducer 2 (AI-2). When both of these molecules are high, virulence factors such as cholera toxin are no longer expressed. In order to disrupt this pathway and reduce virulence, EcN was transformed with a plasmid which constitutively expresses *CqsA*, the gene for CAI-1. In a mouse model, the ingestion of this engineered strain of EcN before *V. cholerae* administration significantly reduced cholera toxin production and mortality [64].

In order to demonstrate the versatility of commensal strains like EcN as carrier systems, efforts were made to create circuits that can be controlled in a temporal and quantitative manner. In line with this, it was shown that EcN can be engineered with synthetic circuits with promoters P_{araBAD}, P_{rhaBAD} and P_{tet} which can be induced with L-arabinose, L-rhamnose or anhydrotetracycline, respectively [86]. These promoters were placed upstream of the *luxCDABE* operon to create an inducible luminescent reporter. When these strains were administered orally and colonised the intestines, each synthetic circuit was shown to have a specific *in vivo* induction profile once the respective inducer substances were administered either orally or intravenously. Tools like this demonstrate the feasibility of precisely controlling gene expression when a chosen vector reaches and colonises a specific niche in the host.

As well as precise control, synthetic biology has also been used to incorporate more complex genetic parts into these synthetic circuits (Figure 1.7). A circuit harbouring both a switch element and memory element could be used in a non-pathogenic laboratory strain of *E. coli* to sense and report on stimuli directly from the gut of a mouse model [67]. Once the stimuli was sensed in the gut, in this case the inducer tetracycline (ATC), the chassis uses a stable memory element to hold the state over a number of passages and days. More recently, another stimuli sensing memory switch was used in *Bacteroides thetaiotaomicron* but with CRISPR-interference technology instead [81]. The incorporation of an integrase element into a sensor circuit also enabled researchers to amplify the detection limits of a bacterial biosensor that could detect pathological biomarkers in human clinical samples [90]. Other examples include the use of toxin-antitoxin (TA) systems (Chapter 2) to stabilise genetics circuits in EcN so that it can non-invasively detect and signal liver metastasis after oral administration [91]. Meth-

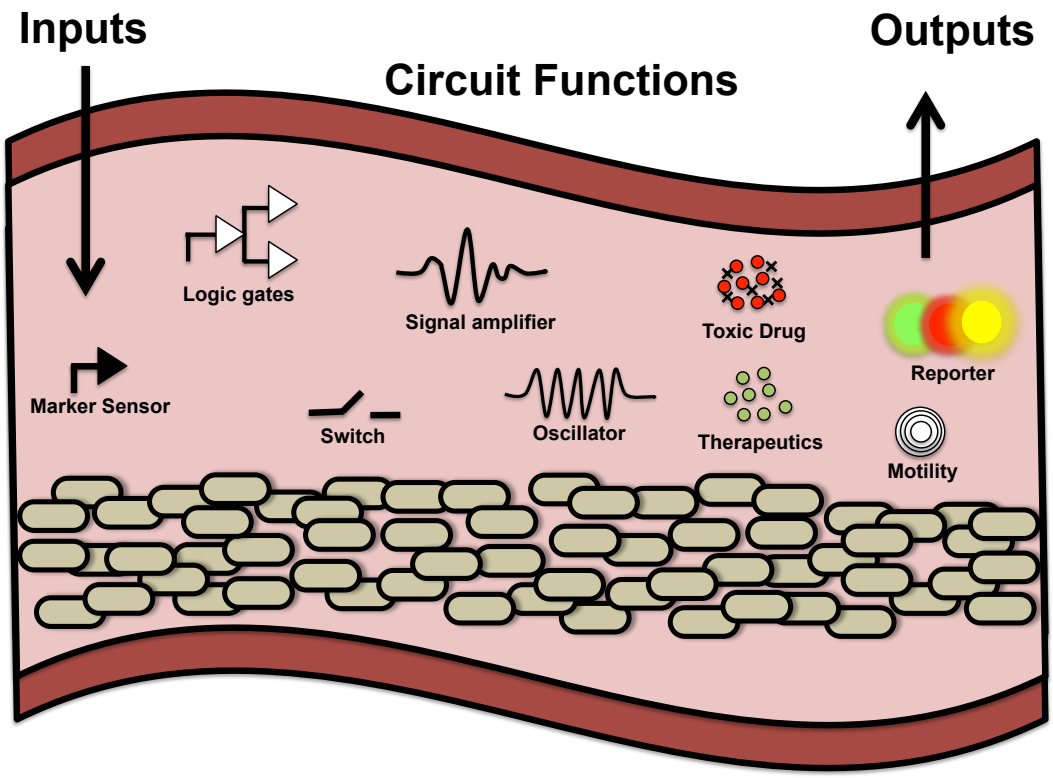

Figure 1.7: Examples of the repertoire of synthetic circuit functions that can be incorporated into engineered strains for intestinal microbiome investigations.

ods like this indicate that it is possible to monitor the complex environment of the gut and in turn elucidate mechanisms behind perturbations and pathologies.

1.4 Thesis Aims

This body of work set out to investigate the use of synthetic biology tools for unraveling the underlying mechanisms of the complex and multifaceted intestinal microbiota. In addition to building on the latest research in these dynamic fields, attempts were made to broaden the established methodologies and approaches currently in use.

Chapter 2: This piece of work aimed to design, test and evaluate the functionality of a number of different PSK systems in stabilising fluorescent and bioluminescent reporter circuits in the probiotic EcN strain *in vitro* and *in vivo*. This included:

1. The TA Hok/*sok* (HS) system derived from the *parB* locus of *E. coli*.
2. The TA Axe/Txe (AT) system derived from the pRUM plasmid of *E. faecium*.
3. The microcin V (MCC) bacteriocin system derived from *E. coli*.

Chapter 3: This piece of work aimed to design, test and evaluate a range of therapeutically relevant sensors in the probiotic EcN strain. This included:

1. A sensor based on the *yeaR-yoaG* operon that can detect a range of RNS such as nitric oxide, nitrate and nitrite.
2. A sensor based on the *prpBCDE* operon that can detect the SCFA propionate.
3. A sensor based on the *cadBA* operon that can detect changes in external pH.
4. A sensor based on the putative promoter region of the *BBr_0838* gene that can detect bile acids.

Chapter 4: This piece of work aimed to investigate the use of *C. elegans* as a live model for characterising an inducible EcN bacterial biosensor *in vivo*. This included:

1. Developing an inducible reporter system that can be detected quantitatively *in vivo*.
2. To establish whether *C. elegans* can develop and grow solely on EcN.
3. The development of an induction assay whereby the signal of an EcN biosensor can be detected and quantified from the *C. elegans* intestines *in vivo*.

1.5 Thesis Organisation

This thesis is organised in the following manner:

- Chapter 1: Background.
- Chapter 2: Stabilising Plasmids in *E. coli* Nissle 1917 Through Post-segregational Killing Mechanisms.
- Chapter 3: Design and Construction of Therapeutically Relevant Bacterial Sensors.
- Chapter 4: *Caenorhabditis elegans*: An Emerging Model for Studying the Intestinal Microbiota.
- Chapter 5: Conclusions.
- References.
- Appendix.

Experimental Chapters 2, 3 and 4 include their own introductory Background section and a stand-alone Materials and Method section.

1.6 Work Carried Out by Other Individuals

Chapter 2: Alex Fedorec (Barnes Lab, UCL) was responsible for cloning the MCC constructs and we jointly ran the plasmid loss experiments throughout. Alex also plotted all the plasmid loss curves for the experiments. Anjali Doshi (Danino Lab, Columbia University, USA) was responsible for cloning the pHelp promoter into all the p26_Lux constructs. Anjali also performed all animal model experiments with the luminescent constructs and kindly shared the experimental results.

Chapter 4: The IPTG inducible pLac_GFP plasmid was cloned from the OG241 plasmid by David Gonzales (MRes student in Barnes Lab).

2. Stabilising Plasmids in *E. coli* Nissle 1917 Through Post-segregational Killing Mechanisms

2.1 Introduction

The rapid advancement of microbiology techniques and DNA manipulation methods has facilitated an increasing level of complexity in genetic engineering. These DNA manipulation methods have evolved from standard restriction enzyme and PCR cloning to more recent methods such as Golden Gate cloning [92] and Gibson assembly [93]. It is fundamental that with this engineering, the desired outcome is stable and reproducible. To date, genetic engineering of prokaryotes has either been carried out directly on the host chromosome or on plasmids; small circular DNA molecules that can replicate independently of the chromosome [94]. These plasmids are naturally found in most bacteria and often carry beneficial genes such as antibiotic resistance [95]. Due to their easy manipulation with DNA polymerases and molecular restriction enzymes, artificial plasmids are a fundamental biological tool and have been widely used as vectors in molecular cloning.

In the case of engineering a chosen host to contain a length of foreign DNA such as a reporter circuit, it would be ideal to integrate the DNA sequence directly into the genome to achieve a stable transformation. However, integration of a large number of genes such as those found on a synthetic gene circuit can be technically challenging and time consuming [96]. Whereas next generation tools such as lambda Red [97] and CRISPR-Cas9 [98] are rapidly changing this landscape, there is still much debate

on the unintended consequences of inserting large amounts of foreign DNA into the genome of bacterial hosts. In light of these factors, non-integrating plasmids are still widely used as DNA cloning vectors. However, these plasmids are not inherently stable in the transformed host after division. If a gene on a plasmid confers a metabolic burden on the host, plasmid-free progeny can rapidly outgrow plasmid containing cells due to the negative selective pressure [99]. This would result in the complete loss of the desired synthetic construct and therefore antibiotic resistance markers are widely used in a research environment to impose a selective pressure and maintain plasmid stability. However, the likelihood of horizontal gene transfer makes the use of antibiotics unsuitable in many clinical [100] and industrial [101] applications of synthetic biology. In the case of the intestinal microbiota, the use of antibiotics would also immensely alter the native environment and significantly impact investigations [102].

Some plasmids have naturally evolved a number of mechanisms to prevent themselves from being dropped from the constantly dividing host. All plasmids studied to date have been shown to contain an origin of replication that uses negative feedback control to narrow the distribution of plasmid copy numbers across cells and reduce the risk of plasmid loss during division [103, 104]. However, this alone is not sufficient to maintain full stability. In light of these limitations, efforts have already been made to re-use a variety of existing microbial machinery to ensure plasmid persistence in more complex environments [105]. Successful alternatives have been demonstrated with the use of post-segregational killing systems [106, 91], active-partitioning mechanisms [91, 107] and auxotrophy [108].

Toxin-antitoxin (TA) systems are a type of post-segregation killing mechanism that consists of a self regulated fragment with two or more genes that separately encode for a toxic protein and an equivalent antidote protein. The toxic protein is normally stable and is not broken down quickly while the antidote is normally unstable and short-lived [109]. Due to these dynamics, the presence of a TA cassette on a plasmid ensures that only the daughter cell that possesses the plasmid survives after a cell undergoes division (Figure 2.1). Whereas the toxin in the system is always a protein, the method of the antitoxin distinguishes the two types of systems. Type I systems are found in *E. coli* and other Gram-negative bacteria and comprise of a small cell membrane damaging hydrophobic protein and an RNA antitoxin that inhibits protein translation. Type

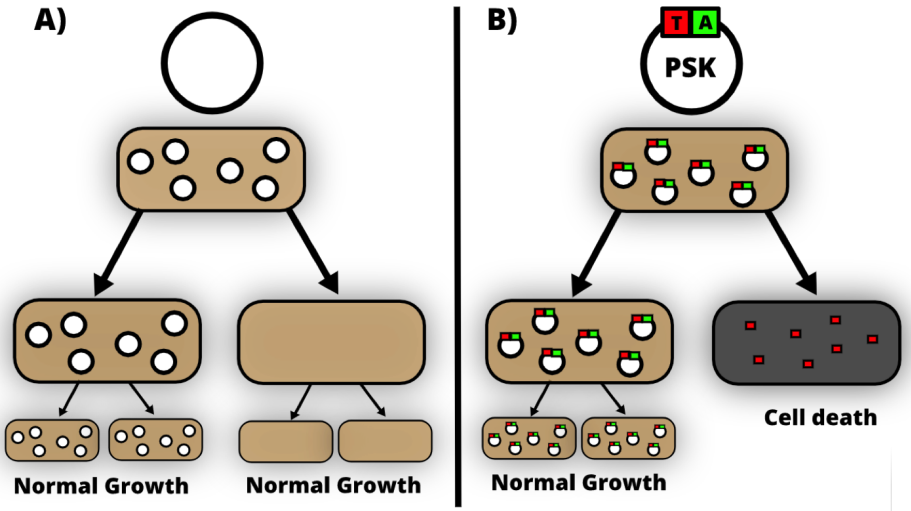

Figure 2.1: Toxin-antitoxin (TA) post-segregation killing (PSK) systems for plasmid maintenance. A) Plasmid loss in a population without a PSK system. B) PSK system maintaining a plasmid in a population by preventing the growth of daughter cells without the plasmids. Red indicates toxic element and green indicates antidote.

II systems consist of an unstable antitoxin protein that neutralises the toxin through proteic complex formation [110]. Over the last few decades, a number of systems have been discovered and characterised from across a variety of microbes [105].

2.2 Toxin-antitoxin Systems

In order to improve the functionality and stability of plasmids in synthetic biology approaches, researchers have incorporated TA systems into the design of synthetic circuits for microbiota investigations.

Hok/*sok* is a type I system that originates from the *parB* locus of the *E. coli* plasmid R1 and has been shown to be effective in its native *E. coli* as well as the Gram-negative *Pseudomonas putida* [111] (Figure 2.2A). It is a bactericidal system where the toxin leads to cell death. The use of Hok/*sok* was recently demonstrated in EcN with the introduction of the TA system into a synthetic circuit that could non-invasively detect and signal liver metastasis [91]. Surprisingly, the introduction of the Hok/*sok* cassette was found to show hardly any improvement in the stability of the constitutive luxCDABE reporter *in vitro* without antibiotic selection. However, the presence of the Hok/*sok* system vastly improved plasmid retention of the reporter construct during *in vivo* tumour experiments after administration of the engineered

EcN strain. This retention was further improved with the addition of the alp active partitioning system on the reporter construct [91].

Axe/txe is a type II system from the *axetxe* locus of the Gram-positive *Enterococcus faecium* plasmid pRUM (Figure 2.2B). It is a bacteriostatic system where the toxin prevents cell growth. The functionality of Axe/Txe in *E. faecium* was demonstrated with the creation of a luminescent reporter that was stable without antibiotic selection [112]. In addition, it was shown that axe/txe could be used to stabilise a luminescent reporter in the closely related Gram-positive *Enterococcus faecalis in vivo* without antibiotic selection for five days [113].

2.3 Bacteriocins

An alternative PSK system to TA are bacteriocins, which are bacterially secreted proteins that have a bactericidal effect on either a narrow or broad spectrum of other bacteria lacking immunity [114]. By secreting these antimicrobials, a plasmid-bearing population is able to police the environment, preventing the growth of plasmid-free cells. In comparison to the TA system, bacteriocins can maintain plasmids even with mutational instability. Whereas a single mutation in the toxin on a TA plasmid would remove the selective pressure in that cell, the selection with bacteriocins is maintained via the surrounding cells. Regardless of whether they are able to produce the bacteriocin, each cell still needs to encode the immunity gene on the plasmid to avoid death [115]. Successful attempts have already been made to use bacteriocins, such as the Lcn972 system, to stabilise plasmids in *L. lactis* [116]. In addition, the colicin A bacteriocin was also able to stabilise a plasmid in *E. coli* for up to 18 daily passages [115]. The microcin V system is encoded on conjugative plasmids in *E. coli* and consists of a low molecular weight toxic bacteriocin, along with the genes for a transporter and

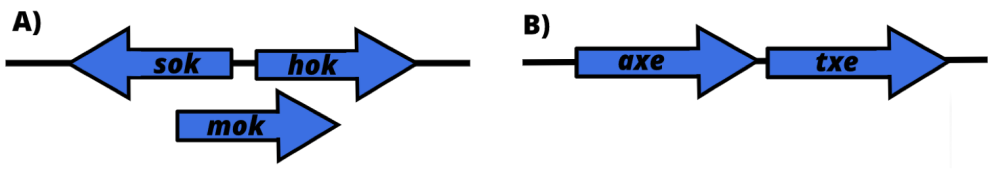

Figure 2.2: A) The 633bp Hok/*sok* system codes for a toxic protein (hok), RNA antitoxin (sok) and modulatory protein (mok) needed for hok translation. B) The 1791bp proteic axe/txe system codes for a single toxic protein (txe) and antidote protein (axe).

immunity protein (Figure 2.3) [114]. It does not undergo any post-translational modification and, as such, does not require any extra enzyme encoding genes. Furthermore, it has been shown that EcN already carries two bacteriocin systems in its chromosome; microcins H47 and M [117]. More recently, it was also shown that native bacteriocins found in EcN were vital in mediating competition in the inflamed gut in a inter and intraspecies manner [118].

Figure 2.3: The 4848bp microcin V (MCC) system consists of genes coding for a toxic protein (cvaC), an immunity protein (cvi) and a transporter system (cvaA and cvaB).

2.4 Aims

Due to the fact that different types of TA and bacteriocin systems originate from different species of prokaryotes and use different molecular mechanisms, there is no consensus on which PSK system is most suitable for use in common laboratory strains or commensal vector strains. In addition to this, the stability of the synthetic circuit will also be affected by the ultimate *in vivo* destination of the commensal strain. The integration of a PSK system into a commensal strain like EcN could pave the way for effective tools in monitoring and engineering the intestinal microbiota.

This piece of work aimed to design, test and evaluate the functionality of a number of different PSK systems in stabilising fluorescent and bioluminescent reporter circuits in the probiotic EcN strain *in vitro* and *in vivo*. These PSK systems include:

1. The TA Hok/*sok* (HS) system derived from the *parB* locus of *E. coli*.
2. The TA Axe/Txe (AT) system derived from the pRUM plasmid of *E. faecium*.
3. The microcin V (MCC) bacteriocin system derived from *E. coli*.

2.5 Materials and Methods

2.5.1 Media and Strains

Lysogeny broth (LB) media and agar was used during propagation and cloning of bacteria. Assays were carried out in LB media and when antibiotic selection was applied, kanamycin was used at 25μg/mL, erythromycin at 100μg/mL and gentamycin at 10μg/mL. All DNA manipulations were performed in *E. coli* DH5α (NEB). All sequences were confirmed via Sanger sequencing (Source Bioscience, UK). *E. coli* Nissle 1917 (EcN) was provided by Prof. Ian Henderson (University of Birmingham, UK). Chemically competent EcN strains were made using the same standard protocol. Briefly, this involved diluting an overnight strain culture 1:100 into 50ml of fresh LB media and grown at 37°C in a shaking incubator to an OD_{540} of 0.25 to 0.3. The culture was then chilled on ice for 15 minutes and then centrifuged for 10 minutes at 5000g and 4°C. The medium was then discarded and the cell pellet resuspended in 30ml of cold 0.1M $CaCl_2$ before being kept on ice for a further 30 minutes. This suspension was then centrifuged for 10 minutes at 5000g and 4°C. The supernatant was once again removed and the cell pellet was resuspended in 3ml of cold 0.1M $CaCl_2$ solution with 15% glycerol. The final cell suspension was then aliquoted and flash frozen before being stored at -80°C.

Initial fluorescent plasmid stability assays were performed in an EcN variant where the mini-Tn7 transposon system was used to genomically integrate gentamycin resistance and constitutive DsRedExpress expression into the chromosome (EcN_Red). Briefly, the Tn7 transposon inserts as a single copy into a specific site named *att* Tn7 which is conserved in most known bacteria and is classed as a neutral chromosomal site where genomic integration should not affect the host [119]. The miniTn7 system takes advantage of these unique characteristics and consists of a helper plasmid with the transposition genes and a delivery plasmid with the Tn7 flanks and DNA insert of choice. The delivery plasmid acts as a suicide vector and consists of an origin of replication that only allows transient propagation in the chosen bacteria. In light of this, the delivery plasmid is eventually dropped from the strain and the genomic insert is only found in the chromosome. Here, the pTNS1 helper plasmid [120] and the pUC18T-mini-Tn7T-Gm-*DsRedExpress* delivery plasmid [121] were used to engineer EcN according

to the specified electroporation protocol. Along with growth in gentamycin and visible DsRedExpress expression, colony PCR was performed to confirm the Tn7 integration into EcN to derive EcN_Red. However, it was eventually discovered that the EcN_Red strain was ampicillin resistant, which implied that the integration was faulty and the delivery plasmid was not dropped after integration as expected. Due to this discovery, all final fluorescent plasmid stability assays were repeated and instead performed in EcN with a genomically integrated erythromycin-resistant *luxCDABE* cassette (EcN_Lux) (Dr Tal Danino from the Columbia University, USA)[91].

All luminescent plasmid stability assays in liquid culture and in animals models were performed in *E. coli* Nissle 1917 (EcN).

2.5.2 Plasmids and Cloning Methods

Fluorescent plasmids were constructed from OXB20_GFP, a plasmid with a pUC high copy origin-of-replication, a kanamycin resistance cassette, an empty multiple cloning site (MCS) and a dasher GFP gene being constitutively expressed in high quantities by the OXB20 promoter (Oxford Genetics, UK) (Figure 2.4). A strong promoter and high copy origin of replication was chosen to maximise the metabolic burden of the plasmid on the host. Using standard DNA manipulation methods, Hok/*sok* (633bp fragment cut with HindIII and SacI from plasmid pKG1022 [111]) and Axe/Txe (1390bp fragment cut with SacI and BamHI from plasmid pREG531 [95]) were ligated and individually cloned into the multiple cloning site of OXB20_GFP to derive plasmids OXB20_GFP_HS and OXB20_GFP_AT. In order to evaluate the TA systems against other PSK mechanisms, these constructs were tested alongside the microcin V (MCC) bacteriocin. Briefly, PCR was used to clone and attach compatible restriction enzyme sites to the MCC system [122]. This was then ligated into to OXB20_GFP to derive OXB20_GFP_MCC. Both EcN_Red and EcN_Lux were transformed individually with these plasmids via heat-shock methods (Figure 2.5).

Luminescent plasmids were constructed from pSEVA246, a plasmid based on the pSEVA format [123] with a ColE1 high copy origin-of-replication, a kanamycin resistance cassette, an empty multiple cloning site (MCS) and a promoterless *LuxCDABE* operon (Figure 2.4). The strong constitutive phelp promoter [124] was cloned upstream of *luxCDABE* to drive expression and derive p24_help-Lux. The 1390bp axe/txe frag-

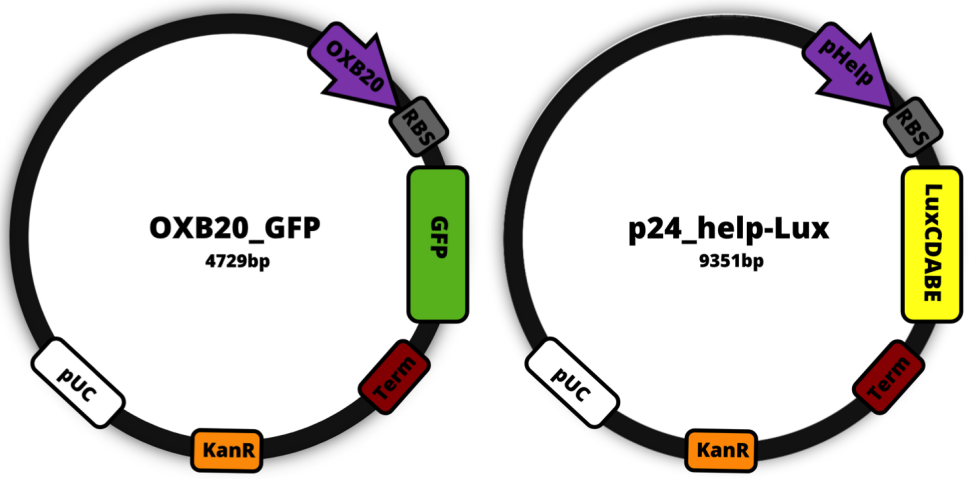

Figure 2.4: Graphical representation of constitutive OXB20_GFP and constitutive p24_help-Lux plasmids.

	Relevant Characteristics	Source
Strain		
EcN	*E.coli* Nissle 1917	Prof. Ian Henderson, UK
EcN_Lux	*E.coli* Nissle 1917 with chromosomal *LuxCDABE* and Er^R	Danino et al. [2015]
EcN_Red	*E.coli* Nissle 1917 with chromosomal *DsRedExpress* and Gm^R	This work
Plasmids		
OXB20_GFP	Constitutive strong OXB20 promoter, GFP, pUC and Kan^R	Oxford Genetics, UK
OXB20_GFP_HS	OXB20_GFP with Hok/Sok cassette	This work
OXB20_GFP_AT	OXB20_GFP with Axe/Txe cassette	This work
OXB20_GFP_MCC	OXB20_GFP with Microcin V cassette	Alex Fedorec (Barnes Lab)
p24_help-Lux	Constitutive strong P_{help} promoter, *LuxCDABE*, pUC and Kan^R	Benedetti et al. [2012]
p24_help-Lux_HS	p24_help-Lux with Hok/Sok cassette	This work
p24_help-Lux_AT	p24_help-Lux with Axe/Txe cassette	This work
p24_help-Lux_MCC	p24_help-Lux with Microcin V cassette	Alex Fedorec (Barnes Lab)

Figure 2.5: Table of strains and plasmids used throughout.

ment was digested from plasmid pREG531 [95] with SacI and BamHI and ligated into the MCS of p24_help-Lux to derive plasmid p24_help-Lux_AT. The 633bp hok/*sok* fragment was PCR amplified from plasmid pKG1022 [111] and cloned into the MCS of p24_help-Lux with SacI and BamHI to derive p24_help-Lux_HS. The MCC system [122] was ligated into into the MCS of p24_help-Lux with SacI and XbaI to derive p24_help-Lux_MCC. EcN was transformed individually with these plasmids via heat-shock methods (Figure 2.5).

2.5.3 Growth Rate Assays

Overnight cultures of each strain were grown in triplicates and diluted 1/1000 into LB media. 200μL from each culture was then transferred into 6 wells of a shallow polystyrene 96-well plate (Corning ®, Sigma-Aldrich, UK) and sealed with a Breathe-

Easy sealing membrane (Sigma-Aldrich, UK). The plate was then grown in a shaking POLARstar Galaxy microplate reader (BMG LABTECH, UK) at 37°C for 20 hours with OD_{540} readings taken every 10 minutes. Growth curves were fitted using a non-parametric Gaussian process method [125].

2.5.4 Fluorescent Plasmid Stability Assays in Liquid Culture

Three colonies of each EcN_Lux_OXB20_GFP strain were picked from LB-agar plates and grown in 5mls of LB media with kanamycin and erythromycin overnight at 37°C and 200RPM to create starter cultures with a 100% plasmid bearing population. Assays were performed with LB in a sterile autoclaved 96-well deep square well (2.2mL) polpropylene plate. The 96-well plate was split into two replicate sections with a random arrangement of wells to minimise contamination and growth variation (Figure 2.6). Each strain had 3 independent replicates and 3 biological replicates. Wells in the first section were filled with 500μL of LB media with erythromycin (100μg/mL) and wells in the second section were filled with 500μL of LB with both erythromycin and kanamycin. With erythromycin resistance integrated into the chromosome of EcN_Lux, the use of the antibiotic would prevent external contamination while running the assay in the absence of kanamycin. 1μL of overnight starter culture was then used to inoculate each well from the respective strain to create passage 1. The plate was then sealed with a System Duetz breathable silicon sandwich (EnzyScreen, The Netherlands) and clamped down in a shaking incubator at 37°C and 350RPM for 24 hours. Subsequent passages were made by using a 8-channel pipet to transfer 1μL of overnight culture into an identical sterile autoclaved 96-well deep square well plate with the same LB well arrangement and grown in the same conditions as before. Plasmid stability was then investigated by using the GFP marker expressed from the plasmids and flow cytometry to calculate the proportion of plasmid-bearing population for each strain over a total of 37 passages. The initial plasmid stability assays performed in EcN_Red were carried out in the same manner for 21 passages but with gentamycin instead of erythroymcin.

Flow Cytometry Analysis and Plotting

Flow cytometry was performed on an Attune NxT Acoustic Focusing Cytometer with Attune NxT Autosampler (Thermo Fisher Scientific, UK). 1μL of the appropriate strain

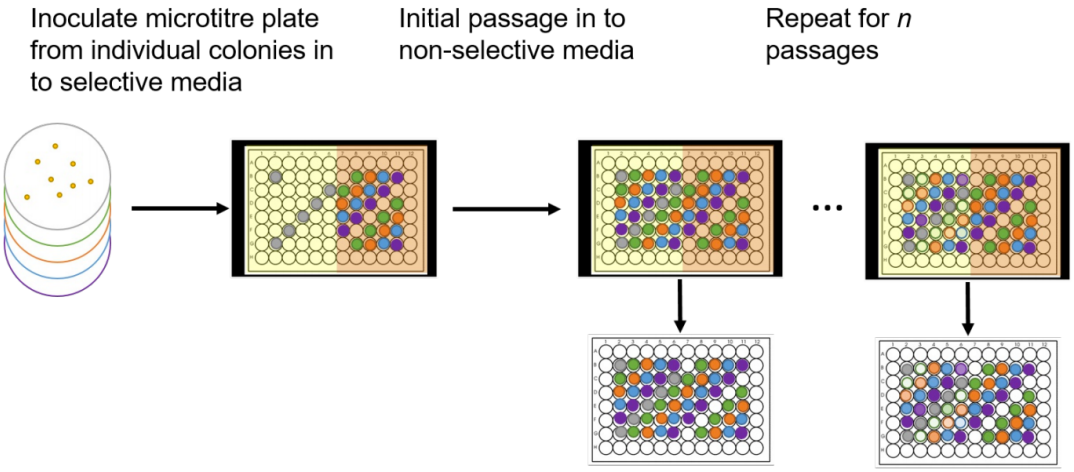

Figure 2.6: Plasmid stability assay with daily passages. Yellow indicates LB with just erythromycin and orange indicates control wells containing LB with both erythromycin and kanamycin. Optical density and GFP fluorescence was measured at each passage.

culture was transferred into 200μL of PBS in a shallow polystyrene 96-well plate. The Attune NxT Autosampler was used to record 10,000 events for each sample with 4 washes between each. GFP was excited using the blue laser (488nm) and was detected using a 530/30nm bandpass filter. In order to prevent operator bias associated with manual drawing of gates and speed up the analysis of samples, a computational pipeline called autoGate was developed by Alexander Fedorec in the Barnes Lab (github.com/ucl-cssb/autoGate) to automate the gating of singlet bacteria while excluding background debris and bacterial doublets. Briefly, the method fits mixture models of one, two and three clusters to the forward-scatter versus side-scatter data. Using integrated completed likelihood (ICL) [126], the number of clusters that best fits the data is calculated and the cluster centred closest to the expected bacterial population coordinate is taken. A linear model is then fit to the side-scatter-height versus side-scatter-area data and points falling too far away are removed as cell doublets. The levels of trimming are shown in Figure 2.7. Python was used for Gaussian process fitting [125] and the ggplot2 package in R was used for plotting. Briefly, this involved expanding on previously published models [127] to incorporate post-segregational killing and using Bayesian methods to fit a model to the plasmid-loss data.

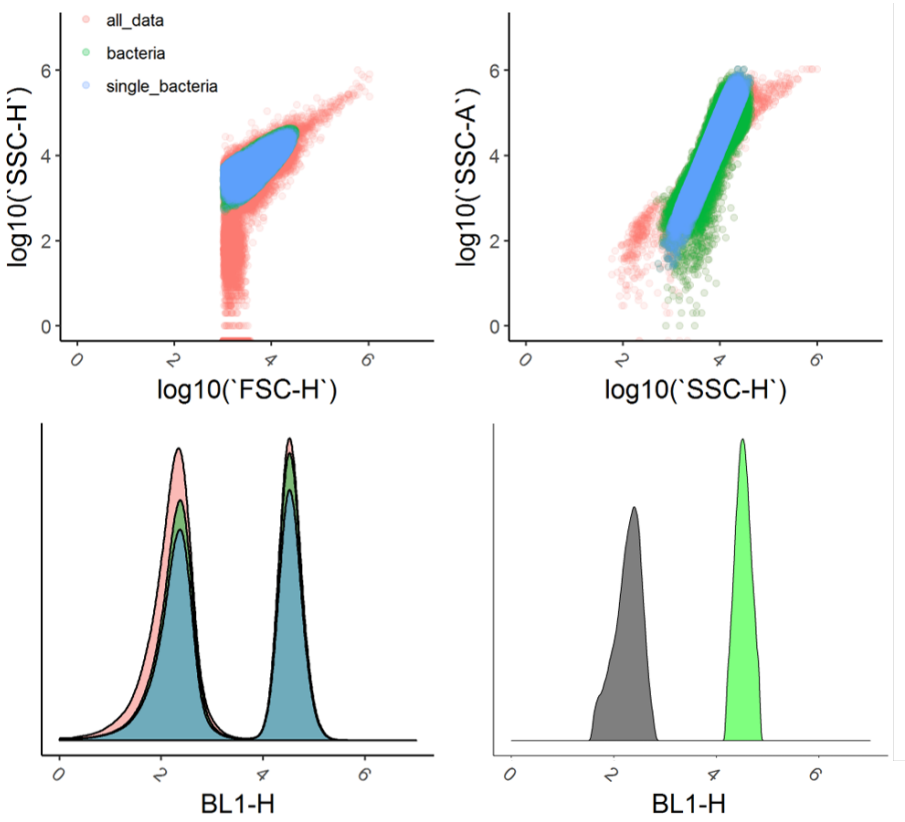

Figure 2.7: autoGate clustering and trimming of flow cytometry data.

2.5.5 Luminescent Plasmid Stability Assays in Liquid Culture

Three colonies of each EcN_p24_help-Lux strain were picked from LB-agar plates and grown in 5mls of LB media with kanamycin overnight at 37°C and 200RPM to create starter cultures with a 100% plasmid bearing population. The assays were then performed with LB in a sterile autoclaved 96-well deep square well (2.2mL) polpropylene plate. In line with the fluorescent assays, the 96-well plate was split into two replicate sections with a random arrangement of wells to minimise growth variation (Figure 2.6). Each strain had 3 independent replicates and 3 biological replicates. Wells in the first section were filled with 500μL of LB media with no antibiotic and wells in the second section were filled with 500μL of LB with kanamycin. Once the wells were filled, the entire plate was exposed to UV light for 40 minutes in a custom built perspex chamber to minimise contamination. 1μL of overnight starter culture was then used to inoculate each well from the respective strain to create passage 1. The plate was then sealed with a System Duetz breathable silicon sandwich (EnzyScreen, The Netherlands) and clamped down in a shaking incubator at 37°C and 350RPM for 24 hours. Subsequent

passages were made by using a 8-channel pipet to transfer 1μL of overnight culture into an identical sterile autoclaved 96-well deep square well plate with the same LB well arrangement and grown in the same conditions as before. Plasmid stability was then investigated at each passage by transferring 200μL from each culture into a shallow polystyrene 96-well plate (Corning ®, Sigma-Aldrich, UK) and detecting luminescence and OD_{410} in a POLARstar Galaxy microplate reader (BMG LABTECH, UK). ggplot2 package in R was used for plotting.

2.5.6 Luminescent Plasmid Stability Assays *in vivo*

These experiments involved using a tumour xenograft model where tumours were initiated by subcutaneous injection of 5x10 ^{6} cells of a human colorectal cancer cell line (LS174T) in 100μl of PBS per flank of 5 6-week-old female nude mice (NcrNu strain; Taconic) and grown for 1 to 2 weeks until they reached a size of 5 to 10mm. Along with a EcN_Lux strain as a control, individual EcN strains with p24_help-Lux, p24_help-Lux_AT, p24_help-Lux_HS and p24_help-Lux_MCC were grown in LB with kanamycin until exponential phase, washed three times in sterile PBS and then injected intravenously at a dosage of 1x10 ^{6} bacteria. After bacterial colonisation of the tumours, animals were monitored daily via IVIS (IVIS 200, Caliper Life Sciences) to detect the presence of the plasmid via bioluminescence. Briefly, this involved anaesthetising the mice with isoflurane and imaging with an open filter on the auto-exposure setting. After 7 days, each of the tumours were sterilely extracted and homogenised using a tissue dissociator (Miltenyi), an aliquot of which was seeded on each of LB plates and LB with kanamycin plates. The ratio was calculated by comparing the mean counts of plasmid bearing colonies on LB plates and LB plates with kanamycin from each tumour [91]. ggplot2 package in R was used for plotting. Statistical significance was demonstrated by the Mann-Whitney U test with R.

2.6 Results

In order to evaluate the ability of the Hok/*sok*, axe/txe and microcin V systems to stabilise a synthetic gene circuit in different environments, the respective gene fragments were independently cloned into the fluorescent OXB20_GFP plasmid and the luminescent p24_help-Lux plasmid to derive a number of constructs (Figure 2.8). The ability of the PSK systems to stabilise the fluorescent OXB20_GFP plasmids in liquid culture were first characterised in the EcN_Red strain and then in the EcN_Lux strain. The luminescent p24_help-Lux constructs were characterised in the EcN strain first in liquid culture and then in an *in vivo* tumour mouse model.

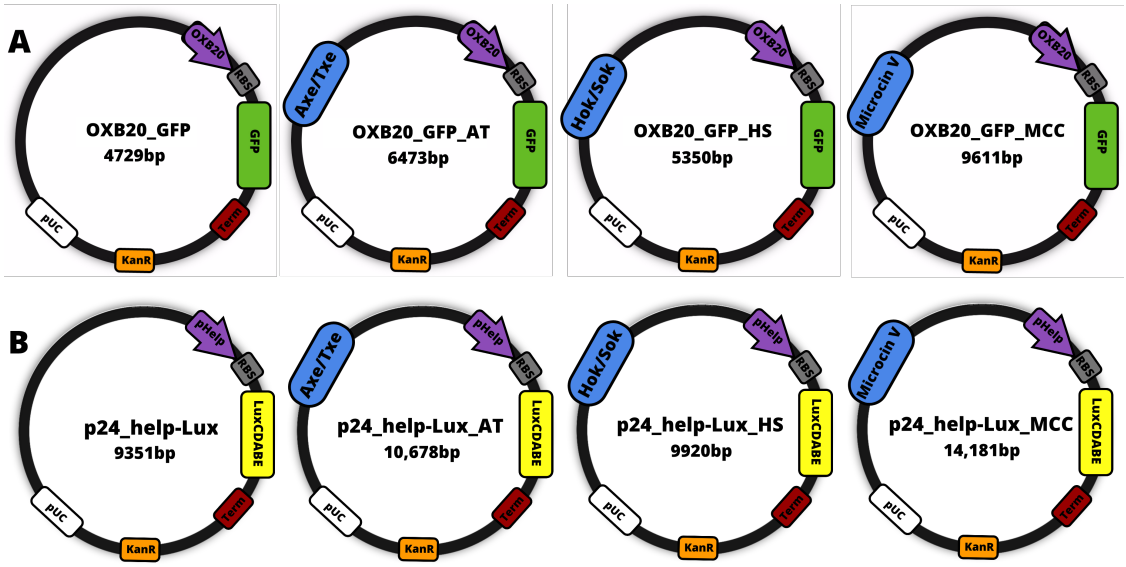

Figure 2.8: A) Control OXB20_GFP plasmid, OXB20_GFP_AT plasmid stabilised with the axe/txe system, OXB20_GFP_HS plasmid stabilised with the Hok/*sok* system and OXB20_GFP_MCC plasmid stabilised with the microcin V system. B) Control p24_help-Lux plasmid, p24_help-Lux_AT plasmid stabilised with the axe/txe system, p24_help-Lux_HS plasmid stabilised with the Hok/*sok* system and p24_help-Lux_MCC plasmid stabilised with the microcin V system.

2.6.1 Plasmid Stability Assays in EcN_Red with OXB20_GFP

The plasmid stability assays in EcN_Red were performed for 21 daily passages. Figure 2.9 shows that the EcN_Red_OXB20_GFP control plasmid started to drop from the population after 7 daily passages without any antibiotic selection. The population was completely plasmid free within 16 passages. The HS system showed a slight level of stabilisation where the plasmid drop was delayed until 10 days. However, the AT and MCC systems demonstrated complete plasmid stability until the end of the experiment (Figure 2.9). At the end of the stability assay it was apparent that the EcN_Red strain still harboured the delivery plasmid used in the transposon genome integration method. The competition resulting from the presence of this plasmid in the strain would have therefore impacted the level of plasmid loss observed in stability assays and it was concluded that the assays must be repeated with a strain of EcN where the correct genomic integration of markers were confirmed.

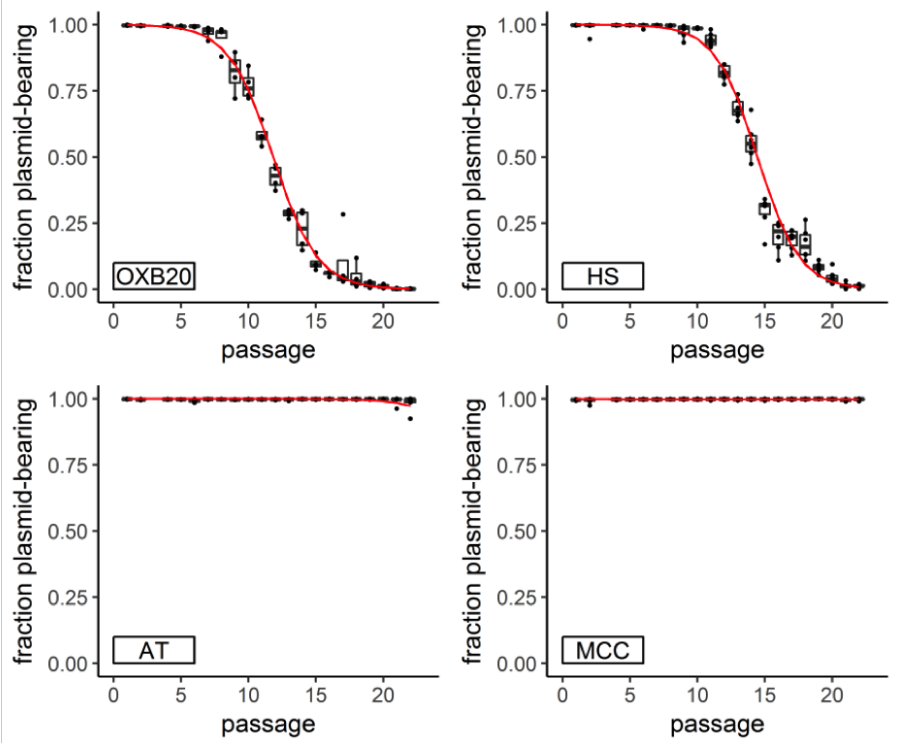

Figure 2.9: Plasmid loss curves of OXB20_GFP, OXB20_GFP_AT, OXB20_GFP_HS and OXB20_GFP_MCC in EcN_Red over 21 daily passages in the absence of antibiotic selection. Fraction of plasmid-bearing population was calculated from flow cytometry data at each daily time point. Plasmid loss curves were fitted to the data using a Bayesian model by Alexander Fedorec (Barnes Lab, UCL).

2.6.2 Plasmid Stability Assays in EcN_Lux with OXB20_GFP

In light of the problems observed with the EcN_Red strain, the stability assays were repeated in EcN with a genomically integrated erythromycin-resistant *luxCDABE* cassette (EcN_Lux) [91]. The plasmid stability assay was performed for 37 daily passages where in addition to GFP fluorescence readings, control measurements of optical density and luminescence were also taken (Appendix, Figures 5.1 and 5.2). Figures 2.10 and 2.11 show that the EcN_Lux_OXB20_GFP control plasmid started to drop from the population after 5 daily passages without any antibiotic selection. The population was completely plasmid free within 12 passages. The HS system was able to stabilise the constructs substantially, and except for one replicate, was completely plasmid free by day 20. The MCC system also stabilised the construct but showed a more inconclusive set of results. A gradual level of plasmid loss was observed from day 21 onwards but four out of nine replicates remained entirely plasmid-bearing up until day 37. The presence of the OXB20_GFP_MCC plasmid in these strains at the end of the 37 day experiment was confirmed by mini-preps (Appendix, Figure 5.4). In comparison to the other systems, AT was able to completely stabilise the GFP construct throughout the entire 37 day experiment (Figure 2.10). The presence of the OXB20_GFP_AT plasmid in the strain at the end of the 37 day experiment was confirmed in all replicates by mini-preps (Appendix, Figure 5.3). Data points missing at days 7,8 and 30-34 were due to equipment failure on the flow cytometer. Data points missing at day 17 were due to human error during culture passaging.

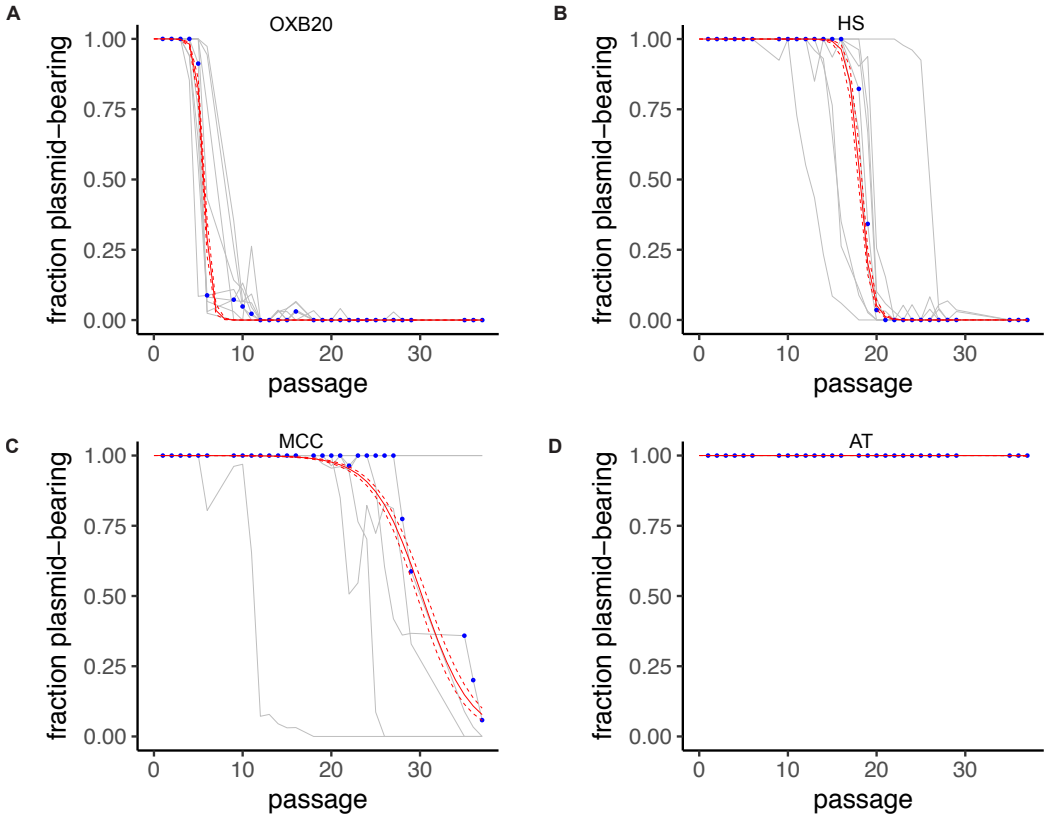

Figure 2.10: Plasmid loss curves of OXB20_GFP, OXB20_GFP_HS, OXB20_GFP_MCC and OXB20_GFP_AT in EcN_lux over 37 daily passages in the absence of antibiotic selection. Fraction of plasmid-bearing population was calculated from flow cytometry data at each daily time point. Plasmid loss curves (in red) were fitted to the data using a Bayesian model by Alexander Fedorec (Barnes Lab, UCL). Assays were carried out with erythromycin selection but not kanamycin. Blue dots represent experimental medians and grey lines indicate individual experimental replicates.

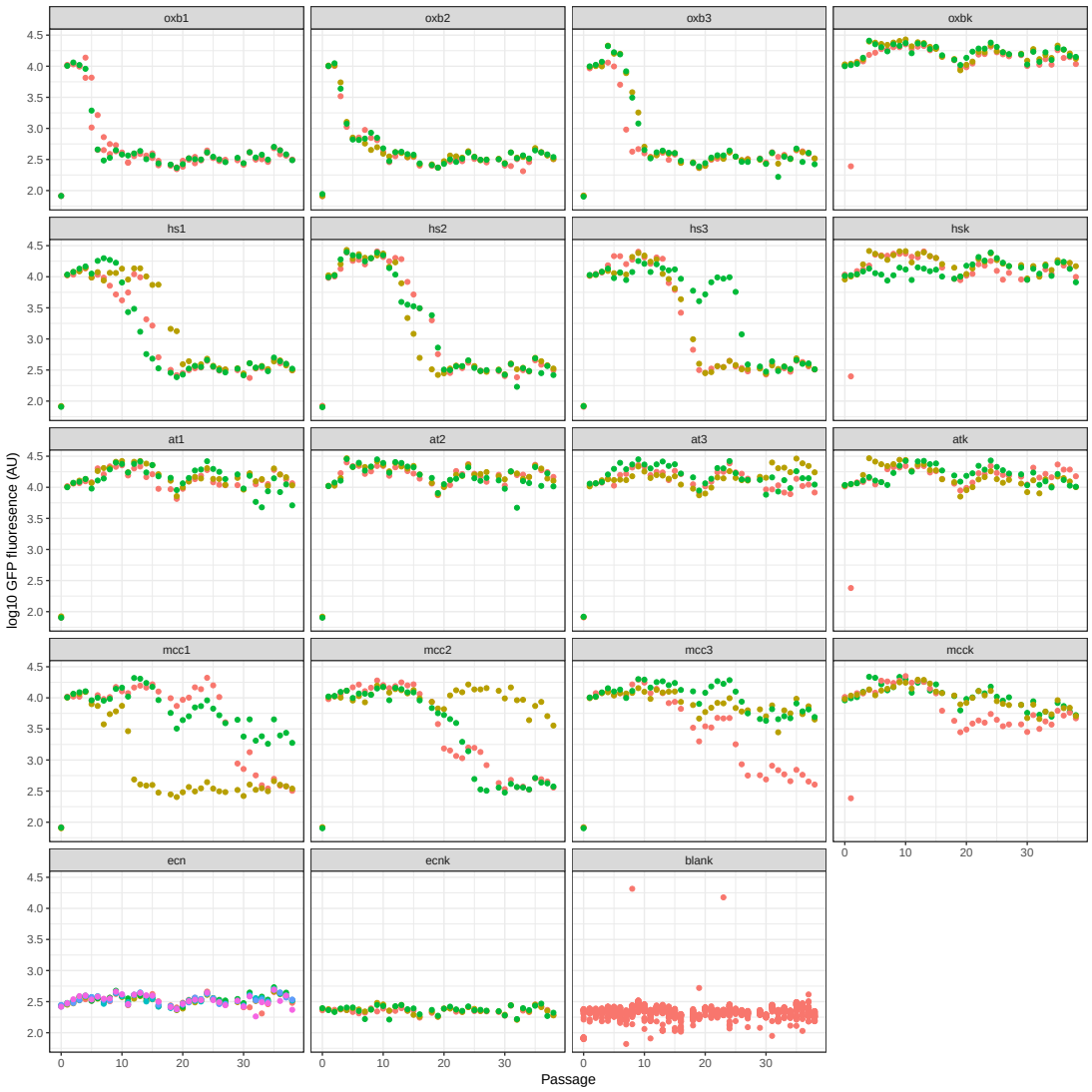

Figure 2.11: Plate-reader GFP fluorescence of OXB20_GFP, OXB20_GFP_AT, OXB20_GFP_HS and OXB20_GFP_MCC over 37 daily passages in the absence of antibiotic selection. OXBK, ATK, HSK and MCCK indicate control wells grown with both erythromycin and kanamycin that should be 100% plasmid-bearing. Ecn and ecnk indicate negative controls. Numbers indicate biological replicates and colours indicate technical replicates.

PSK Mechanisms Impact Growth

Figure 2.12 shows that in comparison to the EcN_Lux control strain, all constructs showed a significant impact on the growth rate of the chassis. In comparison to the control OXB20_GFP plasmid, all three PSK plasmids demonstrated an additional burden on the growth rates with higher lag times. This indicates that while the high copy plasmid and strong GFP expression is particularly burdensome on the host strain, the additional PSK cassette provides a further metabolic load.

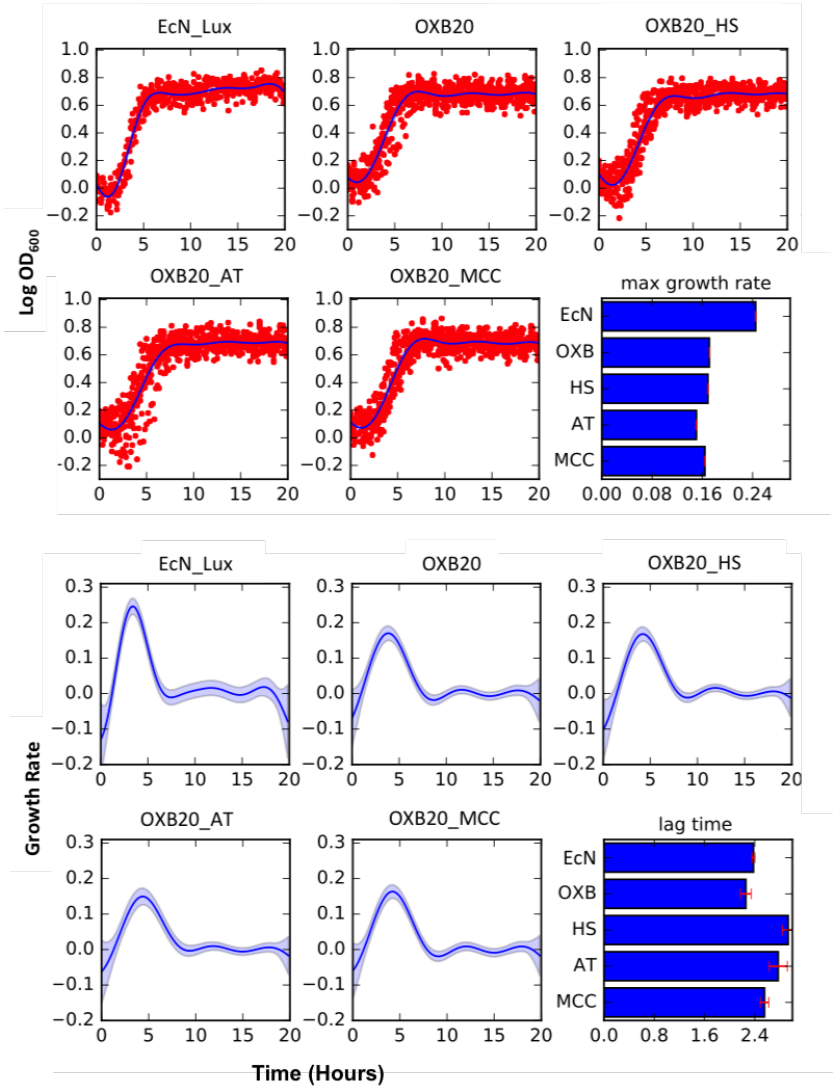

Figure 2.12: Growth curves for all EcN_Lux strains fitted using Gaussian processes. Top, estimated growth rates. Bottom, estimated lag times. N=3.

2.6.3 Plasmid Stability Assays in EcN with p24_help-Lux

After characterising the TA systems with a GFP fluorescent reporter, further work was carried out to investigate their plasmid stabilising capabilities with a *LuxCDABE* reporter construct (p24_help-Lux). This would provide a higher metabolic burden on the plasmid and create a reporter that could then subsequently be characterised *in vivo*. The plasmid stability assay was performed for 14 daily passages where daily luminescence and OD_{410} readings were taken. Figure 2.13 shows that the p24_help-Lux control plasmid was completely dropped from the EcN population after 3 passages without any antibiotic selection. Considering that even the positive kanamycin controls eventually started to drop, it can be inferred that the high metabolic burden of the reporter renders the plasmid unstable even with antibiotic selection. The HS system was able to stabilise the constructs substantially but was completely plasmid free by day 10. MCC also provided substantial stabilisation with two replicates still harbouring the plasmid after 14 days. In comparison to the other systems, AT was able to provide substantial stabilisation to the p24_help-Lux construct throughout the 14 day experiment with only two replicates dropping (Figure 2.13). These findings mainly corroborate with the differences found between the TA systems in the GFP constructs (Figure 2.10).

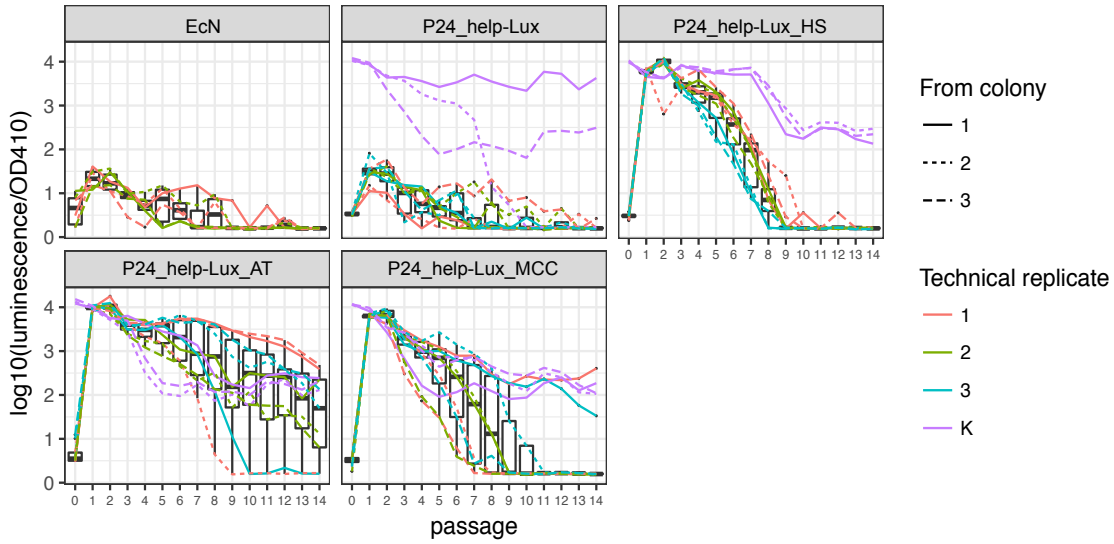

Figure 2.13: Plasmid stabilisation of p24_help-Lux with Axe/Txe, Hok/*sok* and MCC in EcN over 14 daily passages in the absence of antibiotic selection. Luminescence of p24_help-Lux was used to identify the plasmid bearing population from plate-reader data at each daily time point. K replicate is positive kanamycin control.

2.6.4 Stabilising Plasmids with PSK Systems in an *in vivo* Tumour Model

With the TA systems demonstrating stabilisation of a luminescent reporter in liquid culture without antibiotic selection (Figure 2.13), EcN strains containing either the p24_help-Lux_AT, p24_help-Lux_HS, p24_help-Lux_AT or p24_help-Lux control constructs were intravenously injected into a mouse tumour model for *in vivo* characterisation.

Once administered, the EcN strain was shown to colonise the tumours in the mouse flanks within 3 days (Figure 2.14). The tumours were then excised 7 days after injection and a colony count was performed from the homogenised tissue to independently measure the stabilising effect of the Axe/Txe, Hok/*sok* and MCC systems on the reporter construct. Figure 2.14 shows that without any stabilising system, over 52% of the population had dropped the p24_help-Lux plasmid after intravenous injection and tumour colonisation. In comparison, the p24_help-Lux_AT was significantly stabilised with nearly 92% of the population maintaining the plasmids after colonisation ($p < 0.0001$). In comparison to the p24_help-Lux control, p24_help-Lux_HS was also significantly stabilised with nearly 76% of the population maintaining the plasmids after colonisation ($p < 0.005$). There was no significant difference between the plasmid fraction bearing population in p24_help-Lux and p24_help-Lux_MCC. While the levels observed with Axe/Txe were higher, there was no significant difference between the plasmid fraction bearing population in p24_help-Lux_AT and p24_help-Lux_HS. In addition, variability was higher in the p24_help-Lux_HS constructs (Figure 2.14).

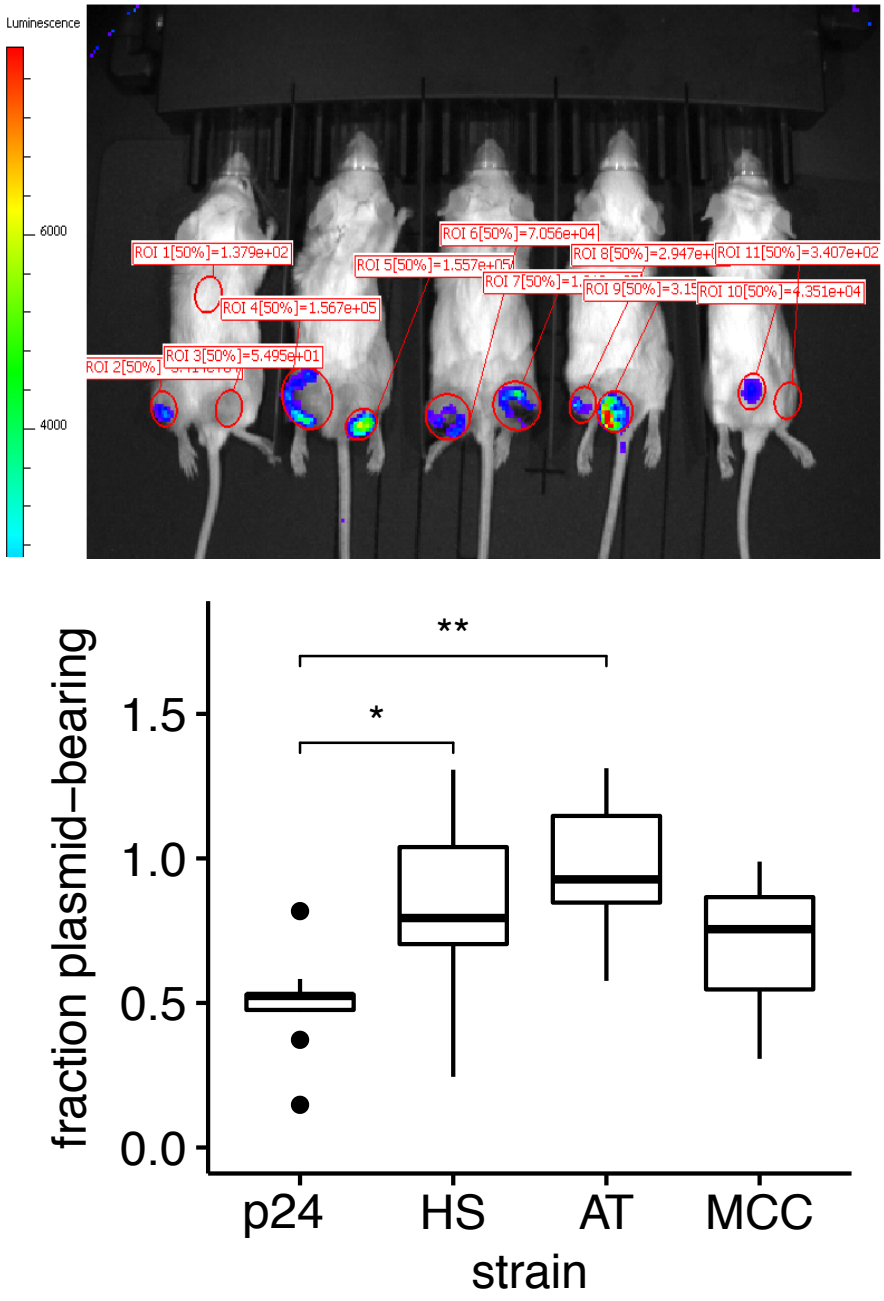

Figure 2.14: PSK systems can stabilise the p24_help-Lux plasmid in EcN *in vivo*. Top, representative IVIS images showing the luminescence of EcN_p24_help-Lux strains in tumours of anaesthetised mice 3 days after intravenous injection. Bottom, comparison of plasmid bearing population fraction after 7 days in excised tumours colonised with a strain containing just the control p24_help-Lux (n=9 tumours) reporter plasmid and strains containing stabilised p24_help-Lux_AT (n=8 tumours), p24_help-Lux_HS (n=7 tumours) and p24_help-Lux_MCC (n=5 tumours) plasmids. P values were calculated using the Mann-Whitney U test. Single asterisk indicates $p < 0.05$ and double asterisk indicates $p < 0.005$.

2.7 Discussion

The use of PSK mechanisms for maintaining synthetic circuits in commensal strains like EcN provide a valuable foundational tool for monitoring and engineering the intestinal microbiome. While a large repertoire of systems exist, there is insufficient data on their functionality and use in common laboratory strains or commensal vectors. Here we successfully evaluate and compare the ability of a variety of TA and bacteriocin PSK systems in stabilising synthetic reporter circuits in the absence of antibiotics in both liquid culture and the *in vivo* environment.

The addition of the Axe/Txe cassette to plasmids provided substantial stabilisation. The AT system provided complete plasmid stability in both the EcN_Red and EcN_Lux liquid culture experiments with the fluorescent OXB20_GFP plasmids (Figures 2.10 and 2.9). In addition, Axe/Txe was able to stabilise the luminescent p24_help-lux plasmid for 14 days in liquid culture (Figure 2.13) and provide almost complete plasmid retention during a 7 day *in vivo* tumour xenograft model (Figure 2.14). Interestingly, the Gram-positive *E. faecium* derived Axe/Txe system was found to be more effective in EcN than the more widely characterised and used Hok/*sok* system from *E. coli*. Furthermore, because Hok/*sok* is bactericidal and Axe/Txe is only bacteriostatic, it would be expected that the static plasmid-free persister cells created from the Txe toxin would begin to divide at a later passage and outcompete the plasmid-bearing population. The Axe/Txe system is also found on pS177, another *E. faecium* plasmid that also harbours the gene for vancomycin resistance [128]. A deeper understanding of the mechanisms behind the Axe/Txe system could further elucidate how clinically relevant multidrug-resistance strains of bacteria like *E. faecium* survive and propagate. This may also lead to further tools in the fight against multi-drug resistance microbes. These findings demonstrate that the Axe/Txe system is an additional and superior synthetic biology tool for maintaining plasmid stability than Hok/*sok*.

In line with published literature [91], the Hok/*sok* cassette provided a substantial level of stability to both fluorescent and luminescent reporters in EcN strains during liquid culture and *in vivo* experiments (Figures 2.9, 2.10 and 2.14). In the EcN_Lux strain, it was able to delay the plasmid drop of OXB20_GFP by a further 20 days in comparison to the control. The earlier drop observed at 10 days passage

with in EcN_Red could be due to the faulty presence of the pUC18T-mini-Tn7T-Gm-*DsRedExpress* delivery plasmid providing further plasmid competition during growth (Figure 2.9). While it was not as effective as the AT system in stabilising the p24_help-lux plasmid in liquid culture, it functioned similarly in the *in vivo* tumour experiments. It would enlightening to see how they compared in an experiment longer than 7 days.

The microcin V bacteriocin system was also successful in delaying the plasmid drop in OXB20_GFP in both EcN_Red and EcN_Lux experiments (Figure 2.9). However, while it demonstrated near enough complete plasmid retention in EcN_Red, it displayed much more variable results in the same experiment with the EcN_lux strain. The form of the loss curves in Figure 2.10 between replicates suggests that the bacteriocin killing system may be functioning variably. In addition, the bacteriocin cassette did not offer a significant stablisation effect *in vivo* in comparison to the p24_help-lux control (Figure 2.14). This raises interesting questions regarding the functionality of the circuit and what environmental conditions favour it. Perhaps the bacteriocin was washed away and concentrations were too low to provide effective cell killing *in vivo*.

2.8 Conclusions and Further Work

As set out in the aims, this piece of work demonstrated that is possible to use PSK systems such as Hok/*sok*, Axe/Txe and microcin V to stabilise synthetic gene networks in the probiotic EcN strain in the absence of antibiotic selection for up to 37 passages in liquid culture. In addition, it was demonstrated that the Axe/Txe and Hok/*sok* systems could substantially stabilise a luminescent reporter plasmid in an *in vivo* tumour xenograft model without antibiotic selection.

Whereas the stability provided by the Hok/*sok* system corroborates with previous literature, the results in this piece of work demonstrate that Axe/Txe was a superior plasmid stability system in EcN. The *E. faecium* derived Axe/Txe system was particularly effective in preventing a reporter plasmid dropping from the population. In order to further characterise these systems, experiments could be repeated in other commensal strains such as *Salmonella typhimurium* [129] or with different *in vivo* animal models. While a tumour xenograft model was used here, it would be enlightening to see how effective the PSK systems are in stabilising a genetic construct within a

healthy or diseased intestine.

Collectively, these systems can act as foundational components to expand the genetic repertoire of tools available for complex and robust investigations in both synthetic biology and *in vivo* microbiota experiments.

3. Design and Construction of Therapeutically Relevant Bacterial Sensors

3.1 Introduction

Billions of years of evolution has provided prokaryotes with a genome that allows them to survive in almost any habitat found on earth. This repertoire of genes enable bacteria to sense and metabolise a wide variety of compounds and molecules. Synthetic biologists utilise this expansive genome to develop novel synthetic circuits and expand the genetic toolbox. One approach is to utilise bacterial promoters or repressors that finely control the transcription of downstream genes. Building on this, a simple circuit can be designed that can sense and respond to an input (see Section 1.3.3). This linked output can be a fluorescent or luminescent reporter that can in turn be used to qualitatively or quantitively measure the presence of an input. Whereas a large library of well characterised inducible and constitutive promoters such as P_{araBAD} and P_{recA} already exist, researchers are utilising the latest bioinformatics techniques to identify and incorporate less well defined promoters from prokaryotes into genetic circuits for novel functions [130].

While initial attempts set out to detect environmental toxins such as mercury, cadmium and lead [131, 132], researchers are now looking at the creation of therapeutically relevant bacterial sensors. An example of this approach is reengineering an *E. coli* promoter to detect and respond to gut inflammation [133]. The P_{NorR} promoter is used by several strains of *E. coli* to control the expression of nitric oxide reductases that metabolise and detoxify nitric oxide. In a laboratory strain of *E. coli*, this promoter was used to activate a fluorescent switch in response to biological nitric oxide in an *in*

vitro inflammation model with inflamed mouse ileum explants. These approaches could be coupled to a commensal vector to measure inflammation *in vivo*.

Another therapeutic bacterial sensor circuit enabled *E. coli* to sense and destroy the pathogenic *Pseudomonas aeruginosa* [134, 135]. This approach involved placing the quorum molecule sensing P_{LuxR} promoter from *P. aeruginosa* upstream of the genes for an *E. coli* E7 lysis protein and an antimicrobial bacteriocin. Upon detection of quorum sensing molecules specific to *P. aeruginosa*, this strain undergoes lysis and releases the antimicrobial bacteriocin into the immediate vicinity and destroys surrounding *P. aeruginosa*.

3.2 Related Work

Reactive Nitrogen Species

Inflammatory bowel disease (IBD) consists of a group of conditions that are clinically characterised by chronic inflammation of the colon and small intestines. It is estimated to affect 2.5-3 million people in Europe alone and the most common variants are ulcerative colitis and Crohn's disease [136].

It is now thought that the chronic condition is caused by the host's immune system interacting pathologically to both genetic and environmental factors [88]. Differences have long been observed in the microbial community structure of IBD patients in comparison to healthy controls. Luminal concentrations of reactive nitrogen species (RNS) like nitrate, nitrite and nitric oxide are also known to be significantly increased in ulcerative colitis [137]. More recently, it was shown that nitrate generated as a byproduct of inflammation provided a significant growth advantage to certain strains of intestinal bacteria [138]. Due to the integral role of the intestinal microbiome in conditions such as this, efforts have already been made to both broaden our understanding and develop new tools for diagnosis and treatment. A recent example includes using an *E. coli* promoter to detect and respond to gut inflammation [133]. The P_{NorR} promoter is used by several strains of *E. coli* to control the expression of nitric oxide reductases that metabolise and detoxify nitric oxide. This promoter was used in a synthetic circuit, implemented within a laboratory strain of *E. coli*, to activate a fluorescent switch in response to biological nitric oxide in an *in vitro* inflammation model with inflamed

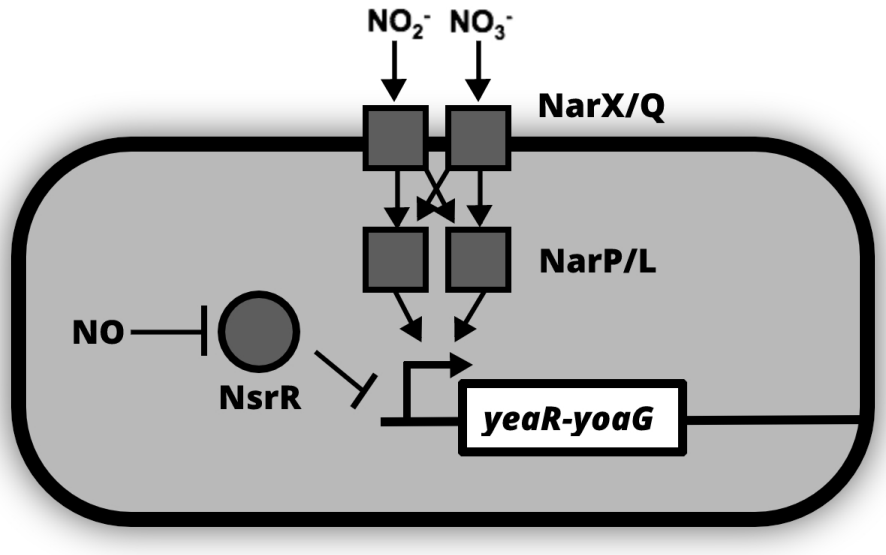

Figure 3.1: Regulation of the *E. coli yeaR-yoaG* operon by the NsrR repressor and the NarX-NarL and NarQ-NarP two-component systems. NsrR represses gene expression upon nitric oxide detection. NarX and NarQ is independently able to detect nitrate and nitrite, respectively. Upon detection, they phosphorylate NarL and NarP which interact with DNA to activate transcription of the operon.

mouse ileum explants.

As a facultative aerobe, *E. coli* K12 strains can use the *yeaR-yoaG* operon to switch to respiratory nitrate ammonification to generate energy during anaerobic growth [139]. This tightly regulated system is known to control gene expression through a combination of the NsrR repressor and the Nar two-component system which is composed of the NarX, NarQ, NarL and NarP proteins (Figure 3.1). While the nitric oxide-responsive NsrR protein represses the transcription of the *yeaR-yoaG* operon, the NarX-NarL and NarQ-NarP two-component system activates transcription upon independent nitrate and nitrite detection.

Through the use of this P_{yearR} promoter region, a team was recently able to create a whole-cell biosensor capable of detecting increasing concentrations of nitrate in clinical samples of serum and urine [90]. Furthermore, they incorporated integrase genes into the sensor circuit that enabled them to create an amplifying switch circuit capable of detecting lower thresholds of nitrate in urine and serum. These results show that by coupling bacterial promoters with more complex genetic components developed through synthetic biology, it is possible to increase the robustness of a circuit and in turn create clinically relevant bacterial biosensors.

Short Chain Fatty Acids

Short chain fatty acids (SCFAs) are microbial fermentation products from ingested carbohydrates. Recent findings have indicated that SCFAs such as butyrate, propionate and acetate have roles in several metabolic and inflammatory conditions such as obesity, diabetes and IBD [140]. It is thought that these SCFAs directly act on the surface exposed G protein-coupled receptors of the host cells in the lumen [42]. SCFA driven signalling interactions with these receptors have been found to mediate anti-inflammatory outcomes by promoting the differentiation of regulatory T cells and IL-10 producing T cells [141, 142]. It is hypothesised that these associations also mediate the protective effects of a high fibre diet on colorectal cancer [143]. The complex interactions of the host's diet and genetics with the intestinal microbiota means that there are many mechanisms yet to be understood.

Based on the ability of some bacterial strains to detect and use propionate as a sole carbon and energy source, a propionate inducible system (pPro) was identified and characterised from the *prpBCDE* operons of *E. coli* and *Salmonella enterica* [144]. It was shown that after intake into the cell, propionate is activated to propionyl-CoA by *prpE*-encoded propionyl-CoA synthetase. This is then catalysed to 2-methylcitrate (2-MC) by the *prpC*-encoded 2-MC synthase. *prpBD* then produces enzymes that convert 2-MC into pyruvate and succinate for energy production in the methylcitrate cycle [145]. Eventually, it was understood that it was 2-MC, and not propionate, that signals the presence of propionate in the environment as transcription is initiated by 2-MC-activated PrpR protein through the sigma-54 factor (Figure 3.2).

Alongside the *prpR* transcriptional activator gene, the P_{prpB} promoter region was used to create the pPro inducible expression system which was shown to be comparable to existing systems based on promoters such as P_{tac} and P_{trc}[145]. Upon induction with 50mM propionate, a maximum 1,500 fold induction of GFP expression was recorded in strains such as *E. coli* BL21, MG1655 and W3110. However, the pPro system was shown to be inactive in other strains such as *E. coli* DH5α and DH510B as they lack the chromosomal *prpBCDE* operon and are therefore unable to produce the enzymes needed for 2-MC production. In addition, it was noted that the supplementary presence of carbon sources like glucose or glycerol in LB media would lead to catabolic repression

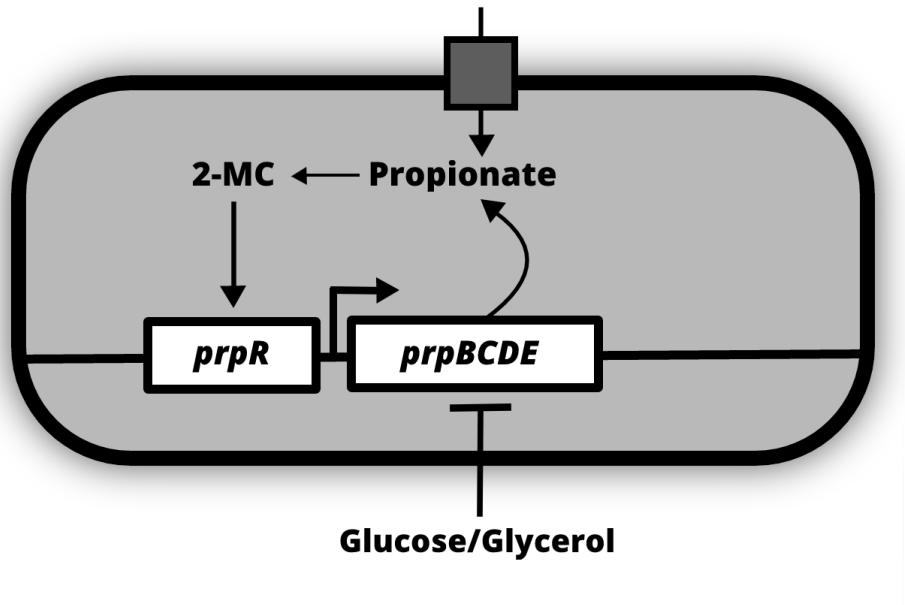

Figure 3.2: Regulation of the *E. coli prpBCDE* operon by propionate and the regulatory prpR protein. After intake into the cell, propionate is activated to propionyl-CoA by *prpE*-encoded propionyl-CoA synthetase and then catalysed to 2-methylcitrate (2-MC) by the *prpC*-encoded 2-MC synthase. *prpBD* then produces enzymes that convert 2-MC into pyruvate and succinate for energy production in the methylcitrate cycle. Transcription is initiated by 2-MC-activated PrpR protein through the sigma-54 factor.

of the system upon propionate induction. This is a vital microbial process where the bacteria adapt to inhibit the production of certain catabolic enzymes so that they can carry on using preferred carbon sources like glucose that allow the fastest growth rates. While the presence of glucose or glycerol inhibited pPro induction with propionate in LB media, it was found to have a minor impact in supplemented M9 media [146]. The pPro induction system can be further evaluated as a potential tool in elucidating the link between SCFA metabolism and intestinal dysbiosis.

pH

The intraluminal pH of the intestinal tract rapidly changes. The extremely acidic conditions in the stomach give way to a pH of 6 in the duodenum which increases further to pH 7.4 in the ileum. This then drops to pH 5.7 in the caecum before reaching pH 6.7 in the rectum [147]. More recently, the interlinked relationship between the microbiome and pH of the niches they occupy have been under investigation in regards to conditions such as acne [148] and bacterial vaginosis [149]. In order to provide some growth or survival advantage in acidic conditions, the P_{cadC} region of the *cadBA* operon in *E. coli* activates transcription under external acidic pH and in the presence of lysine [150] (Figure 3.3). Using β-galactosidase assays, it was shown that P_{cadC} could significantly increase expression when the pH was decreased from 7.6 to 5.4. A system like this could be used to design a biosensor circuit to only activate in predetermined locations or to detect dysbiotic pH at microbial niches within the intestines, skin and vagina.

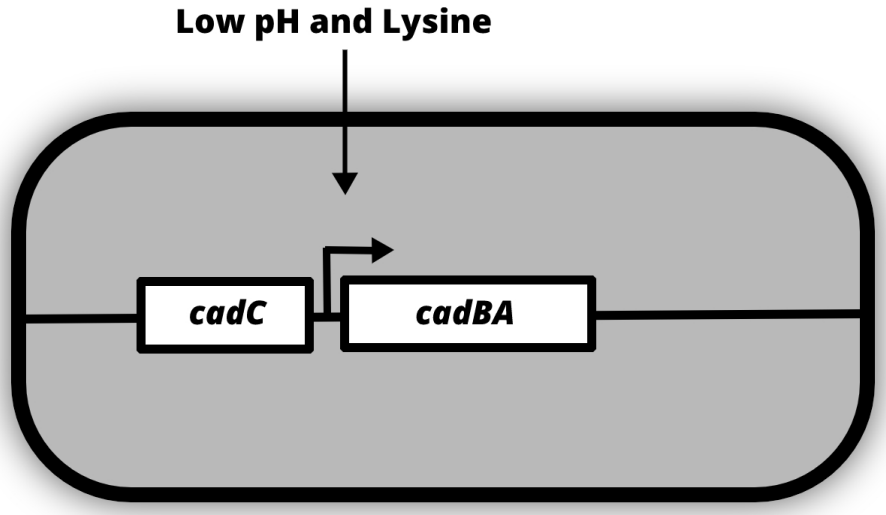

Figure 3.3: Regulation of the *E. coli cadBA* operon by external pH and the positive activator *cadC*. Under acidic conditions and in the presence of lysine, the cadC protein acts as a positive regulator to initiate transcription of the operon through the P_{cadC} promoter region. The operon encodes a lysine-cadaverine antiporter (*cadB*) and a lysine decarboxylase (*cadA*).

Bile Acids

Secondary bile acids are formed from colonic bacteria metabolising the primary bile acids that are synthesised by the liver. They are considered pro-inflammatory bacterial metabolites and are thought to contribute to colorectal carcinogenesis through reactive oxygen species (ROS) and RNS [41, 42, 43]. As well as higher levels of bile acids being found in the faeces of patients with colorectal cancer [151], *in vivo* animal studies have shown that the administration of bile acids results in a higher incidence of tumours in the intestines [152]. In addition to their pro-inflammatory effects, these compounds have also recently been associated with providing resistance to pathogenic *Clostridium difficile* infection [44]. In relation to this, *Bifidobacterium breve* was found to encode a bile-inducible membrane protein (BBr_0838) which provides the bacteria with tolerance against bile acids [153]. The putative promoter region of this membrane protein could be harnessed for bile acid detection.

3.3 Aims

Advancements in sequencing and bioinformatic techniques have resulted in the identification of a large number of confirmed or putative regulatory regions that could be used for *de novo* gene regulation.

By building on this extensive literature, this piece of work aimed to design, test and evaluate a range of therapeutically relevant sensors in the probiotic EcN strain. This included:

1. A sensor based on the *yeaR-yoaG* operon that can detect a range of RNS such as nitric oxide, nitrate and nitrite.

2. A sensor based on the *prpBCDE* operon that can detect the SCFA propionate.

3. A sensor based on the *cadBA* operon that can detect changes in external pH.

4. A sensor based on the putative promoter region of the *BBr_0838* gene that can detect bile acids.

3.4 Materials and Methods

3.4.1 Media and Strains

Lysogeny broth (LB) media and agar was used during propagation and cloning of bacteria. Assays were carried out in M9 minimal media supplemented with 1mM thiamine hydrochloride, 0.4% glycerol, 0.2% casamino acids, 2mM $MgSO_4$ and 0.1mM $CaCl_2$. When antibiotic selection was applied, kanamycin was used at 25μg/mL and ampicillin was used at 100μg/mL.

All DNA manipulations were performed in *E. coli* DH5α (NEB). All sequences were confirmed via Sanger sequencing (Source Bioscience, UK). The bacterial nitric oxide synthase producing $pNOS_{Ban}$ plasmid [154] (Professor Evgeny Nudler from the New York University School of Medicine, USA) was transformed into and expressed in *E. coli* BL21 (DE3) (NEB). This strain was referred to as EcB_$pNOS_{Ban}$. *Bacillus subtilis* 168 was purchased from the Bacillus Genetic Stock Center (Ohio, USA).

All final induction assays were performed in *E. coli* Nissle 1917 (EcN) (Prof. Ian Henderson from the University of Birmingham, UK). Chemically competent EcN was made using standard protocols. Briefly, this involved diluting an overnight EcN LB culture 1:100 into 50ml of fresh LB media and grown at 37°C in a shaking incubator to an OD_{600} of 0.25 to 0.3. The culture was then chilled on ice for 15 minutes and then centrifuged for 10 minutes at 5000g and 4°C. The medium was then discarded and the cell pellet resuspended in 30ml of cold 0.1M $CaCl_2$ before being kept on ice for a further 30 minutes. This suspension was then centrifuged for 10 minutes at 5000g and 4°C. The supernatant was once again removed and the cell pellet was resuspended in 3ml of cold 0.1M $CaCl_2$ solution with 15% glycerol. The final cell suspension was then aliquoted and flash frozen before being stored at -80°C.

3.4.2 Plasmids and Cloning Methods

Sensor assay plasmids were constructed from the promoterless OG241_GFP plasmid (Figure 3.4) which consisted of an upstream multiple cloning site, a dasher GFP reporter gene, a pUC high copy origin-of-replication and a kanamycin resistance cassette (Oxford Genetics, UK). Standard restriction enzyme and PCR cloning was used throughout. As a positive control, the strong constitutive OXB19 promoter (Oxford

Genetics, UK) was placed upstream of GFP to derive OXB19_GFP. The prpR-P_{prpB} region was cloned out by PCR from the pPro24-gfp plasmid [144] and ligated into the MCS of OG241_GFP to derive pProE_GFP. The 100bp promoter region of the *E. coli yeaR/yoaG* operon [155] was cloned out of the genomic DNA of *E. coli* DH5α by PCR and ligated into the MCS of OG241_GFP to derive pYeaR_GFP. The 284bp promoter region of the *BBr_0838* gene from *Bifidobacterium breve* UCC2003 [153] was synthesised as a gBlock Gene Fragment® (IDT DNA, USA) and ligated into the MCS of OG241_GFP to derive pBBr_GFP. The 672bp region of the *cadBA* operon identified as $P_{Cad}600$ [150] was cloned out of the genomic DNA of *E. coli* DH5α by PCR and ligated into the MCS of OG241_GFP to derive pCadC_GFP. SnapGene was used to simulate and plan ligation steps. EcN was transformed individually with these plasmids via heat-shock methods to give the strains listed in Figure 3.5.

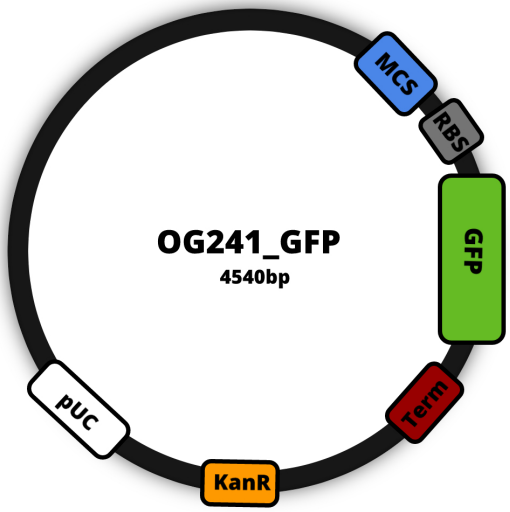

Figure 3.4: Graphical representation of promoterless OG241_GFP plasmid.

Strain Name	Host Bacterium	Plasmid	Plasmid Source
EcN_OG241_GFP	*E.coli* Nissle 1917	OG241_GFP_pUC_Kan^R (promoterless control)	Oxford Genetics, UK
EcN_OXB19_GFP	*E.coli* Nissle 1917	OXB19_GFP_pUC_Kan^R (constitutive control)	This work
EcN_pProE_GFP	*E.coli* Nissle 1917	pProE_GFP_pUC_Kan^R	This work
EcN_pYeaR_GFP	*E.coli* Nissle 1917	pYeaR_GFP_pUC_Kan^R	This work
EcN_pBBr_GFP	*E.coli* Nissle 1917	pBBr_GFP_pUC_Kan^R	This work
EcN_pCadC_GFP	*E.coli* Nissle 1917	pCadC_GFP_pUC_Kan^R	This work
EcB_$pNOS_{BAN}$	*E.coli* BL21 (DE3)	$pNOS_{BAN}$_Amp^R	Gusarov et al. [2008]

Figure 3.5: Table of strains used throughout.

3.4.3 Induction Assays

All induction assays were performed over 16 hours at 37°C and 350RPM at a volume of 750μL in sterile autoclaved 96-well deep square well (2.2mL) polypropylene plates (BRAND®, Sigma-Aldrich, UK) sealed with Breathe-Easy sealing membranes (Sigma-Aldrich, UK). Induction was calculated through flow cytometry analysis. Sodium nitrate, sodium nitrite and sodium nitroprusside (SNP) was used to induce the pYeaR_GFP construct with nitrate, nitrite and nitric oxide, respectively [139, 133]. Sodium propionate was used for investigating the pPro_GFP construct [144]. The pBBr _GFP construct was induced with deoxycholic acid [153].

Concentration Range Induction Assays

Concentration range induction assays were performed by diluting triplicate overnight cultures 1:500 into supplemented M9 media with the appropriate inducer concentration. For induction assays in growing phase, overnight cultures were grown in triplicates and diluted 1:500 into supplemented M9 media with the appropriate inducer. For induction assays in stationary phase, overnight cultures were grown in triplicates and spun down at 4000g before removing the supernatant and resuspending in fresh supplemented M9 media with the appropriate inducer.

$\mathbf{pNOS_{Ban}}$ and *Bacillus subtilis* Induction Assays

The pYeaR_GFP-$pNOS_{Ban}$ liquid induction assay was performed by first removing the supernatant of an overnight culture of EcB_$pNOS_{Ban}$ induced at 2% arabinose and 2mM arginine but without any ampicillin. The assay was then performed in the same manner of a concentration range induction but with varying proportions of $pNOS_{Ban}$ supernatant. The pYeaR_GFP-$pNOS_{Ban}$ agar induction assay was performed by first pipetting 80μL of uninduced EcN_pYeaR_GFP onto an antibiotic free LB agar plate with 2% arabinose and 2mM arginine. The culture was spread evenly and left to dry under a flame. The plate was then seeded at the outlined centre with 20μL of induced overnight $pNOS_{Ban}$ culture and again left to dry under a flame before being left overnight at 37°C. Inoculation loops were then used to collect EcN_pYeaR_GFP samples at set distances from the outlined centre of the plate containing the induced

$pNOS_{Ban}$ strains. Induction was calculated by placing the inoculation loops into PBS solution and analysing through flow cytometry. The control experiments consisted of the same approach but with a plain LB agar plate and uninduced $pNOS_{Ban}$ culture. The EcN_pYear-*B.subtilis* induction assay was performed by first removing the supernatant of an overnight culture of *B.subtilis* without any antibiotic. The assay was then performed in the same manner of a concentration range induction but with varying proportions of *B.subtilis* supernatant.

pH Sensor Assays

The pH sensor assay consisted of growing EcN_pCadC_GFP in media buffered to a pH of either 5, 6, 7 or 8. This was done by first preparing sterile buffers with enough physiological buffering capacity to maintain the pH of the media constant throughout the culture growth. A bench top pH meter (HI-2211, HANNA Instruments) and either 1M HCl or 1M NaOH was used to create acetic acid (0.5M) buffered to pH 5, MES (0.5M) buffered to pH 6, HEPES (0.5M) buffered to pH7 and HEPES (0.5M) buffered to pH 8. The buffers were then sterilised through a 22μm filter and added individually to 1:500 diluted overnight culture of EcN_pCadC_GFP with kanamycin to create a final culture at the desired pH (confirmed using the pH meter). All assays were performed as before in a sealed 96-well deep square well plate over 16 hours at 37°C and 350RPM. The buffering capacity of the buffers and the pH of the overnight cultures were checked using individual pH indicator strips (Whatman, Sigma-Aldrich, UK) (Figure 3.6).

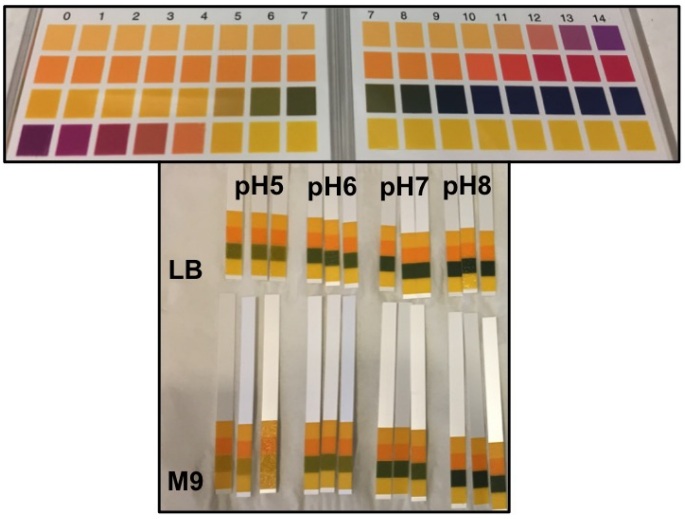

Figure 3.6: Top: colour key indicating pH. Bottom: indicator strips showing the pH of overnight EcN_pCadC_GFP culture buffered to pH 5, 6, 7, or 8 either in M9 or LB.

3.4.4 Flow Cytometry Analysis and Plotting

Flow cytometry was performed on an Attune NxT Acoustic Focusing Cytometer with Attune NxT Autosampler (Thermo Fisher Scientific, UK). 1μL of the appropriate strain culture was transferred into 200μL of PBS in a shallow polystyrene 96-well plate. The Attune NxT Autosampler was used to record 10,000 events for each sample with 4 washes between each one. GFP was excited using the blue laser (488nm) and was detected using a 530/30nm bandpass filter. In order to prevent operator bias associated with manual drawing of gates and speed up the analysis of samples, a computational pipeline called autoGate was developed by Alexander Fedorec in the Barnes Lab (github.com/ucl-cssb/autoGate) to automate the gating of singlet bacteria while excluding background debris and bacterial doublets. Briefly, the method fits mixture models of one, two and three clusters to the forward-scatter versus side-scatter data. Using integrated completed likelihood (ICL) [126], the number of clusters that best fits the data is calculated and the cluster centred closest to the expected bacterial population coordinate is taken. A linear model is then fitted to the side-scatter-height versus side-scatter-area data and points falling too far away are removed as doublets. The levels of trimming are shown in Figure 3.7.

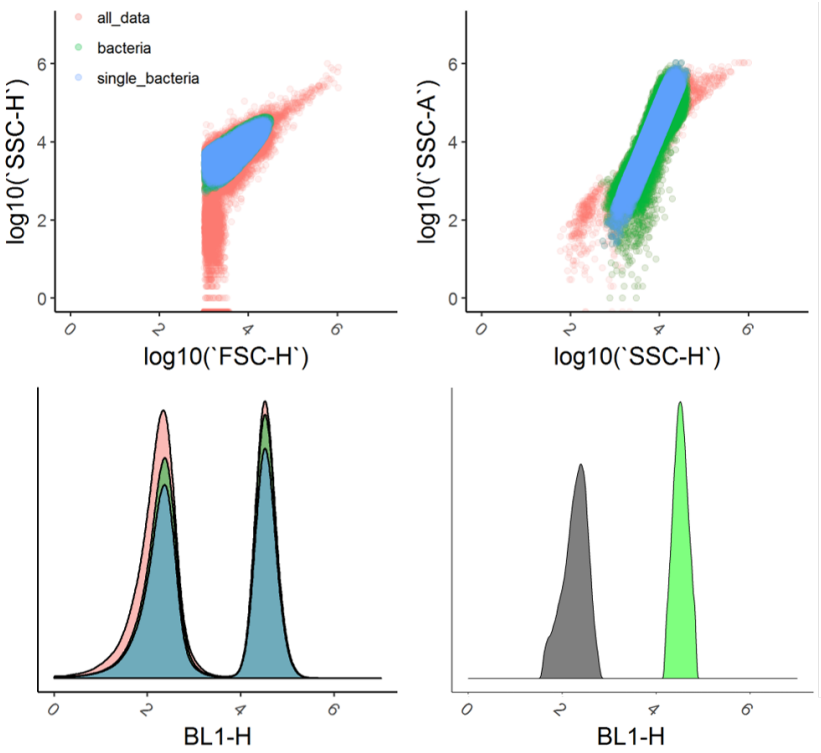

Figure 3.7: autoGate clustering and trimming of flow cytometry data.

All plots were made using the flowCore and ggplot2 R packages. Non-linear least squares (nls function in R) curve fitting was used to fit a line to induction plots. This model approximates the non-linear function using a linear one and iteratively refines the parameter values to the best fit. Locally weighted least square regression smoothing (loess function in R) was used to fit lines on EcN growth curve plots. This uses a local regression model fit to the points to create a smooth line. Relative fluorescent units (RFU) were shown as mean averages along with the standard error of the mean. R was also used for all statistics.

3.4.5 Growth Rate Assays

Overnight cultures were grown in triplicates and diluted 1:100 into supplemented M9 media with the appropriate inducer. A sterile autoclaved 96-well deep square well (2.2mL) polypropylene plate (BRAND®, Sigma-Aldrich, UK) was then filled with 16 replicates of 750μL of each culture. The plate was then sealed with a Breathe-Easy sealing membrane (Sigma-Aldrich, UK) and grown at 37°C and 350RPM for 16 hours. While maintaining the membrane seal for the rest of the plate, 750μL from each strain-culture was taken hourly and the OD_{600} was recorded on a tabletop WPA CO8000 Cell Density Meter (Biochrom).

3.5 Results

Biosensor circuits were designed and built using the promoterless OG241_GFP plasmid to enable evaluation through fluorescent reporting (Figure 3.8). The propionate inducible pPro system (containing the *prpR* transcriptional activator gene and the P_{prpB} promoter region from *E. coli*) was cloned into OG241_GFP to derive pProE_GFP [144]. Likewise, the promoter region of the *yeaR-yoaG* operon was used to derive the nitrate, nitrite and nitric oxide inducible pYeaR_GFP [139]. The promoter region of the *Bbr-0838* gene was cloned in the attempt to derive the bile acid inducible pBBR_GFP [153]. Lastly, the P_{cadC} region of the *cadBA* operon was used to derive the pH sensitive pCadc_GFP [150]. All sensors were characterised in the probiotic EcN strain unless otherwise stated.

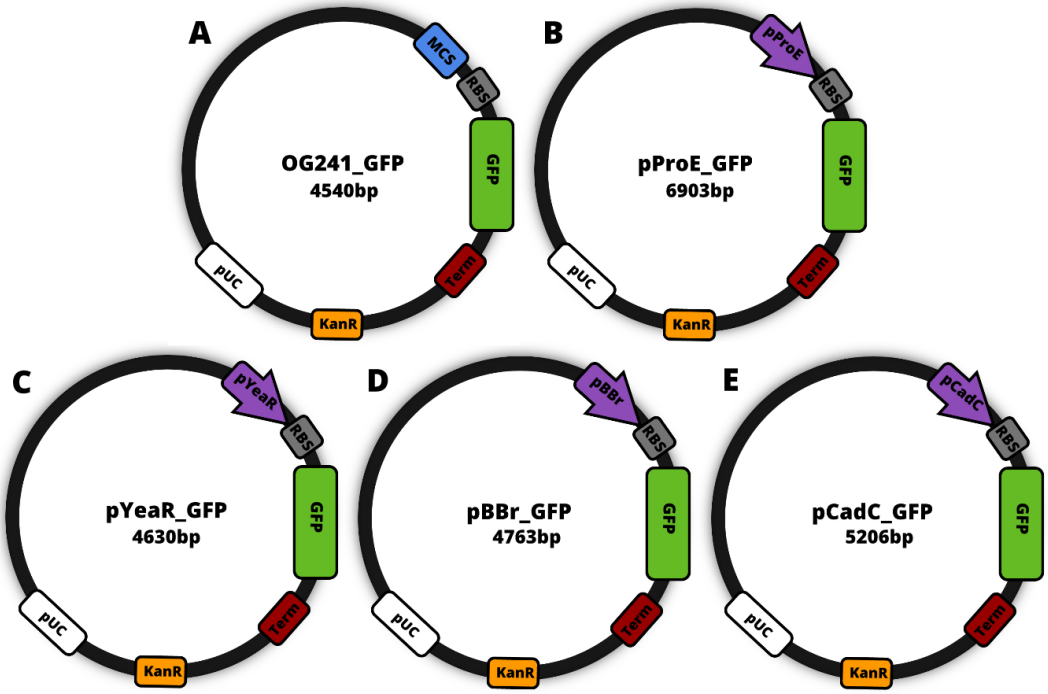

Figure 3.8: Plasmid maps of GFP based reporter sensors. A) Promoterless OG241_daGFP plasmid. B) pProE_GFP propionate sensor. C) pYeaR_GFP nitrate, nitrite and nitric oxide sensor. D) pBBR_GFP bile acid sensor. E) pCadC_GFP pH sensor.

3.5.1 EcN_pProE_GFP - Propionate Inducible Sensor

Figures 3.9 and 3.10 show that the EcN_pProE_GFP sensor demonstrated robust induction over a wide range of propionate concentrations in both supplemented M9 and LB media. In comparison to the maximum fold increase of 19.7 (from 478±84 RFU to 9403±747 RFU) in LB media, the maximum fold increase in supplemented M9 media was 31.4 (from 204±3 RFU to 6510±568 RFU) at 200mM of inducer.

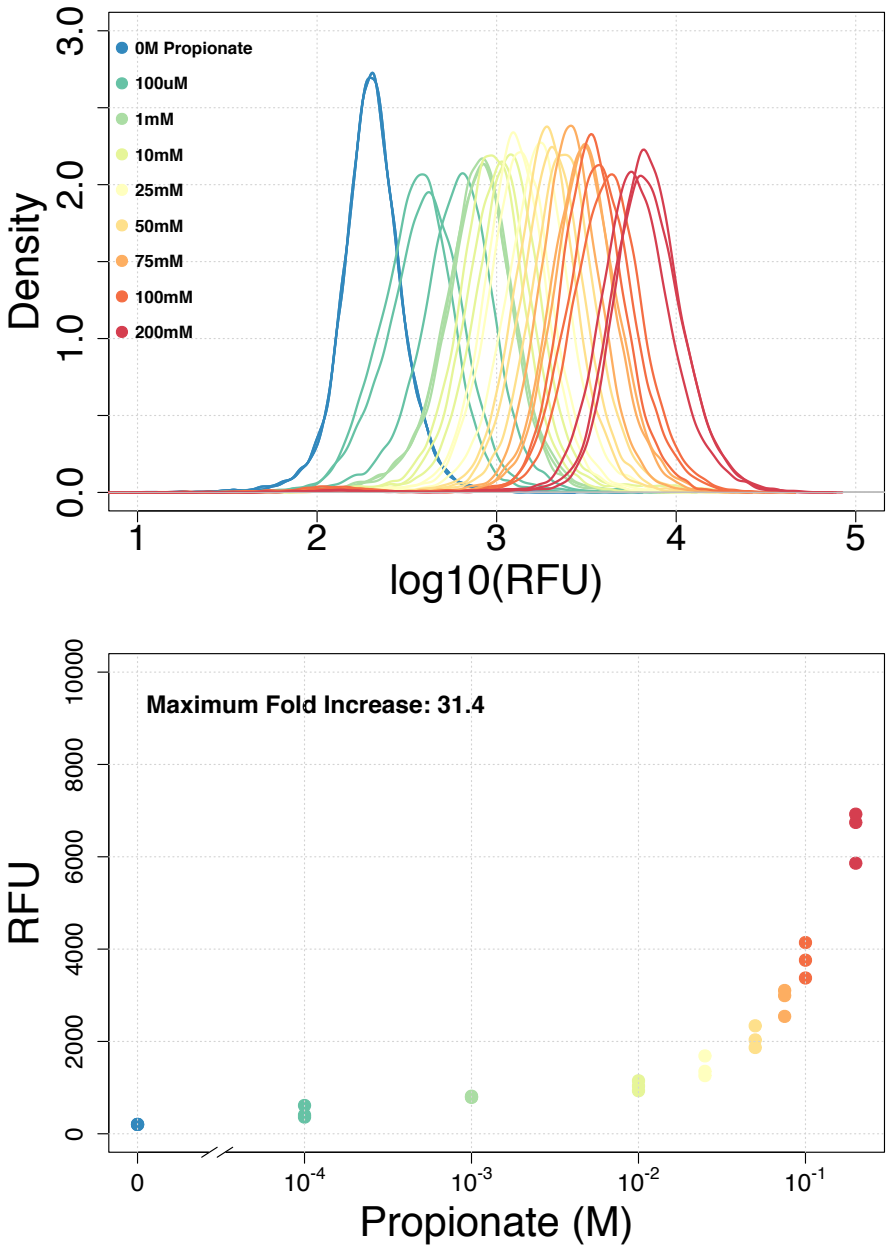

Figure 3.9: EcN_pProE_GFP induction with propionate in supplemented M9 media. Top: histogram density plot of GFP fluorescence after 16 hours induction. Bottom: median GFP fluorescence after 16 hours induction. Flow cytometry data with 10,000 events (n=3).

While a higher level of expression was observed in LB at the maximum induction of 200mM propionate, the difference in fold increase was due to a significantly lower average basal expression in supplemented M9 media (204±3 RFU) than in LB (478±84 RFU). The small population of uninduced cells at 100mM and 200mM could be persister cells that have dropped the plasmid (Figure 3.10).

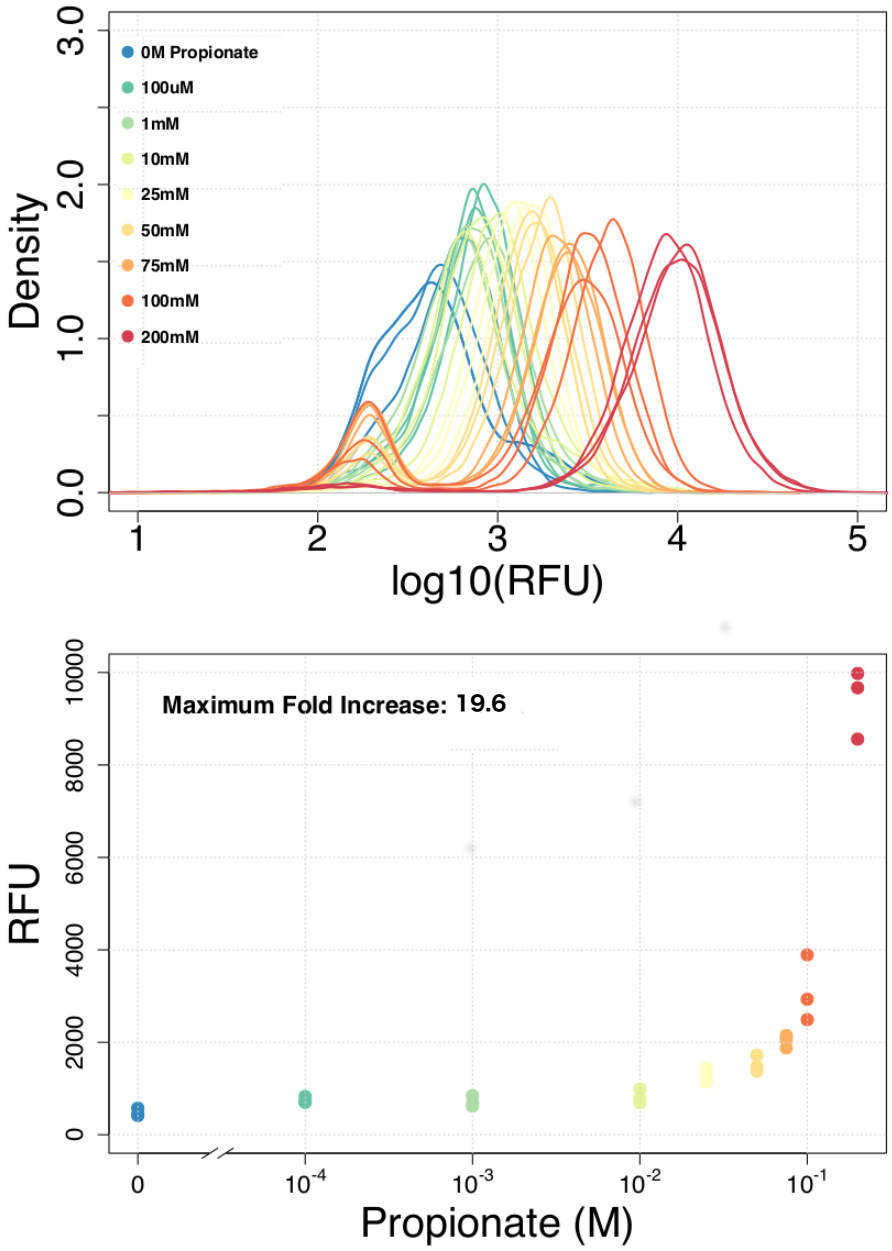

Figure 3.10: EcN_pProE_GFP induction with propionate in LB media. Top: histogram density plot of GFP fluorescence after 16 hours induction. Bottom: median GFP fluorescence after 16 hours induction. Flow cytometry data with 10,000 events (n=3).

Figure 3.11 shows that the concentration of propionate only started having a demonstrable impact on the overnight growth of EcN_pProE_GFP in supplemented M9 media above 10mM. In order to investigate the toxicity of higher concentrations of propionate at which significant levels of induction were observed, a time-course growth assay was conducted with no inducer, 50mM or 100mM propionate (Figure 3.12).

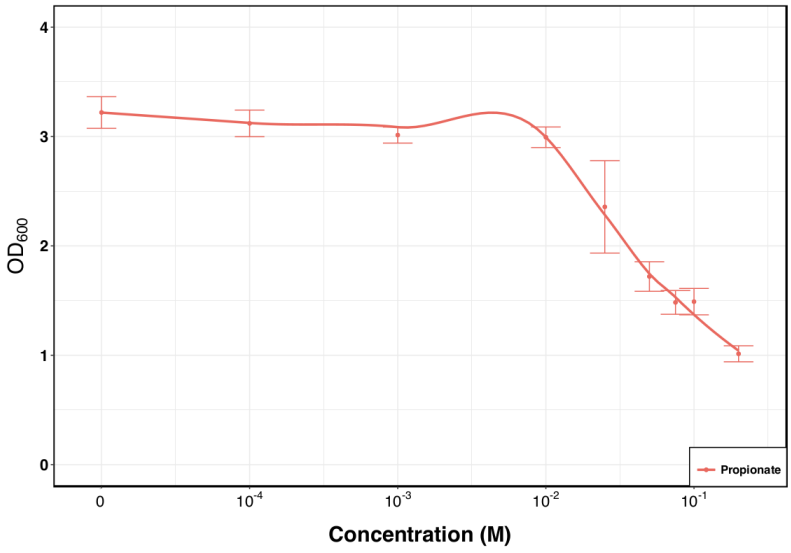

Figure 3.11: EcN_pProE_GFP growth in increasing concentration of propionate in supplemented M9 media after 16 hours (n=3).

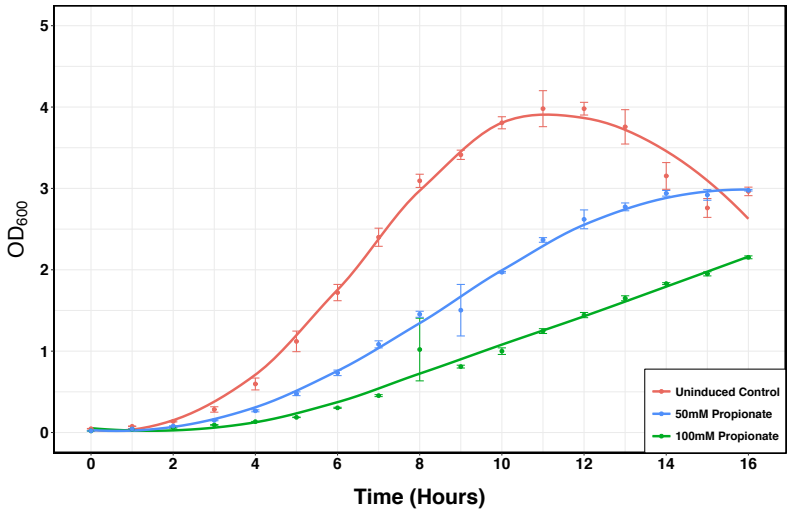

Figure 3.12: EcN_pProE_GFP growth over time with 0M, 50mM or 100mM propionate in supplemented M9 media (n=3).

In order to investigate the dynamic response of EcN_pProE_GFP, a time-course induction with propionate was carried out in supplemented M9 media. The uninduced control showed some basal expression over time before eventually plateauing (Appendix, Figure 5.5). Figures 3.13 and 3.14 show that at both 50mM and 100mM propionate, a rapid response was observed with a large proportion of the population becoming induced within 1 or 2 hours.

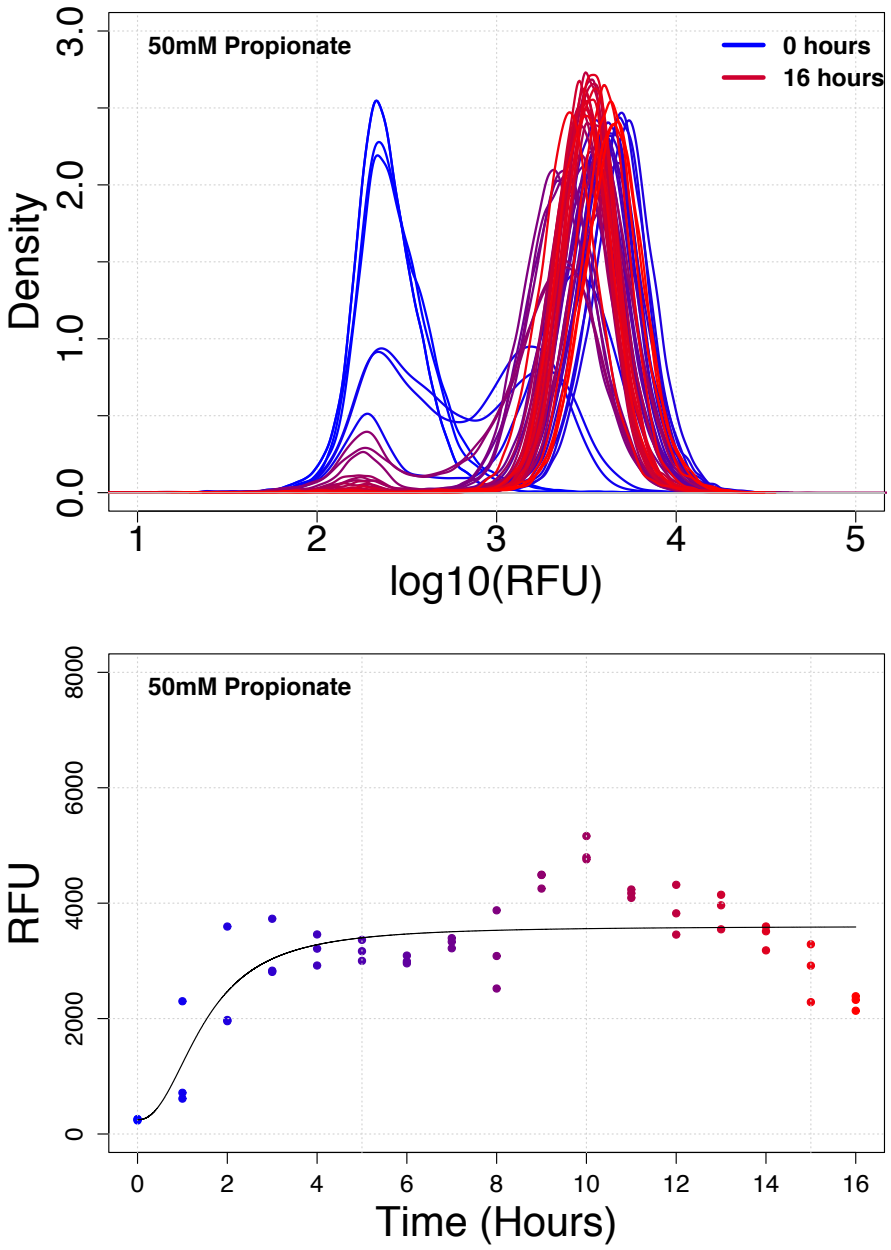

Figure 3.13: Time course EcN_pProE_GFP induction in supplemented M9 media with 50mM propionate over 16 hours. Top: histogram density plot of GFP fluorescence over 16 hours. Bottom: median GFP fluorescence over 16 hours induction. Flow cytometry data with 10,000 events (n=3).

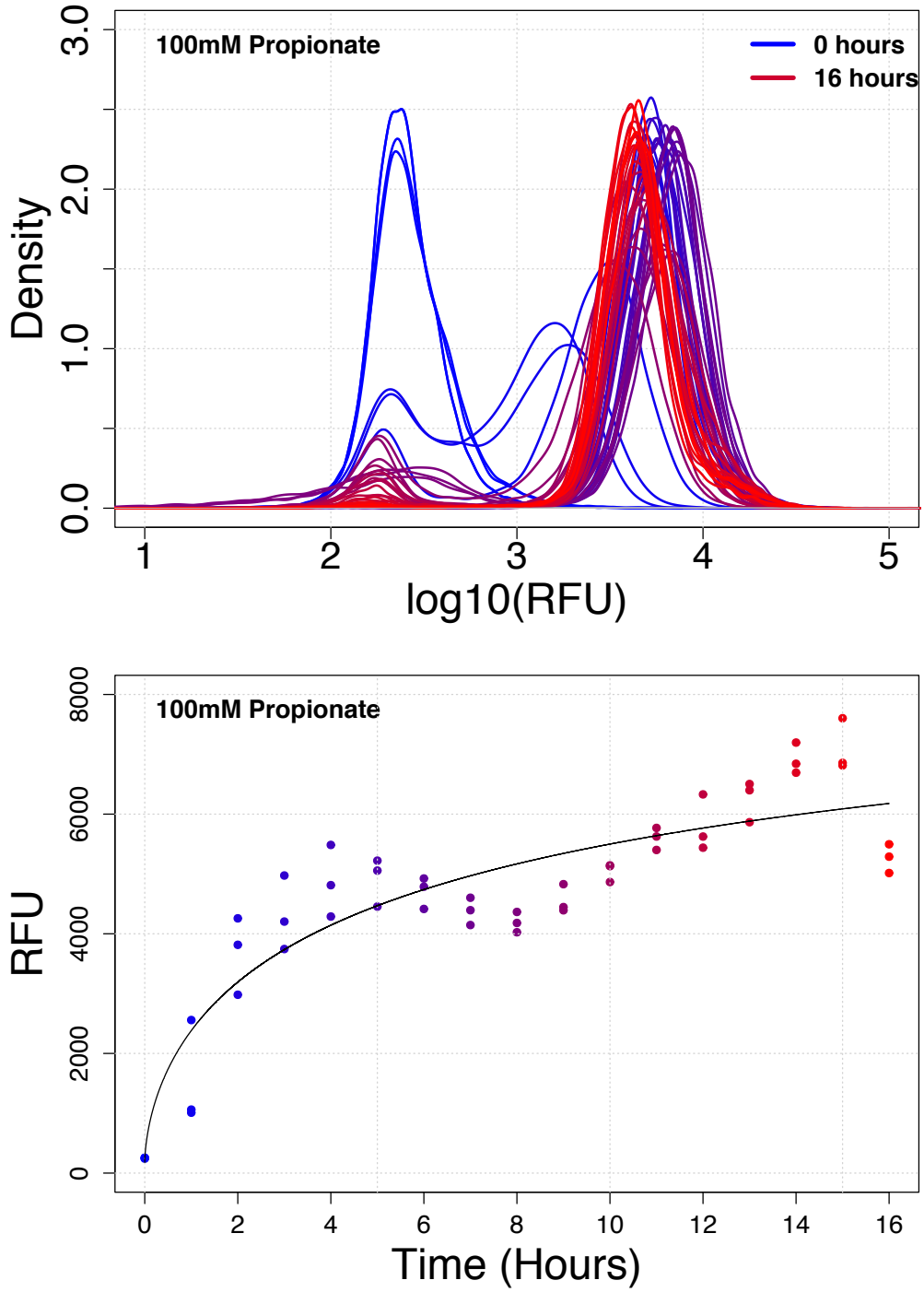

Figure 3.14: Time course EcN_pProE_GFP induction in supplemented M9 media with 100mM propionate over 16 hours. Top: histogram density plot of GFP fluorescence after 16 hours. Bottom: median GFP fluorescence over 16 hours induction. Flow cytometry data with 10,000 events (n=3).

3.5.2 EcN_pYeaR_GFP - Nitrate, Nitrite and Nitric Oxide Inducible Sensor

Figures 3.15, 3.16 and 3.17 show that the EcN_pYeaR_GFP sensor demonstrated robust induction with nitrate, nitrite and nitric oxide in supplemented M9 media. A maximum fold increase of 19.8 (from 459±32 RFU to 9106±552 RFU) was observed in 100mM nitrate, 11.1 (from 439±18 RFU to 5139±998 RFU) in 25mM nitrite and 14.1 (from 458±32 RFU to 6782±385 RFU) in 1mM SNP (nitric oxide donor).

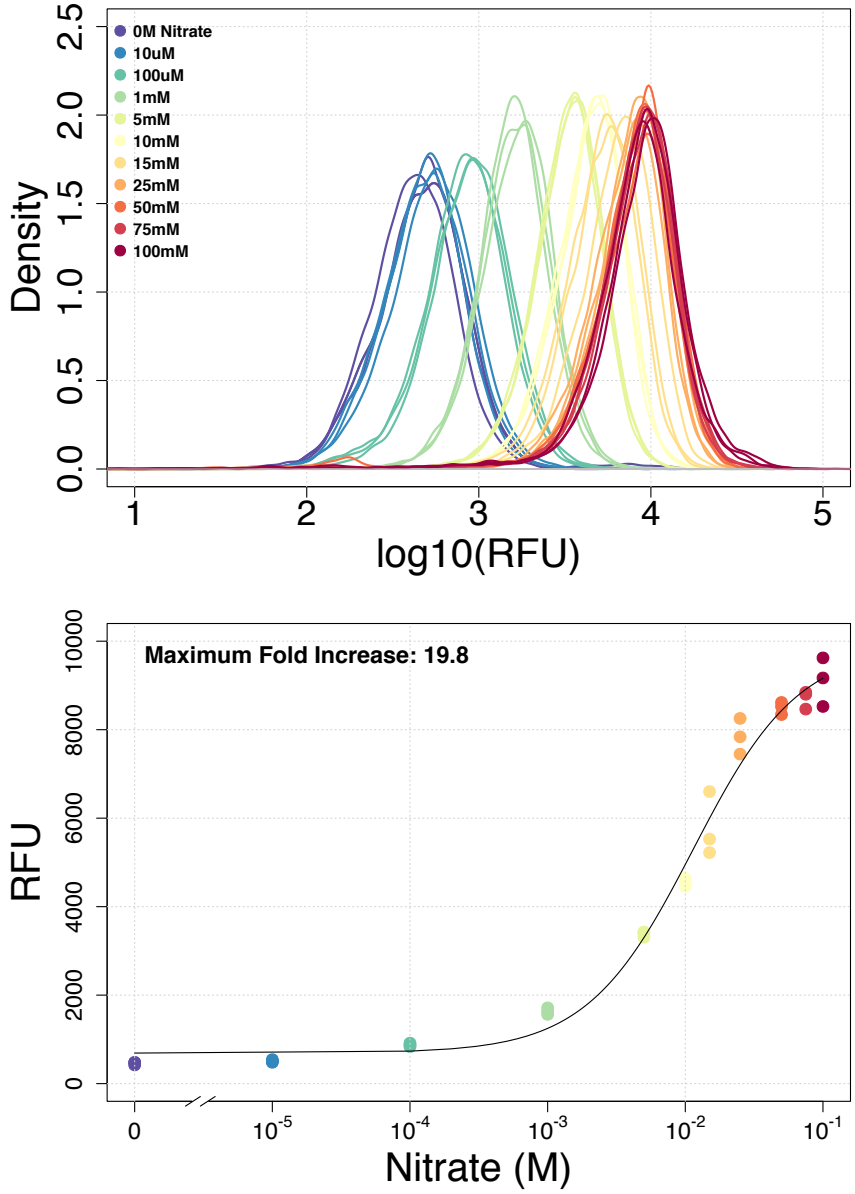

Figure 3.15: EcN_pYeaR_GFP induction with nitrate in supplemented M9 media. Top: histogram density plot of GFP fluorescence after 16 hours induction. Bottom: median GFP fluorescence after 16 hours induction. Flow cytometry data with 10,000 events (n=3).

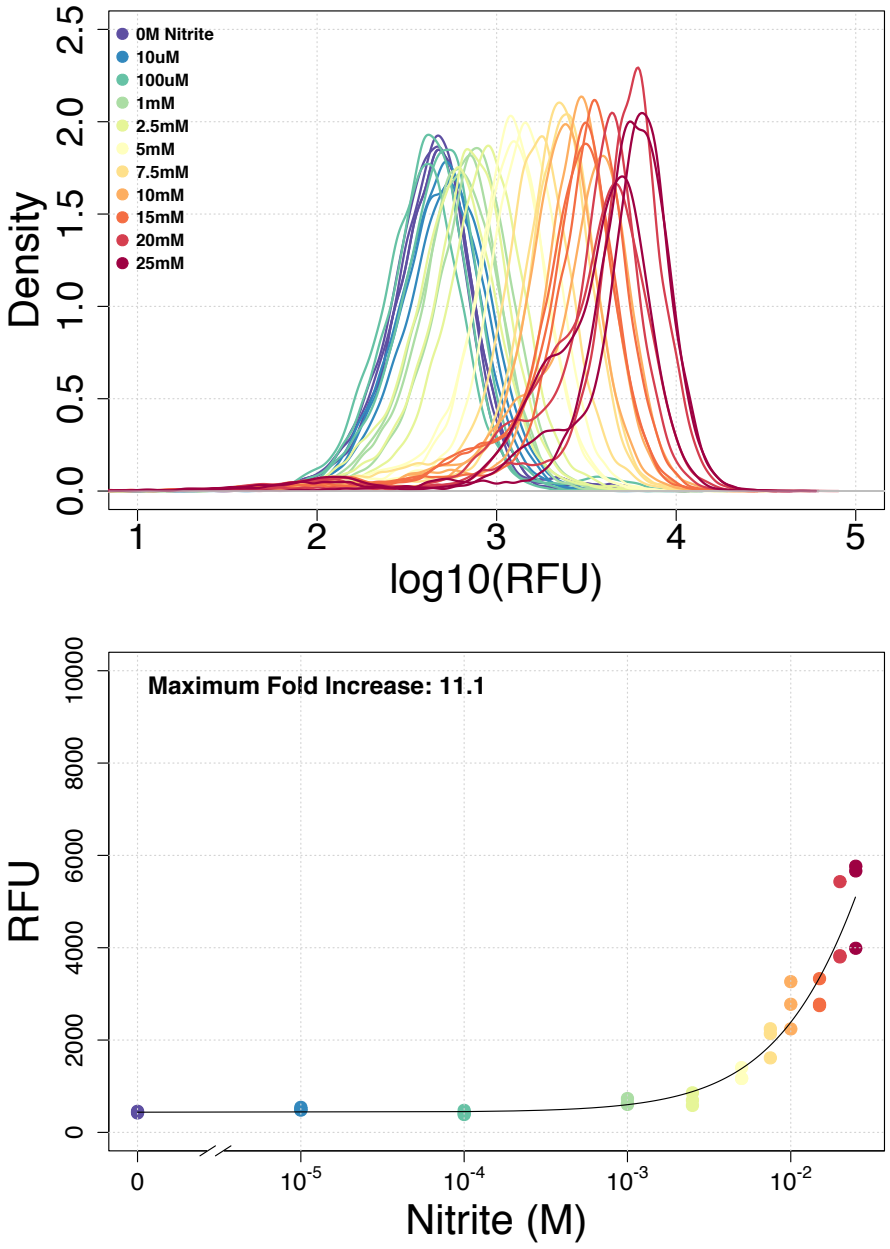

Figure 3.16: EcN_pYeaR_GFP induction with nitrite in supplemented M9 media. Top: histogram density plot of GFP fluorescence after 16 hours induction. Bottom: median GFP fluorescence after 16 hours induction. Flow cytometry data with 10,000 events (n=3). Density plots at higher concentrations showed some uncharacteristic curves. This was most likely due to the toxicity of increasing levels of nitrite.

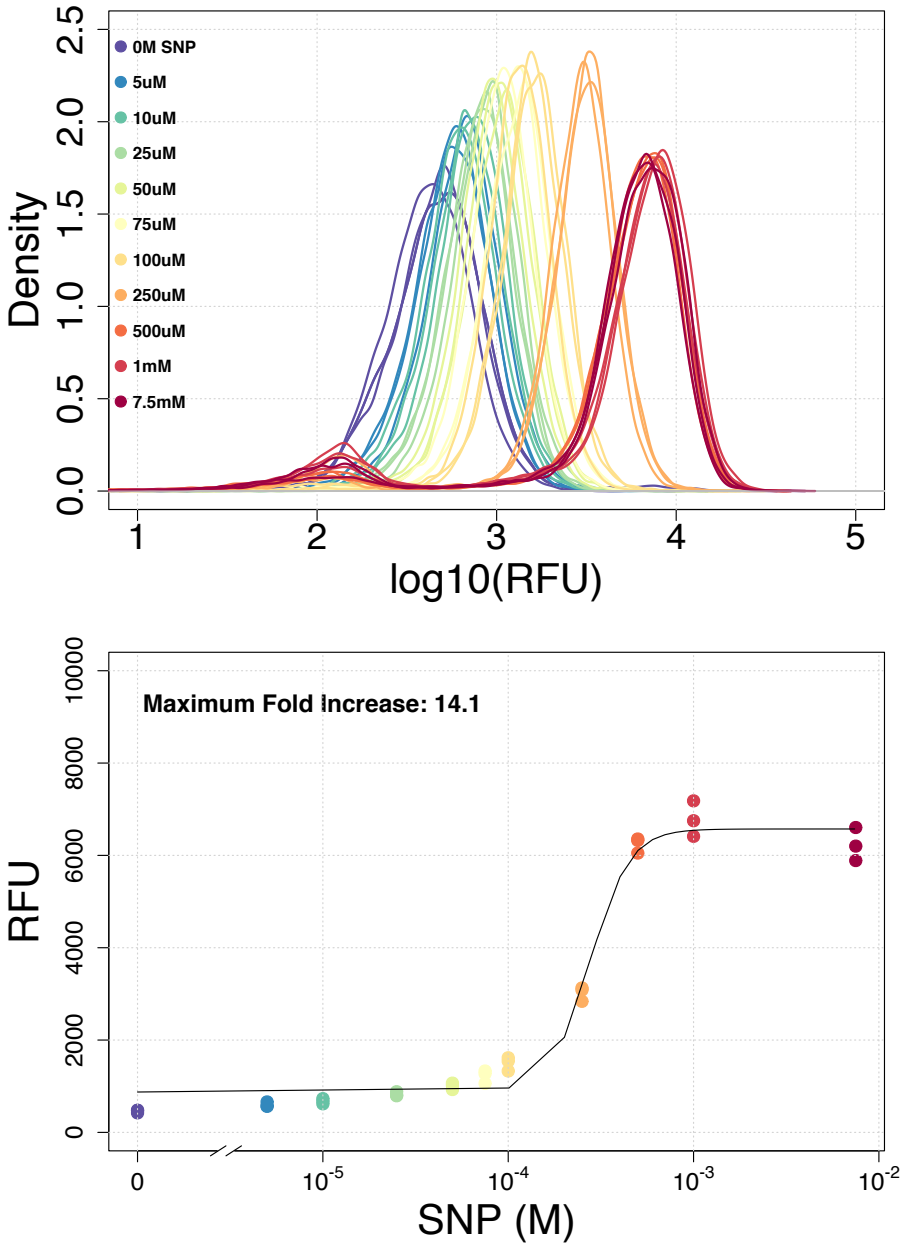

Figure 3.17: EcN_pYeaR_GFP induction with SNP (nitric oxide donor) in supplemented M9 media. Top: histogram density plot of GFP fluorescence after 16 hours induction. Bottom: median GFP fluorescence after 16 hours induction. Flow cytometry data with 10,000 events (n=3). The small population of uninduced cells at 7.5mM could be persister cells that have dropped the plasmid or dead cells.

The EcN_pYeaR_GFP sensor also showed induction with nitrate, nitrite and nitric oxide in LB media (Figure 3.18, 3.19 and 3.20). A maximum fold increase of 44.7 (from 595±17 RFU to 26597±5780 RFU) was observed in 75mM nitrate, 31.9 (from 548±4 RFU to 17467±1743 RFU) in 100mM nitrite and 46.9 (from 542±57 RFU to 25431±1850 RFU) in 100mM SNP (nitric oxide donor). These were significantly higher in comparison to induction in M9 media and was mostly due to the inability of EcN_pYeaR_GFP to tolerate higher inducer concentrations when grown in supplemented M9 media (Figure 3.21).

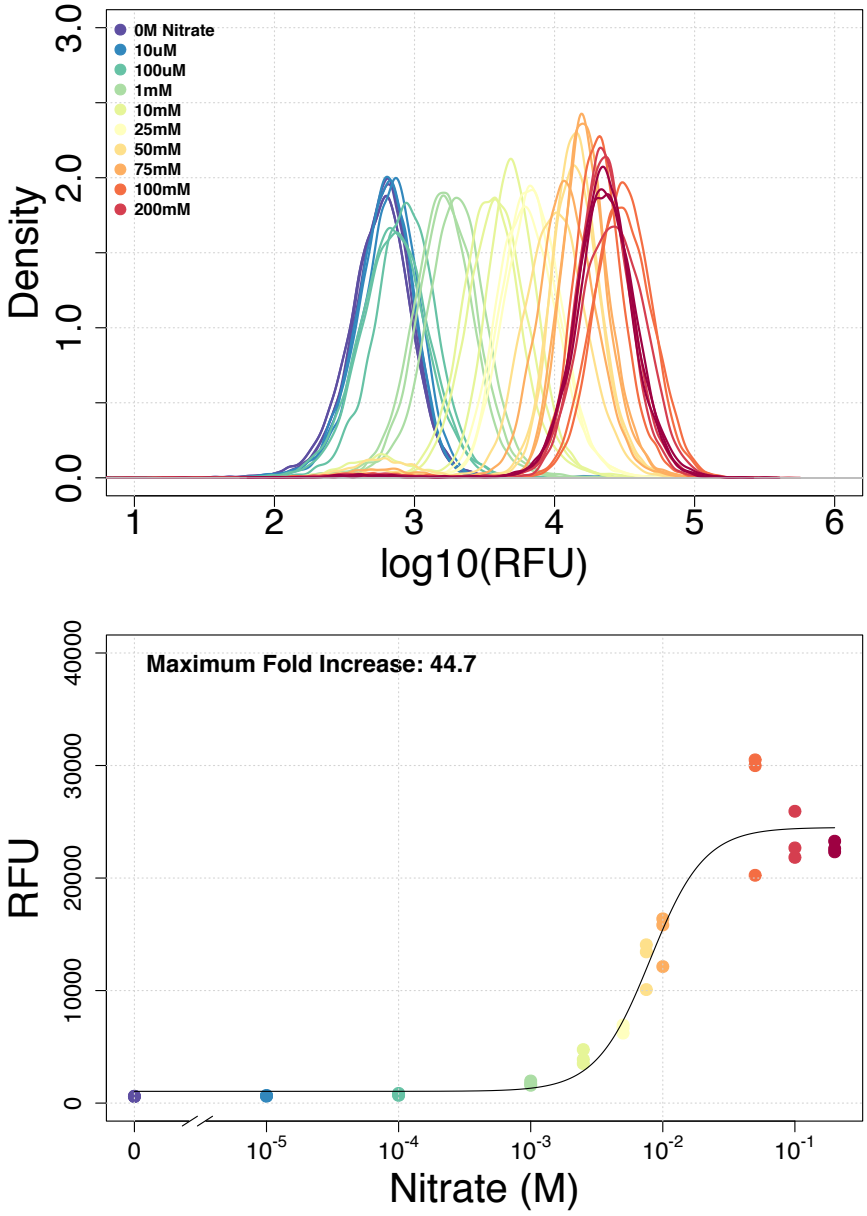

Figure 3.18: EcN_pYeaR_GFP induction with nitrate in LB media. Top: histogram density plot of GFP fluorescence after 16 hours induction. Bottom: median GFP fluorescence after 16 hours induction. Flow cytometry data with 10,000 events (n=3).

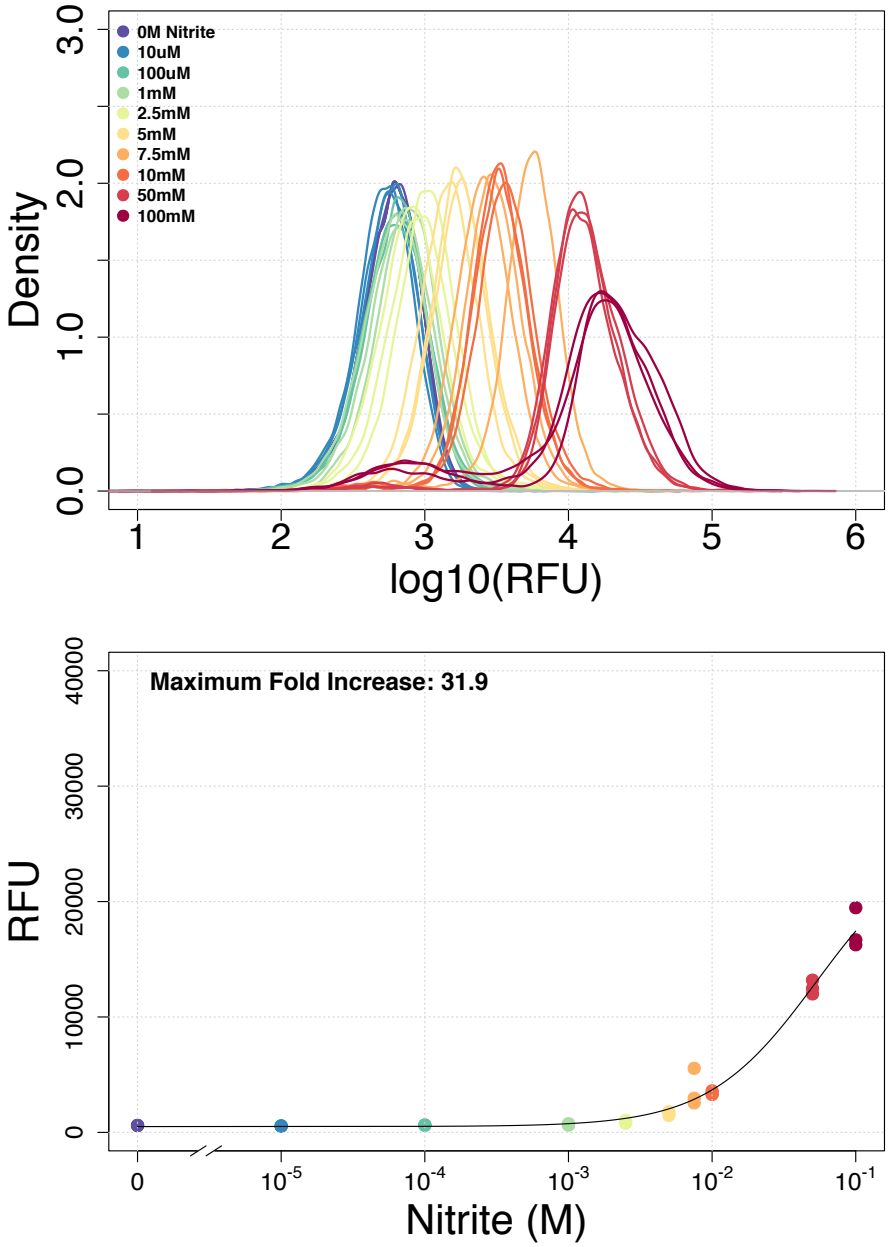

Figure 3.19: EcN_pYeaR_GFP induction with nitrite in LB media. Top: histogram density plot of GFP fluorescence after 16 hours induction. Bottom: median GFP fluorescence after 16 hours induction. Flow cytometry data with 10,000 events (n=3). Density plots at higher concentrations showed some uncharacteristic curves. This was most likely due to the toxicity of increasing levels of nitrite.

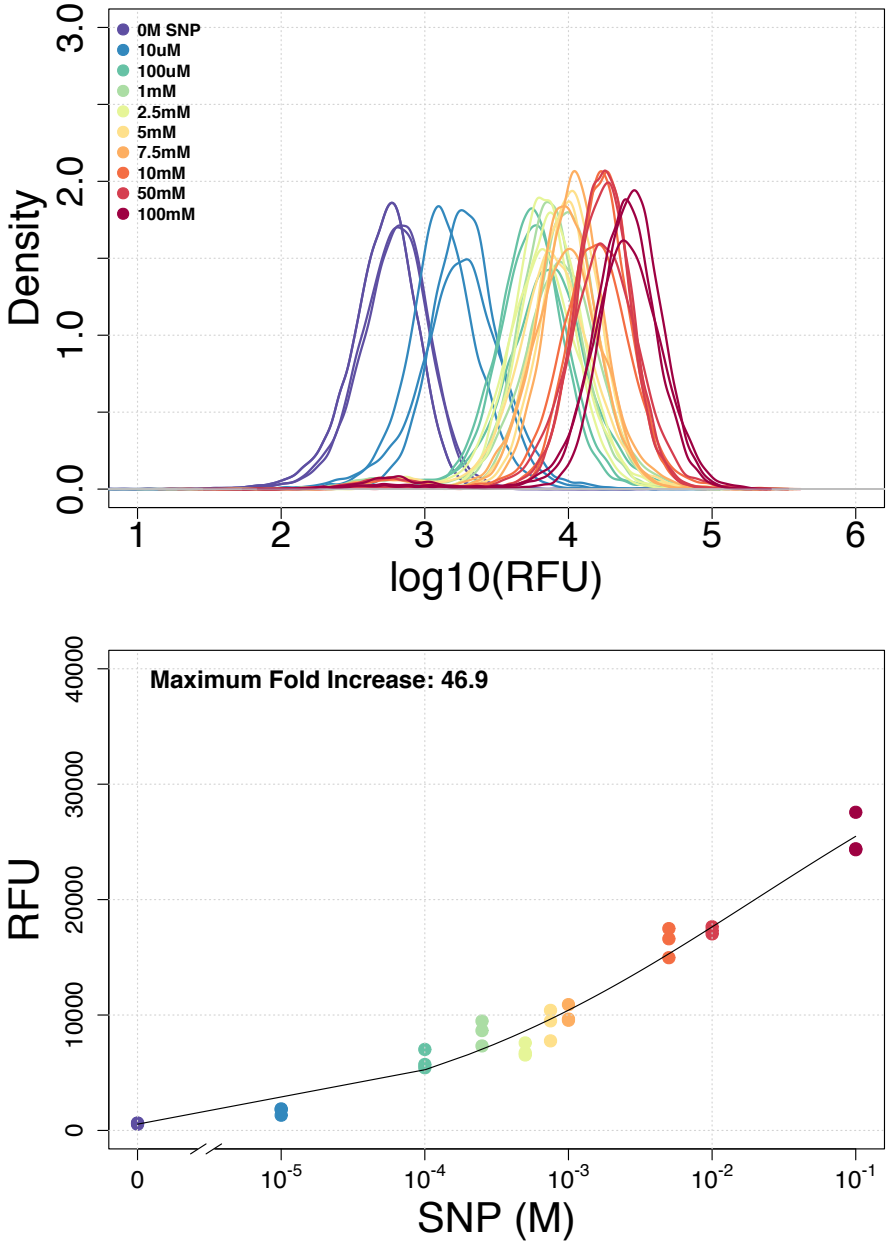

Figure 3.20: EcN_pYeaR_GFP induction with SNP (nitric oxide donor) in LB media. Top: histogram density plot of GFP fluorescence after 16 hours induction. Bottom: median GFP fluorescence after 16 hours induction. Flow cytometry data with 10,000 events (n=3).

Figure 3.21 shows that the RNS inducers started becoming toxic to EcN_pYeaR_GFP in supplemented M9 media at various different concentrations. In order to investigate the toxicity of higher concentrations of inducer at which significant levels of induction was observed, a time-course growth assay was conducted with no inducer, 25mM nitrate, 7.5mM nitrite and 250μM SNP (Figure 3.22).

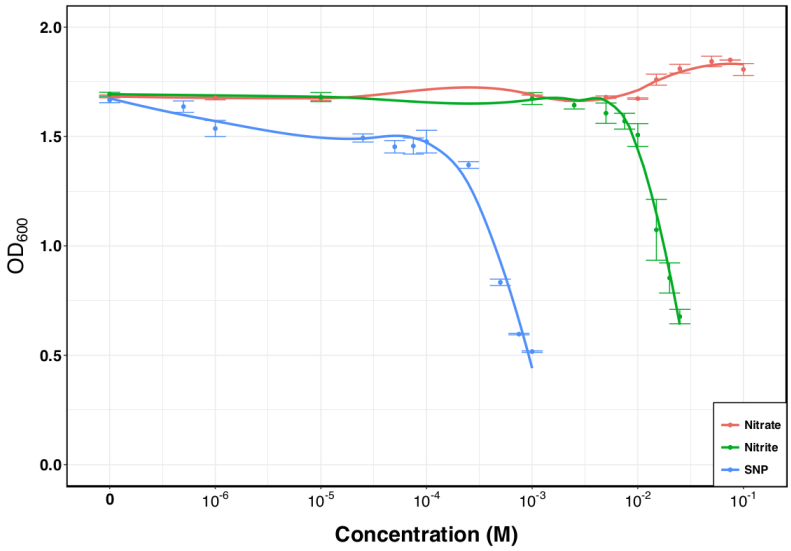

Figure 3.21: EcN_pYeaR_GFP growth with increasing concentrations of nitrate, nitrite or SNP (nitric oxide donor) in supplemented M9 media after 16 hours (n=3).

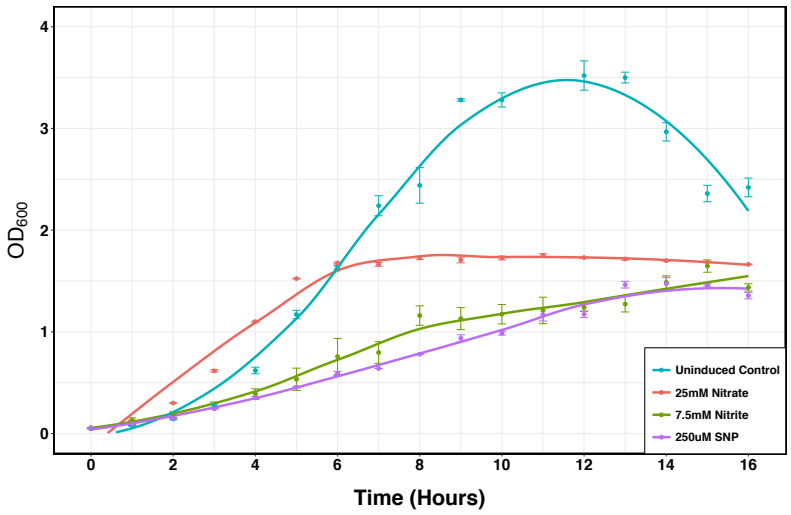

Figure 3.22: EcN_pYeaR_GFP growth over 16 hours with no inducer, 25mM nitrate, 7.5mM nitrite or 250μM SNP (nitric oxide donor) in supplemented M9 media (n=3).

EcN_pYeaR_GFP - Time-course Induction

In order to investigate the dynamic response of EcN_pYeaR_GFP, a time-course induction with the various inducers were carried out in supplemented M9 media in either the growing or stationary phase. Figure 3.23 shows that at 50mM nitrate, EcN_pYeaR_GFP demonstrated rapid induction within 2 to 3 hours during the stationary phase of growth. In comparison, induction was considerably slower during the growth phase where it took 5 to 6 hours (Figure 3.24).

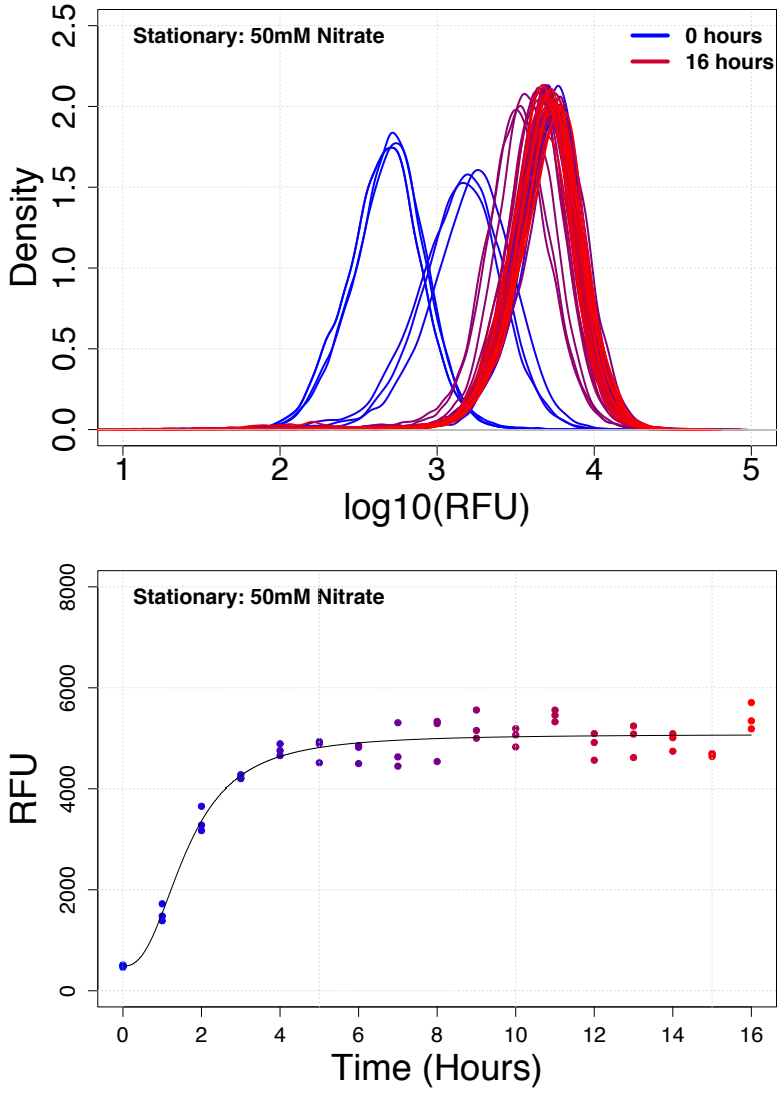

Figure 3.23: Time course EcN_pYeaR_GFP induction during the stationary phase in supplemented M9 media with 50mM nitrate over 16 hours. Top: histogram density plot of GFP fluorescence over 16 hours. Bottom: median GFP fluorescence over 16 hours induction. Stationary phase indicates an overnight culture spun down and resuspended in fresh media before being induced. Flow cytometry data with 10,000 events (n=3).

However, even though induction was slower, EcN_pYeaR_GFP reached a higher level of induction during the growth phase experiment with half the concentration of nitrate (25mm compared to 50mM).

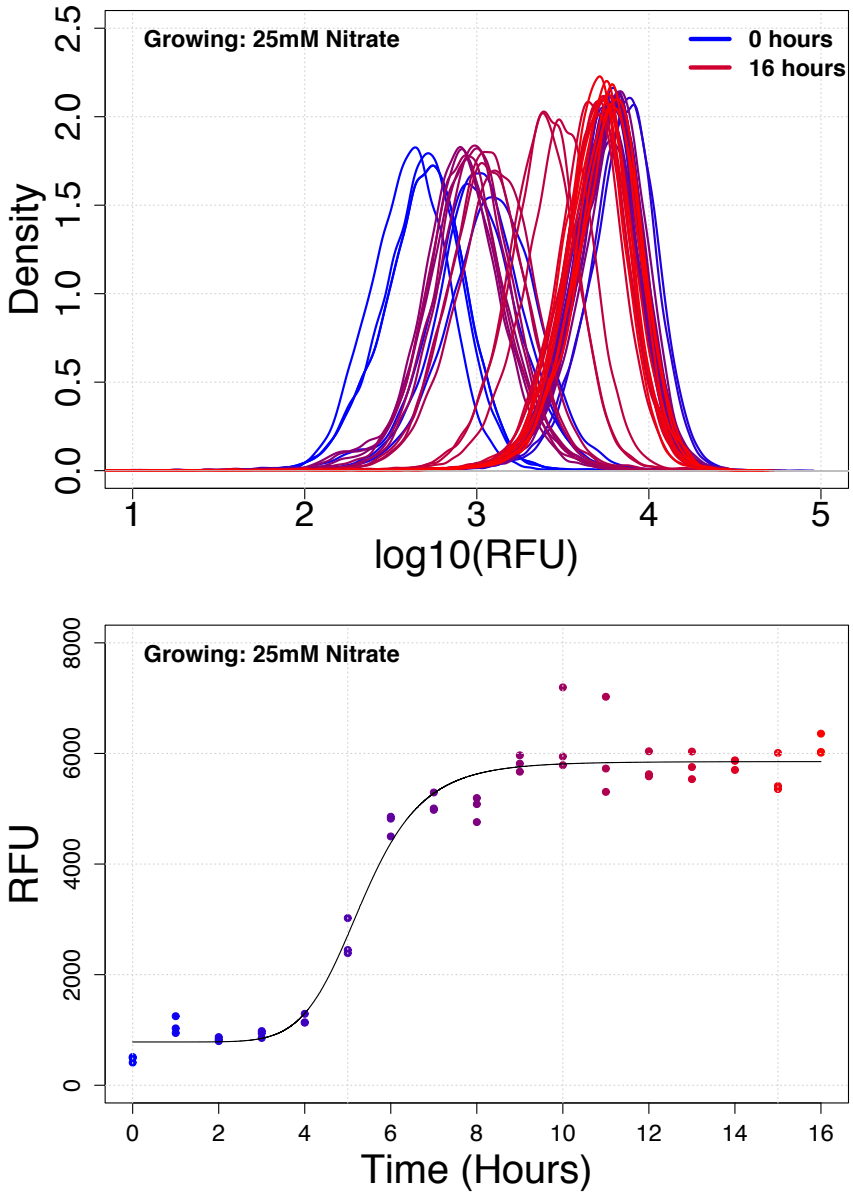

Figure 3.24: Time course EcN_pYeaR_GFP induction during the growing phase in supplemented M9 media with 25mM nitrate over 16 hours. Top: histogram density plot of GFP fluorescence over 16 hours. Bottom: median GFP fluorescence over 16 hours induction. Growing phase indicates an overnight culture that was diluted 1:500 in fresh media before being induced. Flow cytometry data with 10,000 events (n=3).

Figure 3.25 shows that at 15mM nitrite, EcN_pYeaR_GFP demonstrated rapid induction within 2 hours during the stationary phase of growth. Induction during the growth phase was just as rapid in 7.5mM nitrite (Figure 3.26).

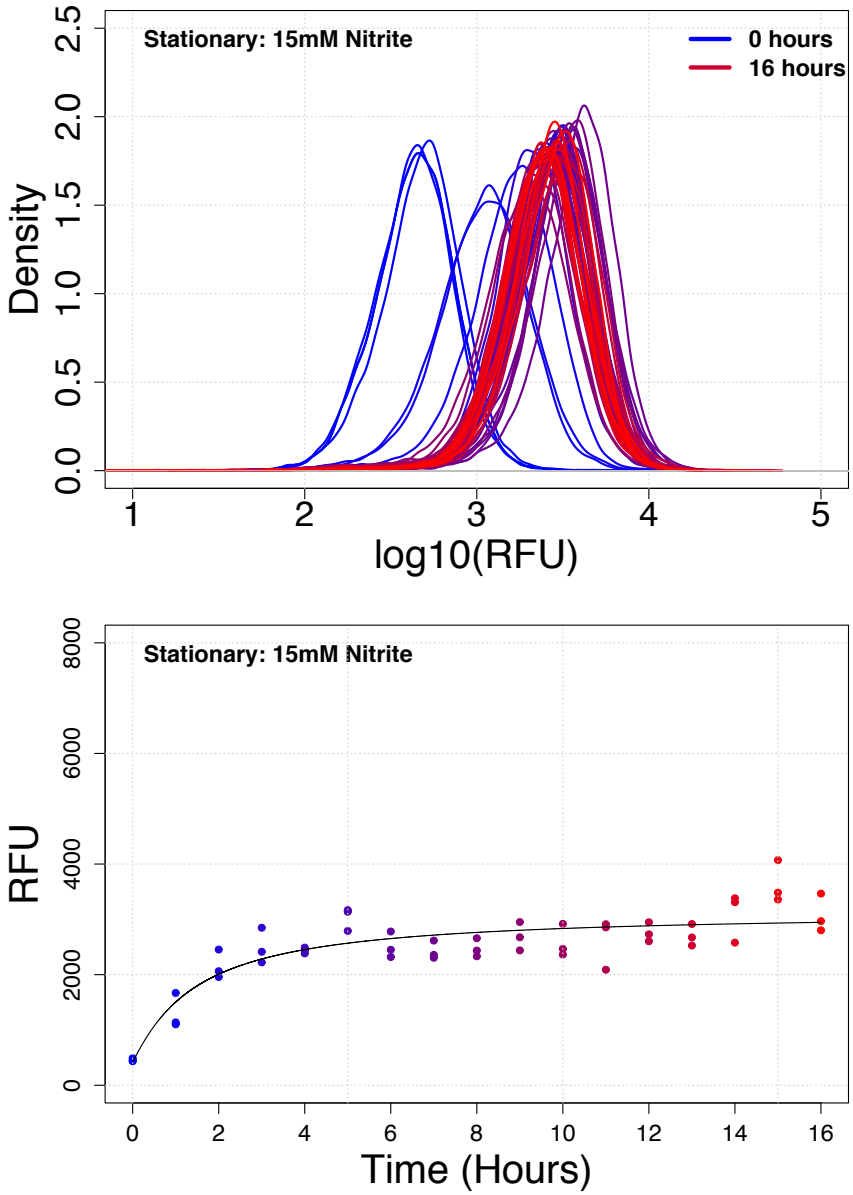

Figure 3.25: Time course EcN_pYeaR_GFP induction during the stationary phase in supplemented M9 media with 15mM nitrite over 16 hours. Top: histogram density plot of GFP fluorescence over 16 hours. Bottom: median GFP fluorescence over 16 hours induction. Stationary phase indicates an overnight culture spun down and resuspended in fresh media before being induced. Flow cytometry data with 10,000 events (n=3).

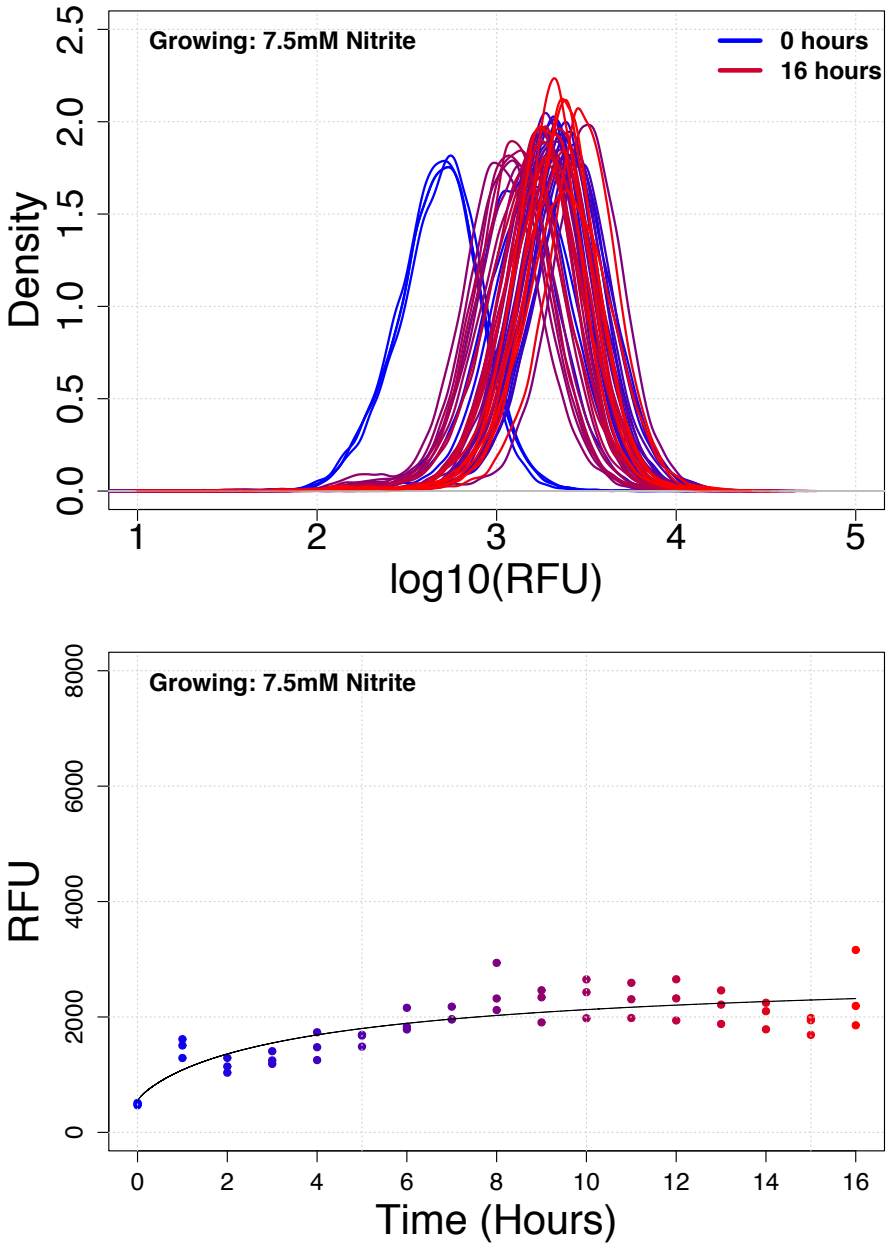

Figure 3.26: Time course EcN_pYeaR_GFP induction during the growing phase in supplemented M9 media with 7.5mM nitrite over 16 hours. Top: histogram density plot of GFP fluorescence over 16 hours. Bottom: median GFP fluorescence over 16 hours induction. Growing phase indicates an overnight culture that was diluted 1:500 in fresh media before being induced. Flow cytometry data with 10,000 events (n=3).

Figure 3.27 shows that at 500μM SNP nitrate, EcN_pYeaR_GFP demonstrated rapid induction within 2 to 3 hours during the stationary phase of growth. In comparison, induction was considerably slower during the growing phase at 250μM SNP where it took 6 to 8 hours (Figure 3.28).

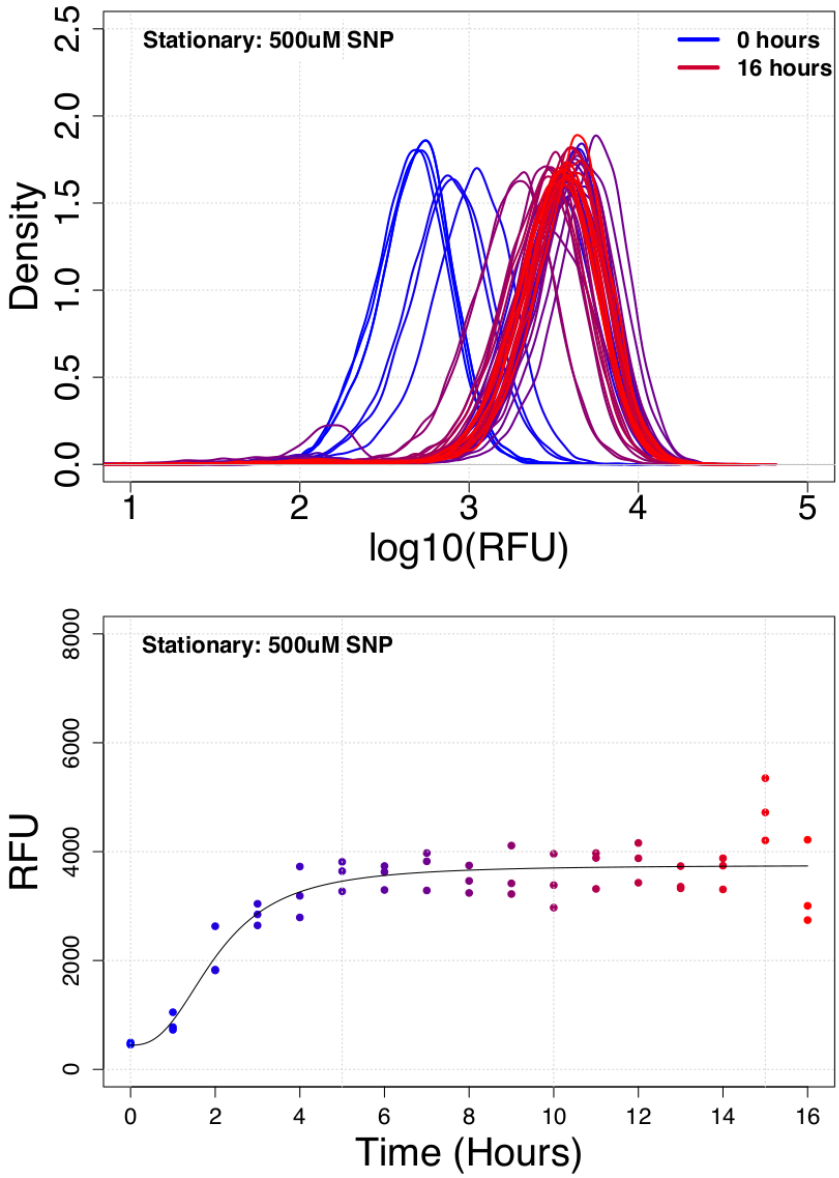

Figure 3.27: Time course EcN_pYeaR_GFP induction during the stationary phase in supplemented M9 media with 500μM SNP (nitric oxide donor) over 16 hours. Top: histogram density plot of GFP fluorescence over 16 hours. Bottom: median GFP fluorescence over 16 hours induction. Stationary phase indicates an overnight culture spun down and resuspended in fresh media before being induced. Flow cytometry data with 10,000 events (n=3).

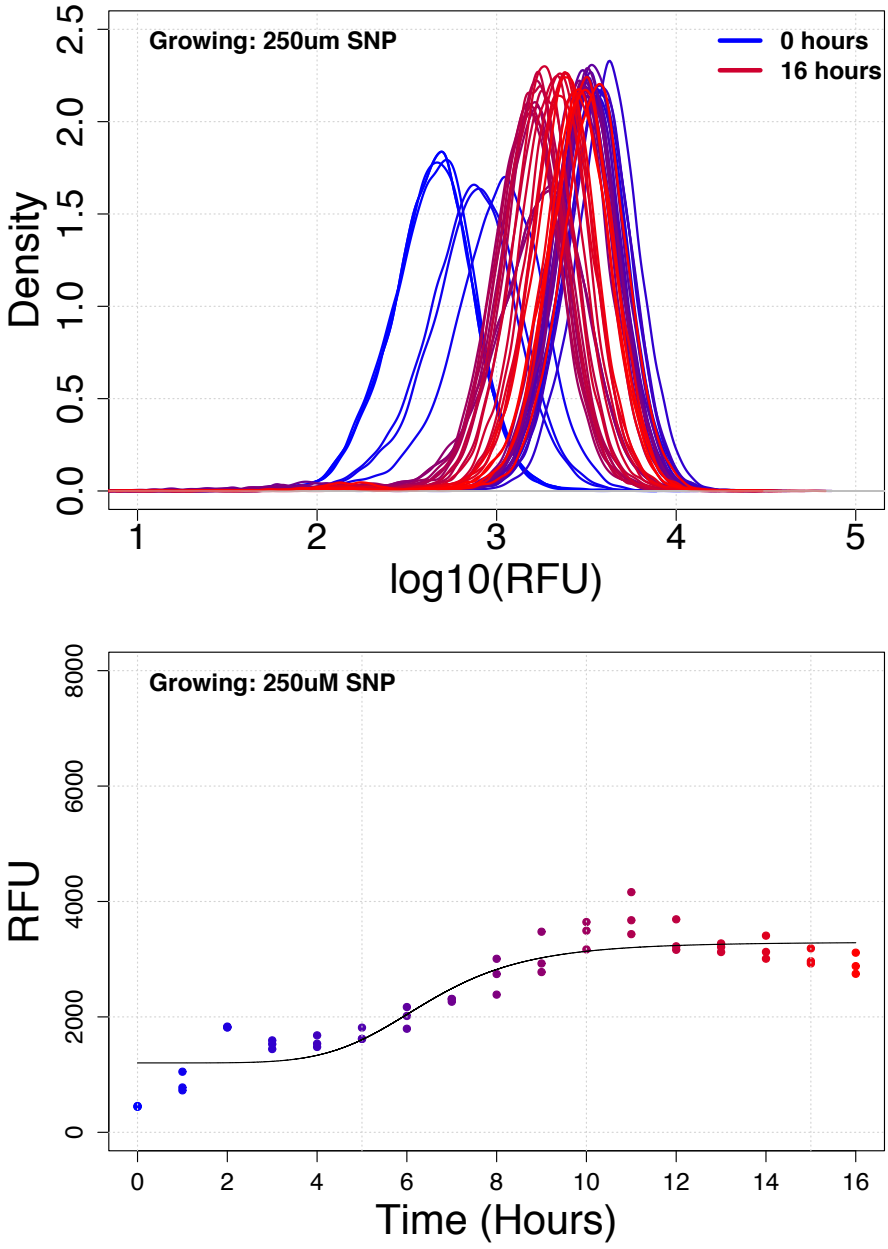

Figure 3.28: Time course EcN_pYeaR_GFP induction during the growing phase in supplemented M9 media with 250μM SNP (nitric oxide donor) over 16 hours. Top: histogram density plot of GFP fluorescence over 16 hours. Bottom: median GFP fluorescence over 16 hours induction. Growing phase indicates an overnight culture that was diluted 1:500 in fresh media before being induced. Flow cytometry data with 10,000 events (n=3).

EcN_pYeaR_GFP - Induction with Bacterial Nitric Oxide Synthase

Through the use of $pNOS_{Ban}$, it was demonstrated that EcN_pYeaR_GFP could also detect RNS direct from bacterial sources. Once induced, $pNOS_{Ban}$ expresses the gene for bacterial nitric oxide synthase (NOS) from *Bacillus anthracis* [154]. The cluster of genes converts arginine into nitric oxide which due to its unstable nature is rapidly broken down into nitrate and nitrite. *E. coli* BL21 was transformed with $pNOS_{Ban}$ to derive EcB_$pNOS_{Ban}$ and induced overnight with 2% arabinose and 2mM arginine as described previously [154].

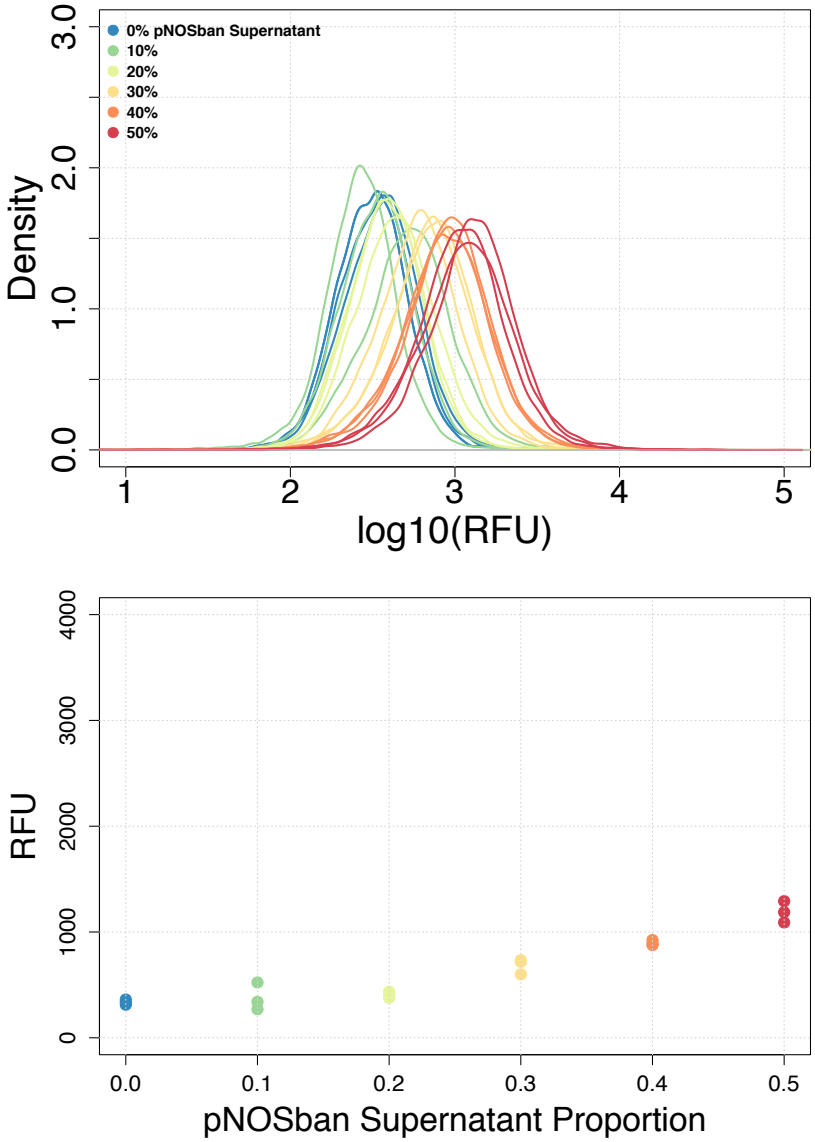

Figure 3.29: EcN_pYeaR_GFP induction with different proportions of induced EcB_$pNOS_{Ban}$ supernatant in supplemented M9 media. Top: histogram density plot of GFP fluorescence after 16 hours induction. Bottom: median GFP fluorescence after 16 hours induction. Flow cytometry data with 10,000 events (n=3).

Figure 3.29 shows that in supplemented M9 media, EcN_pYeaR_GFP demonstrated a 3.5 fold increase in GFP fluorescence with 50% EcB_pNOS$_{Ban}$ supernatant (from 336±24 RFU to 1187±101 RFU). In LB media, this was increased to a 20.1 fold increase (from 264±6 RFU to 5302±2441 RFU) (Figure 3.30).

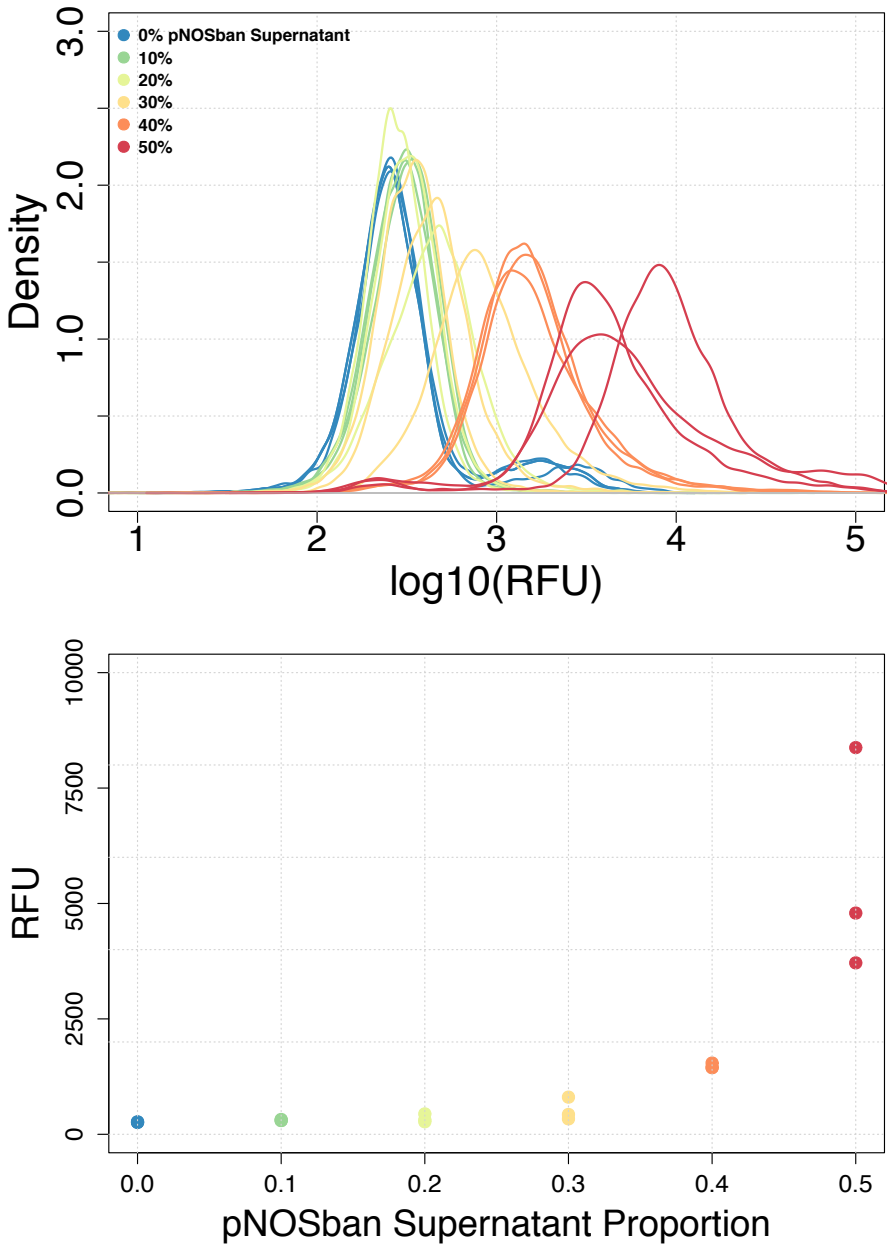

Figure 3.30: EcN_pYeaR_GFP induction with different proportions of induced EcB_pNOS$_{Ban}$ supernatant in LB media. Top: histogram density plot of GFP fluorescence after 16 hours induction. Bottom: median GFP fluorescence after 16 hours induction. Flow cytometry data with 10,000 events (n=3).

As *B. subtilis* 168 also contains a NOS variant, a similar assay was conducted to see whether EcN_pYeaR_GFP could detect RNS from the overnight supernatant of a *B. subtilis* 168 culture. In LB, EcN_pYeaR_GFP demonstrated a 2.5 fold increase in GFP fluorescence with 50% *B. subtilis* 168 supernatant (from 213±1 RFU to 539±111 RFU) (Figure 3.31).

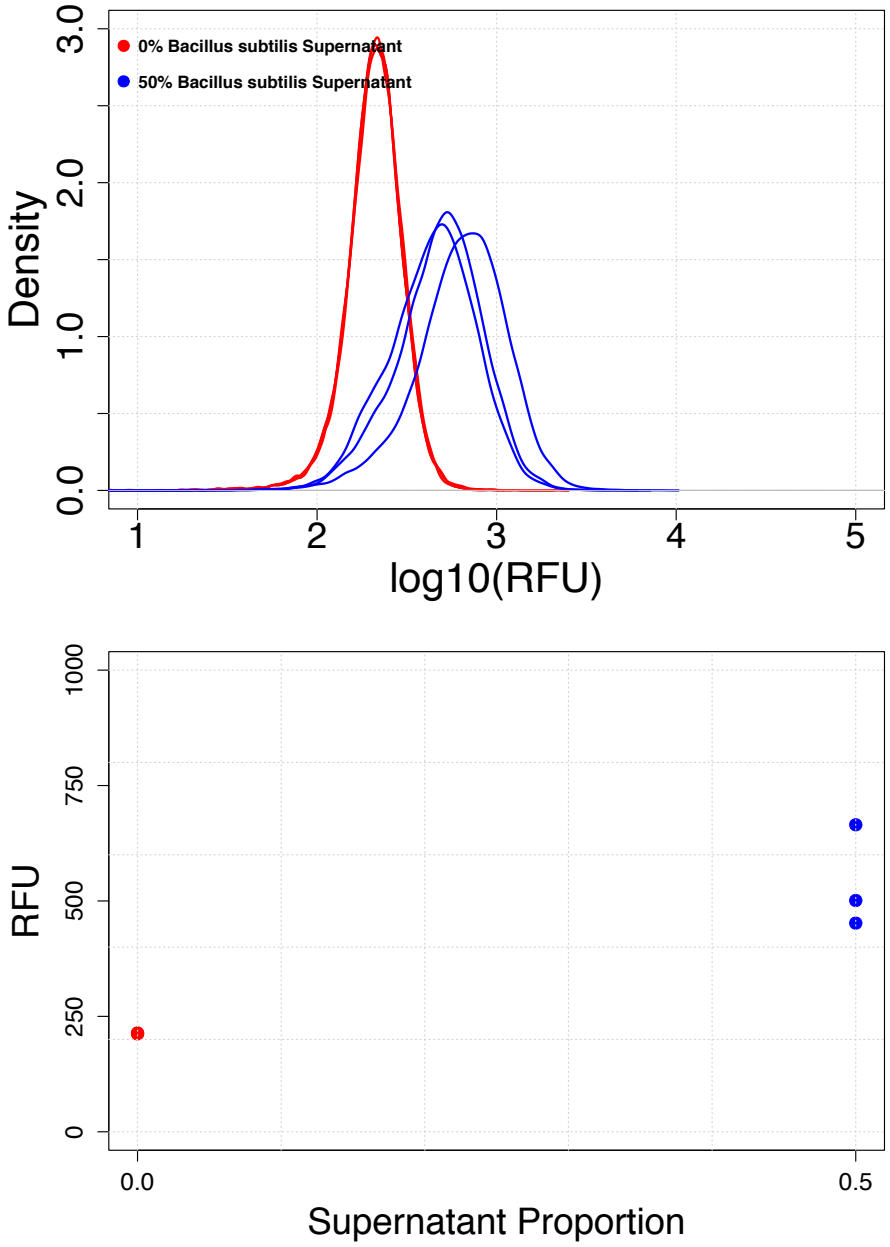

Figure 3.31: EcN_pYeaR_GFP induction with different proportions of *Bacillus subtilis* 168 supernatant in LB media. Top: histogram density plot of GFP fluorescence after 16 hours induction. Bottom: median GFP fluorescence after 16 hours induction. Flow cytometry data with 10,000 events (n=3).

The ability of EcN_pYeaR_GFP to detect RNS from EcB_pNOS$_{Ban}$ was also investigated on an agar co-culture plate (Figure 3.32). A qualitative difference could be seen in the level of GFP fluorescence on an agar plate grown with induced EcB_pNOS$_{Ban}$ in comparison to the uninduced control (Figure 3.33).

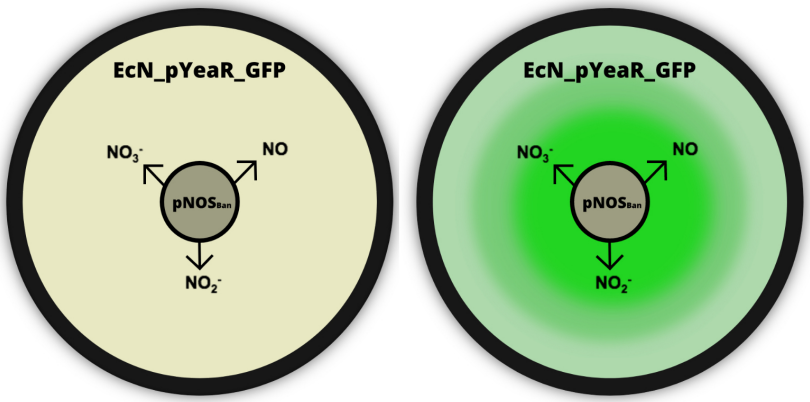

Figure 3.32: Graphical representation of the EcN_pYeaR_GFP - EcB_pNOS$_{Ban}$ agar induction assay demonstrating the induced EcB_pNOS$_{Ban}$ (at the centre) producing nitrates, nitrites and nitric oxide to induce the EcN_pYeaR_GFP lawn grown overnight on the agar plate.

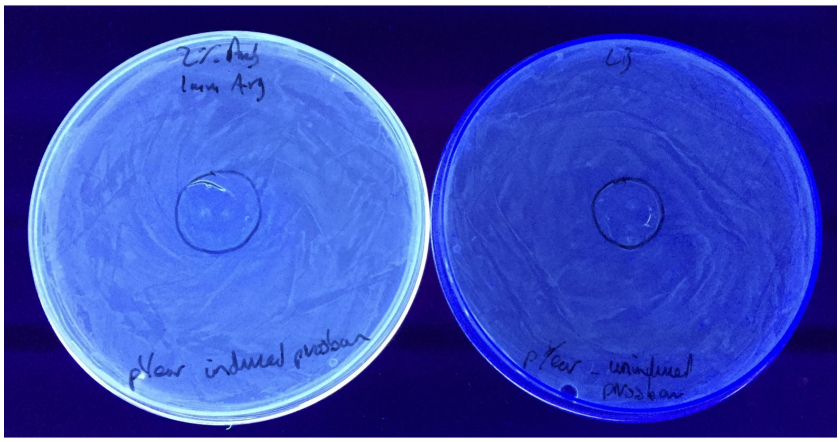

Figure 3.33: Photograph of the EcN_pYeaR_GFP-EcB_pNOS$_{Ban}$ agar induction assay under UV illumination. Left: EcN_pYeaR_GFP grown overnight with induced EcB_pNOS$_{Ban}$ seeded at the centre of the plate. Right: EcN_pYeaR_GFP grown overnight with uninduced EcB_pNOS$_{Ban}$ seeded at the centre of the plate. Images were taken side by side at the same time.

This GFP expression was quantified with flow cytometry as a measure of distance from the centre of the plate. Figure 3.34 shows that at 0mm from the induced EcB_pNOS$_{Ban}$ centre, GFP expression from EcN_pYeaR_G was 7415±797 RFU. This decreased to 4926±125 RFU and 1723±438 RFU at a distance of 15mm and 30mm from the centre, respectively. No demonstrable differences were seen from the basal expression on the control plate with uninduced EcB_pNOS$_{Ban}$ at the centre (Appendix, Figure 5.6).

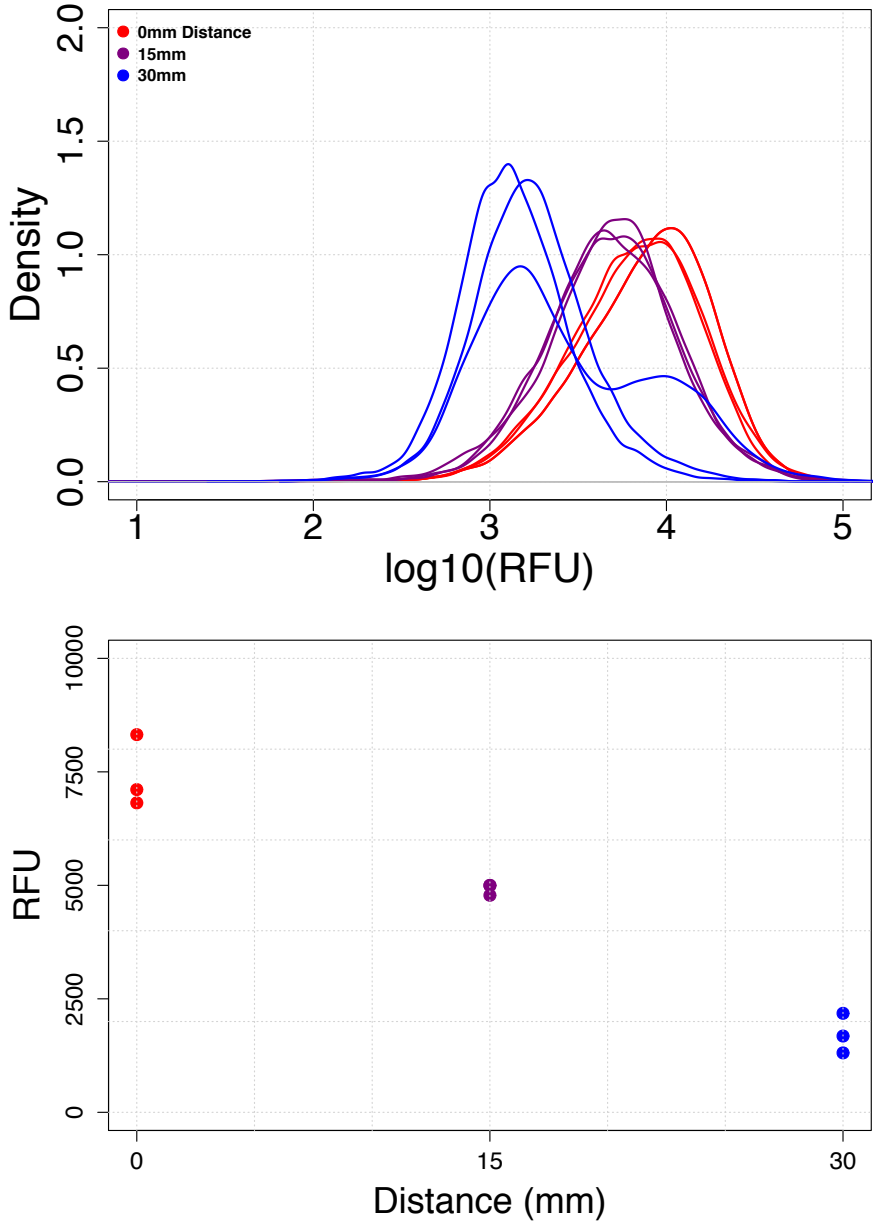

Figure 3.34: EcN_pYeaR_GFP induction on an agar plate at different distances from the induced pEcB_pNOS$_{Ban}$ centre. Top: histogram density plot of GFP fluorescence after 16 hours growth. Bottom: median GFP fluorescence after 16 hours growth. Flow cytometry data with 10,000 events (n=3).

3.5.3 EcN_pCadC_GFP - pH Sensor

Figures 3.36 and 3.35 shows that the EcN_pCadC_GFP sensor demonstrated the ability to induce GFP expression at a lower pH in LB but not in supplemented M9 media. After overnight growth in LB media buffered to pH 8 and 7, GFP expression was at 217±39 RFU and 547±64 RFU, respectively. In LB media buffered to pH 6 and 5, this increased to 2790±170 RFU and 2895±393 RFU, respectively. This results in a 13.3 fold increase from pH 5 to pH 8. These increases were not observed in the EcN_OG241_GFP and EcN_OXB19_GFP controls (Appendix, Figure 5.7 and 5.8).

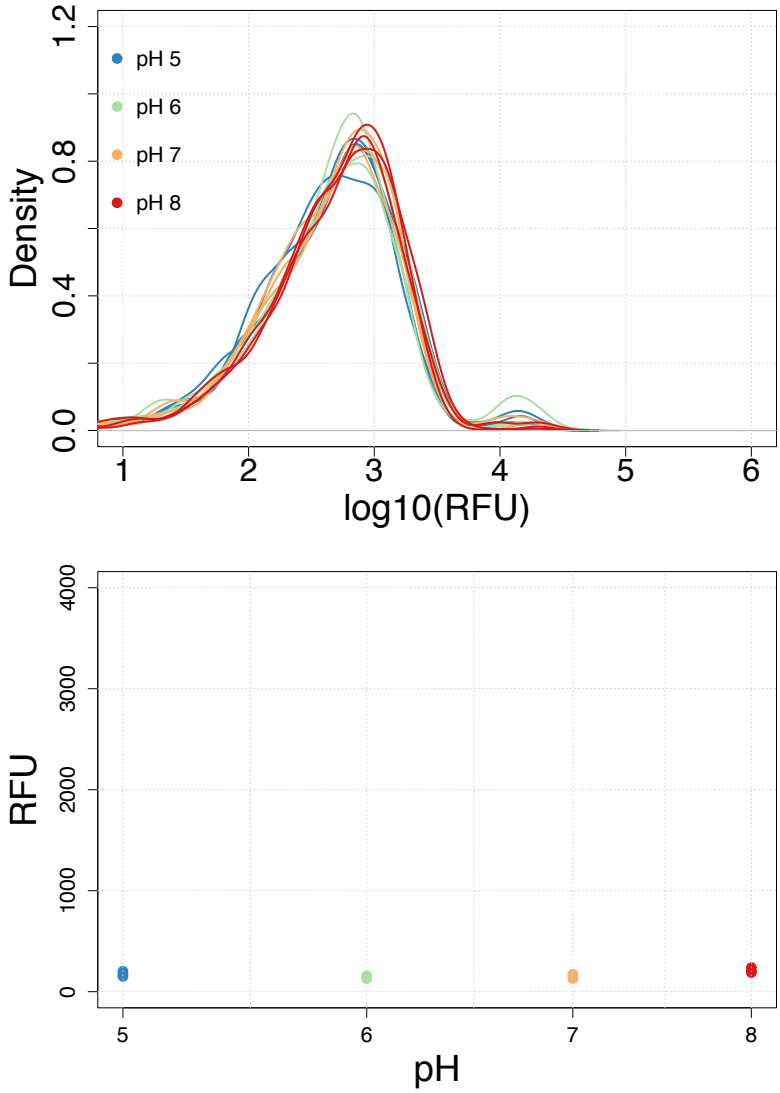

Figure 3.35: EcN_pCadC_GFP induction after 16 hours in supplemented M9 media buffered to pH 5 (with acetic acid), pH 6 (with MES), pH 7 (with HEPES) and pH 8 (with HEPES). Top: histogram density plot of GFP fluorescence after 16 hours growth. Bottom: median GFP fluorescence after 16 hours growth. Flow cytometry data with 10,000 events (n=3).

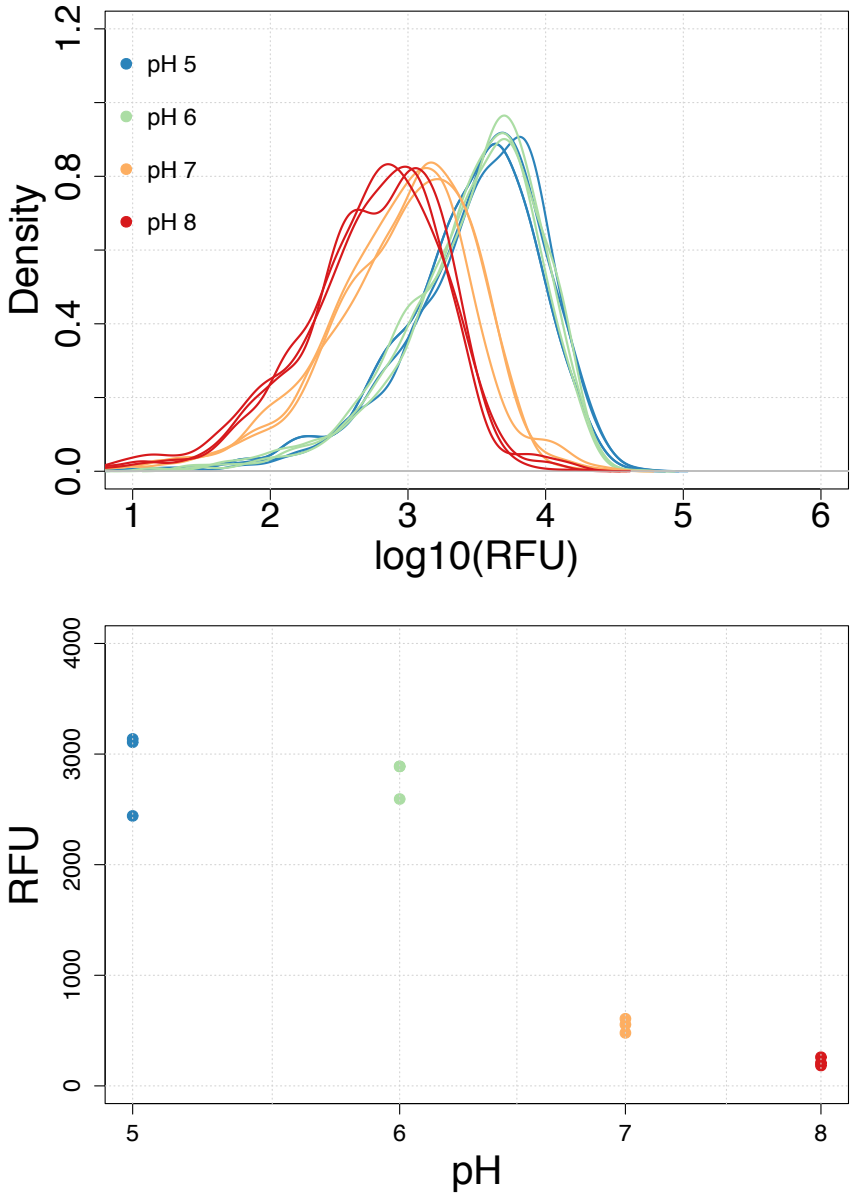

Figure 3.36: EcN_pCadC_GFP induction after 16 hours in LB media buffered to pH 5 (with acetic acid), pH 6 (with MES), pH 7 (with HEPES) and pH 8 (with HEPES). Top: histogram density plot of GFP fluorescence after 16 hours growth. Bottom: median GFP fluorescence after 16 hours growth. Flow cytometry data with 10,000 events (n=3).

3.5.4 EcN_pBBr_GFP

Figure 3.37 shows that even though a slight increase in GFP expression was observed with increasing concentrations of deoxycholic acid inducer, the EcN_pBBr_GFP construct did not demonstrate a feasible level of induction as it had an extremely high level of basal expression (22,911±973 RFU). The EcN_pBBr_GFP construct was also tested with cholate but no induction was observed (data not shown).

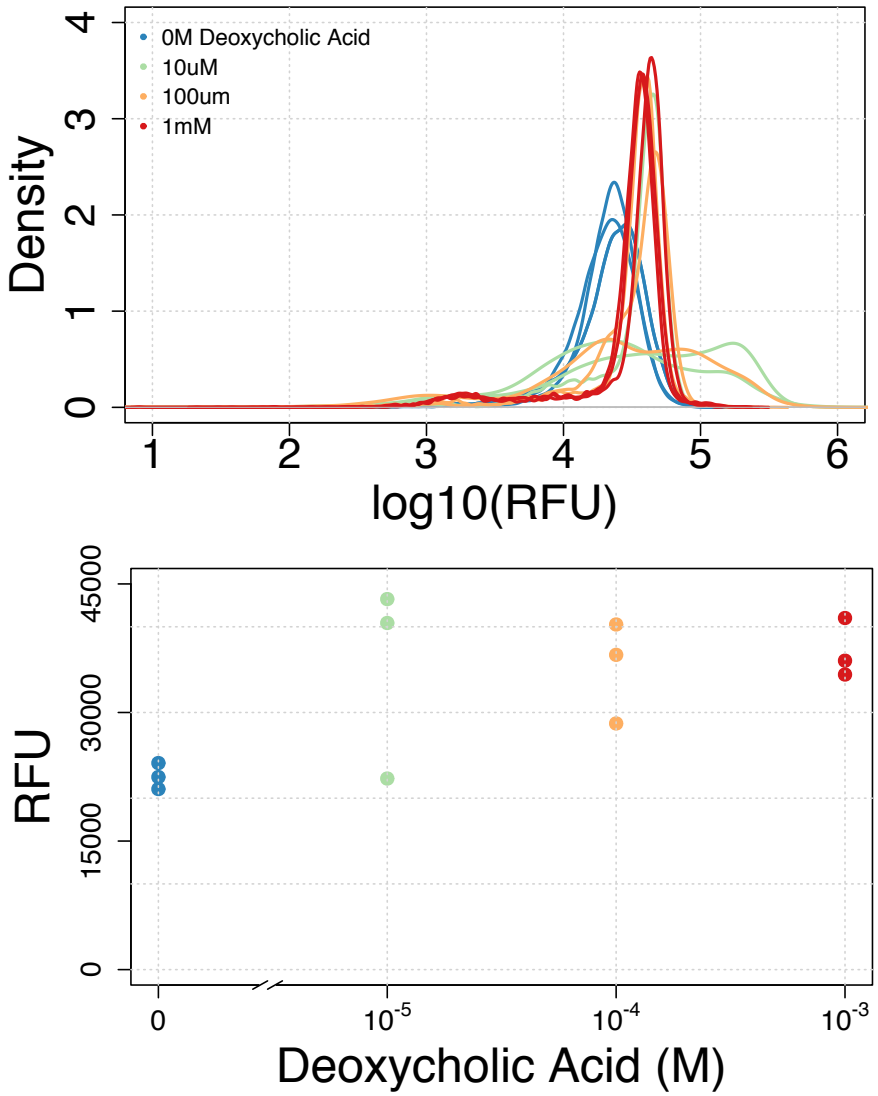

Figure 3.37: EcN_pBBr_GFP induction with deoxycholic acid in LB media. Top: histogram density plot of GFP fluorescence after 16 hours induction. Bottom: median GFP fluorescence after 16 hours induction. Flow cytometry data with 10,000 events (n=3).

3.6 Discussion

Quantitatively detecting markers of interest through inducible reporter systems can enable the design of more complex therapeutic circuits. The ability of EcN to occupy various niches in the intestines means it is particularly relevant to the detection of dysbiotic markers in the gut. Here it was shown that various inducible systems were successfully characterised in the probiotic EcN strain for the first time.

The pPro inducible system has thus far been characterised in laboratory strains such as *E. coli* BL21 (DE3) [144]. As EcN contains the required *prpBCDE* operon in the chromosome (confirmed using the complete genome [87] via NCBI Blast alignment), we were able to demonstrate the system working successfully for the first time in a probiotic bacterial strain. EcN_pProE_GFP was able to robustly detect propionate at a range of concentrations in both supplemented M9 and LB media (Figure 3.9 and 3.10). While the maximum induction fold increases observed here in LB were lower than in the published pPro system (19.7 with EcN_pProE_GFP in 200mM compared to 15000 with pPro in 50mM) this could be due to the fact that the high copy (500) OG241 plasmid would have a considerably higher basal expression level than the low copy (20) pBAD24 plasmid used in pPro [144]. The lower basal expression level observed in supplemented M9 media (204±3 RFU compared to 478±84 RFU) increased the fold change to 31.4 (Figure 3.9). This lower basal expression level in supplemented M9 media corresponds to previous reports of catabolic repression in LB media with the *S. enterica* variant of the pPro system [146]. Nonetheless, EcN_pProE_GFP showed a high level of GFP fluorescence at maximum induction in both M9 (6510±568 RFU) and LB media (9403±747 RFU). The rapid level of induction observed also corresponds to published reports on the system where significant fluorescence was recorded within 90 minutes [144] (Figure 3.13 and 3.14). It is thought that the system evolved for rapid induction in order to enable the host to quickly adapt to carbon sources. In previous reports investigating the effect of diet on SCFA levels in fecal matter, it was shown that the concentration of this particular SCFA ranges from 12mM to 25mM [156, 157]. In light of this, EcN_pProE_GFP could be used with *in vivo* models to elucidate the role of SCFAs in diet, dysbiosis and host genetics. It could also be used to design circuits that can sense low levels of propionate during pathologies and respond to normalise

them by inducing the production of catabolic enzymes.

Using EcN_pYeaR_GFP, it was shown that a range of concentrations of nitrate, nitrite and nitric oxide could be detected with a probiotic strain in both M9 and LB media (Figure 3.15 to 3.20). Previous investigations showed that levels of nitrate can rise to around 500μM at the mucosal layer of the intestines in an inflammation model [138]. In another experiment, it was shown that stool nitrite levels were significantly higher in children with IBD in comparison to healthy controls (162±31 mM vs 77±22 mM) [158]. In comparison to control patients with rectal levels of of nitric oxide at around 2-3μM, patients suffering from Crohn's disease were shown have nitric oxide levels of 25-30μM [159]. As nitric oxide is rapidly degraded, higher levels are expected to be found in the microenvironment surrounding inflamed intestinal tissue. In light of this, EcN_pYeaR_GFP could be used to detect physiologically relevant levels of nitrate, nitrite and nitric oxide directly from the intestines or stool samples. Through the use of $pNOS_{Ban}$, it was also demonstrated that EcN_pYeaR_GFP could detect RNS directly from bacterial sources in both M9 and LB (Figure 3.29 and 3.30). As it was also shown that EcN_pYeaR_GFP could be induced from other bacterial strains on an agar plate (Figure 3.34), the sensor could be further investigated as a communication system with a sensor colony node harbouring the pYeaR plasmid and an effector colony node harbouring the NOS plasmid.

Previously published work on a P_{yearR}-GFP sensor only involved characterisation with nitrate and clinical samples of serum and urine [90]. The findings presented here with nitrate and EcN_pYeaR_GFP closely corroborate the minimal detection levels and maximum fold increases previously published. In line with their work, nitrate was detected from 1mM onwards and demonstrated a 10 fold increase at 10mM in both M9 and LB. It is worth noting that the induction was amplified by 10 fold with the use of integrase genes to create a pYeaR-switch [90]. The work here builds further on our understanding of P_{yearR} through characterisation with nitric oxide and nitrite.

As discussed previously, a synthetic switch circuit was also used to detect intestinal inflammation through the nitric oxide sensitive promoter region of the *norV* gene [133]. As this construct was solely characterised through a fluorescent switch inversion system, a comparison cannot be made with EcN_pYeaR_GFP in terms of fold increase with SNP (nitric oxide) induction. Due to the use of the *norV* promoter region, the circuit

designed was only sensitive to nitric oxide and not to nitrate or nitrite. However, it would be inquisitive to use a similar inflamed mouse ileum explant to investigate the ability of EcN_pYeaR_GFP to detect biological inflammation. More recently, EcN was engineered with a thiosulfate and a tetrathionate sensor to detect colonic inflammation in a *in vivo* mouse model both in the presence or absence of oxygen [160]. While they were able to use fluorescence as an output to detect inflammation in the feces and colon with the thiosulfate sensor, they were unable to detect significant differences with the tetrathionate sensor. This indicates that EcN_pYeaR_GFP would need a low enough detection limit to work in a similar *in vivo* mouse model. Genetic amplification switches could be used to achieve this [90].

It was demonstrated that EcN_pCadC_GFP could successfully induce GFP expression at a lower pH in LB but not in supplemented M9 media (Figure 3.36 and 3.35). The 13.3 fold increase observed here from pH 8 to pH 5 corresponds well to the previously reported 12.5 fold increase observed with the pCadC_lacZ construct in *E. coli* MC4100 [150]. While it was previously reported that the pCadC region is dependent on exogenous lysine to mediate induction, this was not the case with EcN_pCadC_GFP as induction was not affected in the presence or absence of 10mM lysine. In addition, the fact that EcN_pCadC_GFP did not function in supplemented M9 media (with or without lysine) indicates that the pCadC region could be dependent on another exogenous compound for induction. The incorporation of a pH sensitive system like this into a strain such as EcN could enable the design of a chassis that can exploit the pH gradient of the intestines. For example, EcN could be designed to only induce a gene when it is in a low pH niche. In addition, the system could be used to either induce or suppress induction of an output gene when it detects a decreasing pH.

The EcN_pBBr_GFP sensor created with the promoter region of the BBr_0838 gene from *B. breve* UCC2003 [153] did not function as an induction system. While a slight increase was observed with increasing levels of deoxycholic acid (Figure 3.37) and cholate (data not shown), the system showed an extremely high basal expression level. This is in contradiction with previously published work that showed the promoter region increasing expression of GusA by 8 fold in *B. breve* using the pNZ272 promoter probe vector [153]. This discrepancy is most likely due to the fact that the pBBr region was characterised here in EcN instead of *B. breve*. The suitability of the pBBr region

could be further analysed using bioinformatic tools such as PromoterHunter [161].

The ability to quantitively measure therapeutically relevant markers such as SCFA, pH and RNS could shed light onto mechanisms behind dysbiosis in the gut. Through the use of commensal vectors like EcN, precise *in vivo* models with mice or *C. elegans* could be used to investigate the role of the intestinal microbiome in host genetics, diet and pathologies. As well as monitoring the microbiota, these sensor components could eventually be coupled to other genes to design and create dynamic genetic circuits with pre-determined and responsive functions.

3.7 Conclusions and Further Work

As set out in the aims, this piece of work demonstrated that is possible to design and characterise a range of therapeutic sensors using the probiotic EcN.

Elements from the *E. coli yeaR-yoaG* operon were successfully used to create a nitric oxide, nitrate and nitrite inducible sensor with EcN_pYeaR_GFP. In further work, this system could be further characterised by testing induction with the various RNS in combination. This would also further elucidate the interplay between the NsrR repressor and the Nar two-component system. While it was clearly shown that EcN_pYeaR_GFP could detect bacterial NOS from NOS_{Ban}, it would be enlightening to fully quantify the concentration of nitric oxide, nitrate and nitrite produced by this system. Although these systems have been previously reported in the literature, this piece of work shows full and quantitative characterisation of the systems in EcN. The regulatory and promoter region of the *prpBCDE* operon was successfully used to create a sensor induced by propionate; a vital intestinal SCFA. The impact of catabolic repression on the EcN_pProE_GFP sensor could be further investigated by growing the strain with lower concentrations of glycerol or alternative carbon sources such as glucose. The regulatory and promoter region of the *cadBA* operon was also successfully used to create a sensor capable of detecting a decrease in pH. The fact that the system only functioned in LB and not M9 media means that the mechanisms behind the regulation of the *cadBA* operon need to be further investigated.

Collectively, these sensors need to be characterised further to eventually investigate their capabilities with *in vivo* experiments or clinical samples.

4. *Caenorhabditis elegans*: An Emerging Model for Studying the Intestinal Microbiota

4.1 Introduction

The ability of researchers to ask complex questions and unravel the multifaceted role of the microbiome in the health of a host is partly due to the development of informative animal models. In conjunction with the rapid advancement of sequencing and metagenomic pipelines, these models have enabled the design and execution of experiments that have delineated the mechanisms by which the microbiome helps shape the host's physiology and propensity to disease.

These animal models are also vital in the development of novel investigative and therapeutic synthetic biology tools where the eventual aim is to design systems that are robust enough to function in the complex *in vivo* gut environment. Characterisation of tools such as bacterial biosensors (see Chapter 3) *in vivo* as opposed to just in culture is critical for their iterative development and eventual use in a clinical setting.

4.1.1 Current Model Systems for Studying the Intestinal Microbiota

Although there can be significant interindividual variation observed within species, a broad trend exists in the composition of the intestinal microbiota, particularly at the phylum level [23]. Experimental model based systems including mice, insects and fish continue to provide valuable and striking insights into how the microbiota interacts with the host in the gut. The abundance of historic biological tools developed for use

in these systems provide opportunities to perturb, engineer, and study this interplay with a level of experimental control that is not possible in humans. Several factors within the organism's anatomy and physiology dictate the suitability of the model for the investigative experiment. For instance, whether the intestines are anaerobic, as is the case for mice and zebrafish, or aerobic, as is the case for *Drosophila* [162].

Due to their high reproductive capacity, genetic tractability and vast abundance of tools, *Drosophila* has been used to broaden our understanding of cellular and developmental biology for decades. Recent studies have shown that they have a reduced microbiota consisting of less than 30 species that are both aerobic and culturable [163]. This provides a potentially valuable symbiont model where the microbial community can be easily engineered in a highly genetically malleable host. A recent unexpected finding demonstrated that *Drosophila* prefer to mate with flies with similar intestinal microbes [164]. After initial results linking diet to their mating preferences, researchers discovered that this could be sufficiently manipulated with antibiotics and the introduction of a single symbiont strain.

The zebrafish offers another tractable model but with a more complex physiology and diverse microbiota [23]. The optical transparency and rapid development of embryos and larvae enable a host with powerful genetic and chemical screens. As a vertebrate, the zebrafish bears an adaptive immune system; a vital and complex layer in the interplay between the host and the intestinal microbiota. In light of this, it has even been used as a model of inflammatory bowel disease [165].

The mouse is by far the most widely used model to study the intestinal microbiome [166]. As well possessing similar taxonomic levels of the microbiota to humans, the mammalian physiology offers a closer mimicry of the interaction between the gut and the host's diet, genetics and immune system. There is extensive knowledge of their genetic background with custom genotypes and phenotypes. A particularly powerful capability of this model is the use of humanised gnotobiotic mice where germ free mice are inoculated with a human gut microbiota sample. This leads to a mimicry of the human gut microbiota phylogenic composition and allows researcher to investigate perturbations in a human-like system [167, 168, 169]. Almost every synthetic biology approach to engineer or monitor the intestinal microbiota *in vivo* has been demonstrated with the mouse model [64, 65, 67, 91, 160, 68]. However, it is this very complexity

of the mouse intestinal microbiome that provides doubt over the suitability of the model to some investigative questions. While our understanding of this interplay is still significantly lacking, the complexity in the model could mask findings and prevent the ability to ask precise fundamental questions between the host and the intestinal microbiota. This is particularly important considering that the majority of the cross-talk between the gut microbiota and the host is host-specific [162]. Furthermore, there is a considerable problem with non-reproducible findings due to genetic variability, handling techniques, mouse vendors and diet [170, 171]. Unlike other models, the anaerobic conditions of the mouse intestines also prevents the use of oxygenase reporters such as fluorescent or luminescent proteins for live spatiotemporal information *in vivo*.

The cost, time and specialist skillsets needed to run mammalian models for these studies struggle to complement the underlying approach of the 'design, test and build cycle' that is fundamental in the field of synthetic biology (see Section 1.2). In light of this, there is a desire to use models that are compatible with this approach but are still robust and informative enough to ask elucidative questions. Considerations include interactions with the immune system, throughput and timescale of experiments and regulatory hurdles (Figure 4.1).

	Advantages	Disadvantages
Drosophila	Powerful host genetic system; simple culturable microbiota	No adaptive immune system
Zebrafish	Powerful host genetic system; adaptive immunity	Very simple digestive track
C.elegans	Powerful host genetic system; innate immunity; simple culturable microbiota	Very simple digestive track
Mice	Many similarities to the human digestive tract; controlled environment	Limited throughput; limited controls, expensive
Humans	Most clinically relevant	Limited experiment controls

Figure 4.1: Table of considerations in choosing a model organism for microbiome studies. Adapted from [23].

4.1.2 *C. elegans* as a Model for Host-Microbiota Studies

Caenorhabditis elegans is a transparent nematode worm 1mm in length that lives in temperate soil environments and feeds on soil bacteria. It was the first multicellular organism to have its whole genome sequenced in 1998 [172] and the combination of a short 2-3 week lifespan, transparent cell wall and genetic tractability has enabled it to become a biological workhorse used to extensively study energy metabolism, immunity and ageing [173].

While the *C. elegans* worm demonstrates a diverse microbiota in the wild [174], it

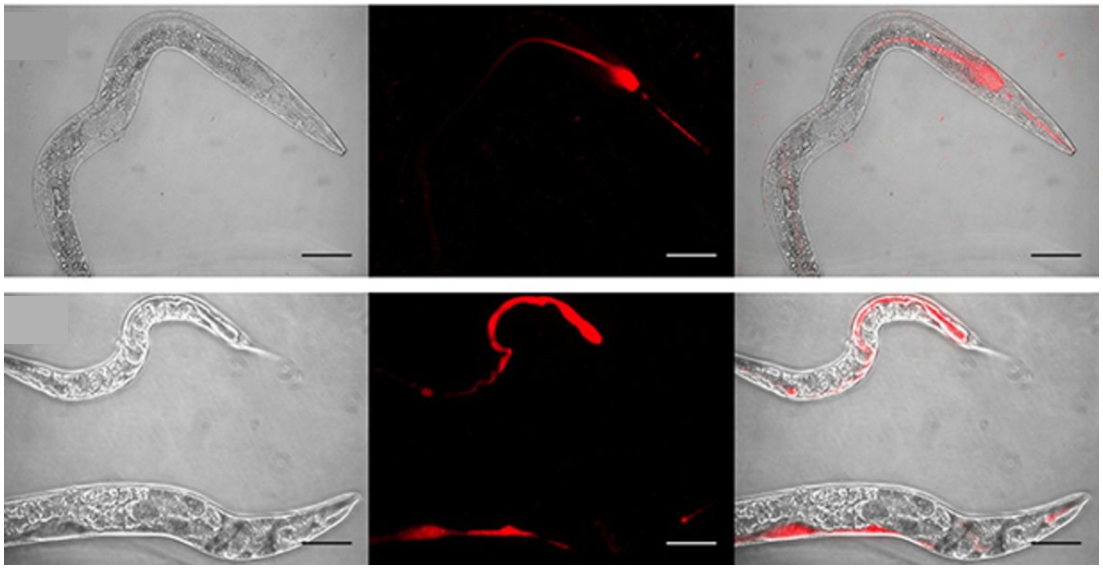

Figure 4.2: Representative image of *C. elegans* after feeding on *E. coli* OP50 expressing a tomato red fluorescent protein (Adapted from [179]). Red indicates the shape and length of the intestines. Left is brightfield, centre is fluorescent and right is merged. Scale bars are 50μm.

is typically monoxenically grown with one species in the lab. This enables researchers to easily create and maintain a defined intestinal microbiota. The intestines are one of the major organs and constitutes roughly a third of their somatic mass [175]. The transparent cell wall and aerobic lumen also enable the simple visualisation of fluorescent proteins and markers (Figure 4.2). Even though it is not as advanced as the adaptive system observed in vertebrates, the worm possesses an innate immune system which is used to regulate the intestinal bacterial load as it ages [176]. Peak transition of bacteria through the intestines can be as short as 2 minutes during young adulthood, although they eventually colonise the lumen in a number of days as the worm ages [177]. The ability to create a powerful yet simple and defined host-microbiota model system is leading to a growing number of investigations using *C. elegans*.

A recent demonstration of the potential power of *C. elegans* as a microbiome model was done using high-throughput screens to elucidate the complexity underlying host-microbe-drug interactions and inter-individual variability [178]. Using *C. elegans* and *E. coli*, researchers showed that bacterial metabolism could boost or suppress the effects of a common cancer drug through microbial metabolic drug interconversion.

More recently, *C. elegans* was used as a live *in vivo* model to demonstrate a synthetic biology approach to prevent gut infection with an engineered probiotic *E. coli* Nissle

1917 (EcN) strain [135]. After designing and characterising a sense-and-kill synthetic circuit in EcN, the researchers were able to show that the engineered EcN strain could colonise the worm to prevent a *Pseudomonas aeruginosa* gut infection. Furthermore, the use of *C. elegans* and fluorescent proteins in EcN enabled them to visualise this approach in a spatiotemporal manner *in vivo*. This work demonstrates that it is indeed possible to formulate and test synthetic biological approaches to engineering the intestinal microbiome with the use of *C. elegans*.

Recent work with *C. elegans* and their bacterial diets further uncovered the role of certain metabolites in worm gene expression and lifespan [180]. Using system biology approaches, it was shown that the bacterial derived vitamin B12 not only affects worm development but also prevents a toxic build up of propionate in the intestines.

The discussed characteristics of *C. elegans* could pave the way for further investigations into host-microbiome interactions in the intestines with synthetic biology. EcN bacterial sensors could also be be characterised *in vivo* using *C. elegans* as a model system.

4.2 Aims

The emerging need for both convenient and robust tools to investigate the relationship between the host and microbiome has resulted in a growing interest in the use of *C. elegans* as a live animal model. This piece of work aimed to investigate whether *C. elegans* can indeed be used as a live animal model for characterising an inducible EcN bacterial biosensor *in vivo*. These aims included:

1. Developing an inducible bacterial sensor system that can be detected quantitatively *in vivo*.

2. To establish whether *C. elegans* can develop and grow solely on EcN.

3. The development of an induction assay whereby the signal of an EcN biosensor can be detected and quantified from the *C. elegans* intestines *in vivo*.

4.3 Materials and Methods

4.3.1 Media and Strains

Lysogeny broth (LB) media and agar was used during propagation and cloning of bacteria. Assays were carried out in LB or M9 minimal media supplemented with 1mM thiamine hydrochloride, 0.4% glycerol, 0.2% casamino acids, 2mM $MgSO_4$ and 0.1mM $CaCl_2$. When antibiotic selection was applied, kanamycin was used at 25μg/mL and streptomycin was used at 50μg/mL.

All DNA manipulations were performed in *E. coli* DH5α (NEB). All sequences were confirmed via Sanger sequencing (Source Bioscience, UK). All final induction assays were performed in *E. coli* Nissle 1917 (EcN) (Prof. Ian Henderson from the University of Birmingham, UK). Chemically competent EcN was made using standard protocols. Briefly, this involved diluting an overnight EcN LB culture 1:100 into 50ml of fresh LB media and grown at 37°C in a shaking incubator to an OD_{600} of 0.25 to 0.3. The culture was then chilled on ice for 15 minutes and then centrifuged for 10 minutes at 5000g and 4°C. The medium was then discarded and the cell pellet resuspended in 30ml of cold 0.1M $CaCl_2$ before being kept on ice for a further 30 minutes. This suspension was then centrifuged for 10 minutes at 5000g and 4°C. The supernatant was once again removed and the cell pellet was resuspended in 3ml of cold 0.1M $CaCl_2$ solution with 15% glycerol. The final cell suspension was then aliquoted and flash frozen before being stored at -80°C.

4.3.2 Plasmids and Cloning Methods

Ratiometric sensor assay systems were designed with a constitutive mCherry reporter plasmid and a separate GFP reporter plasmid. The GFP reporter plasmids consisted of the OG241_GFP constructs previously described in Section 3.4. This included the promoterless OG241_GFP plasmid (Figure 3.4) which consisted of an upstream multiple cloning site, a dasher GFP reporter gene, a pUC high copy origin-of-replication and a kanamycin resistance cassette (Oxford Genetics, UK). As a positive control, the strong constitutive OXB19 promoter (Oxford Genetics, UK) was placed upstream of GFP to derive OXB19_GFP. In addition to these constructs, an isopropyl β-D-1-thiogalactopyranoside (IPTG) inducible GFP sensor (pLac_GFP) was created. Briefly,

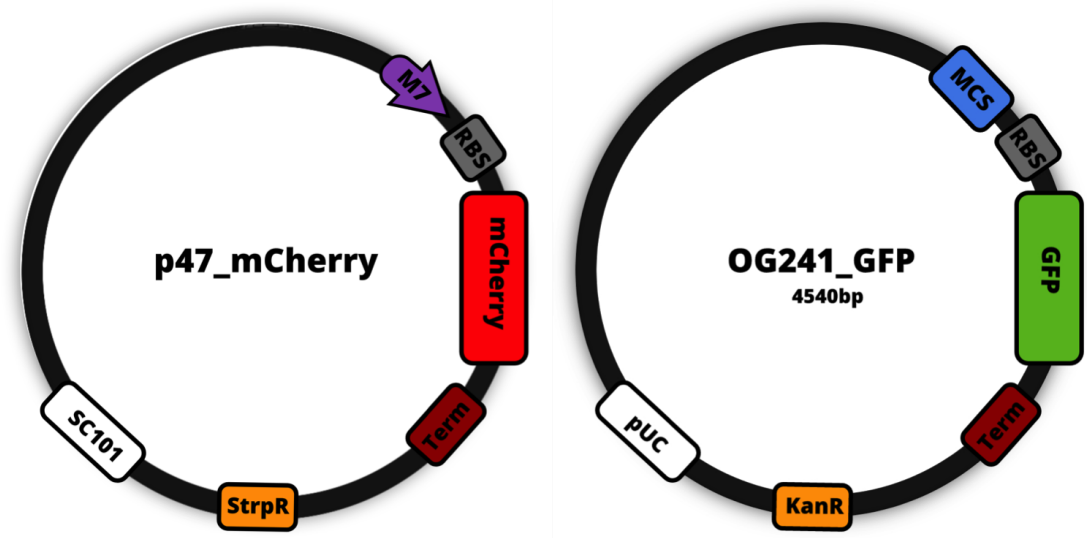

Figure 4.3: Graphical representation of constitutive mCherry plasmid and promoterless OG241_GFP control plasmid.

Strain Name	Host Bacterium	Plasmids	Plasmid Source
EcN_OG241_GFP_mCherry	*E.coli* Nissle 1917	OG241_GFP_pUC_Kan^R (promoterless control) p47_M7_mCherry_SC101_Strp^R	Oxford Genetics, UK
EcN_OXB19_GFP_mCherry	*E.coli* Nissle 1917	OXB19_GFP_pUC_Kan^R (constitutive control) p47_M7_mCherry_SC101_Strp^R	This work
EcN_pLac_GFP_mCherry	*E.coli* Nissle 1917	pLac_GFP_pUC_Kan^R (inducible control) p47_M7_mCherry_SC101_Strp^R	This work

Figure 4.4: Table of strains used.

this was created by PCR cloning the region containing the lacI protein, tetR promoter and trc promoter from pKDL071 [181] and adding SpeI and EcoRI flanks. This region was then cloned into the MCS of OG241_GFP with the appropriate restriction enzymes. The p47_mCherry construct was created from pSEVA471, a 3120bp plasmid based on the pSEVA format [182]. This involved using pacI and SpeI to clone out the constitutively expressed mCherry fragment from pTn7-M-pEM7-mCherry and ligate into the empty MCS of pSEVA471 to derive a low copy SC101 plasmid with streptomycin resistance and strong constitutive mCherry expression under the pEM7 promoter (Figure 4.3). EcN was then simultaneously transformed with p47_mCherry and the respective GFP plasmid via heat-shock methods to give the strains listed in Figure 4.4.

4.3.3 Induction Assays in Liquid Culture

All induction assays were performed over 16 hours at 37°C and 350RPM at a volume of 750μL in sterile autoclaved 96-well deep square well (2.2mL) polypropylene plates

(BRAND®, Sigma-Aldrich, UK) sealed with Breathe-Easy sealing membranes (Sigma-Aldrich, UK). Induction was calculated through flow cytometry analysis. IPTG was used to induce pLac_GFP. Concentration range induction assays were performed by diluting triplicate overnight cultures 1:500 into LB or supplemented M9 media with the appropriate inducer concentration. For induction assays in growing phase, overnight cultures were grown in triplicates and diluted 1:500 into media with the appropriate inducer. For induction assays in stationary phase, overnight cultures were grown in triplicates and spun down at 4000g before removing the supernatant and resuspending in fresh media with the appropriate inducer.

4.3.4 Growth Rate Assays

Overnight cultures were grown in triplicates and diluted 1:500 into LB media with the appropriate inducer. A sterile autoclaved 96-well deep square well (2.2mL) polypropylene plate (BRAND®, Sigma-Aldrich, UK) was then filled with 16 replicates of 750μL of each culture. The plate was then sealed with a Breathe-Easy sealing membrane (Sigma-Aldrich, UK) and grown at 37°C and 350RPM for 16 hours. While maintaining the membrane seal for the rest of the plate, 750μL from each strain-culture was taken hourly and the OD_{700} was recorded on a WPA CO8000 Cell Density Meter (Biochrom). OD_{700} was measured instead of OD_{600} to minimise the impact of mCherry fluorescence on the readings [183].

4.3.5 Flow Cytometry Analysis and Plotting

Flow cytometry was performed on an Attune NxT Acoustic Focusing Cytometer with Attune NxT Autosampler (Thermo Fisher Scientific, UK). 1μL of the appropriate strain culture was transferred into 200μL of PBS in a shallow polystyrene 96-well plate. The Attune NxT Autosampler was used to record 10,000 events for each sample with 4 washes between each one. GFP was excited using the blue laser (488nm) and was detected using a 530/30nm bandpass filter. mCherry was excited with the yellow laser (561nm) and was detected using a 620/15 bandpass filter. In order to prevent operator bias associated with manual drawing of gates and speed up the analysis of samples, a computational pipeline called autoGate was developed by Alexander Fedorec in the Barnes Lab (github.com/ucl-cssb/autoGate) to automate the gating of singlet bacteria

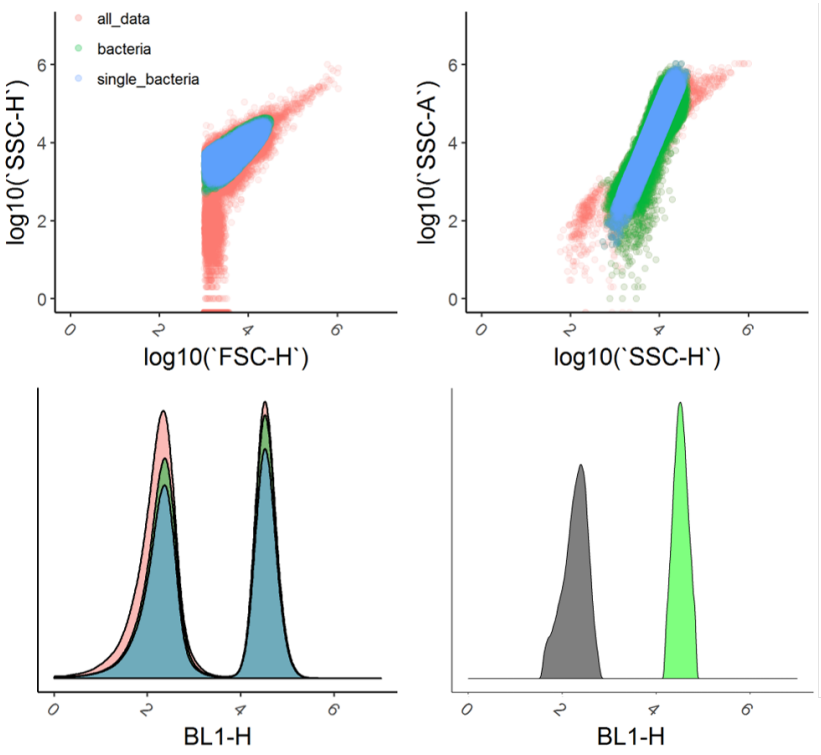

Figure 4.5: autoGate clustering and trimming of flow cytometry data.

while excluding background debris and bacterial doublets. Briefly, the method fits mixture models of one, two and three clusters to the forward-scatter versus side-scatter data. Using integrated completed likelihood (ICL) [126], the number of clusters that best fits the data is calculated and the cluster centred closest to the expected bacterial population coordinate is taken. A linear model is then fitted to the side-scatter-height versus side-scatter-area data and points falling too far away are removed as doublets. The levels of trimming are shown in Figure 4.5.

All plots were made using the flowCore and ggplot2 R packages. Non-linear least squares (nls function in R) curve fitting was used to fit a line to induction plots. This model approximates the non-linear function using a linear one and iteratively refines the parameter values to the best fit. Locally weighted least sqaure regression smoothing (loess function in R) was used to fit lines on EcN growth curve plots. This uses a local regression model fit to the points to create a smooth line. Relative fluorescent units (RFU) were shown as mean averages along with the standard error of the mean. R was also used for all statistics. GFP sensor induction was calculated as a ratio of median GFP fluorescence to median mCherry fluorescence (GFP:mCherry). The ratio of GFP:mCherry was calculated by dividing the median GFP fluorescence (x) by the

median mCherry fluorescence (y) (Equation 4.1). The standard error of the ratio (σ_R) was calculated with Equation 4.2 where s_x is the standard error x and s_y is the standard error of y.

$$R = \frac{x}{y} \tag{4.1}$$

$$\sigma_R^2 = R^2((\frac{s_x}{x})^2 + (\frac{s_y}{y})^2) \tag{4.2}$$

4.3.6 *C. elegans* Strains and Handling

All *C. elegans* experiments were carried out in the wild-type lab strain N2 Bristol (provided by the Caenorhabditis Genetics Center, USA). Unless stated otherwise, worms were maintained and raised at 20°C on nematode growth medium (NGM) seeded with *E. coli* OP50, an auxotroph lab strain whose growth is limited on NGM.

Adult worms were maintained and passaged according to normal protocols. Briefly, this involved seeding NGM agar plates with 150μL of overnight *E. coli* OP50 culture and incubating for 48 hours at 20°C to create a bacterial lawn for food. Five to six L4-stage worms were picked and transferred to seeded NGM plates and incubated for 24 hours so that they become adults and start laying eggs. After 24 hours, the adult worms are removed from each plate and killed. The plates are incubated for a further 48 hours to enable the large number of eggs to hatch, feed on the bacterial lawn and become heavily pregnant with eggs.

After 48 hours, an egg prep was carried out to isolate the eggs from the pregnant worms. This involved washing NGM plates with M9 media to collect all worms and transferring to a falcon tube. Once settled, the M9 media was aspirated and the remaining worms were washed with 2mls of bleach and NaOH at a ratio of 7:8. The mixture was then vortexed for 3-4 minutes and then neutralised with 13mls of M9. The tube was then centrifuged for 3 minutes at 4000RPM and once again the M9 media was aspirated without disturbing the pellet. This wash was repeated twice more before the egg pellet was resuspended with 10mls of M9 media and transferred into an empty dish for 24 hours incubation. This incubation allows the eggs to hatch but since there is no food the larvae does not develop past the first larval stage (L1) and

provides an entirely synchronised population. After 24 hours incubation, 400 L1s were seeded on the appropriate bacterial NGM plate for experiments or re-passaging. Where described, worms were passaged as sterile and non-reproductive adults with the drug fluorodeoxyuridine (FUdR). This involved picking L4 worms and transferring them to seeded NGM plates coated with FUdR at a concentration of 20μM for at least 24 hours. This enables the maintenance of a synchronously ageing population of worms.

Individual EcN-NGM plates were prepared in the same manner as with *E. coli* OP50 but with an overnight antibiotic culture of the respective EcN sensor strain or control instead. After preparing the worms as previously described, synchronised 400 L1 stage worms were transferred to NGM plates seeded with the respective EcN strain. These included EcN_OXB19_GFP_mCherry and EcN_OG241_GFP_mCherry as positive and negative controls, respectively. The inducible EcN_pLac_GFP_mCherry was used to investigate the sensor assay. After 48 hours of growth on the respective EcN-NGM plates, 45-50 L4 worms were picked and transferred to FUdR coated NGM plates seeded with the same EcN strain as before. Adult worms were picked and transferred to fresh FUdR coated EcN-NGM plates every 3-4 days.

4.3.7 EcN Biosensor Induction Assays in *C. elegans*

Figure 4.6 gives a graphical representation of the induction assay. As the worms age, the peristaltic movements in their intestines decrease and they eventually become constipated while the bacteria proliferates in the gut [173]. Induction assays were carried out on 7 day old adult worms after being grown on NGM plates with EcN. 25 to 30 worms were picked from the respective EcN-NGM plates and transferred to either an unseeded plain NGM agar plate (without bacteria) or an unseeded NGM agar plate (without bacteria) containing 1mM of IPTG. Plates were then stored at 20°C for the duration of the assay. After 8 hours induction, worms were picked from either the control NGM plate or the the assay plate and transferred to a separate plain NGM agar plate before being anaesthetised for imaging with 0.2% levamisole.

4.3.8 *C. elegans* Imaging and Biosensor Quantification

Anaesthetised worms were imaged with a Zeiss Axio Scope using GFP (excitation: 470nm; emission: 525nm) and mCherry (excitation: 560nm; emission: 630nm) filters.

Exposure times were set at 500ms for each and laser intensities were kept constant. Images were acquired using the Zen software and analysed using FIJI. For both GFP and mCherry images, the background was subtracted with a rolling ball radius of a 1000 pixels. The mCherry channel was then used to manually draw a region of interest (ROI) identifying the worm intestines. Using the same ROI, the mean pixel density was measured for both mCherry and GFP channels. The two values were then used to derive the GFP:mCherry ratio for each worm imaged. Where appropriate, the Mann-Whitney U test used to demonstrate statistical significance. All plots were done with the ggplot2 package in R.

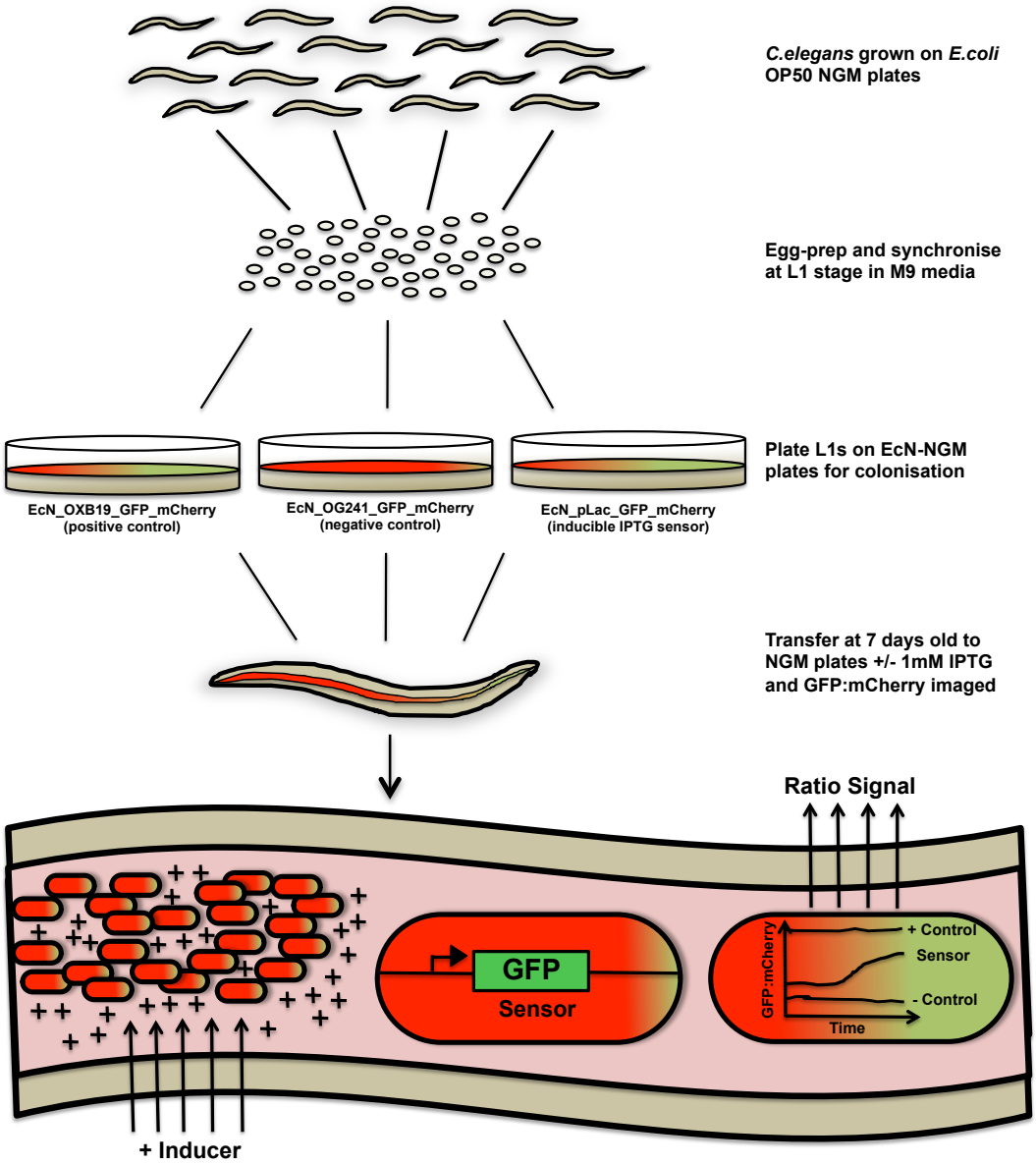

Figure 4.6: Graphical representation of induction assay protocol with EcN-NGM plates and sensor induction quantification using GFP:mCherry ratio.

4.4 Results

In order to quantitatively and accurately detect biosensor circuit signals in an *in vivo* environment, a dual-plasmid system was designed and created in EcN (Figure 4.7). This approach would enable the detection of the sensor circuit GFP signal irrespective of the surrounding environment. Here a constitutively expressing mCherry plasmid was designed and transformed into EcN in conjunction with the previously characterised sensors in Section 3.5. The GFP induction of the sensor circuit could be quantified by detecting the ratio of GFP signal to the constant mCherry signal.

Initial attempts to incorporate an mCherry fragment onto the same existing GFP sensor plasmids were unsuccessful in EcN. While initial cloning attempts were successful, protein expression and plasmid propagation were faulty. This was most likely due to the high burden of the plasmid leading to recombination. Using the dual plasmid approach instead, a variety of ratiometric constructs were designed and created in EcN using the p47_mCherry and OG241 plasmids (Figure 4.7).

EcN_OG241_GFP_mCherry was created as a negative control with the promoterless OG241_GFP plasmid. The EcN_OXB19_GFP_mCherry was created as a positive control with the constitutive OXB19_GFP plasmid. The IPTG inducible EcN_pLac_GFP_mCherry sensor strain with the pLac_GFP plasmid. All constructs were subsequently characterised in EcN.

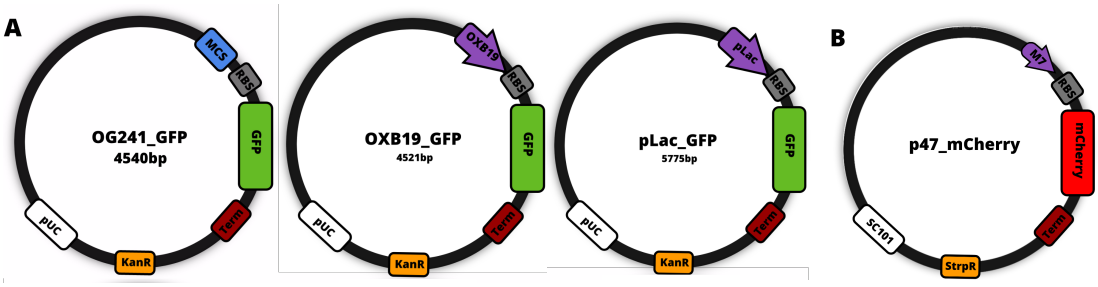

Figure 4.7: A) Plasmid maps of GFP based reporter sensors consisting of a promoterless OG241_daGFP plasmid, constitutive OXB19_GFP reporter and IPTG inducible pLac_GFP reporter. B) Constitutive p47_mCherry reporter.

4.4.1 GFP:mCherry Ratio Quantifies Sensor Induction *in vitro*

Figures 4.8 to 4.11 show that while mCherry expression was identical in both the negative promoterless and positive constitutive control strains, the maturation of the red protein took far longer than the maturation of GFP. This delay in median mCherry fluorescence over the time-assay indicates that while the production of mCherry may be constitutively and constantly driven by the promoter during cell growth, there will be delay in detection until the protein matures. In comparison, the fast maturation of GFP only results in a slight delay in detection during growth (Figure 4.11).

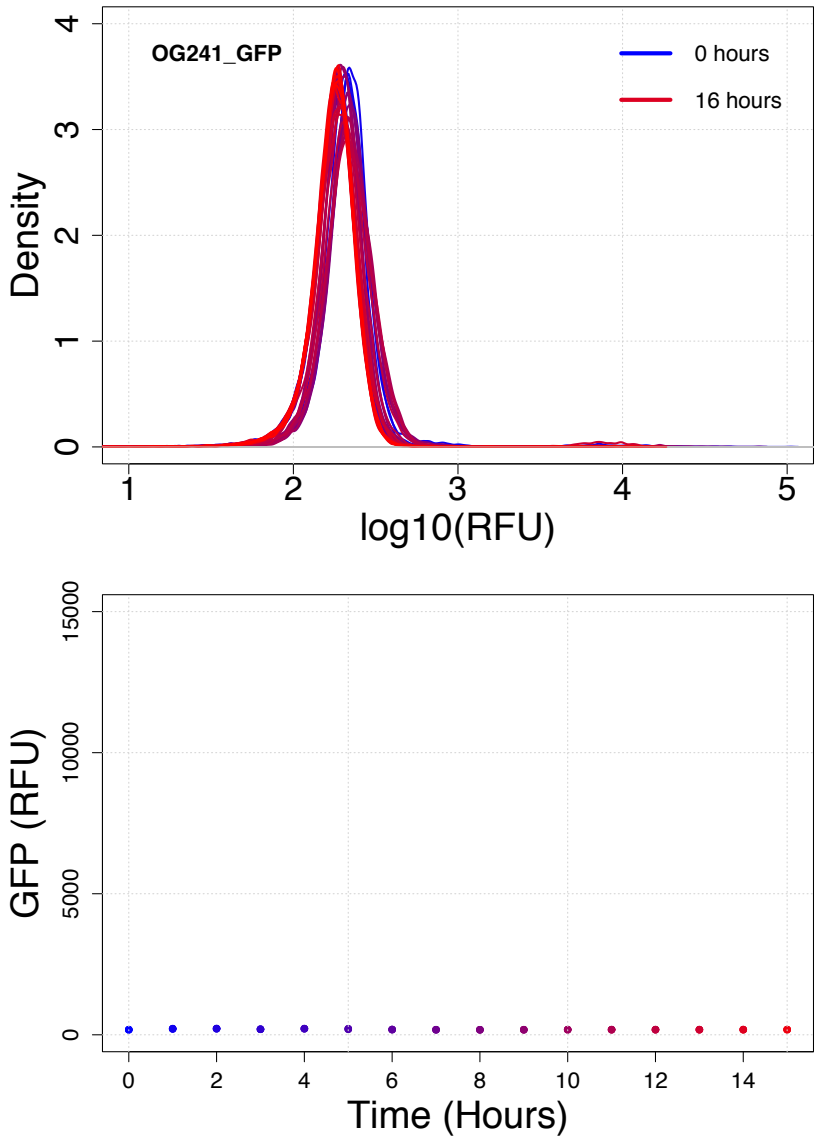

Figure 4.8: EcN_OG241_GFP_mCherry (negative promoterless GFP control) GFP induction over 15 hours in LB. Top, histogram density plot of GFP fluorescence over 15 hours growth. Bottom, median GFP fluorescence over 15 hours growth. Flow cytometry data with 10,000 events (n=3).

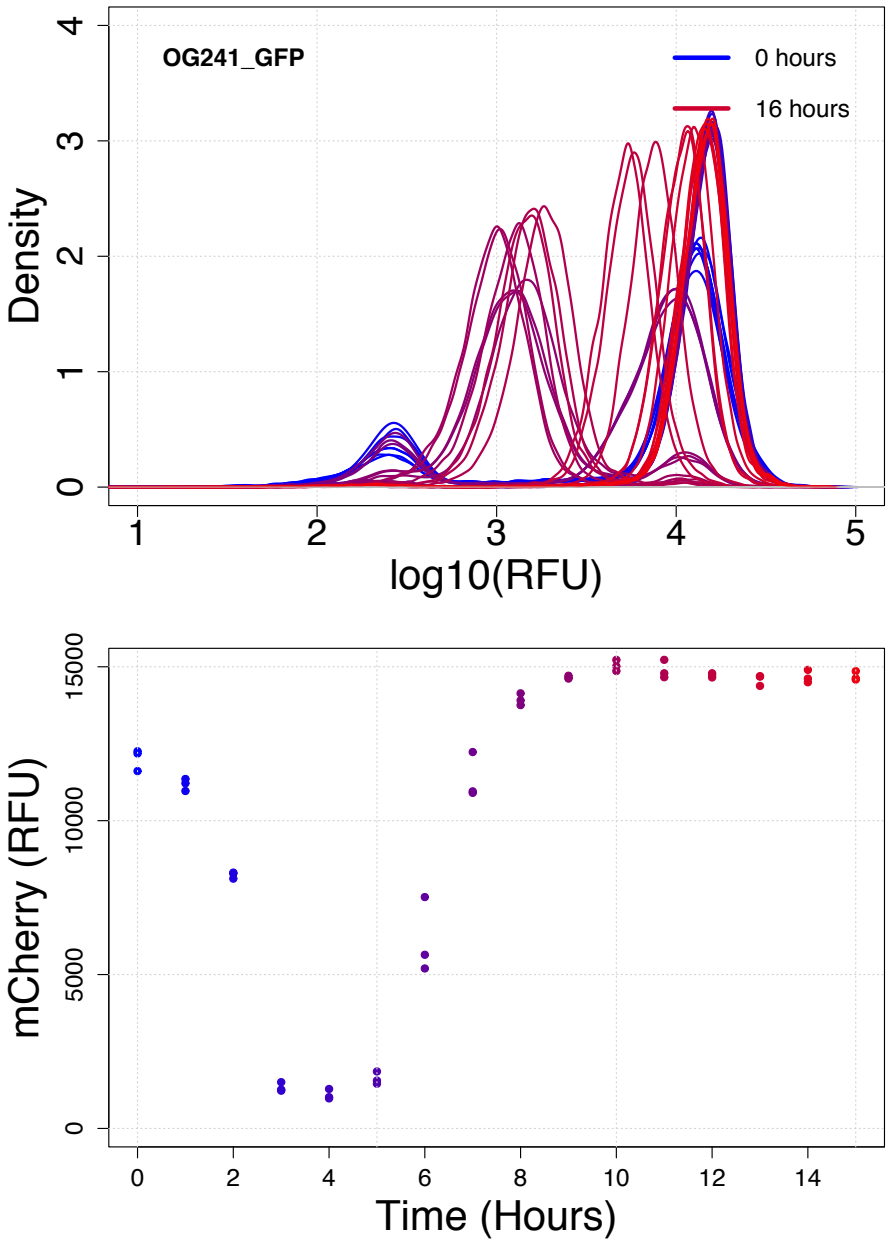

Figure 4.9: EcN_OG241_GFP_mCherry (negative promoterless GFP control) mCherry induction over 15 hours in LB. Top, histogram density plot of mCherry fluorescence after 15 hours growth. Bottom, median mCherry fluorescence after 15 hours growth. Flow cytometry data with 10,000 events (n=3).

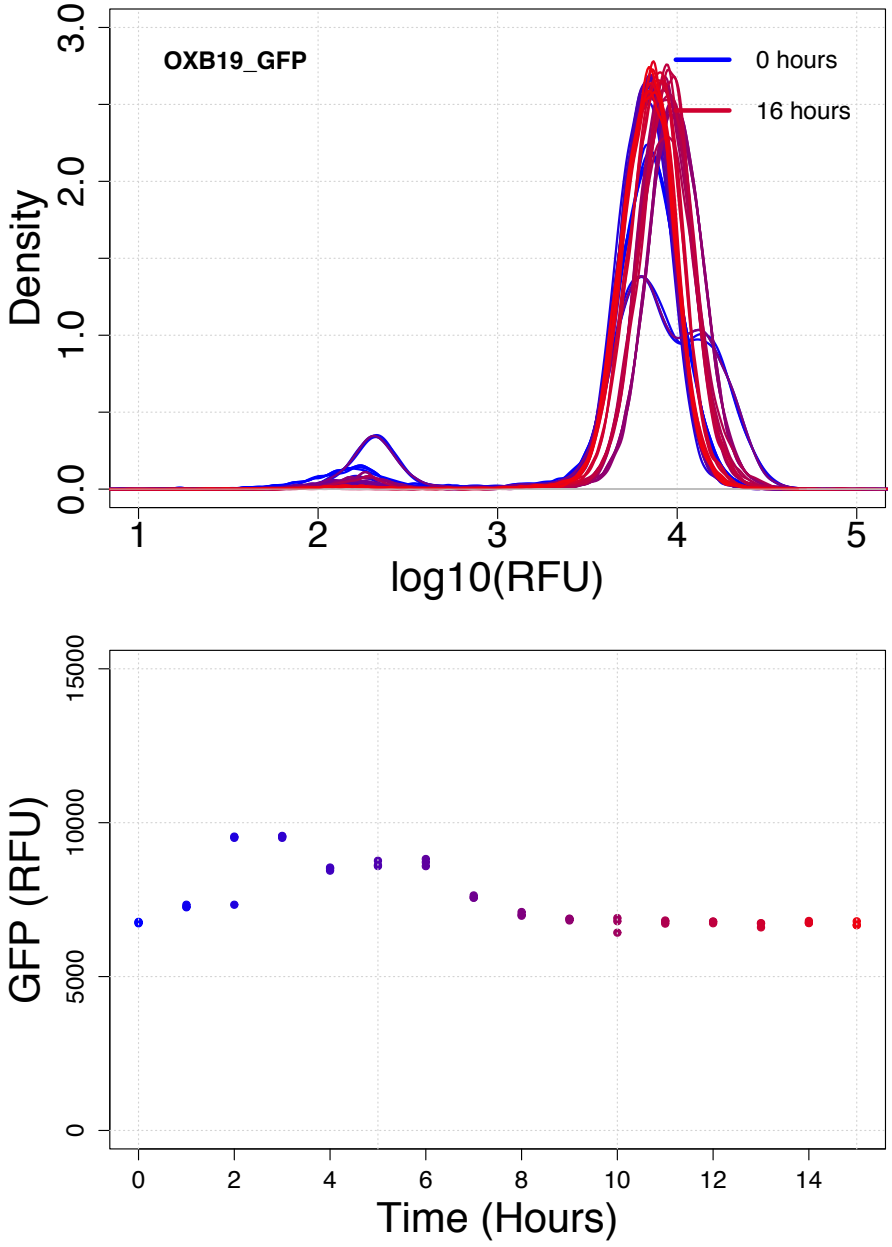

Figure 4.10: EcN_OXB19_GFP_mCherry (positive constitutive GFP control) GFP induction over 15 hours in LB. Top, histogram density plot of GFP fluorescence after 15 hours growth. Bottom, median GFP fluorescence after 15 hours growth. Flow cytometry data with 10,000 events (n=3).

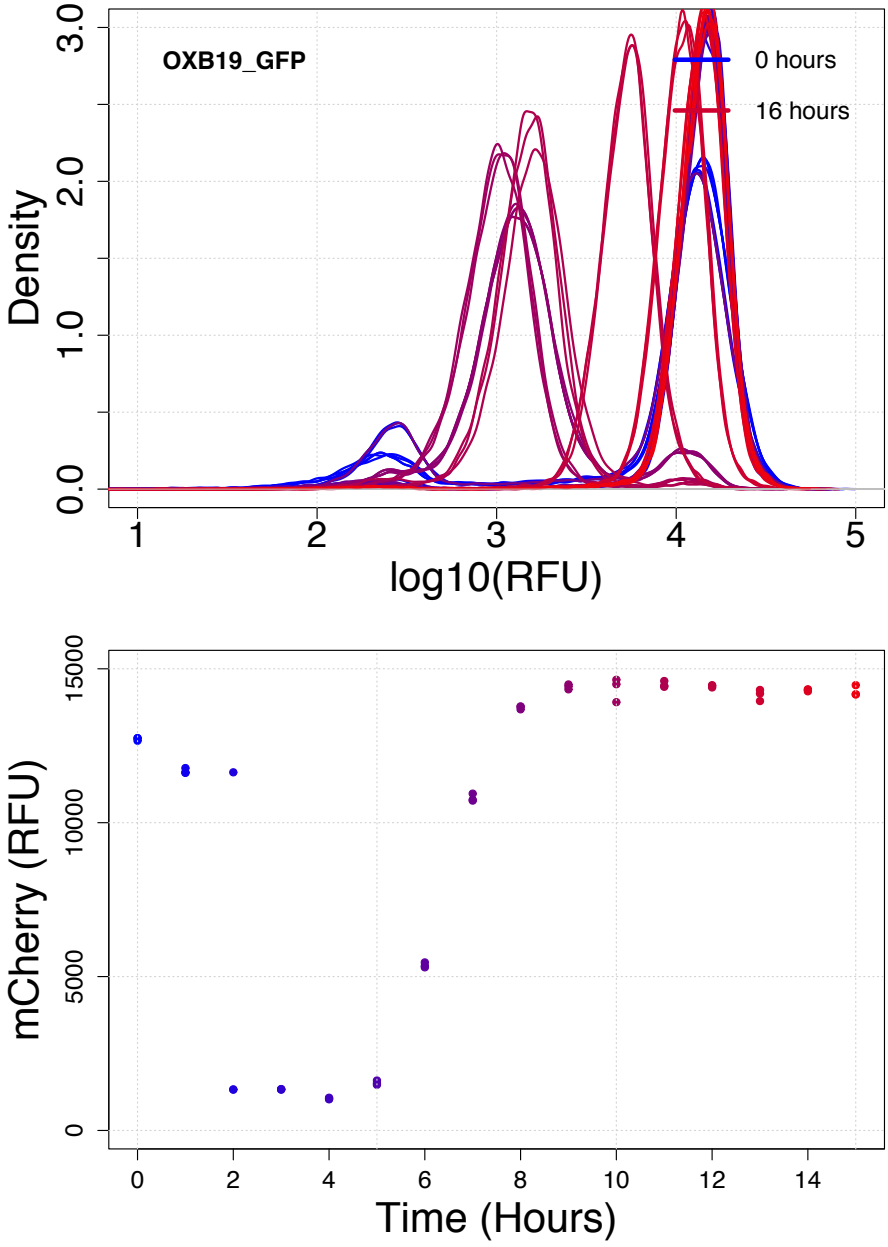

Figure 4.11: EcN_OXB19_GFP_mCherry (positive constitutive GFP control) mCherry induction over 15 hours in LB. Top, histogram density plot of mCherry fluorescence after 15 hours growth. Bottom, median mCherry fluorescence after 15 hours growth. Flow cytometry data with 10,000 events (n=3).

Even with the differences in maturation times, a distinctively higher GFP:mCherry ratio can be detected between the negative EcN_OG241_GFP_mCherry and the positive EcN_OXB19_GFP_mCherry control (0.0125±0.0001 compared to 0.471±0.004 at 15 hours of growth) (Figure 4.12). Due to the lag of maturation, the ratio of GFP:mCherry is particularly high during the logarithmic stages of growth (0 to 8 hours)(Figures 4.13 and 4.14). In line with this, the difference in ratio between the strains is also apparent at the stationary phase of growth when the OD700 is larger than 1.5 (Appendix Figure 5.9).

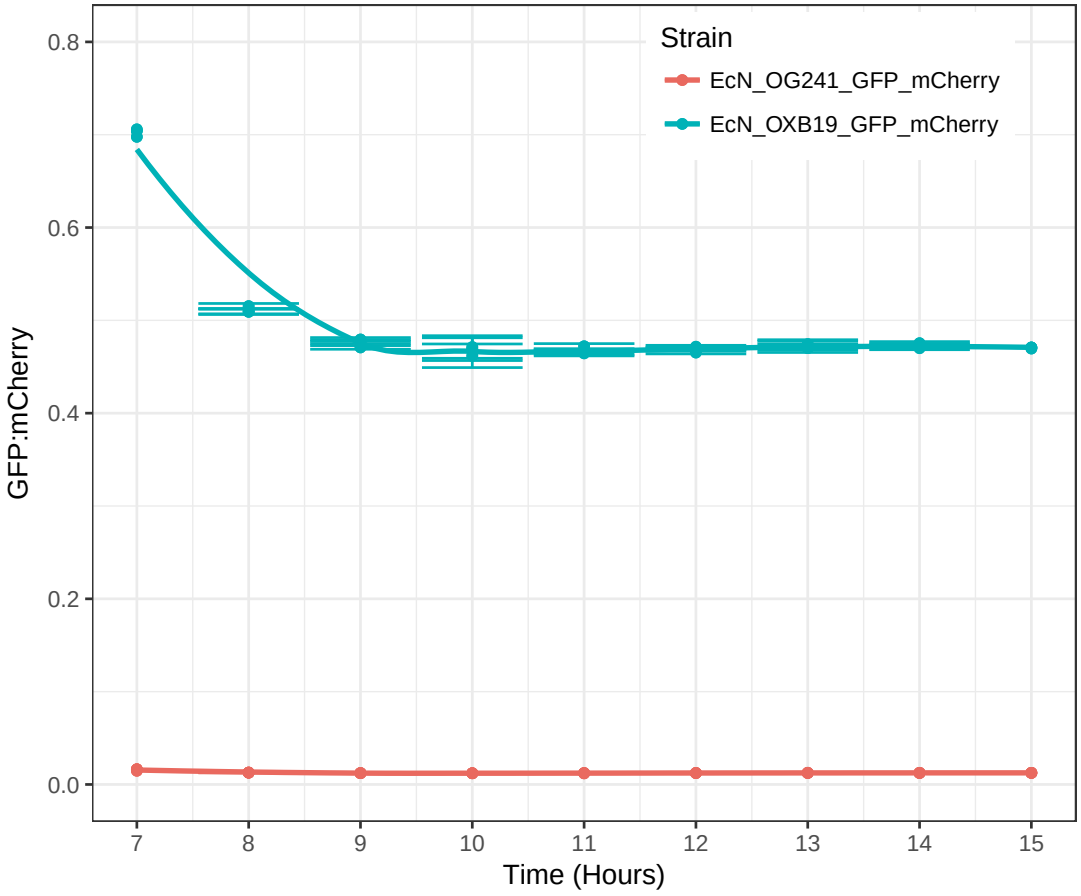

Figure 4.12: GFP to mCherry ratio in EcN_OG241_GFP_mCherry and EcN_OXB19_GFP_mCherry during growth in LB media from 8 to 15 hours. Ratio calculated using median fluorescence for each reporter from flow cytometry data with 10,000 events (n=3).

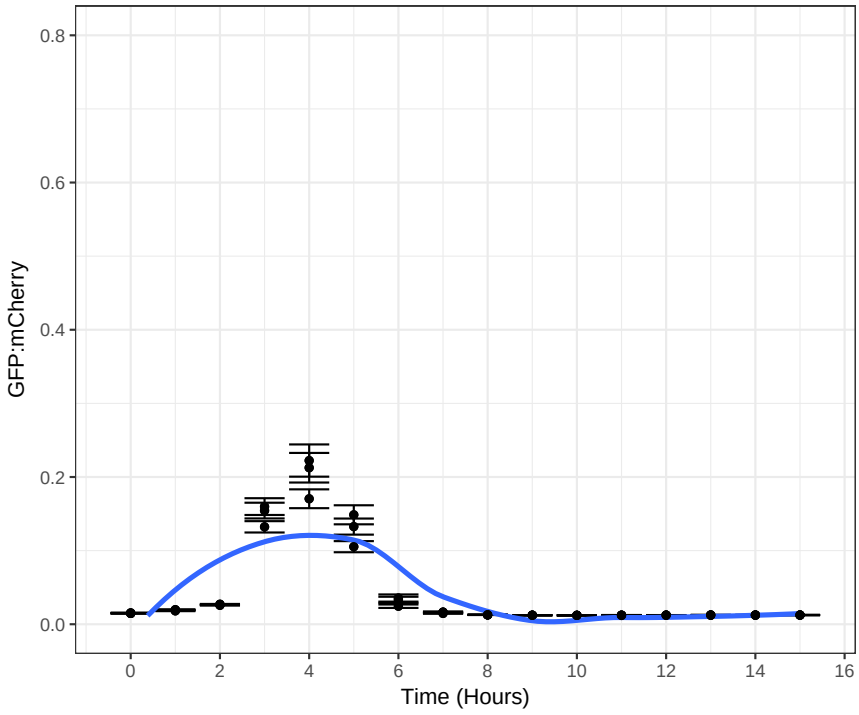

Figure 4.13: GFP to mCherry ratio in EcN_OG241_GFP_mCherry during growth in LB media for 15 hours. Ratio calculated using median fluorescence for each reporter from flow cytometry data with 10,000 events (n=3).

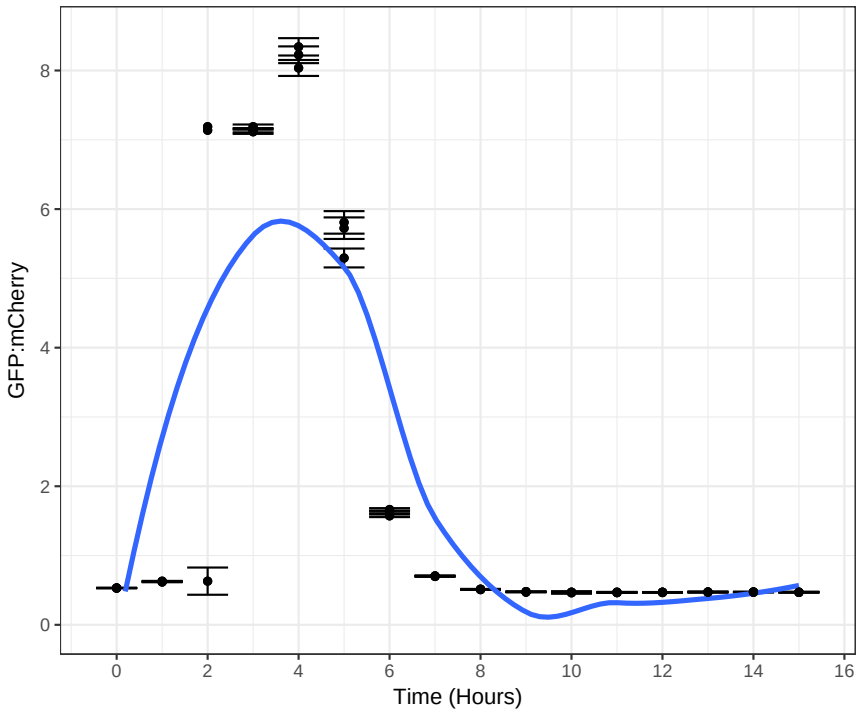

Figure 4.14: GFP to mCherry ratio in EcN_OXB19_GFP_mCherry during growth in LB media for 15 hours. Ratio calculated using median fluorescence for each reporter from flow cytometry data with 10,000 events (n=3).

Figures 4.15 and 4.16 show that increasing concentrations of IPTG can be used to achieve a maximum 25 fold increase in GFP fluorescence in EcN_pLac_GFP_mCherry with minimal impact on mCherry expression. Similar results were observed in induction with supplemented M9 media instead of LB (Figures 4.17 and 4.18). In a similar manner to the negative promoterless and positive constitutive controls, the uninduced EcN_pLac_GFP_mCherry strain demonstrated a lagged but steady level of mCherry expression over 15 hours (Figures 4.19 and 4.20).

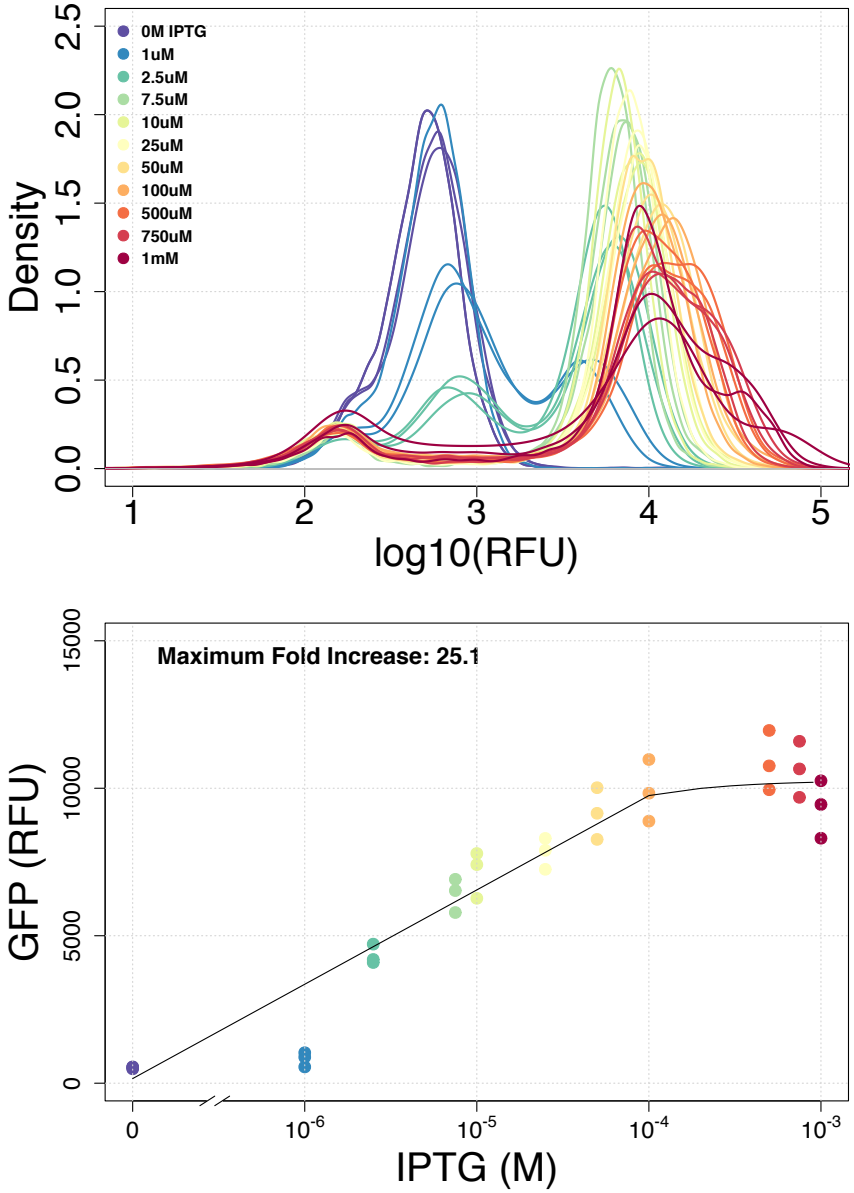

Figure 4.15: EcN_pLac_GFP_mCherry induction with IPTG in LB media. Top: histogram density plot of GFP fluorescence after 16 hours induction. Bottom: median GFP fluorescence after 16 hours induction. Flow cytometry data with 10,000 events (n=3).

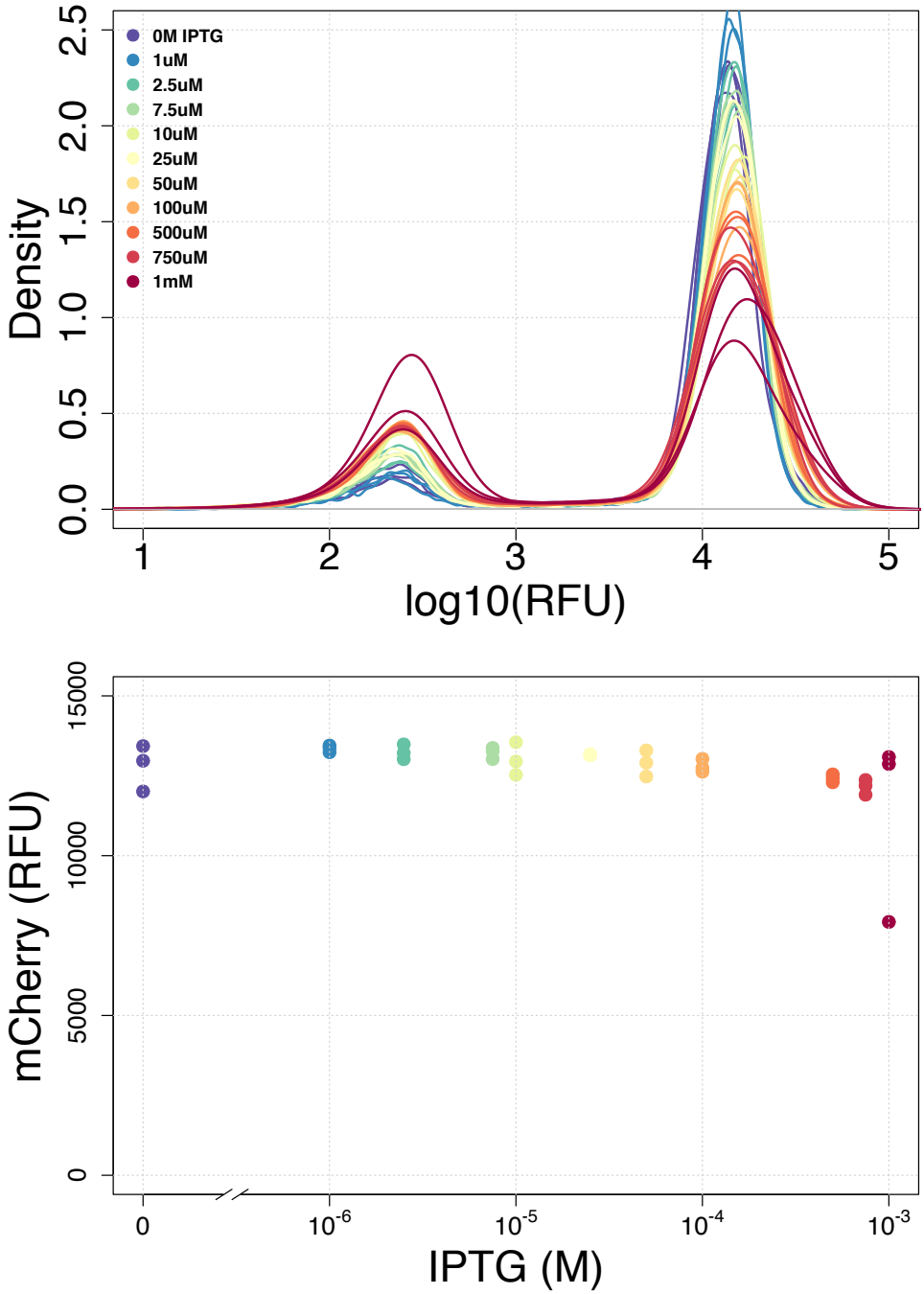

Figure 4.16: EcN_pLac_GFP_mCherry induction with IPTG in LB media. Top: histogram density plot of mCherry fluorescence after 16 hours induction. Bottom: median mCherry fluorescence after 16 hours induction. Flow cytometry data with 10,000 events (n=3).

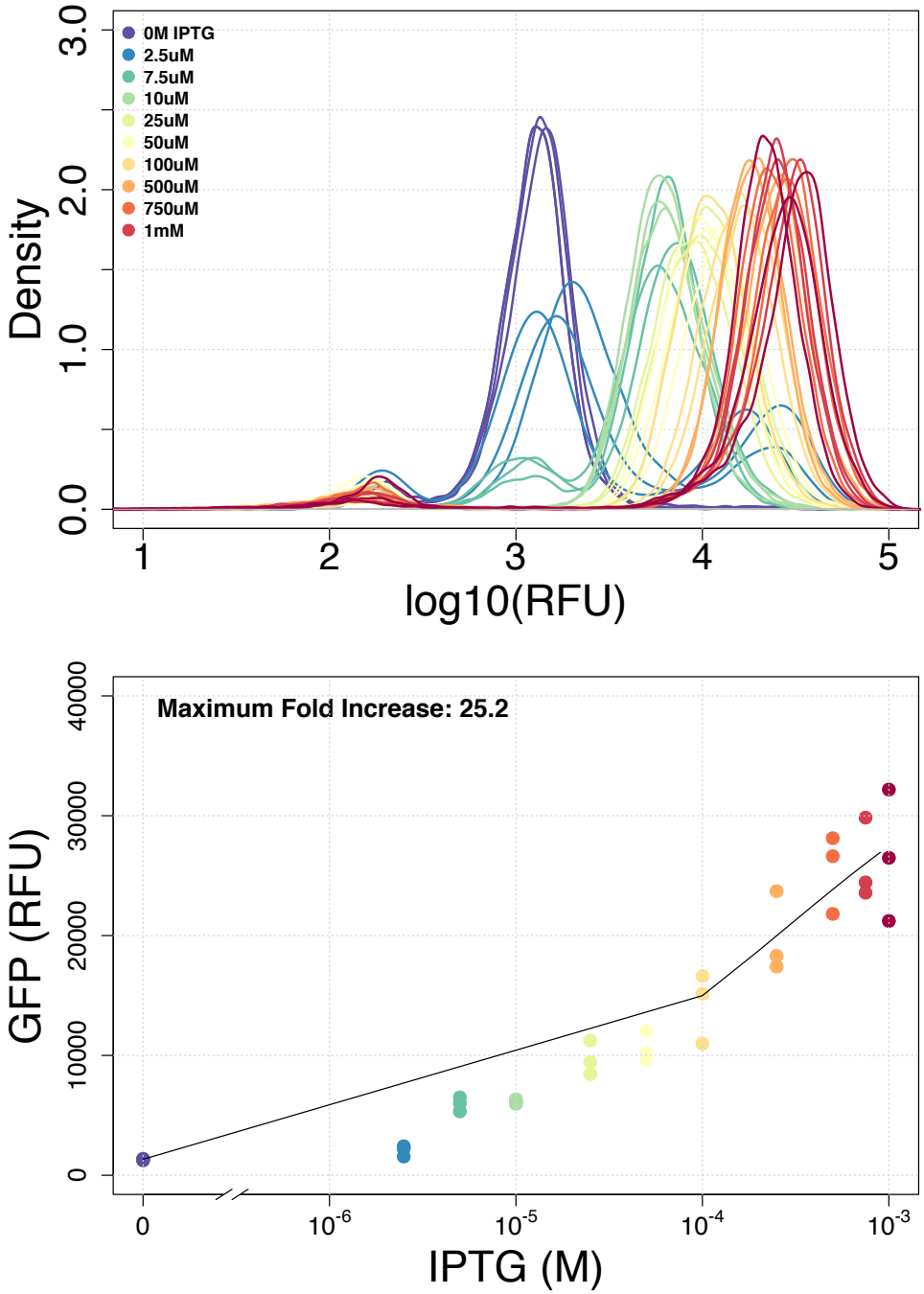

Figure 4.17: EcN_pLac_GFP_mCherry induction with IPTG in M9 media. Top: histogram density plot of GFP fluorescence after 16 hours induction. Bottom: median GFP fluorescence after 16 hours induction. Flow cytometry data with 10,000 events (n=3).

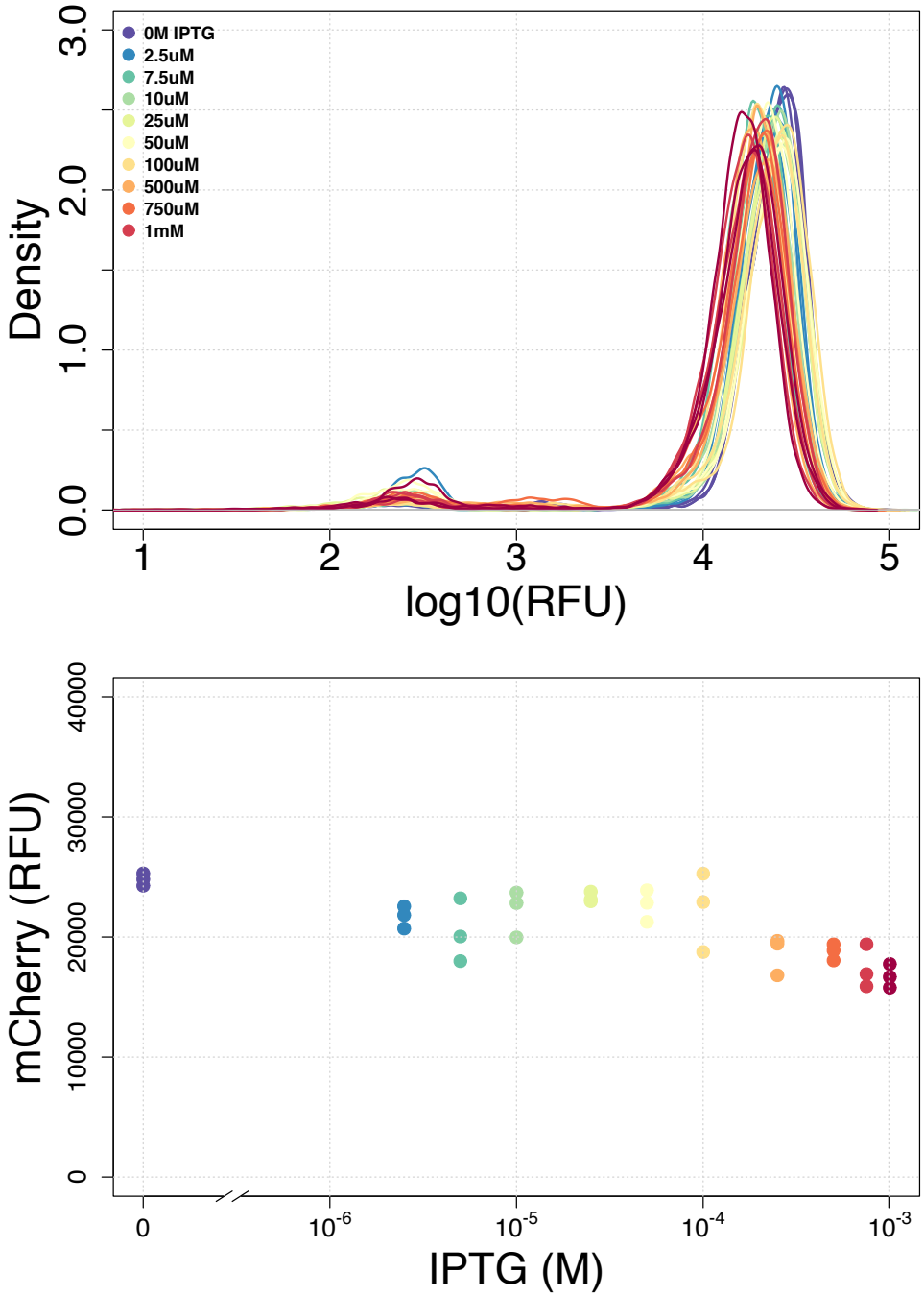

Figure 4.18: EcN_pLac_GFP_mCherry induction with IPTG in M9 media. Top: histogram density plot of mCherry fluorescence after 16 hours induction. Bottom: median mCherry fluorescence after 16 hours induction. Flow cytometry data with 10,000 events (n=3).

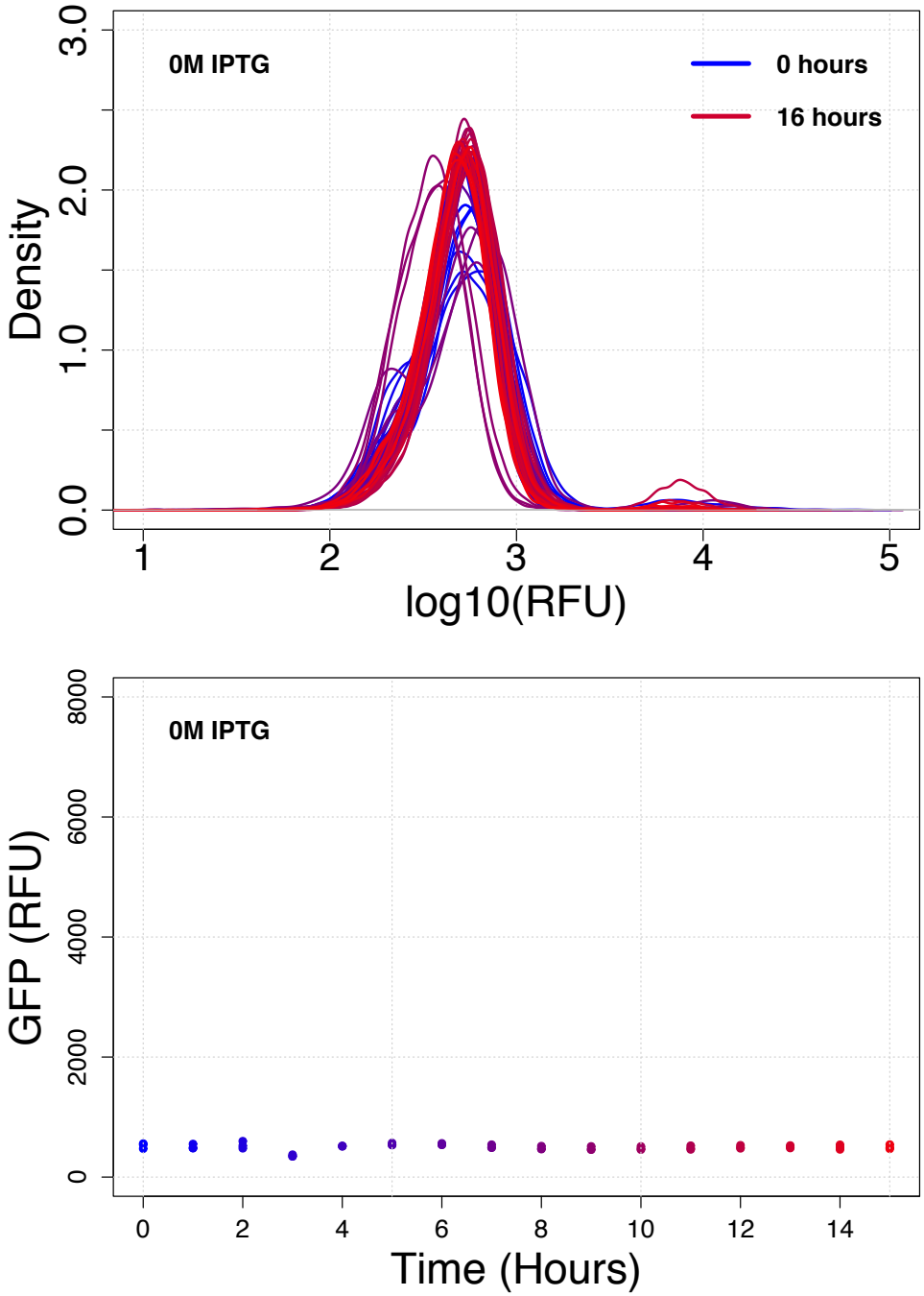

Figure 4.19: GFP expression in uninduced EcN_pLac_GFP_mCherry during 15 hours of growth in LB media. Top: histogram density plot of GFP fluorescence over 15 hours. Bottom: median GFP fluorescence over 15 hours. Flow cytometry data with 10,000 events (n=3).

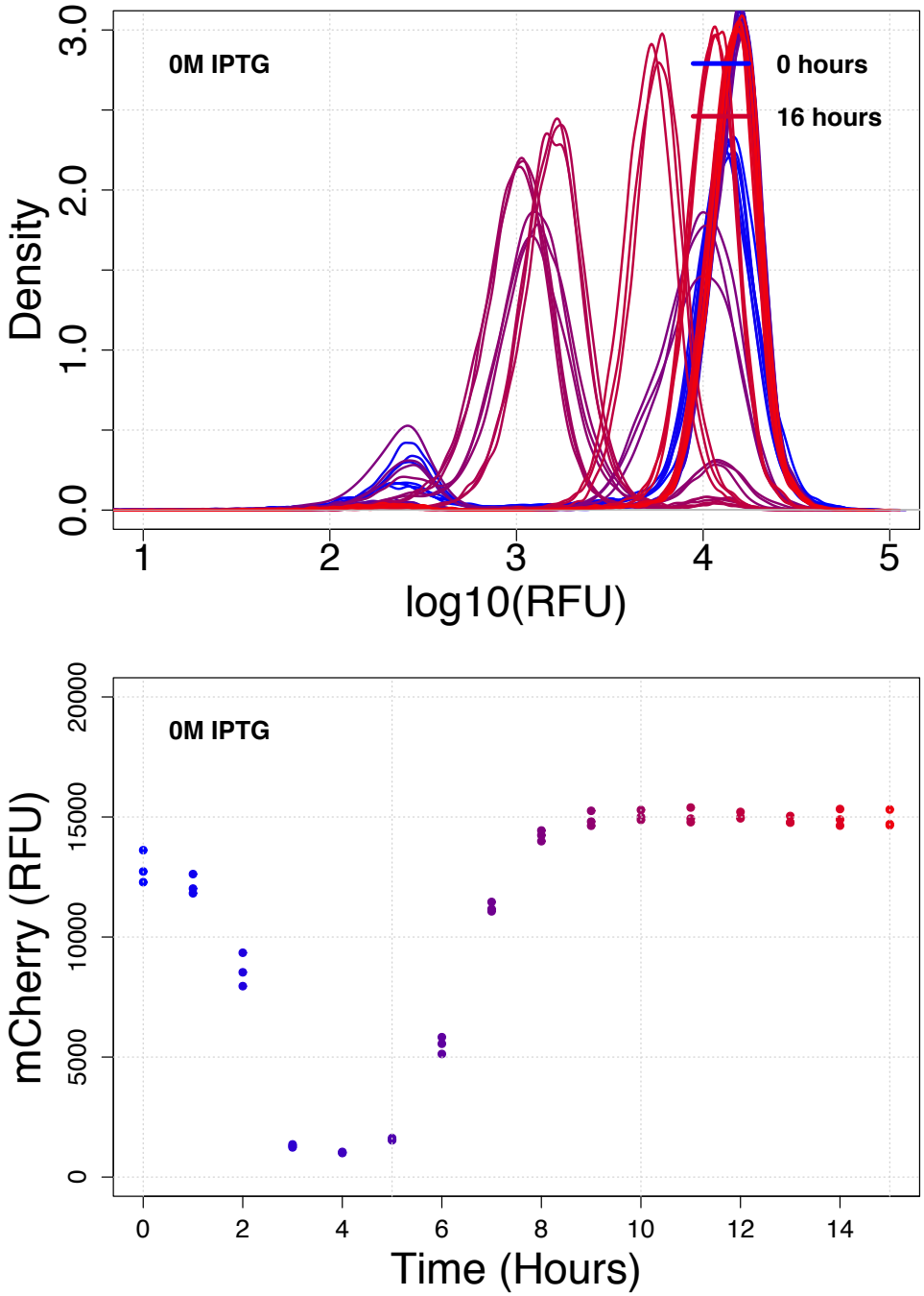

Figure 4.20: mCherry expression in uninduced EcN_pLac_GFP_mCherry during 15 hours of growth in LB media. Top: histogram density plot of mCherry fluorescence over 15 hours. Bottom: median mCherry fluorescence over 15 hours. Flow cytometry data with 10,000 events (n=3).

Figure 4.21 shows that the ratio of GFP:mCherry markedly increases from 0.037±0.0002 whilst uninduced to 0.82±0.0008 after overnight induction in 750μM of IPTG. Higher fold increases in this ratio were also observed in induction assays carried out in supplemented M9 media (from 0.032±0.0002 to 1.43±0.16) (Figure 4.22). This was most likely due to lower levels of basal expression whilst uninduced.

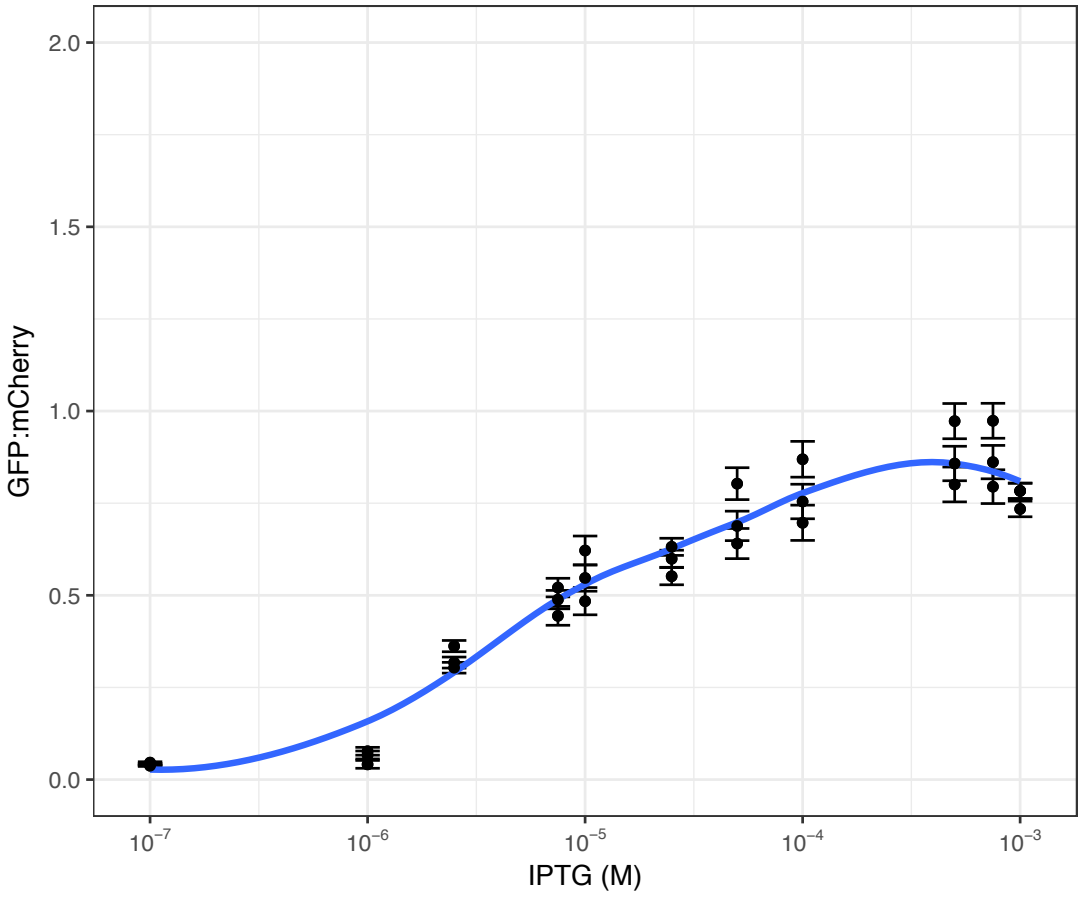

Figure 4.21: GFP to mCherry ratio in EcN_pLac_GFP_mCherry after induction with IPTG in LB media overnight. Ratio calculated using median fluorescence for each reporter from flow cytometry data with 10,000 events (n=3).

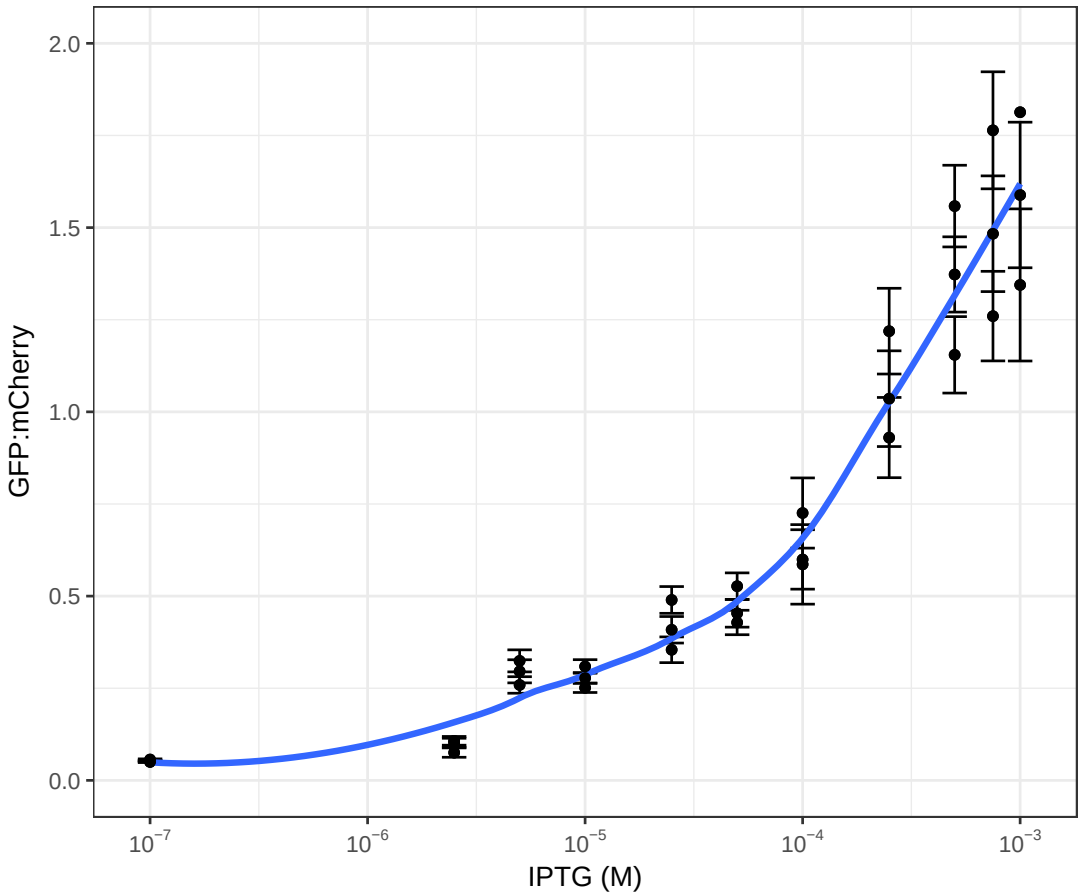

Figure 4.22: GFP to mCherry ratio in EcN_pLac_GFP_mCherry after induction with IPTG in M9 media overnight. Ratio calculated using median fluorescence for each reporter from flow cytometry data with 10,000 events (n=3).

Figure 4.23 demonstrates that once induced at 1mM IPTG after 7 hours of growth, the induction of the pLac_GFP plasmid results in a significant increase in the GFP to mCherry ratio in EcN_pLac_GFP_mCherry in comparison to the uninduced control. After 15 hours of growth, the GFP:mCherry ratio was 0.21±0.0006 in the induced strains in comparison to the uninduced ratio of 0.026±0.001. Figure 4.24 shows the increase of GFP expression rapidly upon induction while mCherry returns to its constant expression levels. Due to the lag of mCherry maturation, the ratio of GFP:mCherry is particularly high during the logarithmic stages of growth (0 to 8 hours)(Figures 4.25 and 4.26). The difference in ratio between the uninduced and induced strains is also apparent at the stationary phase of growth when the OD700 is larger than 1.5 (Appendix Figure 5.10). The discrepancy observed between the ratio here at 1mM (0.21±0.0006) and the ratio after overnight growth in 1mM (0.76±0.0005) (Figure 4.21) is most likely due the strain not being induced at the logarithmic phase of growth.

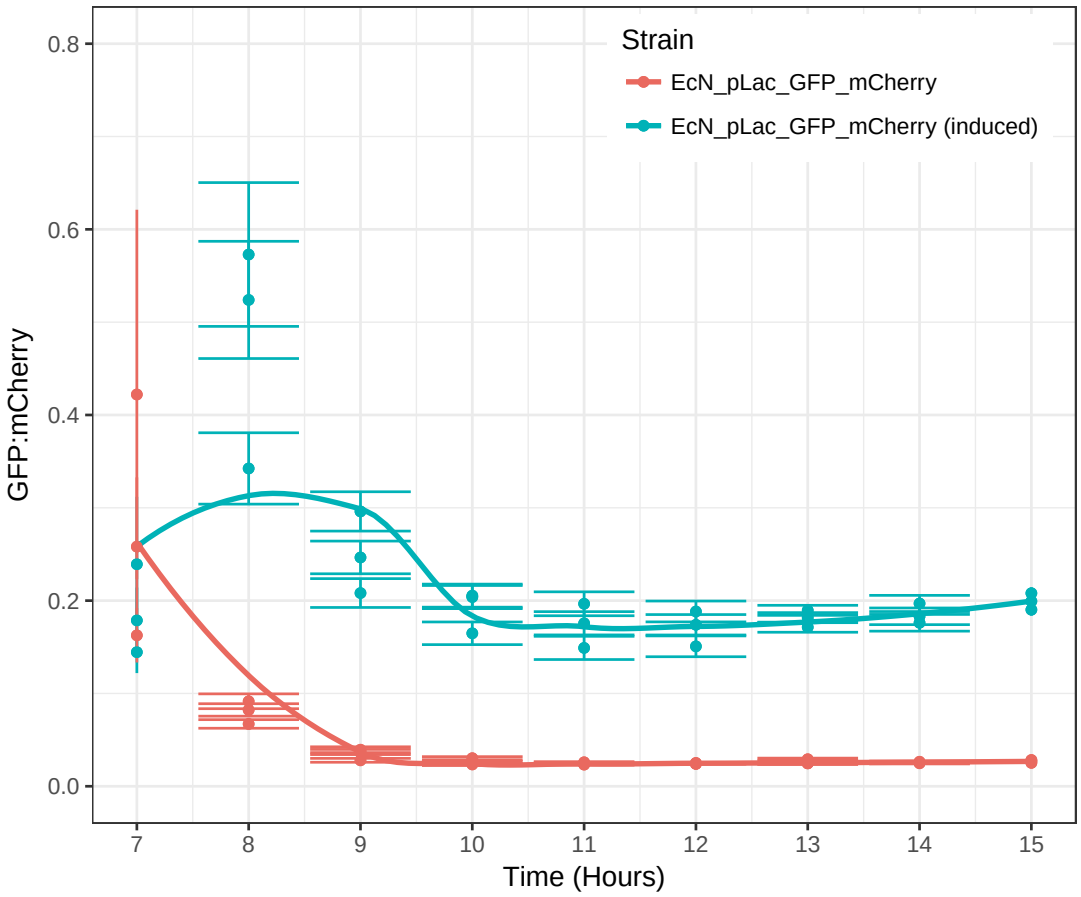

Figure 4.23: GFP to mCherry ratio in EcN_pLac_GFP_mCherry after induction with 1mM IPTG at 7 hours of growth in LB media. Ratio calculated using median fluorescence for each reporter from flow cytometry data with 10,000 events (n=3).

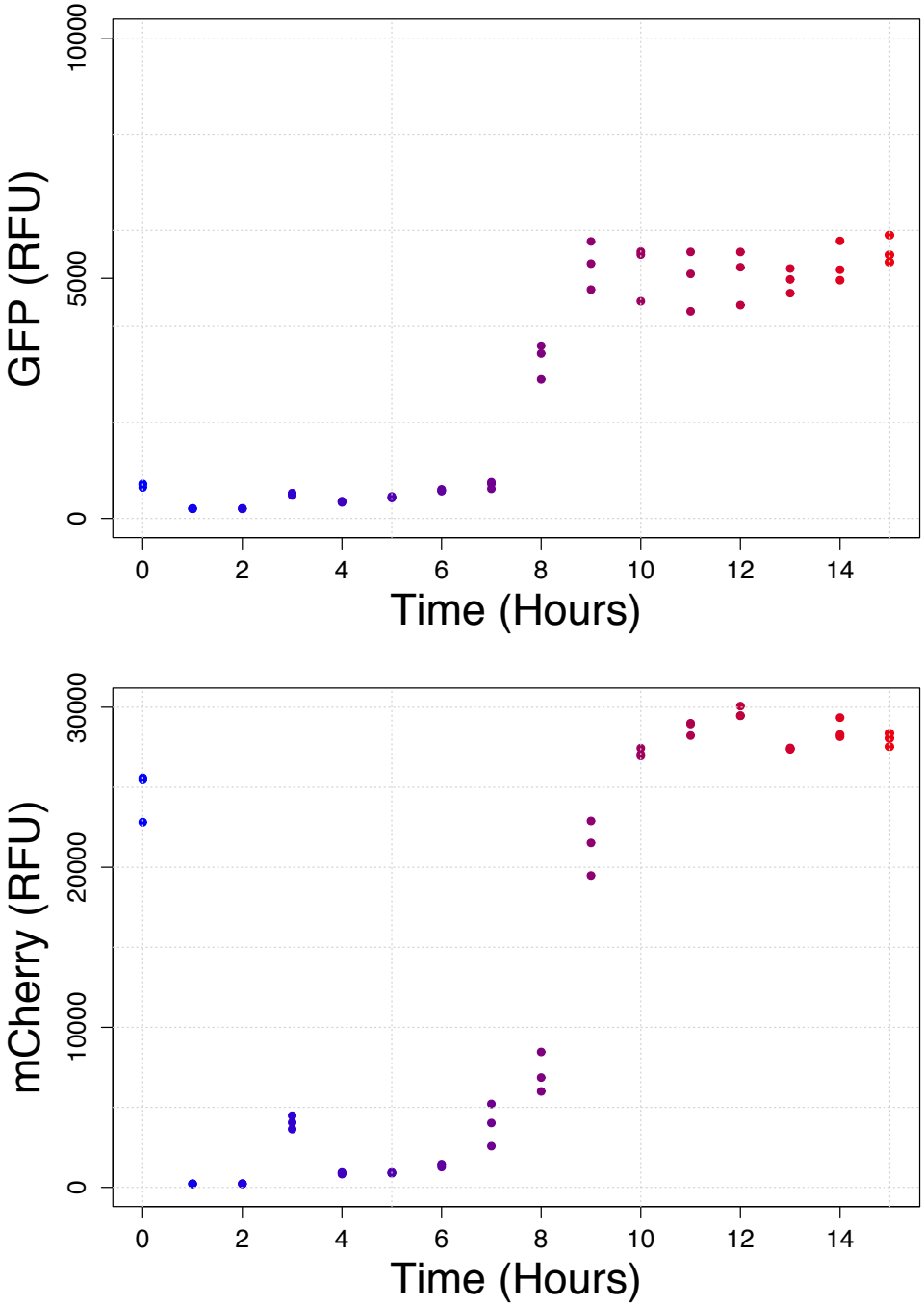

Figure 4.24: GFP and mCherry expression in EcN_pLac_GFP_mCherry after induction with 1mM IPTG at 7 hours of growth in LB media. Top: median GFP fluorescence over 15 hours. Bottom: median mCherry fluorescence over 15 hours. Flow cytometry data with 10,000 events (n=3).

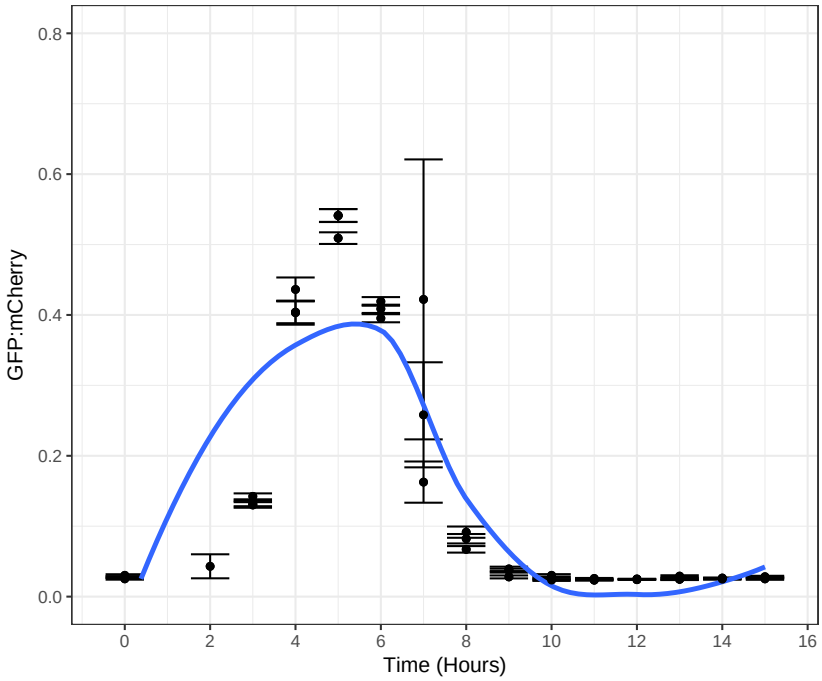

Figure 4.25: GFP to mCherry ratio in EcN_pLac_GFP_mCherry during growth uninduced in LB media. Ratio calculated using median fluorescence for each reporter from flow cytometry data with 10,000 events (n=3).

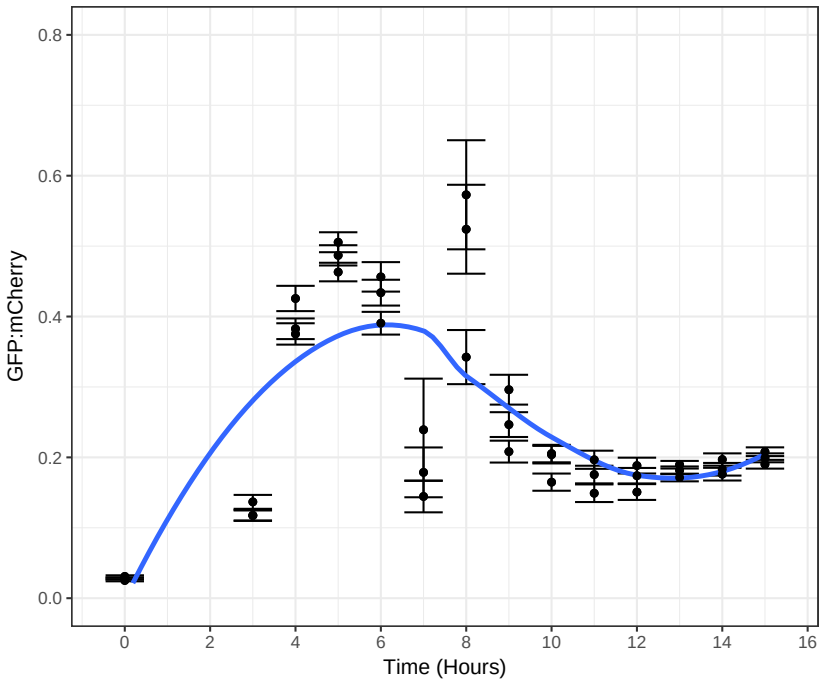

Figure 4.26: GFP to mCherry ratio in EcN_pLac_GFP_mCherry during growth induced at 1mM IPTG at 7 hours in LB media. Ratio calculated using median fluorescence for each reporter from flow cytometry data with 10,000 events (n=3).

4.4.2 EcN Sensors can Detect and Report on Signals in *C. elegans in vivo*

While both EcN and *C. elegans* are widely used as model organisms in a plethora of investigative fields, there is only one published example of their combined use [135]. In that example, it was shown that *C. elegans* can be used as a live *in vivo* model to demonstrate a synthetic biology approach to prevent gut infection with an engineered probiotic *E. coli* Nissle 1917 (EcN) strain. It has not been investigated whether bacterial biosensors can be characterised in *C. elegans*. Initial preliminary experiments here showed that the wild type lab BW *C. elegans* strain could indeed grow and develop successfully with a EcN_OXB19_GFP control strain constitutively expressing GFP. In addition, the GFP signal could be successfully used to image the *C. elegans* intestine (Figure 4.27).

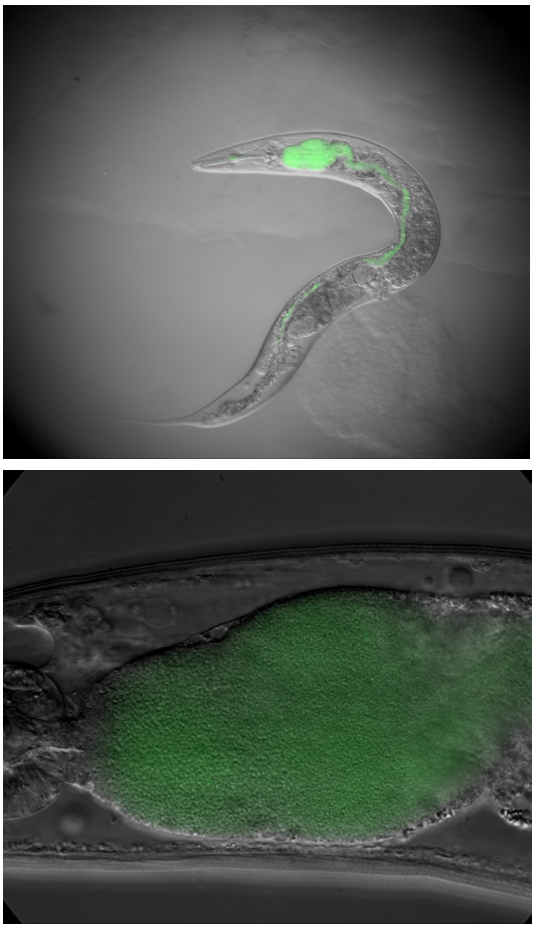

Figure 4.27: Representative image of 7 day old *C. elegans* worm grown on EcN_OXB19_GFP constitutively expressing GFP. GFP shows localisation of the strain from the pharynx onwards and throughout the intestines. Top, imaged at 120x magnification. Bottom, imaged at 200x magnification.

Figures 4.28 and 4.29 demonstrate the positive and negative EcN_GFP_mCherry strains functioning as expected *in vivo*. EcN_OXB19_GFP_mCherry shows direct co-localisation with strong expression of both GFP and mCherry throughout (Figure 4.28). The negative GFP control EcN_OG241_GFP_mCherry shows only high levels of mCherry throughout (Figure 4.29).

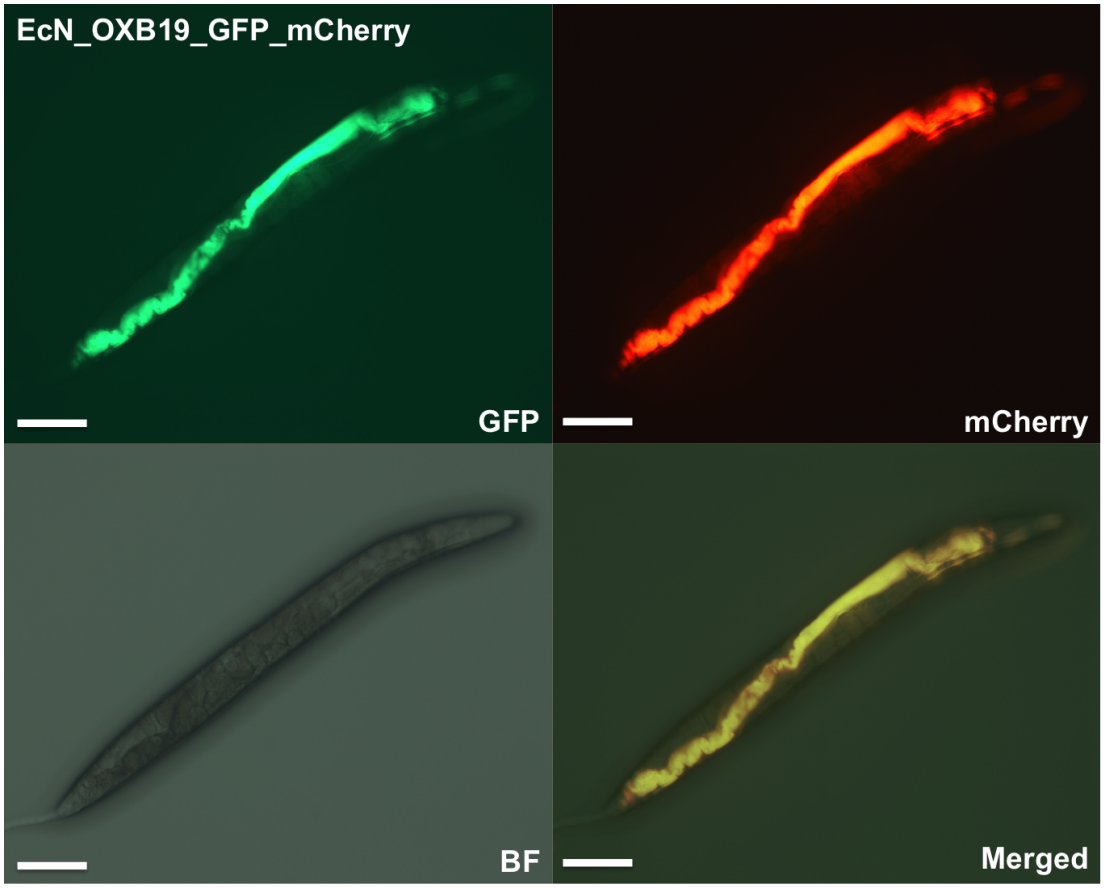

Figure 4.28: Representative image of 5 day old *C. elegans* worm grown on EcN_OXB19_GFP_mCherry constitutively expressing GFP and mCherry as a positive control. Both channels show localisation of the strain from the pharynx onwards and throughout the intestines. All images at 160x magnification. Scale bars are 50μm. BF indicates brightfield image.

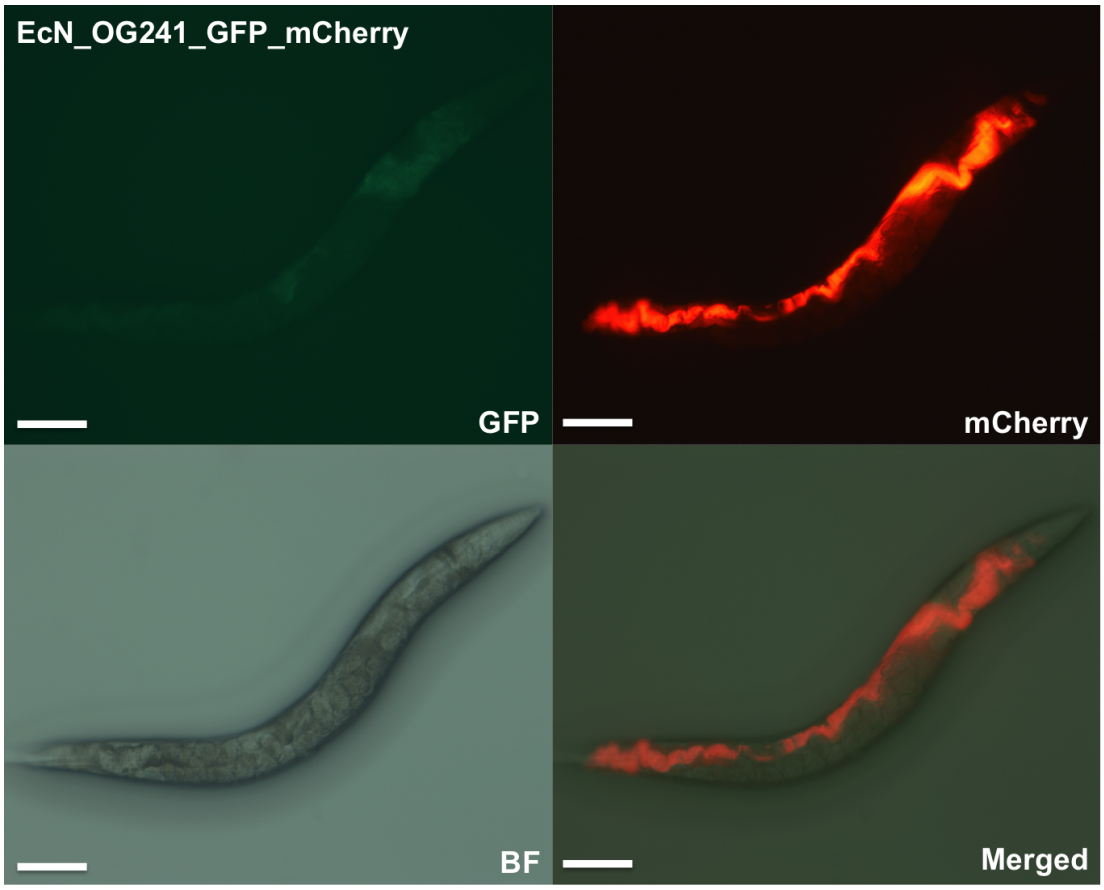

Figure 4.29: Representative image of 5 day old *C. elegans* worm grown on EcN_OG241_GFP_mCherry constitutively expressing mCherry. The promoterless OG241 plasmid acts as a negative sensor control. mCherry shows localisation of the strain from the pharynx onwards and throughout the intestines. All images at 160x magnification. Scale bars are 50μm. BF indicates brightfield image.

As expected, the IPTG inducible EcN_pLac_GFP_mCherry strain showed negligible levels of GFP fluorescent in the *C. elegans* intestines when plated and grown on plain NGM agar plates after an egg-prep (Figure 4.30). However, when the worms and EcN_pLac_GFP_mCherry strain were plated on NGM agar plates supplemented with 1mM IPTG, strong levels of GFP expression were observed co-localised with the mCherry signal in the intestines (Figure 4.31). This indicates that the pLac sensor plasmid could report on the IPTG in the surrounding environment from the *C. elegans* intestines.

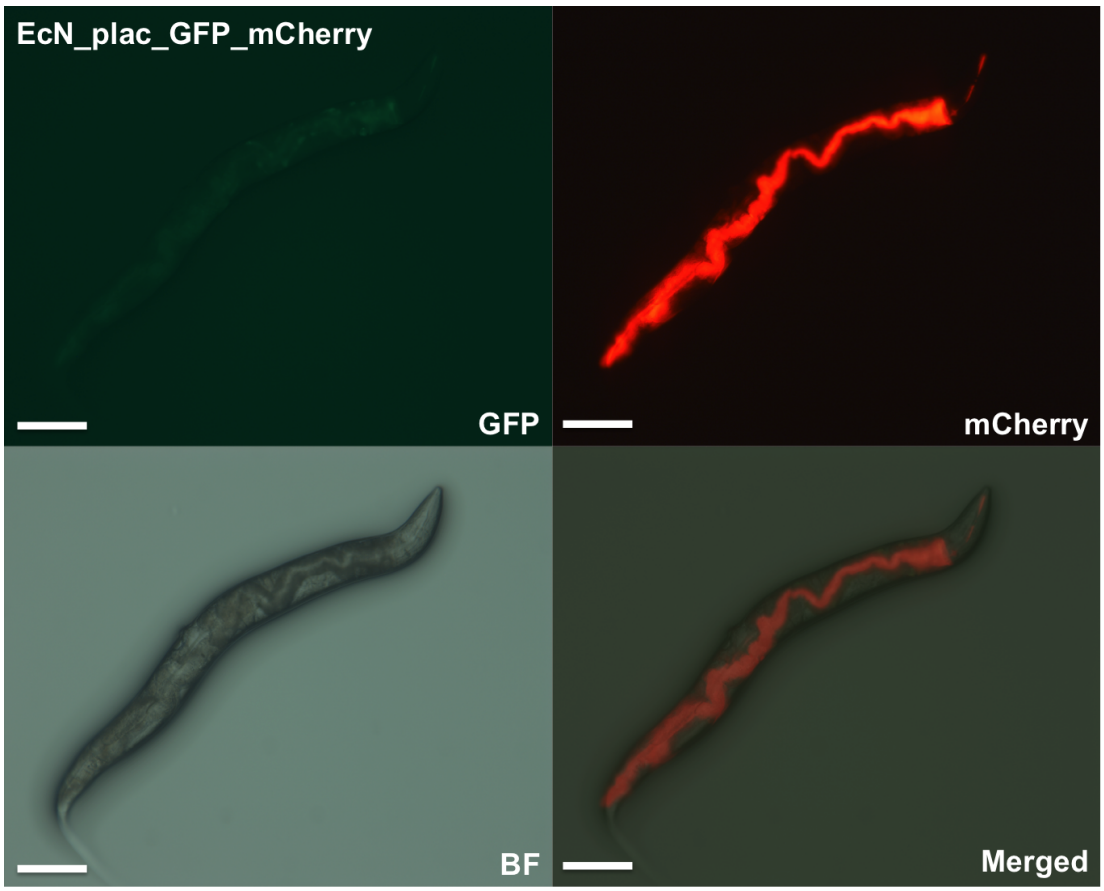

Figure 4.30: Representative image of 5 day old *C. elegans* worm grown on uninduced EcN_pLac_GFP_mCherry constitutively expressing mCherry. The pLac plasmid is IPTG inducible. mCherry shows localisation of the strain from the pharynx onwards and throughout the intestines. All images at 160x magnification. Scale bars are 50μm. BF indicates brightfield image.

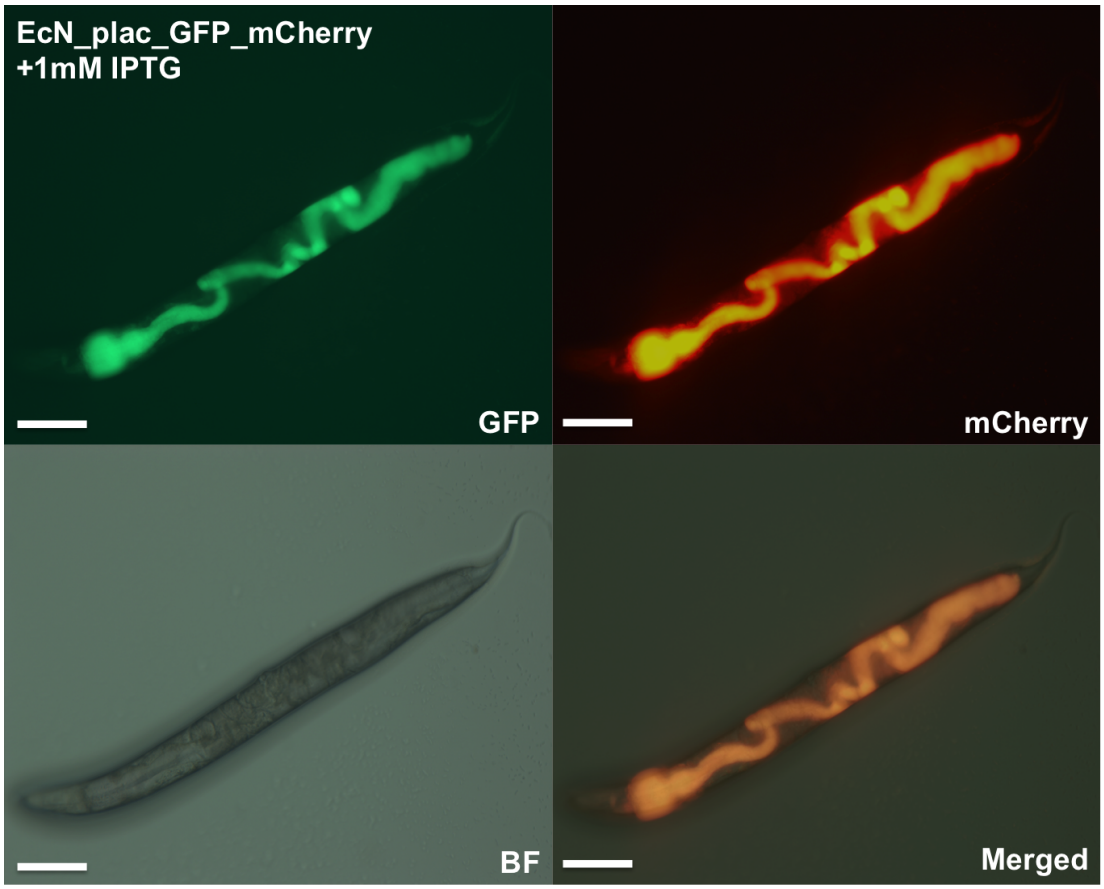

Figure 4.31: Representative image of 5 day old *C. elegans* worm grown on the EcN_pLac_GFP_mCherry strain plated on NGM agar plates with 1mM IPTG. The GFP expression indicates the pLac sensor plasmid detecting the IPTG in the environment. All images at 160x magnification. Scale bars are 50μm. BF indicates brightfield image.

Figure 4.32 shows that the differences between the strains can be sufficiently quantified using the ratio of GFP:mCherry. Furthermore, the induction of GFP in the pLac plasmid could be clearly observed on worms colonised by EcN_pLac_GFP_mCherry and plated on NGM agar with IPTG for 7 days.

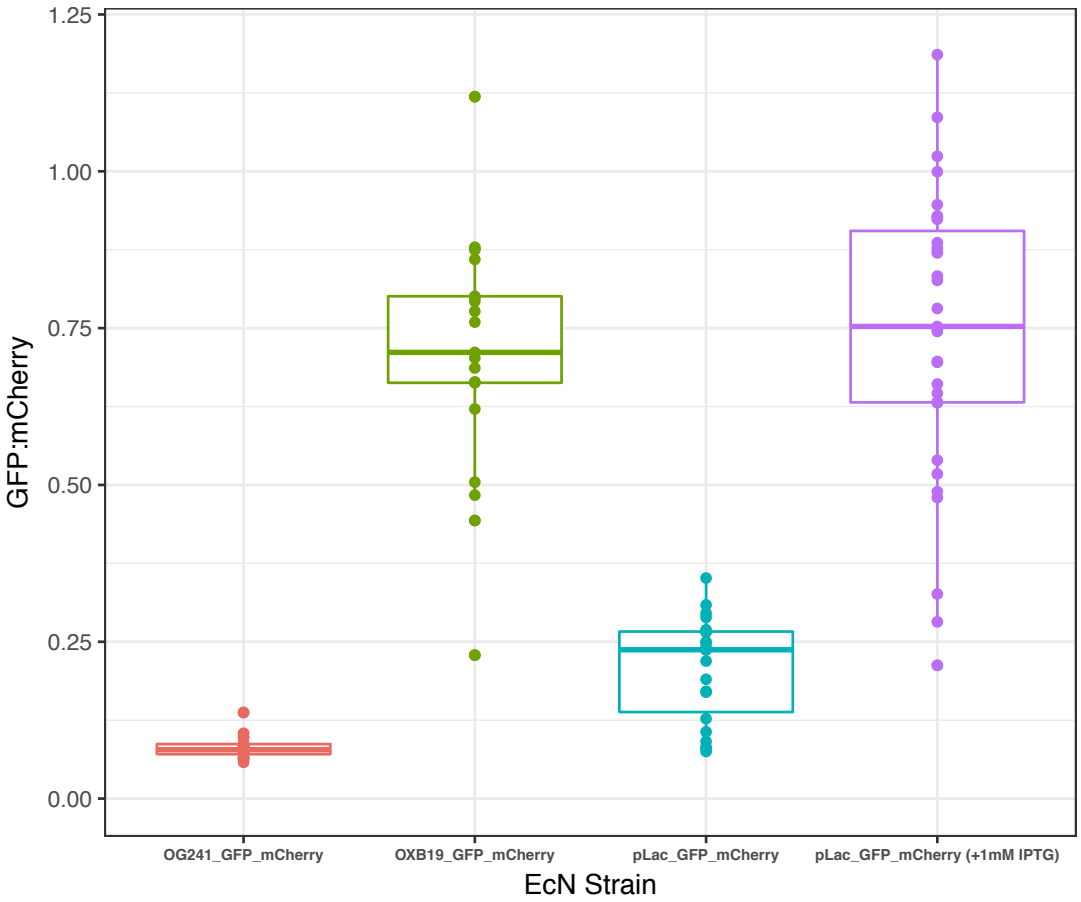

Figure 4.32: Box plot of GFP:mCherry ratio in individual 7 day old *C. elegans* worms grown on EcN sensor strains and plated on NGM agar plates. Worms colonised with EcN_pLac_GFP_mCherry were additionally plated on NGM agar plates with 1mM IPTG to demonstrate sensor induction over 7 days. 25 to 30 worms imaged for each condition.

In order to demonstrate that the EcN_pLac_GFP_mCherry strain could detect and report on an environmental signal from within the *C. elegans* intestines in a dynamic manner, an induction assay was carried out where worms grown on the sensor strain with NGM agar plates were transferred 7 days later to NGM agar plates supplemented with 1mM IPTG (see Section 4.3). Worms were then imaged after 8 hours to detect GFP and mCherry levels as a way of quantifying the sensor induction over time. Figure 4.33 shows that there was no significant increase in the ratio on the worms transferred from a plain NGM agar plate to another plain plate. However, significant differences were observed in the ratios when the worms were transferred to a NGM agar plate supplemented with 1mM IPTG. Within 8 hours, the median GFP:mCherry ratio was significantly higher on those on the IPTG plates in comparison to the plain NGM plates (0.39 compared to 0.21, $p < 0.0001$). No differences were observed in the negative OG241 and positive OXB19 controls (Appendix Figure 5.11).

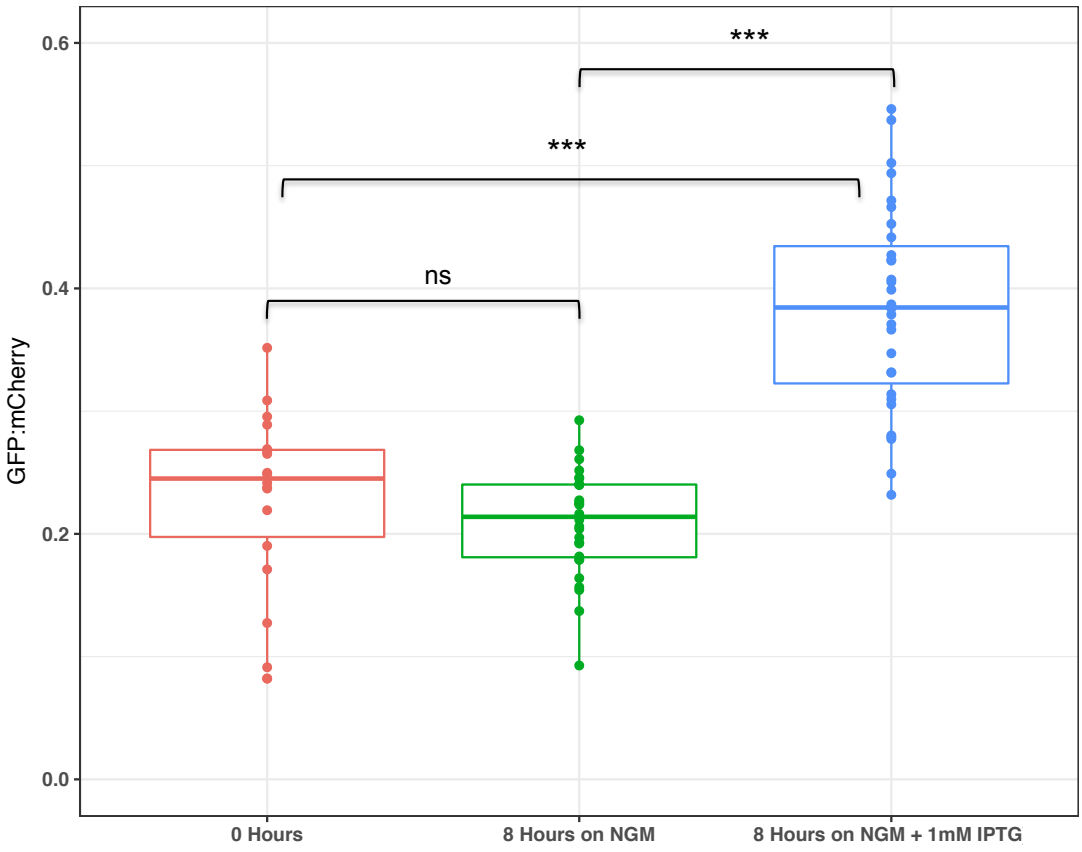

Figure 4.33: Box plot of GFP:mCherry ratio in individual 7 day old *C. elegans* worms grown on EcN_pLac_GFP_mCherry sensor strains and transferred to either plain NGM agar plates or plates supplemented with 1mM IPTG for 8 hours. 27 to 30 worms imaged for each condition and triple asterisk indicates $p < 0.0001$.

4.5 Discussion

Detecting markers of interest through inducible reporter systems can enable the design of more complex therapeutic circuits. The ability of EcN to occupy various niches in the intestines means it is particularly relevant to the detection of dysbiotic markers in the gut. In line with this, a dual reporter system with both mCherry and GFP was created in EcN. While GFP is inducible in the circuit, mCherry is constitutively expressed and could be used to calculate a ratiometric fold increase in GFP induction as opposed to absolute induction. This approach is considered to be more effective in reducing background noise and fluctuation of diverse conditions *in vivo* [184, 185].

The dual mCherry and GFP system was initially characterised with EcN in liquid LB culture. In comparison to the positive constitutive OXB19_GFP_mCherry and negative promoterless OG241_GFP_mCherry controls where the GFP:mCherry remained constant (Figure 4.12), the pLac inducible system showed a robust increase in the ratio upon induction (Figures 4.21 to 4.22).

The pLac_GFP_mCherry system was capable of showing an increase in the ratio from 0.037±0.0002 whilst uninduced to 0.82±0.0008 after overnight induction in 750μM of IPTG (Figure 4.21) in LB. Timecourse experiments indicated that this increase could be detected rapidly within 2 hours of induction (Figure 4.23).

While the half-time for mCherry was initially published at being similar to that of GFP at 15 minutes [186], several reports indicate that the maturation can in fact range from 40 to 100 minutes in *E. coli* [187, 188]. This difference corresponds to data presented here where there was a substantial lag in mCherry detection in comparison to GFP in flow cytometry experiments (Figures 4.10 and 4.11). Even so, the use of the GFP:mCherry was viable after 7 or 8 hours when the EcN strains were out of logarithmic growth.

In line with the sole piece of published research on the combined use of EcN and *C. elegans* [135], preliminary experiments showed that the wild type lab BW *C. elegans* strain could indeed grow and develop successfully with an EcN strain expressing GFP. In addition, the GFP signal could be successfully used to clearly image the intestines (Figure 4.27).

Figures 4.28 to 4.31 show that it is possible to clearly visualise the dual plasmid

GFP and mCherry EcN strains in *C. elegans*. Furthermore, Figure 4.31 shows that a substantial increase in GFP expression can be observed from EcN_pLac_GFP_mCherry throughout the intestines when the worms were plated on NGM plates supplemented with 1mM of the IPTG inducer. In addition, Figure 4.32 shows that the increase in GFP:mCherry from this strain can be clearly recorded and quantified from live *C. elegans in vivo*. This demonstrates that the bacteria can detect and respond to environmental signals from within the worm intestines during colonisation.

To further confirm this finding in a dynamic and spatiotemporal manner, a time-course induction assay was performed where worms with EcN_pLac_GFP_mCherry that were grown on plain seeded NGM plates throughout were transferred to unseeded NGM agar plates with no bacteria but supplemented with 1mM IPTG. Due to there being no bacteria on these induction plates, it would also be possible to confirm that it was in fact the intestinal bacteria detecting and responding to the environmental signal. Figure 4.33 shows that a significant increase in GFP:mCherry ratio from 0.21 to 0.39 ($p < 0.0001$) can be detected from within the intestines after only 8 hours of placing the worms on an IPTG plate. While this was a near 100% increase in the ratio, it can be argued that a higher fold increase like the one in Figure 4.31 (0.24 to 0.76) could have been recorded if the worms were incubated for longer than 8 hours. However, it is not known what impact the lack of bacterial food would have on the worms for such a long time. In line with the liquid culture experiments, it would also be inquisitive to investigate the limits of this detection system *in vivo* by using a diverse range of IPTG concentrations on the NGM induction plates.

4.6 Conclusions and Further Work

As set out in the aims, this piece of work demonstrated that it was possible to use *C. elegans* as a live animal model for characterising EcN sensors *in vivo*. Initially, it was shown that EcN sensors could be further developed to work in liquid culture in a ratiometric manner using a constitutive mCherry signal and inducible GFP signal. The incorporation of this approach allow EcN sensors to function with less background noise and in a more independent manner from the surrounding environmental conditions both in culture and *in vivo*. It was shown that *C. elegans* can survive and grow on these dual reporter EcN strains and that the fluorescent signal could be easily detected from the intestines of the live model. After colonisation, the dual signals were quantified in a ratiometric manner *in vivo*. Finally, it was shown that the EcN_pLac_GFP_mCherry strain could detect and respond to environmental signals directly from within the intestines of the live *C. elegans* model.

Further work would build on the propionate inducible EcN_pProE_GFP and pH sensitive EcN_pCadC_GFP sensors described in Section 3. The sensors could be altered into a dual system with the mCherry plasmid and investigated *in vivo* in *C. elegans*. Building on previous work on host-derived metabolites in *C. elegans* [180], the pProE sensor could be used to demonstrate the precise detection of a worm derived compound directly from within the intestines. Furthermore, the pCadC system could be used to elucidate the changing pH gradient of the worm intestines throughout development. Initial attempts were made to create a dual GFP:mCherry reporter system on a single plasmid. In light of these constructs being unstable in EcN, a dual plasmid approach was used. Further work could include reattempting the single-plasmid approach as it should in theory enable more accurate ratiometric analysis than a system with fluorescent reporters on two separate plasmids that have two independent origins of replication. As these origins of replication maintain plasmid copy number independently in the host, it can add an additional variable to the ratio of the two fluorescent reporters during sensor induction and readout.

Collectively, these findings indicate that the live *C. elegans* model can be used to design precise intestinal investigations. With minimal regulatory and time constraints, experiments can be carried out on a powerful yet simple and defined host-microbiota

model system. Furthermore, this model has the potential to complement the underlying approach of the 'design, test and build cycle' that is crucial to synthetic biology.

5. Conclusions

This body of work set out to investigate the use of synthetic biology tools for unraveling the underlying mechanisms of the complex and multifaceted intestinal microbiota. In addition to building on the latest research in these dynamic fields, the attempts made here tried to broaden the established methodologies and approaches currently in use. The commensal attributes and research already carried out on *E.coli* Nissle 1917 (EcN) made it an ideal chassis to base these approaches on. Novel insights and findings like these could eventually be utilised to help further elucidate the underlying role of the microbiota in conditions such as inflammatory bowel disease (IBD) and cancers of the gasterointestinal tract.

Initially, it was shown here that it is possible to use PSK systems such as Hok/*sok*, Axe/Txe and microcin V to stabilise synthetic gene networks in the probiotic EcN strain in the absence of antibiotic selection for up to 37 passages in liquid culture. In addition, it was demonstrated that the Axe/Txe and Hok/*sok* systems could substantially stabilise a luminescent reporter plasmid in an *in vivo* tumour xenograft model without antibiotic selection. Whereas the stability provided by the Hok/*sok* system corroborates with previous literature, the novel findings here show that Axe/Txe was a superior plasmid stability system in EcN. The *E.faecium* derived Axe/Txe system was particularly effective in preventing a reporter plasmid dropping from the population. These novel findings can be used to design and execute more robust *in vivo* investigations into the intestinal microbiota without the use of antibiotics. Experiments could be repeated in other commensal strains such as *Salmonella typhimurium* or with different *in vivo* animal models. While a tumour xenograft model was investigated here, it would be enlightening to see how effective the Axe/Txe system is in stabilising a genetic construct within a healthy or diseased intestine.

Next it was demonstrated that is possible to design and characterise a range of therapeutic sensors in EcN that could detect RNS, propionate and changes in pH. As RNS are a common marker within intestinal inflammation, the RNS inducible pYeaR_EcN sensor could be used to investigate the underlying mechanisms of IBD *in vivo* or from clinical samples. The propionate inducible pProE_EcN sensor could be used during *in vivo* investigations to broaden our understanding of the role SCFAs play in intestinal pathologies. The pH sensitive pCadC_EcN sensor could be eventually used to investigate the changing pH in the intestines of an organism, or be used to create a circuit switch that only initiates protein expression at a given pH range.

Finally, work presented here demonstrated that it was possible to use *C.elegans* as a live animal model for quantitatively characterising EcN biosensors *in vivo*. While this live animal model is used extensively throughout biological experiments, it has only been recently proposed as a useful model for investigating host-microbe interactions in the intestines. It was shown that *C.elegans* can survive and grow on EcN strains with dual reporters and that the fluorescent signals could be easily detected from the intestines of the live model. After colonisation, the dual signals could be detected in a ratiometric manner *in vivo*. Using this approach, it was shown that an IPTG inducible EcN strain could detect and respond to environmental signals directly from within the intestines of the live *C.elegans* model in a time dependent manner. Further work would consist of employing this approach to the propionate inducible EcN_pProE_GFP and pH sensitive EcN_pCadC_GFP sensors described in Chapter 3. Experiments could be devised that show these sensors dynamically responding to host-derived metabolites *in vivo* directly from the intestines. Collectively, these novel findings indicate that the live *C.elegans* model can be used to design precise intestinal microbiome investigations. With minimal regulatory and time constraints, experiments can be carried out on a powerful yet simple and defined host-microbiota model system. Furthermore, this model has the potential to complement the underlying approach of the 'design, test and build cycle' that is fundamental in the field of synthetic biology.

Taken together, these findings indicate that it is possible to build on existing literature to expand the foundational components and genetic repertoire of synthetic biology tools for robust investigations into the intestinal microbiota. By incorporating approaches like these, we will be able to first elucidate mechanisms behind perturba-

tions and pathologies and in turn develop novel therapeutics. Our ability to devise and characterise complex circuits with a hierarchical output is rapidly evolving. However, these circuits need to truly function in a robust and pre-determined state if they are to ever be used for the production and delivery of therapeutic compounds *in vivo*.

The use of engineered commensal chassis like EcN provide a promising approach for the development of these therapeutics. Building on the wealth of tools available for *E.coli*, it is relatively convenient to develop approaches based on the 'laboratory friendly' EcN strain. Indeed, this is currently reflected in the biotechnology industry where Synlogic Therapeutics (Boston, USA) is using EcN as a chassis for a novel class of medicines. Through the use of EcN, they have designed an orally administered strain that harbours a complementary metabolic pathway that can remove excess ammonia from the blood of a patient suffering from urea cycle disorders (UCD). They have recently dosed patients in a Phase 1 clinical trial to assess the safety of the approach and hope to use the platform as a pipeline for numerous other errors of metabolism and metabolic coniditions.

We are slowly uncovering the vast number of strains in the intestines, and in turn the unique and diverse protein coding genes they harbour. The relevance and merits of synthetic biology tools need to be coupled to the chosen delivery chassis. In light of this, efforts must also be made to devise tools for strains from the *Bacteroidetes* and *Firmicutes* phyla that are more difficult to work with but colonise the intestines in a much more abundant and longterm manner. The sheer abundance of these strains in the intestines could enable the design of much more powerful therapeutic strategies. Regardless of the chassis chosen to manipulate this complex ecosystem with recombinant DNA, it is imperative that we employ robust biocontainement strategies to prevent genetic sharing between strains and the escape of the DNA to the environment or other humans.

References

[1] Turnbaugh, P. J. *et al.* The human microbiome project. *Nature* **449**, 804–810 (2007).

[2] Qin, J. *et al.* A human gut microbial gene catalogue established by metagenomic sequencing. *Nature* **464**, 59–65 (2010). URL `http://www.nature.com/nature/journal/v464/n7285/full/nature08821.html`.

[3] Consortium, T. H. M. P. Structure, function and diversity of the healthy human microbiome. *Nature* **486**, 207–214 (2012). URL `http://www.nature.com/nature/journal/v486/n7402/full/nature11234.html`.

[4] NIH, N. NIDDK Image Library. URL `https://catalog.niddk.nih.gov/catalog/ImageLibrary/searchresults.cfm?keyword=1609&type=keyword`.

[5] Parfrey, L. W. & Knight, R. Spatial and temporal variability of the human microbiota. *Clinical Microbiology and Infection: The Official Publication of the European Society of Clinical Microbiology and Infectious Diseases* **18 Suppl 4**, 8–11 (2012).

[6] Falony, G., Vlachou, A., Verbrugghe, K. & De Vuyst, L. Cross-feeding between Bifidobacterium longum BB536 and acetate-converting, butyrate-producing colon

bacteria during growth on oligofructose. *Applied and Environmental Microbiology* **72**, 7835–7841 (2006).

[7] Salazar, N., Gueimonde, M., Hernandez-Barranco, A. M., Ruas-Madiedo, P. & de los Reyes-Gavilian, C. G. Exopolysaccharides Produced by Intestinal Bifidobacterium Strains Act as Fermentable Substrates for Human Intestinal Bacteria. *Applied and Environmental Microbiology* **74**, 4737–4745 (2008). URL `http://www.ncbi.nlm.nih.gov/pmc/articles/PMC2519331/`.

[8] Bassler, B. L. & Losick, R. Bacterially speaking. *Cell* **125**, 237–246 (2006).

[9] Miller, M. B. & Bassler, B. L. Quorum sensing in bacteria. *Annual Review of Microbiology* **55**, 165–199 (2001).

[10] Frost, L. S., Leplae, R., Summers, A. O. & Toussaint, A. Mobile genetic elements: the agents of open source evolution. *Nature Reviews. Microbiology* **3**, 722–732 (2005).

[11] Gogarten, J. P. & Townsend, J. P. Horizontal gene transfer, genome innovation and evolution. *Nature Reviews. Microbiology* **3**, 679–687 (2005).

[12] Norman, A., Hansen, L. H. & Sorensen, S. J. Conjugative plasmids: vessels of the communal gene pool. *Philosophical Transactions of the Royal Society of London. Series B, Biological Sciences* **364**, 2275–2289 (2009).

[13] Cerf-Bensussan, N. & Gaboriau-Routhiau, V. The immune system and the gut microbiota: friends or foes? *Nature Reviews Immunology* **10**, 735–744 (2010). URL `http://www.nature.com.libproxy.ucl.ac.uk/nri/journal/v10/n10/full/nri2850.html`.

[14] Yatsunenko, T. *et al.* Human gut microbiome viewed across age and geography. *Nature* **486**, 222–227 (2012).

[15] Serino, M. *et al.* Metabolic adaptation to a high-fat diet is associated with a change in the gut microbiota. *Gut* gutjnl–2011–301012 (2011). URL `http://gut.bmj.com/content/early/2011/11/22/gutjnl-2011-301012`.

[16] Honda, K. & Littman, D. R. The microbiome in infectious disease and inflammation. *Annual Review of Immunology* **30**, 759–795 (2012).

[17] Eckburg, P. B. *et al.* Diversity of the human intestinal microbial flora. *Science (New York, N.Y.)* **308**, 1635–1638 (2005).

[18] Guarner, F. & Malagelada, J.-R. Gut flora in health and disease. *The Lancet* **361**, 512–519 (2003). URL http://www.sciencedirect.com/science/article/pii/S0140673603124890.

[19] Cryan, J. F. & Dinan, T. G. Mind-altering microorganisms: the impact of the gut microbiota on brain and behaviour. *Nature Reviews Neuroscience* **13**, 701–712 (2012). URL http://www.nature.com.libproxy.ucl.ac.uk/nrn/journal/v13/n10/full/nrn3346.html.

[20] Mortensen, P. B. & Clausen, M. R. Short-Chain Fatty Acids in the Human Colon: Relation to Gastrointestinal Health and Disease. *Scandinavian Journal of Gastroenterology* **31**, 132–148 (1996). URL http://www.tandfonline.com/doi/abs/10.3109/00365529609094568.

[21] Furusawa, Y. *et al.* Commensal microbe-derived butyrate induces the differentiation of colonic regulatory T cells. *Nature* **504**, 446–450 (2013). URL http://www.nature.com/nature/journal/v504/n7480/full/nature12721.html.

[22] Yaung, S. J., Church, G. M. & Wang, H. H. Recent progress in engineering human-associated microbiomes. *Methods in Molecular Biology (Clifton, N.J.)* **1151**, 3–25 (2014).

[23] Kostic, A. D., Howitt, M. R. & Garrett, W. S. Exploring host-microbiota interactions in animal models and humans. *Genes & Development* **27**, 701–718 (2013). URL http://genesdev.cshlp.org/content/27/7/701.

[24] Pham, T. A. N. & Lawley, T. D. Emerging insights on intestinal dysbiosis during bacterial infections. *Current Opinion in Microbiology* **17**, 67–74 (2014). URL http://www.ncbi.nlm.nih.gov/pmc/articles/PMC3969284/.

[25] Shreiner, A. B., Kao, J. Y. & Young, V. B. The gut microbiome in health and in disease. *Current Ppinion in Gastroenterology* **31**, 69–75 (2015). URL http://www.ncbi.nlm.nih.gov/pmc/articles/PMC4290017/.

[26] Blekhman, R. *et al.* Host genetic variation impacts microbiome composition across human body sites. *Genome Biology* **16**, 191 (2015). URL `https://doi.org/10.1186/s13059-015-0759-1`.

[27] Li, D. *et al.* A Pleiotropic Missense Variant in SLC39a8 Is Associated With Crohn's Disease and Human Gut Microbiome Composition. *Gastroenterology* **151**, 724–732 (2016).

[28] Glocker, E.-O. *et al.* Inflammatory Bowel Disease and Mutations Affecting the Interleukin-10 Receptor. *New England Journal of Medicine* **361**, 2033–2045 (2009). URL `http://dx.doi.org/10.1056/NEJMoa0907206`.

[29] Noverr, M. C. & Huffnagle, G. B. The microflora hypothesis of allergic diseases. *Clinical & Experimental Allergy* **35**, 1511–1520 (2005). URL `http://onlinelibrary.wiley.com/doi/10.1111/j.1365-2222.2005.02379.x/abstract`.

[30] Wu, H.-J. *et al.* Gut-residing segmented filamentous bacteria drive autoimmune arthritis via T helper 17 cells. *Immunity* **32**, 815–827 (2010).

[31] Vieira, S. M., Pagovich, O. E. & Kriegel, M. A. Diet, Microbiota and Autoimmune Diseases. *Lupus* **23**, 518–526 (2014). URL `http://www.ncbi.nlm.nih.gov/pmc/articles/PMC4009622/`.

[32] Giongo, A. *et al.* Toward defining the autoimmune microbiome for type 1 diabetes. *The ISME journal* **5**, 82–91 (2011).

[33] Nicholson, J. K. *et al.* Host-gut microbiota metabolic interactions. *Science (New York, N.Y.)* **336**, 1262–1267 (2012).

[34] Ley, R. E. *et al.* Obesity alters gut microbial ecology. *Proceedings of the National Academy of Sciences of the United States of America* **102**, 11070–11075 (2005). URL `http://www.pnas.org/content/102/31/11070`.

[35] Turnbaugh, P. J. *et al.* An obesity-associated gut microbiome with increased capacity for energy harvest. *Nature* **444**, 1027–131 (2006). URL `http://www.nature.com/nature/journal/v444/n7122/full/nature05414.html`.

[36] Wang, Z. *et al.* Gut flora metabolism of phosphatidylcholine promotes cardiovascular disease. *Nature* **472**, 57–63 (2011).

[37] Vijay-Kumar, M. *et al.* Metabolic syndrome and altered gut microbiota in mice lacking Toll-like receptor 5. *Science (New York, N.Y.)* **328**, 228–231 (2010).

[38] Jemal, A. *et al.* Global cancer statistics. *CA: A Cancer Journal for Clinicians* **61**, 69–90 (2011). URL http://onlinelibrary.wiley.com/doi/10.3322/caac.20107/abstract.

[39] Chang, P. V., Hao, L., Offermanns, S. & Medzhitov, R. The microbial metabolite butyrate regulates intestinal macrophage function via histone deacetylase inhibition. *Proceedings of the National Academy of Sciences* **111**, 2247–2252 (2014). URL http://www.pnas.org/content/111/6/2247.

[40] Buda, A. *et al.* Butyrate downregulates a2b1 integrin: a possible role in the induction of apoptosis in colorectal cancer cell lines. *Gut* **52**, 729–734 (2003). URL http://gut.bmj.com/content/52/5/729.

[41] Barrasa, J. I., Olmo, N., Lizarbe, M. A. & Turnay, J. Bile acids in the colon, from healthy to cytotoxic molecules. *Toxicology in Vitro* **27**, 964–977 (2013). URL http://www.sciencedirect.com/science/article/pii/S088723331200358X.

[42] Louis, P., Hold, G. L. & Flint, H. J. The gut microbiota, bacterial metabolites and colorectal cancer. *Nature Reviews Microbiology* **12**, 661–672 (2014). URL http://www.nature.com.libproxy.ucl.ac.uk/nrmicro/journal/v12/n10/full/nrmicro3344.html.

[43] Attene-Ramos, M. S., Wagner, E. D., Gaskins, H. R. & Plewa, M. J. Hydrogen Sulfide Induces Direct Radical-Associated DNA Damage. *Molecular Cancer Research* **5**, 455–459 (2007). URL http://mcr.aacrjournals.org/content/5/5/455.

[44] Buffie, C. G. *et al.* Precision microbiome reconstitution restores bile acid mediated resistance to Clostridium difficile. *Nature* **517**, 205–208 (2015). URL http://www.nature.com/nature/journal/v517/n7533/full/nature13828.html.

[45] Chen, Y. Y., Galloway, K. E. & Smolke, C. D. Synthetic biology: advancing biological frontiers by building synthetic systems. *Genome Biology* **13**, 240 (2012). URL http://genomebiology.com/2012/13/2/240/abstract.

[46] Cheng, A. A. & Lu, T. K. Synthetic Biology: An Emerging Engineering Discipline. *Annual Review of Biomedical Engineering* **14**, 155–178 (2012). URL http://www.annualreviews.org/doi/abs/10.1146/annurev-bioeng-071811-150118.

[47] Endy, D. Foundations for engineering biology. *Nature* **438**, 449–453 (2005). URL http://www.nature.com.libproxy.ucl.ac.uk/nature/journal/v438/n7067/full/nature04342.html.

[48] Ellis, T., Adie, T. & Baldwin, G. S. DNA assembly for synthetic biology: from parts to pathways and beyond. *Integrative Biology* **3**, 109–118 (2011). URL http://pubs.rsc.org/en/content/articlelanding/2011/ib/c0ib00070a.

[49] Gardner, T. S., Cantor, C. R. & Collins, J. J. Construction of a genetic toggle switch in Escherichia coli. *Nature* **403**, 339–342 (2000).

[50] Weber, W., Kramer, B. P. & Fussenegger, M. A genetic time-delay circuitry in mammalian cells. *Biotechnology and bioengineering* **98**, 894–902 (2007).

[51] Friedland, A. E. *et al.* Synthetic Gene Networks that Count. *Science (New York, N.Y.)* **324**, 1199–1202 (2009). URL http://www.ncbi.nlm.nih.gov/pmc/articles/PMC2690711/.

[52] Anderson, J. C., Voigt, C. A. & Arkin, A. P. Environmental signal integration by a modular AND gate. *Molecular Systems Biology* **3** (2007). URL http://www.ncbi.nlm.nih.gov/pmc/articles/PMC1964800/.

[53] Stricker, J. *et al.* A fast, robust and tunable synthetic gene oscillator. *Nature* **456**, 516–519 (2008). URL http://www.nature.com/nature/journal/v456/n7221/full/nature07389.html.

[54] Pinheiro, V. B. *et al.* Synthetic genetic polymers capable of heredity and evolution. *Science (New York, N.Y.)* **336**, 341–344 (2012). URL http://www.ncbi.nlm.nih.gov/pmc/articles/PMC3362463/.

[55] Annaluru, N. *et al.* Total Synthesis of a Functional Designer Eukaryotic Chromosome. *Science* **344**, 55–58 (2014). URL http://www.sciencemag.org/content/344/6179/55.

[56] Ro, D.-K. *et al.* Production of the antimalarial drug precursor artemisinic acid in engineered yeast. *Nature* **440**, 940–943 (2006). URL http://www.nature.com/nature/journal/v440/n7086/full/nature04640.html.

[57] Galanie, S., Thodey, K., Trenchard, I. J., Interrante, M. F. & Smolke, C. D. Complete biosynthesis of opioids in yeast. *Science* **349**, 1095–1100 (2015). URL http://www.sciencemag.org/content/349/6252/1095.

[58] Lu, T. K., Khalil, A. S. & Collins, J. J. Next-generation synthetic gene networks. *Nature Biotechnology* **27**, 1139–1150 (2009). URL http://www.nature.com/nbt/journal/v27/n12/abs/nbt.1591.html.

[59] Hwang, I. Y. *et al.* Reprogramming Microbes to Be Pathogen-Seeking Killers. *ACS Synthetic Biology* (2013). URL http://dx.doi.org/10.1021/sb400077j.

[60] Forbes, N. S. Engineering the perfect (bacterial) cancer therapy. *Nature Reviews Cancer* **10**, 785–794 (2010). URL http://www.nature.com/nrc/journal/v10/n11/full/nrc2934.html.

[61] Wright, C. M., Wright, R. C., Eshleman, J. R. & Ostermeier, M. A protein therapeutic modality founded on molecular regulation. *Proceedings of the National Academy of Sciences of the United States of America* **108**, 16206–16211 (2011). URL http://www.ncbi.nlm.nih.gov/pmc/articles/PMC3182702/.

[62] Jinek, M. *et al.* A programmable dual-RNA-guided DNA endonuclease in adaptive bacterial immunity. *Science (New York, N.Y.)* **337**, 816–821 (2012).

[63] Yang, L. *et al.* Genome-wide inactivation of porcine endogenous retroviruses (PERVs). *Science (New York, N.Y.)* (2015).

[64] Duan, F. & March, J. C. Engineered bacterial communication prevents Vibrio cholerae virulence in an infant mouse model. *Proceedings of the National Academy of Sciences* **107**, 11260–11264 (2010). URL http://www.pnas.org/content/107/25/11260.

[65] Chen, Z. *et al.* Incorporation of therapeutically modified bacteria into gut microbiota inhibits obesity. *The Journal of Clinical Investigation* (2014).

[66] Xu, Y.-F. *et al.* A new expression plasmid in Bifidobacterium longum as a delivery system of endostatin for cancer gene therapy. *Cancer Gene Therapy* **14**, 151–157 (2007).

[67] Kotula, J. W. *et al.* Programmable bacteria detect and record an environmental signal in the mammalian gut. *Proceedings of the National Academy of Sciences* 201321321 (2014). URL `http://www.pnas.org/content/early/2014/03/12/1321321111`.

[68] Myhrvold, C., Kotula, J. W., Hicks, W. M., Conway, N. J. & Silver, P. A. A distributed cell division counter reveals growth dynamics in the gut microbiota. *Nature Communications* **6**, ncomms10039 (2015). URL `https://www.nature.com/articles/ncomms10039`.

[69] Smillie, C. S. *et al.* Ecology drives a global network of gene exchange connecting the human microbiome. *Nature* **480**, 241–244 (2011). URL `https://www.nature.com/nature/journal/v480/n7376/full/nature10571.html`.

[70] Chan, C. T. Y., Lee, J. W., Cameron, D. E., Bashor, C. J. & Collins, J. J. 'Deadman' and 'Passcode' microbial kill switches for bacterial containment. *Nature Chemical Biology* **12**, 82–86 (2016). URL `https://www.nature.com/nchembio/journal/v12/n2/full/nchembio.1979.html`.

[71] Steidler, L. *et al.* Biological containment of genetically modified Lactococcus lactis for intestinal delivery of human interleukin 10. *Nature Biotechnology* **21**, 785–789 (2003). URL `https://www.nature.com/nbt/journal/v21/n7/full/nbt840.html`.

[72] Braat, H. *et al.* A Phase I Trial With Transgenic Bacteria Expressing Interleukin-10 in Crohns Disease. *Clinical Gastroenterology and Hepatology* **4**, 754–759 (2006). URL `http://www.cghjournal.org/article/S1542-3565(06)00331-4/fulltext`.

[73] Al-Kobaisi, M. F. Jawetz, Melnick & Adelbergs Medical Microbiology. *Sultan Qaboos University Medical Journal* **7**, 273–275 (2007). URL http://www.ncbi.nlm.nih.gov/pmc/articles/PMC3074881/.

[74] Browne, H. P. *et al.* Culturing of unculturable human microbiota reveals novel taxa and extensive sporulation. *Nature* **533**, 543–546 (2016). URL https://www.nature.com/nature/journal/v533/n7604/full/nature17645.html.

[75] Schultz, M. Clinical use of E. coli Nissle 1917 in inflammatory bowel disease. *Inflammatory Bowel Diseases* **14**, 1012–1018 (2008). URL http://onlinelibrary.wiley.com/doi/10.1002/ibd.20377/abstract.

[76] Sonnenborn, U. & Schulze, J. The non-pathogenic Escherichia coli strain Nissle 1917 - features of a versatile probiotic. *Microbial Ecology in Health and Disease* **21**, 122–158 (2009). URL http://informahealthcare.com/doi/abs/10.3109/08910600903444267.

[77] Malchow, H. A. Crohn's disease and Escherichia coli. A new approach in therapy to maintain remission of colonic Crohn's disease? *Journal of Clinical Gastroenterology* **25**, 653–658 (1997).

[78] Henker, J. *et al.* The probiotic Escherichia coli strain Nissle 1917 (EcN) stops acute diarrhoea in infants and toddlers. *European Journal of Pediatrics* **166**, 311–318 (2007).

[79] Kruis, W. *et al.* Double-blind comparison of an oral Escherichia coli preparation and mesalazine in maintaining remission of ulcerative colitis. *Alimentary Pharmacology & Therapeutics* **11**, 853–858 (1997). URL http://onlinelibrary.wiley.com/doi/10.1046/j.1365-2036.1997.00225.x/abstract.

[80] Massa, P. E., Paniccia, A., Monegal, A., Marco, A. d. & Rescigno, M. Salmonella engineered to express CD20-targeting antibodies and a drug-converting enzyme can eradicate human lymphomas. *Blood* **122**, 705–714 (2013). URL http://bloodjournal.hematologylibrary.org/content/122/5/705.

[81] Mimee, M., Tucker, A. C., Voigt, C. A. & Lu, T. K. Programming a Human Commensal Bacterium, Bacteroides thetaiotaomicron, to Sense and Respond to

Stimuli in the Murine Gut Microbiota. *Cell Systems* **1**, 62–71 (2015). URL http://www.cell.com/article/S240547121500006X/abstract.

[82] Parker, A. C. & Smith, C. J. Development of an IPTG Inducible Expression Vector Adapted for Bacteroides fragilis. *Plasmid* **68**, 86–92 (2012). URL http://www.ncbi.nlm.nih.gov/pmc/articles/PMC3389198/.

[83] SÃÂ¡nchez, B. *et al.* A flagellin-producing Lactococcus strain: interactions with mucin and enteropathogens. *FEMS microbiology letters* **318**, 101–107 (2011).

[84] Lagenaur, L. A. *et al.* Prevention of vaginal SHIV transmission in macaques by a live recombinant Lactobacillus. *Mucosal Immunology* **4**, 648–657 (2011).

[85] Yamamoto, S. *et al.* Genetically modified Bifidobacterium displaying Salmonella-antigen protects mice from lethal challenge of Salmonella Typhimurium in a murine typhoid fever model. *Vaccine* **28**, 6684–6691 (2010).

[86] Loessner, H. *et al.* Drug-inducible remote control of gene expression by probiotic Escherichia coli Nissle 1917 in intestine, tumor and gall bladder of mice. *Microbes and infection / Institut Pasteur* **11**, 1097–1105 (2009).

[87] Reister, M. *et al.* Complete genome sequence of the gram-negative probiotic Escherichia coli strain Nissle 1917. *Journal of Biotechnology* **187**, 106–107 (2014).

[88] Steidler, L. *et al.* Treatment of murine colitis by Lactococcus lactis secreting interleukin-10. *Science (New York, N.Y.)* **289**, 1352–1355 (2000).

[89] Miller, J. K. *et al.* B-Carotene Biosynthesis in Probiotic Bacteria. *Probiotics and Antimicrobial Proteins* **5**, 69–80 (2013). URL http://link.springer.com/article/10.1007/s12602-013-9133-3.

[90] Courbet, A., Endy, D., Renard, E., Molina, F. & Bonnet, J. Detection of pathological biomarkers in human clinical samples via amplifying genetic switches and logic gates. *Science Translational Medicine* **7**, 289ra83–289ra83 (2015). URL http://stm.sciencemag.org/content/7/289/289ra83.

[91] Danino, T. *et al.* Programmable probiotics for detection of cancer in urine. *Science Translational Medicine* **7**, 289ra84 (2015).

[92] Engler, C. & Marillonnet, S. Combinatorial DNA assembly using Golden Gate cloning. *Methods in Molecular Biology (Clifton, N.J.)* **1073**, 141–156 (2013).

[93] Gibson, D. G., Smith, H. O., Hutchison, C. A., Venter, J. C. & Merryman, C. Chemical synthesis of the mouse mitochondrial genome. *Nature Methods* **7**, 901–903 (2010).

[94] Thomas, C. M. & Summers, D. Bacterial Plasmids. In *eLS* (John Wiley & Sons, Ltd, 2001). URL `http://onlinelibrary.wiley.com/doi/10.1002/9780470015902.a0000468.pub2/abstract`.

[95] Grady, R. & Hayes, F. Axe-Txe, a broad-spectrum proteic toxin-antitoxin system specified by a multidrug-resistant, clinical isolate of Enterococcus faecium. *Molecular Microbiology* **47**, 1419–1432 (2003). URL `http://onlinelibrary.wiley.com/doi/10.1046/j.1365-2958.2003.03387.x/abstract`.

[96] Lee, J. W. *et al.* Creating Single-Copy Genetic Circuits. *Molecular Cell* **63**, 329–336 (2016).

[97] Murphy, K. C. & Campellone, K. G. Lambda Red-mediated recombinogenic engineering of enterohemorrhagic and enteropathogenic E. coli. *BMC Molecular Biology* **4**, 11 (2003). URL `https://doi.org/10.1186/1471-2199-4-11`.

[98] Jiang, S.-N. *et al.* Engineering of Bacteria for the Visualization of Targeted Delivery of a Cytolytic Anticancer Agent. *Molecular Therapy* **21**, 1985–1995 (2013). URL `http://www.nature.com/mt/journal/v21/n11/full/mt2013183a.html`.

[99] Summers, D. K. The kinetics of plasmid loss. *Trends in Biotechnology* **9**, 273–278 (1991).

[100] Stecher, B. *et al.* Gut inflammation can boost horizontal gene transfer between pathogenic and commensal Enterobacteriaceae. *Proceedings of the National Academy of Sciences* **109**, 1269–1274 (2012). URL `http://www.pnas.org/content/109/4/1269`.

[101] Wright, M. S. *et al.* Influence of industrial contamination on mobile genetic elements: class 1 integron abundance and gene cassette structure in aquatic bacterial communities. *The ISME journal* **2**, 417–428 (2008).

[102] Langdon, A., Crook, N. & Dantas, G. The effects of antibiotics on the microbiome throughout development and alternative approaches for therapeutic modulation. *Genome Medicine* **8** (2016). URL http://www.ncbi.nlm.nih.gov/pmc/articles/PMC4831151/.

[103] Lobner-Olesen, A. Distribution of minichromosomes in individual Escherichia coli cells: implications for replication control. *The EMBO Journal* **18**, 1712–1721 (1999). URL http://www.ncbi.nlm.nih.gov/pmc/articles/PMC1171257/.

[104] Brantl, S. Antisense RNAs in plasmids: control of replication and maintenance. *Plasmid* **48**, 165–173 (2002). URL http://www.sciencedirect.com/science/article/pii/S0147619X02001087.

[105] Wright, O., Stan, G.-B. & Ellis, T. Building-in biosafety for synthetic biology. *Microbiology (Reading, England)* **159**, 1221–1235 (2013).

[106] Loh, J. M. S. & Proft, T. Toxin antitoxin stabilized reporter plasmids for biophotonic imaging of Group A streptococcus. *Applied Microbiology and Biotechnology* **97**, 9737–9745 (2013). URL http://link.springer.com/article/10.1007/s00253-013-5200-7.

[107] Salje, J., Gayathri, P. & Lowe, J. The ParMRC system: molecular mechanisms of plasmid segregation by actin-like filaments. *Nature Reviews Microbiology* **8**, 683–692 (2010). URL http://www.nature.com/nrmicro/journal/v8/n10/full/nrmicro2425.html.

[108] Velur Selvamani, R. S., Friehs, K. & Flaschel, E. Extracellular recombinant protein production under continuous culture conditions with escherichia coli using an alternative plasmid selection mechanism. *Bioprocess and biosystems engineering* **37**, 401–413 (2014).

[109] Ghafourian, S., Raftari, M., Sadeghifard, N. & Sekawi, Z. Toxin-antitoxin Systems: Classification, Biological Function and Application in Biotechnology. *Current issues in molecular biology* **16**, 9–14 (2013).

[110] Van Melderen, L. & Saavedra De Bast, M. Bacterial ToxinÃÂÂAntitoxin Systems: More Than Selfish Entities? *PLoS Genet* **5**, e1000437 (2009). URL http://dx.doi.org/10.1371/journal.pgen.1000437.

[111] Gerdes, K. The parB (hok/sok) Locus of Plasmid R1: A General Purpose Plasmid Stabilization System. *Nature Biotechnology* **6**, 1402–1405 (1988). URL http://www.nature.com/nbt/journal/v6/n12/abs/nbt1288-1402.html.

[112] Leanti La Rosa, S., Diep, D. B., Nes, I. F. & Brede, D. A. Construction and Application of a luxABCDE Reporter System for Real-Time Monitoring of Enterococcus faecalis Gene Expression and Growth. *Applied and Environmental Microbiology* **78**, 7003–7011 (2012). URL http://www.ncbi.nlm.nih.gov/pmc/articles/PMC3457518/.

[113] Rosa, S. L. L. *et al.* In Vivo Assessment of Growth and Virulence Gene Expression during Commensal and Pathogenic Lifestyles of luxABCDE-Tagged Enterococcus faecalis Strains in Murine Gastrointestinal and Intravenous Infection Models. *Applied and Environmental Microbiology* **79**, 3986–3997 (2013). URL http://aem.asm.org/content/79/13/3986.

[114] Azpiroz, M. F. & Lavia, M. Modular Structure of Microcin H47 and Colicin V. *Antimicrobial Agents and Chemotherapy* **51**, 2412–2419 (2007). URL http://www.ncbi.nlm.nih.gov/pmc/articles/PMC1913283/.

[115] Inglis, R. F., Bayramoglu, B., Gillor, O. & Ackermann, M. The role of bacteriocins as selfish genetic elements. *Biology Letters* **9** (2013). URL http://www.ncbi.nlm.nih.gov/pmc/articles/PMC3645024/.

[116] Campelo, A. B. *et al.* A bacteriocin gene cluster able to enhance plasmid maintenance in Lactococcus lactis. *Microbial Cell Factories* **13**, 77 (2014). URL http://dx.doi.org/10.1186/1475-2859-13-77.

[117] Grozdanov, L. *et al.* Analysis of the genome structure of the nonpathogenic probiotic Escherichia coli strain Nissle 1917. *Journal of Bacteriology* **186**, 5432–5441 (2004).

[118] Sassone-Corsi, M. *et al.* Microcins mediate competition among Enterobacteriaceae in the inflamed gut. *Nature* **540**, 280–283 (2016). URL http://www.nature.com/nature/journal/v540/n7632/full/nature20557.html#affil-auth.

[119] Koch, B., Jensen, L. E. & Nybroe, O. A panel of Tn7-based vectors for insertion of the gfp marker gene or for delivery of cloned DNA into Gram-negative bacteria at a neutral chromosomal site. *Journal of Microbiological Methods* **45**, 187–195 (2001). URL http://www.sciencedirect.com/science/article/pii/S0167701201002469.

[120] Choi, K.-H. *et al.* A Tn7-based broad-range bacterial cloning and expression system. *Nature Methods* **2**, 443–448 (2005).

[121] Choi, K.-H. & Schweizer, H. P. mini-Tn: 7: insertion in bacteria with single : att: Tn: 7: sites: example : Pseudomonas aeruginosa : Article : Nature Protocols. *Nat. Protocols* **1**, 153–161 (2006). URL https://www.nature.com/nprot/journal/v1/n1/full/nprot.2006.24.html.

[122] Gilson, L., Mahanty, H. K. & Kolter, R. Four plasmid genes are required for colicin V synthesis, export, and immunity. *Journal of Bacteriology* **169**, 2466–2470 (1987).

[123] Benedetti, I. M., Lorenzo, V. d. & Silva-Rocha, R. Quantitative, Non-Disruptive Monitoring of Transcription in Single Cells with a Broad-Host Range GFP-luxCDABE Dual Reporter System. *PLOS ONE* **7**, e52000 (2012). URL http://journals.plos.org/plosone/article?id=10.1371/journal.pone.0052000.

[124] Riedel, C. U. *et al.* Construction of p16slux, a Novel Vector for Improved Bioluminescent Labeling of Gram-Negative Bacteria. *Applied and Environmental Microbiology* **73**, 7092–7095 (2007). URL http://www.ncbi.nlm.nih.gov/pmc/articles/PMC2074938/.

[125] Swain, P. S. *et al.* Inferring time derivatives including cell growth rates using Gaussian processes. *Nature Communications* **7**, ncomms13766 (2016). URL https://www.nature.com/articles/ncomms13766.

[126] Biernacki, Celeux & Govaert. Assessing a mixture model for clustering with the integrated completed likelihood. *IEEE Transactions on Pattern Analysis and Machine Intelligence* **22**, 719ÃÂÂ725 (2000).

[127] Boe, L. Estimation of plasmid loss rates in bacterial populations with a reference to the reproducibility of stability experiments. *Plasmid* **36**, 161–167 (1996).

[128] Halvorsen, E. M., Williams, J. J., Bhimani, A. J., Billings, E. A. & Hergenrother, P. J. Txe, an endoribonuclease of the enterococcal Axe-Txe toxin-antitoxin system, cleaves mRNA and inhibits protein synthesis. *Microbiology* **157**, 387–397 (2011). URL `http://www.ncbi.nlm.nih.gov/pmc/articles/PMC3090131/`.

[129] Prindle, A. *et al.* Genetic Circuits in Salmonella typhimurium. *ACS Synthetic Biology* **1**, 458–464 (2012). URL `http://dx.doi.org/10.1021/sb300060e`.

[130] Stanton, B. C. *et al.* Genomic mining of prokaryotic repressors for orthogonal logic gates. *Nature Chemical Biology* **10**, 99–105 (2014). URL `http://www.nature.com/nchembio/journal/v10/n2/abs/nchembio.1411.html`.

[131] Tauriainen, S., Karp, M., Chang, W. & Virta, M. Luminescent bacterial sensor for cadmium and lead. *Biosensors and Bioelectronics* **13**, 931–938 (1998). URL `http://www.sciencedirect.com/science/article/pii/S095656639800027X`.

[132] Omura, T., Kiyono, M. & Pan-Hou, H. Development of a Specific and Sensitive Bacteria Sensor for Detection of Mercury at Picomolar Levels in Environment. *Journal of Health Science* **50**, 379–383 (2004).

[133] Archer, E. J., Robinson, A. B. & Suel, G. M. Engineered E. coli That Detect and Respond to Gut Inflammation through Nitric Oxide Sensing. *ACS Synthetic Biology* **1**, 451–457 (2012). URL `http://dx.doi.org/10.1021/sb3000595`.

[134] Saeidi, N. *et al.* Engineering microbes to sense and eradicate Pseudomonas aeruginosa, a human pathogen. *Molecular systems biology* **7**, 521 (2011).

[135] Hwang, I. Y. *et al.* Engineered probiotic Escherichia coli can eliminate and prevent Pseudomonas aeruginosa gut infection in animal models. *Nature Communications* **8**, 15028 (2017). URL `http://www.nature.com/ncomms/2017/170411/ncomms15028/full/ncomms15028.html`.

[136] Burisch, J., Jess, T., Martinato, M. & Lakatos, P. L. The burden of inflammatory bowel disease in Europe. *Journal of Crohn's and Colitis* **7**, 322–337 (2013). URL https://academic.oup.com/ecco-jcc/article/7/4/322/386167/The-burden-of-inflammatory-bowel-disease-in-Europe.

[137] Lundberg, J. O., Hellstram, P. M., Lundberg, J. M. & Alving, K. Greatly increased luminal nitric oxide in ulcerative colitis. *Lancet (London, England)* **344**, 1673–1674 (1994).

[138] Winter, S. E. *et al.* Host-derived nitrate boosts growth of E. coli in the inflamed gut. *Science (New York, N.Y.)* **339**, 708–711 (2013). URL http://www.ncbi.nlm.nih.gov/pmc/articles/PMC4004111/.

[139] Lin, H.-Y., Bledsoe, P. J. & Stewart, V. Activation of yeaR-yoaG Operon Transcription by the Nitrate-Responsive Regulator NarL Is Independent of Oxygen-Responsive Regulator Fnr in Escherichia coli K-12. *Journal of Bacteriology* **189**, 7539–7548 (2007). URL http://www.ncbi.nlm.nih.gov/pmc/articles/PMC2168752/.

[140] Puertollano, E., Kolida, S. & Yaqoob, P. Biological significance of short-chain fatty acid metabolism by the intestinal microbiome. *Current Opinion in Clinical Nutrition and Metabolic Care* **17**, 139–144 (2014).

[141] Smith, P. M. *et al.* The Microbial Metabolites, Short-Chain Fatty Acids, Regulate Colonic Treg Cell Homeostasis. *Science* **341**, 569–573 (2013). URL http://www.sciencemag.org/content/341/6145/569.

[142] Maslowski, K. M. *et al.* Regulation of inflammatory responses by gut microbiota and chemoattractant receptor GPR43. *Nature* **461**, 1282–1286 (2009).

[143] Ganapathy, V., Thangaraju, M., Prasad, P. D., Martin, P. M. & Singh, N. Transporters and receptors for short-chain fatty acids as the molecular link between colonic bacteria and the host. *Current Opinion in Pharmacology* **13**, 869–874 (2013).

[144] Lee, S. K. & Keasling, J. D. A Propionate-Inducible Expression System for Enteric Bacteria. *Applied and Environmental Microbiology* **71**, 6856–6862 (2005). URL http://www.ncbi.nlm.nih.gov/pmc/articles/PMC1287719/.

[145] Lee, S. K. & Keasling, J. D. Propionate-regulated high-yield protein production in Escherichia coli. *Biotechnology and Bioengineering* **93**, 912–918 (2006). URL http://onlinelibrary.wiley.com/doi/10.1002/bit.20784/abstract.

[146] Lee, S. K. & Keasling, J. D. Effect of Glucose or Glycerol as the Sole Carbon Source on Gene Expression from the Salmonella prpBCDE Promoter in Escherichia coli. *Biotechnology Progress* **22**, 1547–1551 (2006). URL http://onlinelibrary.wiley.com/doi/10.1021/bp060193f/abstract.

[147] Fallingborg, J. Intraluminal pH of the human gastrointestinal tract. *Danish Medical Bulletin* **46**, 183–196 (1999).

[148] Barnard, E., Shi, B., Kang, D., Craft, N. & Li, H. The balance of metagenomic elements shapes the skin microbiome in acne and health. *Scientific Reports* **6**, 39491 (2016). URL http://www.nature.com/srep/2016/161221/srep39491/full/srep39491.html.

[149] Hemmerling, A. *et al.* Phase 1 dose-ranging safety trial of Lactobacillus crispatus CTV-05 for the prevention of bacterial vaginosis. *Sexually Transmitted Diseases* **36**, 564–569 (2009).

[150] Kuper, C. & Jung, K. CadC-mediated activation of the cadBA promoter in Escherichia coli. *Journal of Molecular Microbiology and Biotechnology* **10**, 26–39 (2005).

[151] Ou, J., DeLany, J. P., Zhang, M., Sharma, S. & O'Keefe, S. J. D. Association between low colonic short-chain fatty acids and high bile acids in high colon cancer risk populations. *Nutrition and Cancer* **64**, 34–40 (2012).

[152] Bernstein, H., Bernstein, C., Payne, C. M. & Dvorak, K. Bile acids as endogenous etiologic agents in gastrointestinal cancer. *World Journal of Gastroenterology* **15**, 3329–3340 (2009).

[153] Ruiz, L. *et al.* A bile-inducible membrane protein mediates bifidobacterial bile resistance. *Microbial Biotechnology* **5**, 523–535 (2012). URL http://onlinelibrary.wiley.com/doi/10.1111/j.1751-7915.2011.00329.x/abstract.

[154] Gusarov, I. *et al.* Bacterial Nitric-oxide Synthases Operate without a Dedicated Redox Partner. *The Journal of Biological Chemistry* **283**, 13140–13147 (2008). URL http://www.ncbi.nlm.nih.gov/pmc/articles/PMC2442334/.

[155] Lin, H.-Y., Bledsoe, P. J. & Stewart, V. Activation of yeaR-yoaG Operon Transcription by the Nitrate-Responsive Regulator NarL Is Independent of Oxygen-Responsive Regulator Fnr in Escherichia coli K-12. *Journal of Bacteriology* **189**, 7539–7548 (2007). URL http://www.ncbi.nlm.nih.gov/pmc/articles/PMC2168752/.

[156] Takahashi, H. *et al.* Effect of partially hydrolyzed guar gum on fecal output in human volunteers. *Nutrition Research* **13**, 649–657 (1993). URL http://www.nrjournal.com/article/S0271-5317(05)80557-3/abstract.

[157] Muir, J. G. *et al.* Modulation of fecal markers relevant to colon cancer risk: a high-starch Chinese diet did not generate expected beneficial changes relative to a Western-type diet. *The American Journal of Clinical Nutrition* **68**, 372–379 (1998). URL http://ajcn.nutrition.org/content/68/2/372.

[158] Levine, J. J. *et al.* Nitric oxide and inflammatory bowel disease: evidence for local intestinal production in children with active colonic disease. *Journal of Pediatric Gastroenterology and Nutrition* **26**, 34–38 (1998).

[159] Bruzzese, E. *et al.* Intestinal inflammation is a frequent feature of cystic fibrosis and is reduced by probiotic administration. *Alimentary Pharmacology & Therapeutics* **20**, 813–819 (2004).

[160] Daeffler, K. N.-M. *et al.* Engineering bacterial thiosulfate and tetrathionate sensors for detecting gut inflammation. *Molecular Systems Biology* **13**, 923 (2017). URL http://msb.embopress.org/content/13/4/923.

[161] Stano, M. & Klucar, L. phiGENOME: An integrative navigation throughout bacteriophage genomes. *Genomics* **98**, 376–380 (2011). URL http://www.sciencedirect.com/science/article/pii/S0888754311001777.

[162] Rawls, J. F., Mahowald, M. A., Ley, R. E. & Gordon, J. I. Reciprocal Gut Microbiota Transplants from Zebrafish and Mice to Germ-free Recipients Reveal Host Habitat Selection. *Cell* **127**, 423–433 (2006). URL http://www.ncbi.nlm.nih.gov/pmc/articles/PMC4839475/.

[163] Chandler, J. A., Lang, J. M., Bhatnagar, S., Eisen, J. A. & Kopp, A. Bacterial Communities of Diverse Drosophila Species: Ecological Context of a Host Microbe Model System. *PLOS Genetics* **7**, e1002272 (2011). URL http://journals.plos.org/plosgenetics/article?id=10.1371/journal.pgen.1002272.

[164] Sharon, G. *et al.* Commensal bacteria play a role in mating preference of Drosophila melanogaster. *Proceedings of the National Academy of Sciences* **107**, 20051–20056 (2010). URL http://www.pnas.org/content/107/46/20051.

[165] Brugman, S. *et al.* Oxazolone-Induced Enterocolitis in Zebrafish Depends on the Composition of the Intestinal Microbiota. *Gastroenterology* **137**, 1757–1767.e1 (2009). URL http://www.sciencedirect.com/science/article/pii/S0016508509014085.

[166] Nguyen, T. L. A., Vieira-Silva, S., Liston, A. & Raes, J. How informative is the mouse for human gut microbiota research? *Disease Models & Mechanisms* **8**, 1–16 (2015). URL http://www.ncbi.nlm.nih.gov/pmc/articles/PMC4283646/.

[167] Faith, J. J., McNulty, N. P., Rey, F. E. & Gordon, J. I. Predicting a human gut microbiota's response to diet in gnotobiotic mice. *Science (New York, N.Y.)* **333**, 101–104 (2011).

[168] Goodman, A. L. *et al.* Extensive personal human gut microbiota culture collections characterized and manipulated in gnotobiotic mice. *Proceedings of the National Academy of Sciences of the United States of America* **108**, 6252–6257 (2011).

[169] Turnbaugh, P. J. *et al.* The Effect of Diet on the Human Gut Microbiome: A Metagenomic Analysis in Humanized Gnotobiotic Mice. *Science translational medicine* **1**, 6ra14 (2009). URL http://www.ncbi.nlm.nih.gov/pmc/articles/PMC2894525/.

[170] Laukens, D., Brinkman, B. M., Raes, J., De Vos, M. & Vandenabeele, P. Heterogeneity of the gut microbiome in mice: guidelines for optimizing experimental design. *FEMS microbiology reviews* **40**, 117–132 (2016).

[171] Macpherson, A. J. & McCoy, K. D. Standardised animal models of host microbial mutualism. *Mucosal Immunology* **8**, 476–486 (2015). URL http://www.nature.com/mi/journal/v8/n3/full/mi2014113a.html.

[172] Consortium, T. C. e. S. Genome Sequence of the Nematode C. elegans: A Platform for Investigating Biology. *Science* **282**, 2012–2018 (1998). URL http://science.sciencemag.org/content/282/5396/2012.

[173] Cabreiro, F. & Gems, D. Worms need microbes too: microbiota, health and aging in Caenorhabditis elegans. *EMBO Molecular Medicine* **5**, 1300–1310 (2013). URL http://www.ncbi.nlm.nih.gov/pmc/articles/PMC3799487/.

[174] Samuel, B. S., Rowedder, H., Braendle, C., Felix, M.-A. & Ruvkun, G. Caenorhabditis elegans responses to bacteria from its natural habitats. *Proceedings of the National Academy of Sciences* **113**, E3941–E3949 (2016). URL http://www.pnas.org/content/113/27/E3941.

[175] Avery, L. & Shtonda, B. B. Food transport in the C. elegans pharynx. *Journal of Experimental Biology* **206**, 2441–2457 (2003). URL http://jeb.biologists.org/content/206/14/2441.

[176] Portal-Celhay, C., Bradley, E. R. & Blaser, M. J. Control of intestinal bacterial proliferation in regulation of lifespan in Caenorhabditis elegans. *BMC microbiology* **12**, 49 (2012).

[177] Ghafouri, S. & McGhee, J. D. Bacterial residence time in the intestine of *Caenorhabditis elegans*. *Nematology* **9**, 87–91 (2007). URL

http://booksandjournals.brillonline.com/content/journals/10.1163/156854107779969718.

[178] Scott, T. A. *et al.* Host-Microbe Co-metabolism Dictates Cancer Drug Efficacy in C. elegans. *Cell* **169**, 442–456.e18 (2017). URL http://www.cell.com/cell/abstract/S0092-8674(17)30369-0.

[179] Everman, J. L., Ziaie, N. R., Bechler, J. & Bermudez, L. E. Establishing Caenorhabditis elegans as a model for Mycobacterium avium subspecies hominissuis infection and intestinal colonization. *Biology Open* bio.012260 (2015). URL http://bio.biologists.org/content/early/2015/09/14/bio.012260.

[180] Watson, E. *et al.* Interspecies Systems Biology Uncovers Metabolites Affecting C. elegans Gene Expression and Life History Traits. *Cell* **156**, 759–770 (2014). URL http://www.ncbi.nlm.nih.gov/pmc/articles/PMC4169190/.

[181] Litcofsky, K. D., Afeyan, R. B., Krom, R. J., Khalil, A. S. & Collins, J. J. Iterative plug-and-play methodology for constructing and modifying synthetic gene networks. *Nature methods* **9**, 1077–1080 (2012). URL http://www.ncbi.nlm.nih.gov/pmc/articles/PMC3492501/.

[182] Martinez-Garcia, E., Aparicio, T., Goni-Moreno, A., Fraile, S. & de Lorenzo, V. SEVA 2.0: an update of the Standard European Vector Architecture for de-/re-construction of bacterial functionalities. *Nucleic Acids Research* **43**, D1183–D1189 (2015). URL http://www.ncbi.nlm.nih.gov/pmc/articles/PMC4383931/.

[183] Hecht, A., Endy, D., Salit, M. & Munson, M. S. When Wavelengths Collide: Bias in Cell Abundance Measurements Due to Expressed Fluorescent Proteins. *ACS synthetic biology* **5**, 1024–1027 (2016).

[184] Wang, J. *et al.* Ratio-metric sensor to detect riboflavin via fluorescence resonance energy transfer with ultrahigh sensitivity. *Physica E: Low-dimensional Systems and Nanostructures* **72**, 17–24 (2015). URL http://www.sciencedirect.com/science/article/pii/S1386947715300126.

[185] Shynkar, V. V. *et al.* Fluorescent Biomembrane Probe for Ratiometric Detection of Apoptosis. *Journal of the American Chemical Society* **129**, 2187–2193 (2007). URL http://dx.doi.org/10.1021/ja068008h.

[186] Shaner, N. C. *et al.* Improved monomeric red, orange and yellow fluorescent proteins derived from Discosoma sp. red fluorescent protein. *Nature Biotechnology* **22**, 1567–1572 (2004). URL http://www.nature.com/nbt/journal/v22/n12/full/nbt1037.html?foxtrotcallback=true.

[187] Khmelinskii, A. *et al.* Tandem fluorescent protein timers for in vivo analysis of protein dynamics. *Nature Biotechnology* **30**, 708–714 (2012). URL http://www.nature.com/nbt/journal/v30/n7/full/nbt.2281.html.

[188] Hebisch, E., Knebel, J., Landsberg, J., Frey, E. & Leisner, M. High Variation of Fluorescence Protein Maturation Times in Closely Related Escherichia coli Strains. *PLOS ONE* **8**, e75991 (2013). URL http://journals.plos.org/plosone/article?id=10.1371/journal.pone.0075991.

Appendix

Plasmid Stability

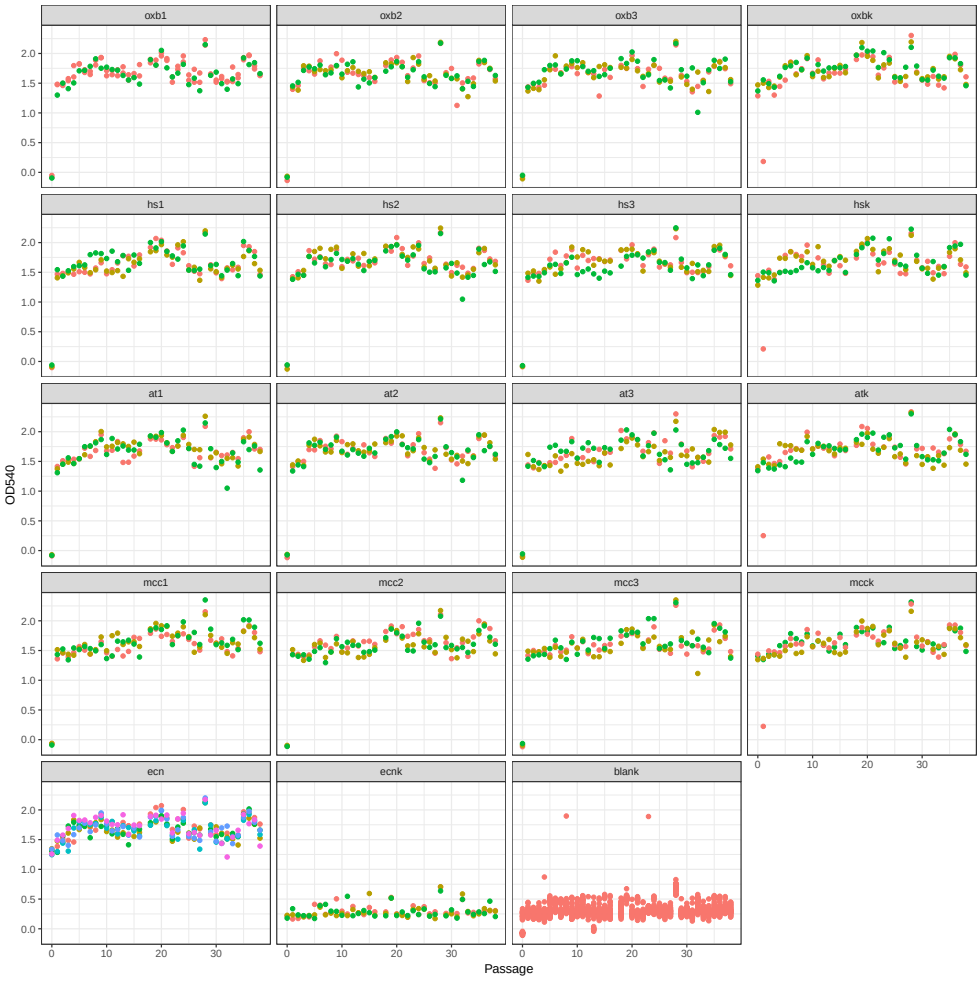

Figure 5.1: Plate-reader OD_{540} absorbance of OXB20_GFP, OXB20_GFP_AT, OXB20_GFP_HS and OXB20_GFP_MCC over 37 daily passages in the absence of antibiotic selection. OXBK, ATK, HSK and MCCK indicate control wells grown with both erythromycin and kanamycin that should be 100% plasmid-bearing. Ecn and ecnk indicate negative controls. Numbers indicate biological replicates and colours indicate technical replicates.

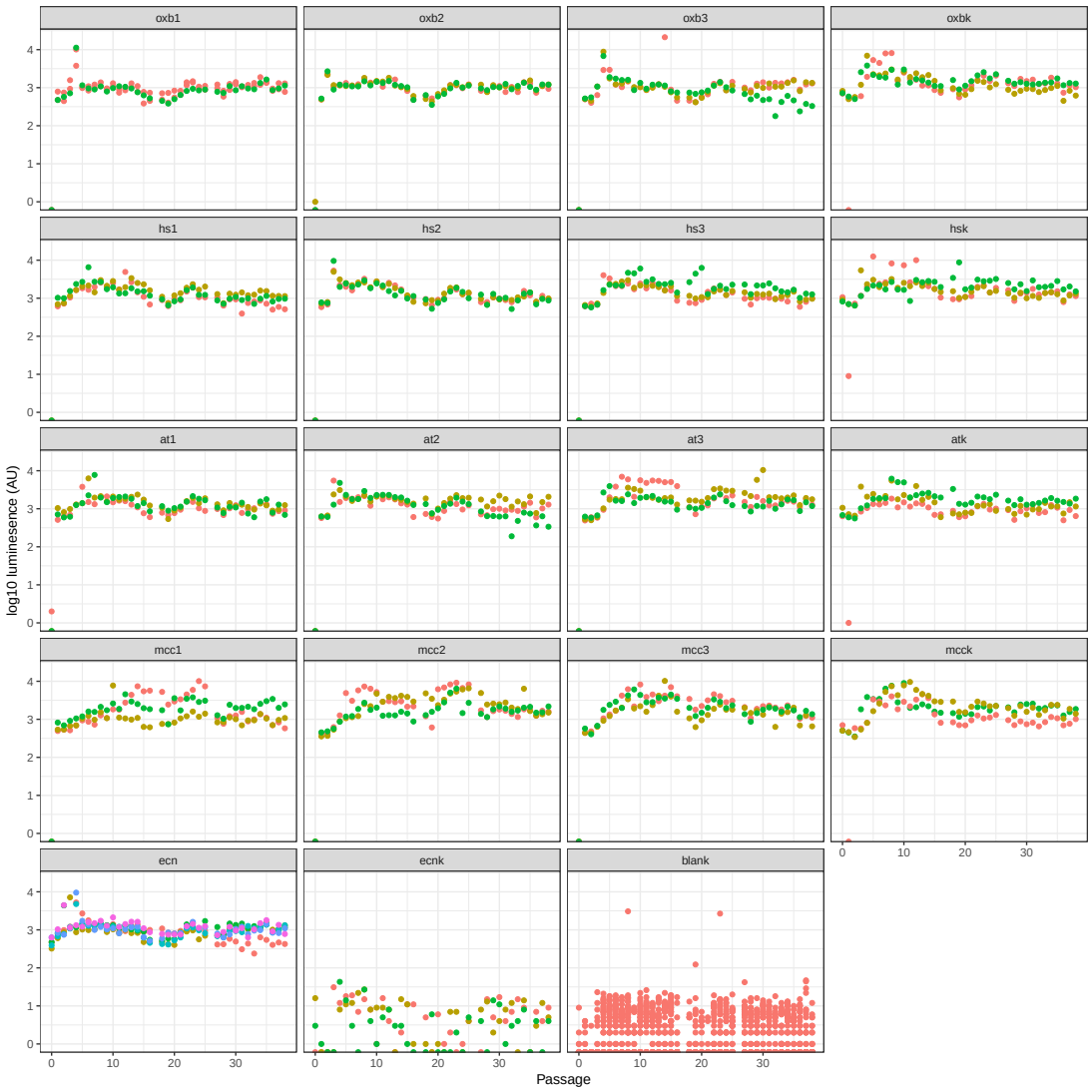

Figure 5.2: Plate-reader luminescence of OXB20_GFP, OXB20_GFP_AT, OXB20_GFP_HS and OXB20_GFP_MCC over 37 daily passages in the absence of antibiotic selection. OXBK, ATK, HSK and MCCK indicate control wells grown with both erythromycin and kanamycin that should be 100% plasmid-bearing. Ecn and ecnk indicate negative controls. Numbers indicate biological replicates and colours indicate technical replicates.

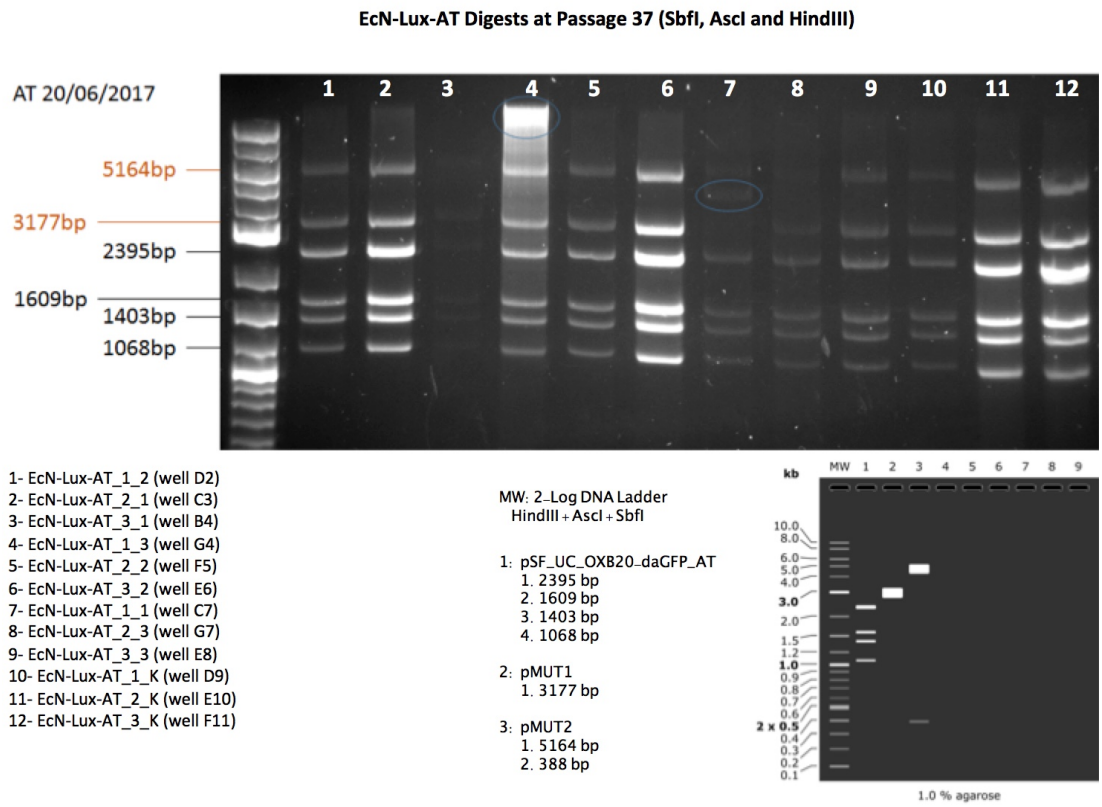

Figure 5.3: Restriction enzyme digests identifying the presence of the OXB20_GFP_AT plasmid in EcN_Lux after 37 daily passages in the absence of antibiotic selection. Lane 1-9 indicate the 9 replicates grown only in erythromycin and lanes 10-12 indicate the control strains grown in erythromycin and kanamycin. Simulated digests on the bottom right show the two EcN cryptic plasmids (at 5164bp and 3177bp) and the 4 identifiable fragments of the OXB20_GFP_AT plasmid.

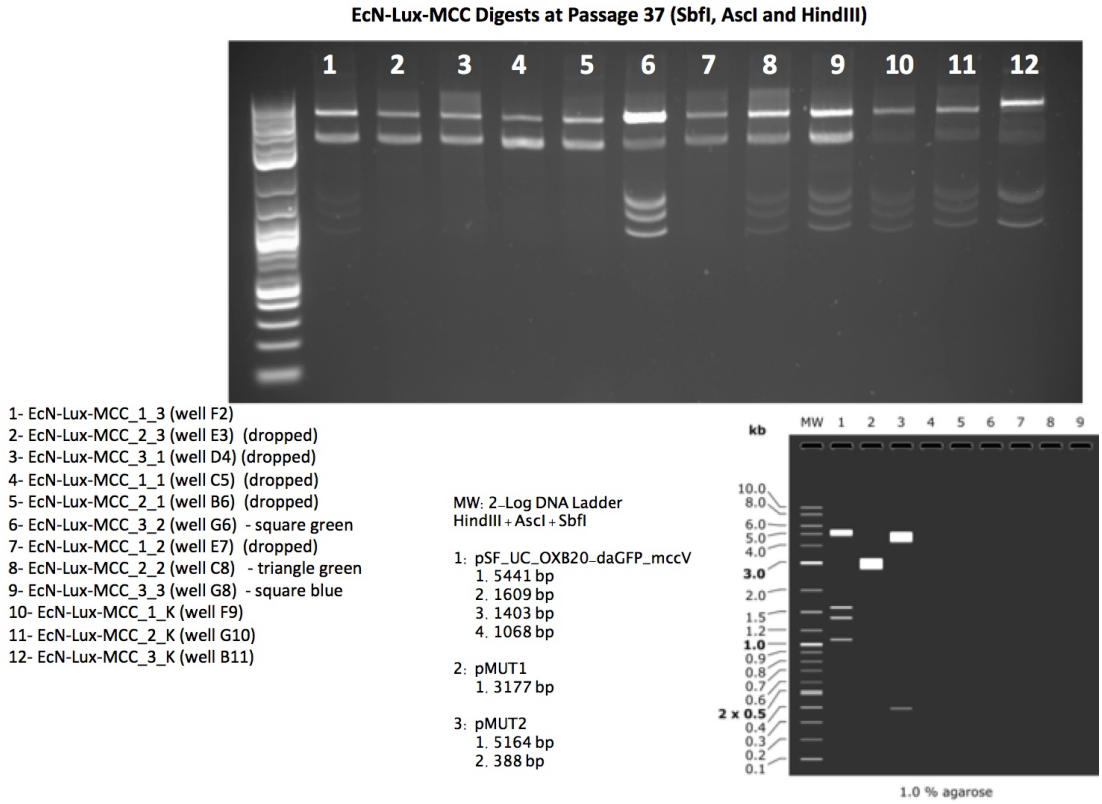

Figure 5.4: Restriction enzyme digests identifying the partial presence of the OXB20_GFP_MCC plasmid in EcN_Lux after 37 daily passages in the absence of antibiotic selection. Lane 1-9 indicate the 9 replicates grown only in erythromycin and lanes 10-12 indicate the control strains grown in erythromycin and kanamycin. Simulated digests on the bottom right show the two EcN cryptic plasmids (at 5164bp and 3177bp) and the 4 identifiable fragments of the OXB20_GFP_MCC plasmid. Digests correlate with fluorescence data indicating that the plasmid was only present in 4 out of 9 replicates (lane 1,6, 8 and 9).

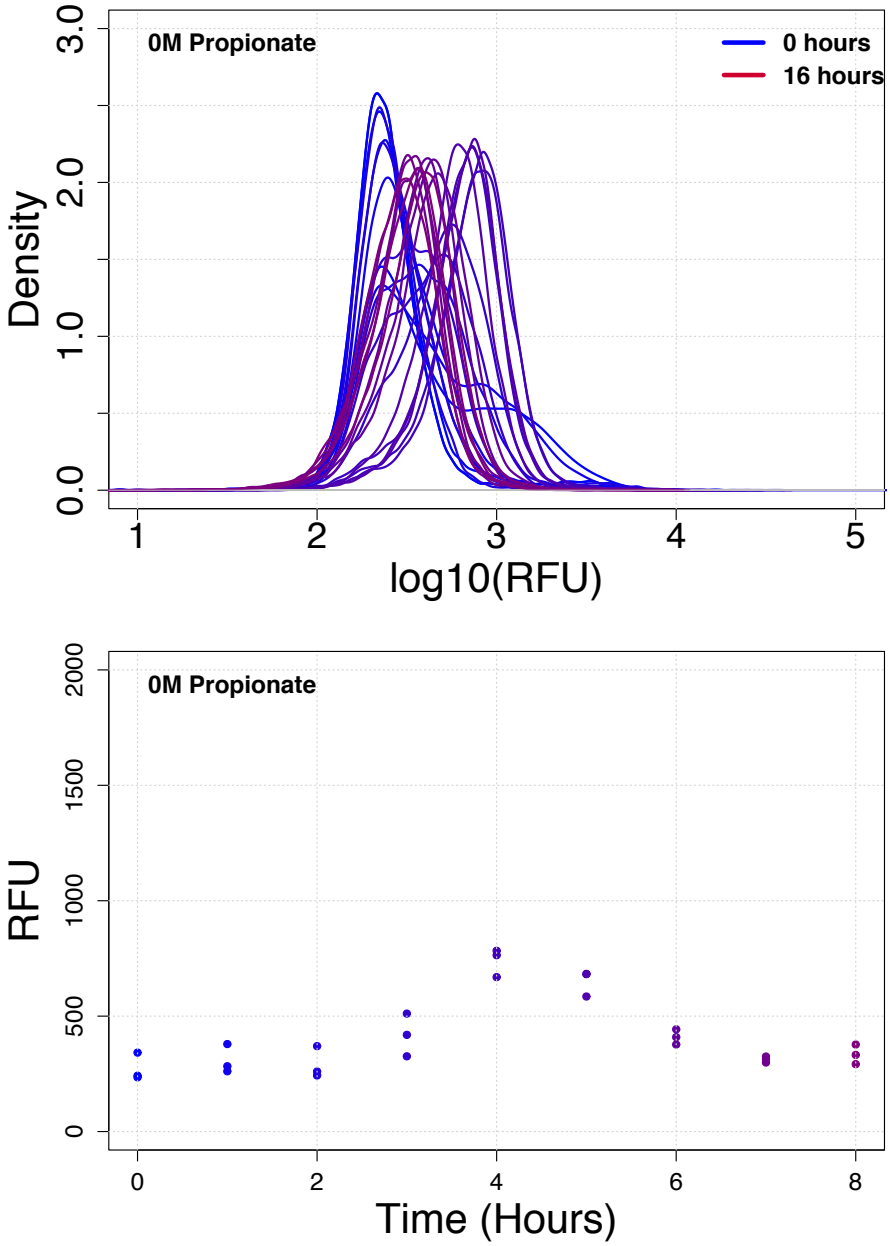

Figure 5.5: EcN_pProE_GFP induction after 16 hours in M9 media with 0M Propionate. Top, histogram density plot of GFP fluorescence after 16 hours induction. Bottom, median GFP fluorescence over 16 hours. Flow cytometry data with 10,000 events (n=3).

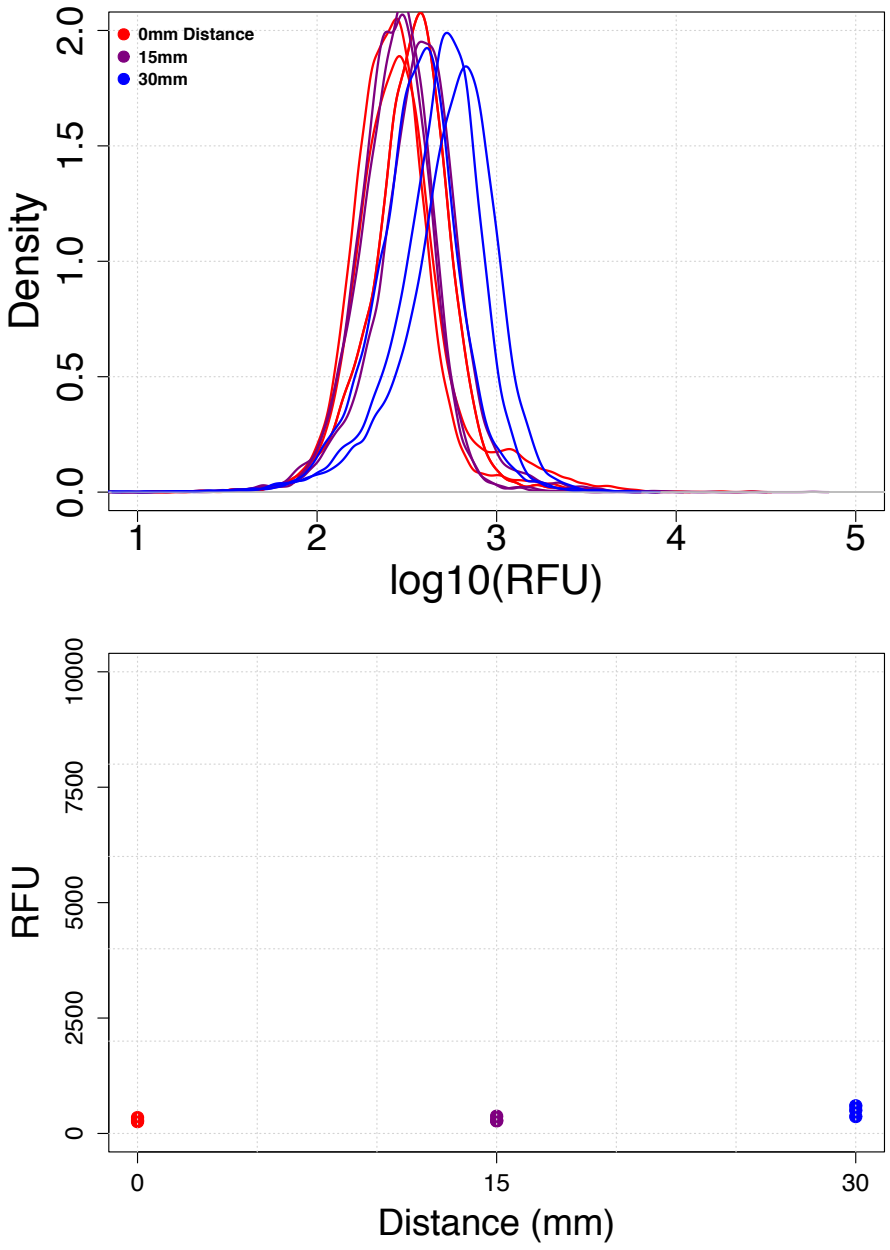

Figure 5.6: EcN_pYeaR_GFP induction on an agar plate at different distances from the uninduced EcB_pNOS$_{Ban}$ centre. Top, histogram density plot of GFP fluorescence after 16 hours growth. Bottom, median GFP fluorescence after 16 hours growth. Flow cytometry data with 10,000 events (n=3).

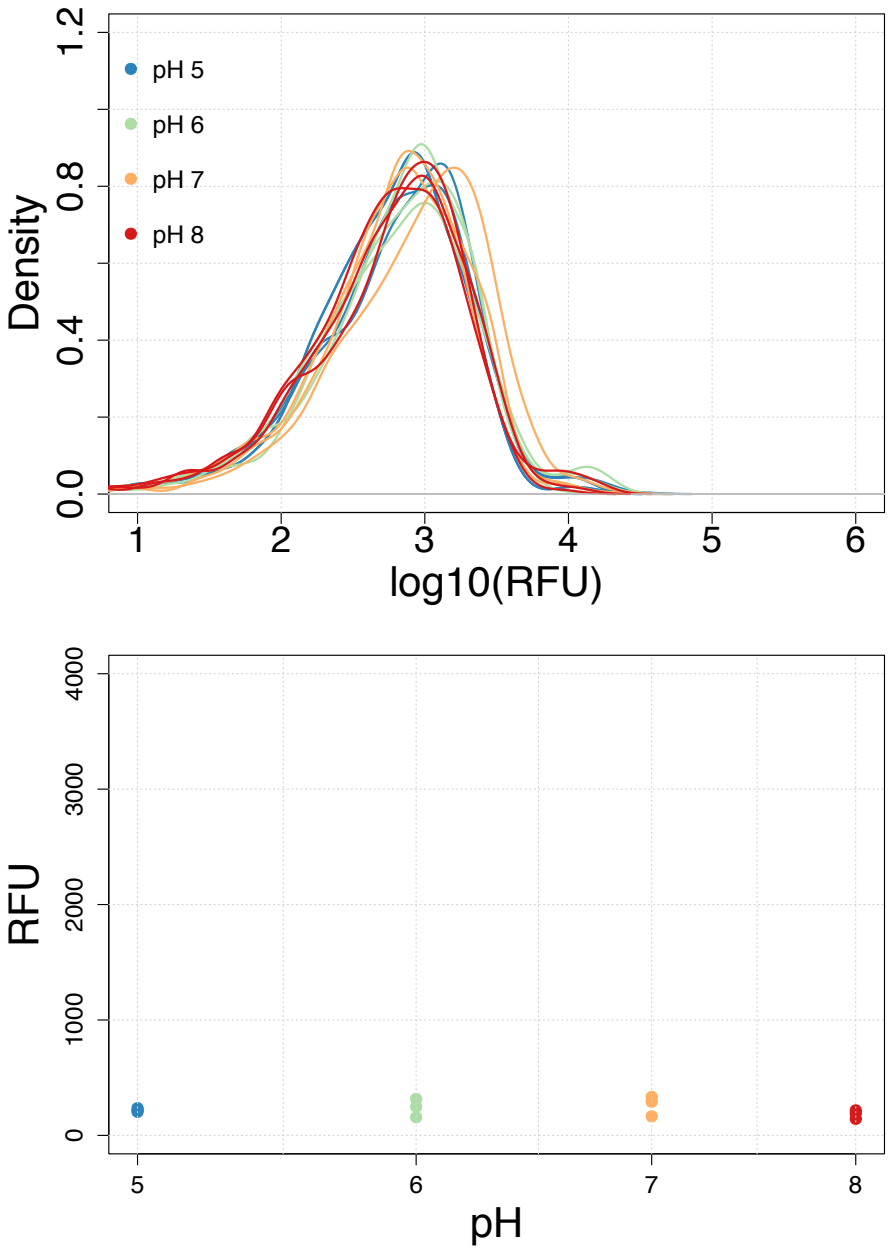

Figure 5.7: EcN_OG241_GFP (negative promoterless control) induction after 16 hours in LB media buffered to pH 5 (with acetic acid), pH 6 (with MES), pH 7 (with HEPES) and pH 8 (with HEPES). Top, histogram density plot of GFP fluorescence after 16 hours growth. Bottom, median GFP fluorescence after 16 hours growth. Flow cytometry data with 10,000 events (n=3).

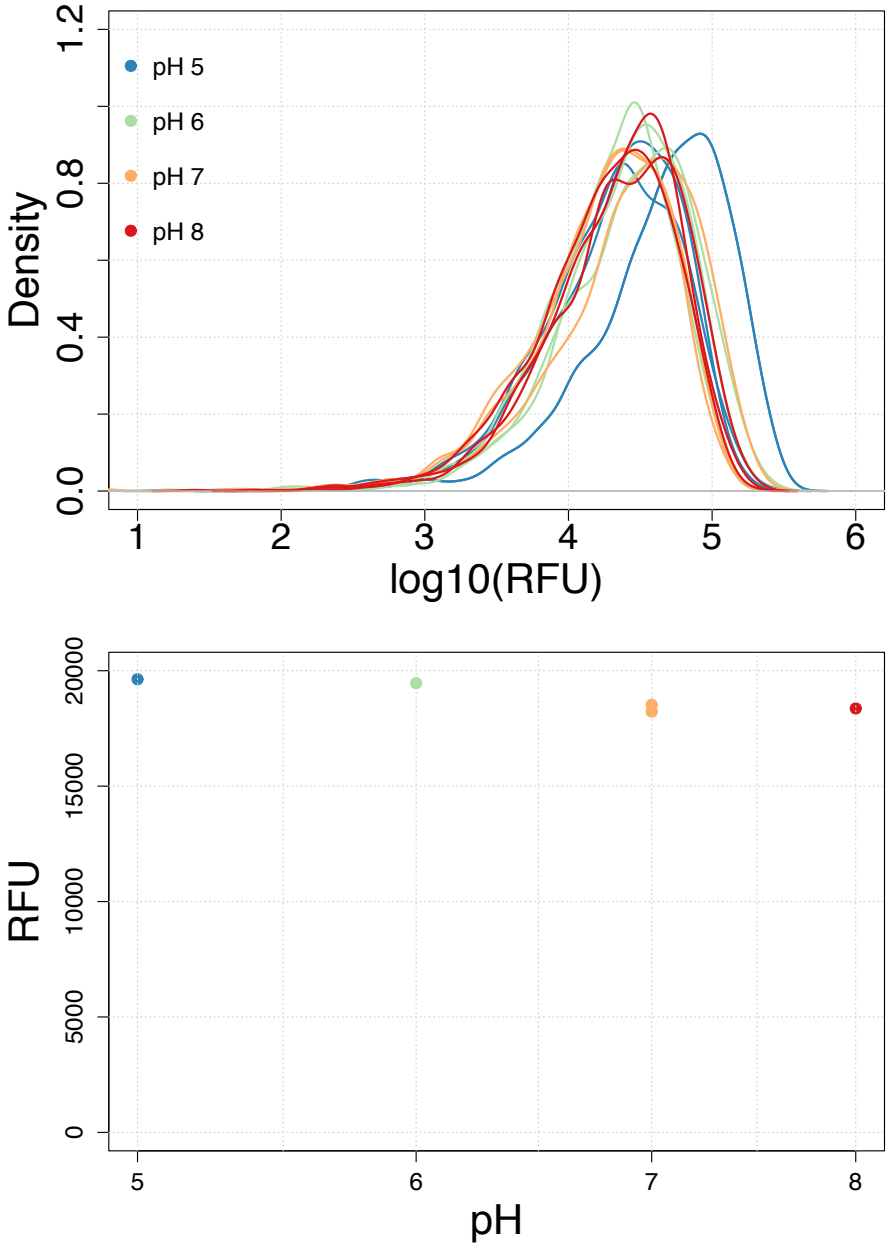

Figure 5.8: EcN_OXB19_GFP (positive constitutive control) induction after 16 hours in LB media buffered to pH 5 (with acetic acid), pH 6 (with MES), pH 7 (with HEPES) and pH 8 (with HEPES). Top, histogram density plot of GFP fluorescence after 16 hours growth. Bottom, median GFP fluorescence after 16 hours growth. Flow cytometry data with 10,000 events (n=3).

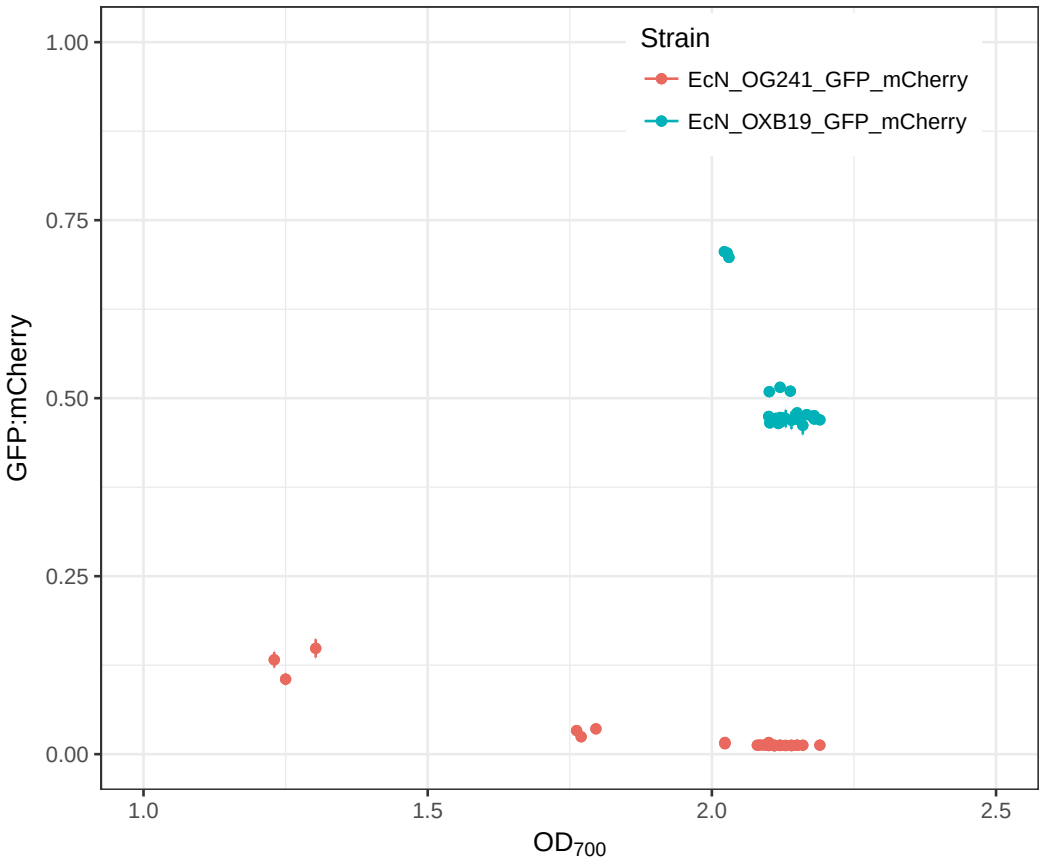

Figure 5.9: GFP:mCherry ratio in EcN_OXB19_GFP_mCherry and EcN_OG241_GFP_mCherry With Increasing OD700. Ratio calculated using median fluorescence for each reporter from flow cytometry data with 10,000 events (n=3).

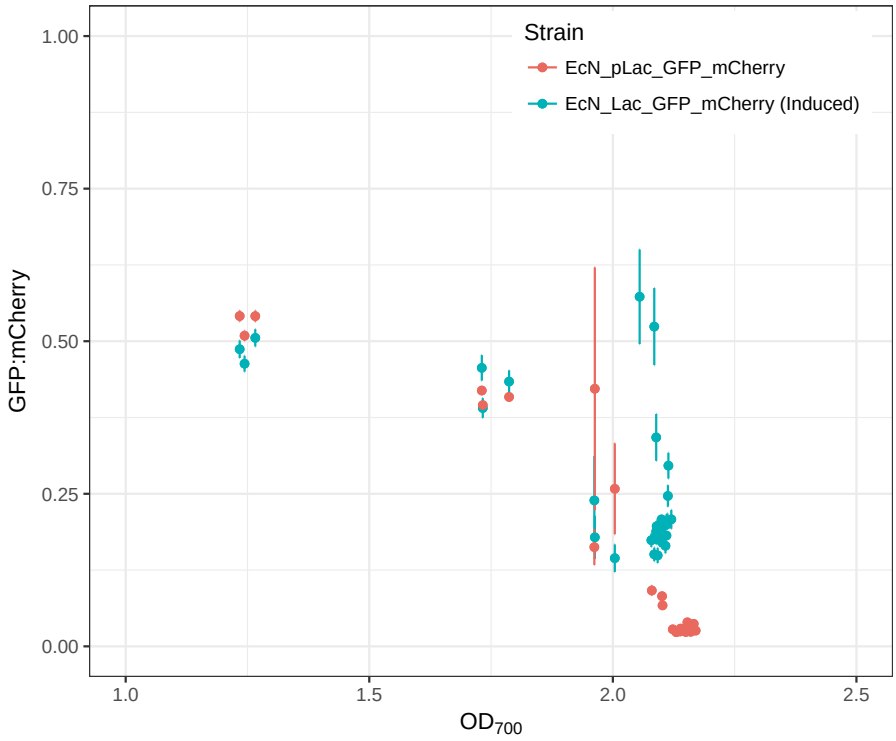

Figure 5.10: GFP to mCherry ratio in uninduced or induced (1mM IPTG) EcN_pLac_GFP_mCherry with increasing OD700. Ratio calculated using median fluorescence for each reporter from flow cytometry data with 10,000 events (n=3).

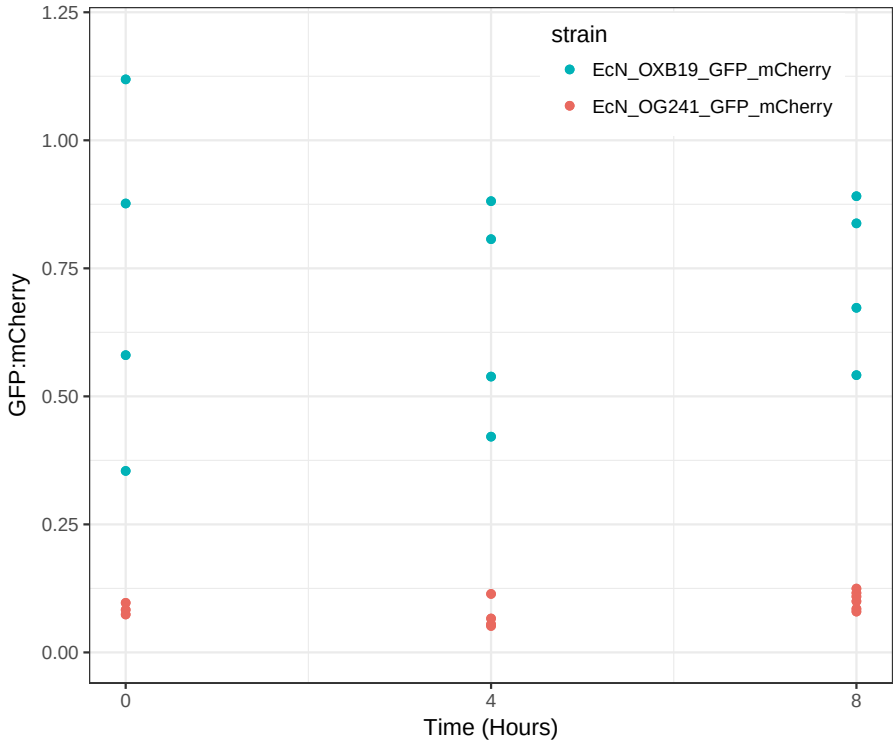

Figure 5.11: Box plot of GFP:mCherry ratio in individual 7 day old *C.elegans* worms grown on EcN_OG241_GFP_mCherry and EcN_OXB19_GFP_mCherry control strains and transferred to a NGM plate supplemented with 1mM IPTG for 8 hours.